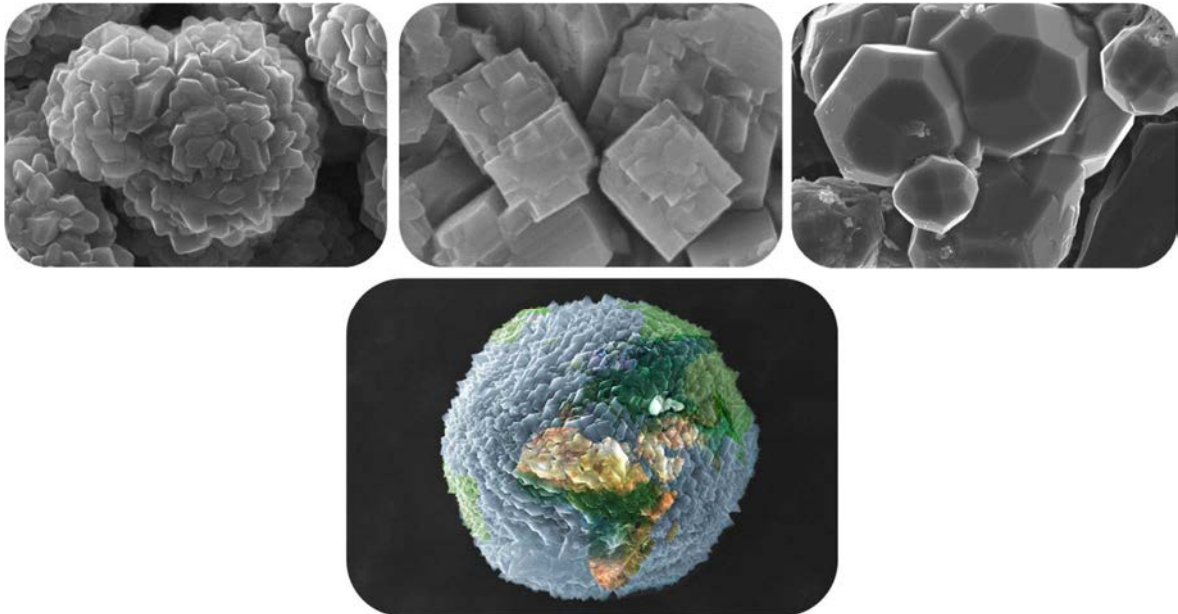


PhD Thesis

Complete transformation of aluminum waste into zeolite and its use in the removal of pollutants from aqueous solution



Ruth Sánchez Hernández



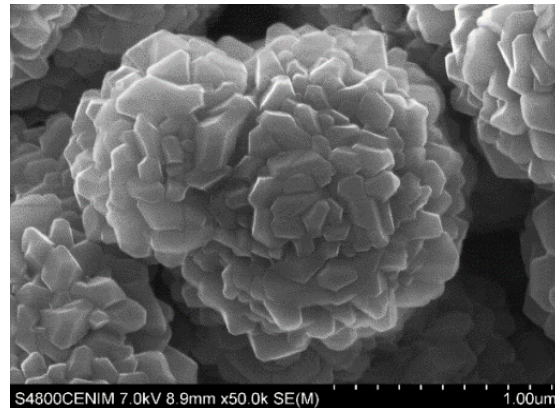
Consejo Superior de Investigaciones Científicas
Centro Nacional de Investigaciones Metalúrgicas



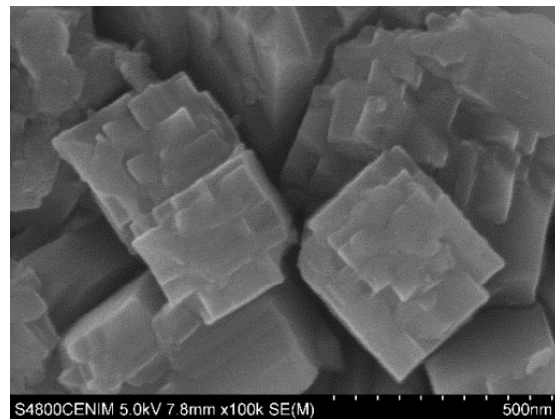
Leganes, Madrid. 2018

Cover Pictures

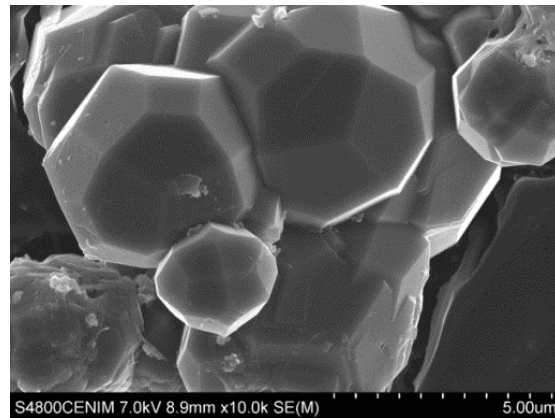
SEM image of the sodalite zeolite obtained from aluminum waste, in this Thesis



SEM image of the NaP1 zeolite obtained from aluminum waste, in this Thesis

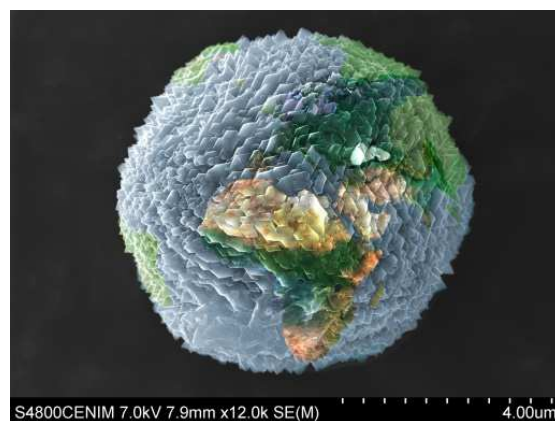


SEM image of the analcime zeolite obtained from aluminum waste, in this Thesis



SEM image of the NaP1 zeolite obtained from aluminum waste

Picture “*Mundo Sostenible*” awarded with the first prize of the micro category in:
Fotography Competition FOTCIENCIA13



PhD THESIS

Complete transformation of aluminum waste into zeolite and its use in the removal of pollutants from aqueous solution

Author:

Ruth Sánchez Hernández

Supervisors:

Aurora López Delgado (CENIM, CSIC)

Sol López Andrés (UCM)

Tutor:

Antonia Jiménez Morales (UC3M)

MATERIALS SCIENCE AND ENGINEERING

Leganés, June 2018

PhD TESIS

**COMPLETE TRANSFORMATION OF ALUMINUM WASTE INTO
ZEOLITE AND ITS USE IN THE REMOVAL OF POLLUTANTS FROM
AQUEOUS SOLUTION**

Author: Ruth Sánchez Hernández

Supervisors: Aurora López Delgado
Sol López Andrés

Firma del Tribunal Calificador:

Firma

Presidente: (Nombre y apellidos)

Vocal: (Nombre y apellidos)

Secretario: (Nombre y apellidos)

Calificación:

Leganés, de de

AGRADECIMIENTOS

Quisiera expresar mi más sincero agradecimiento a todas aquellas personas e instituciones que de alguno u otro modo han hecho posible la realización de este trabajo.

En primer lugar, me gustaría expresar mi gratitud a mis directoras de tesis, Dra. Aurora López Delgado y Prof. Sol López Andrés, por su confianza y apoyo prestados a lo largo del desarrollo de esta tesis. Les agradezco su gran dirección, valiosa dedicación e inestimable ayuda, las cuales han sido clave para poder alcanzar esta meta. Gracias de todo corazón por haber creado una atmósfera de trabajo tan agradable y propicia para mi desarrollo personal y profesional.

Me gustaría agradecer con cariño a la Dra. Isabel Padilla por haberme ayudado y apoyado durante estos años, siempre dispuesta a colaborar desinteresadamente.

Agradecer también al Dr. Roberto Galindo por sus consejos y ayuda durante mi primera etapa de la tesis.

Quisiera dar las gracias a todo el personal del CENIM por su ayuda y por haberme facilitado las herramientas y los medios necesarios para el desarrollo de este trabajo.

Agradecer también a todo el equipo humano que forma parte del CAI de Técnicas Geológicas, de la UCM, por haberme abierto sus puertas y por su gran ayuda.

En especial, me gustaría mostrar mi más sincero agradecimiento y cariño a todos y cada uno de mis compañeros de trabajo y amigos.

Por último, agradecer a mi familia, y en especial, a Javi, por su paciencia, comprensión y apoyo.

A mis padres, Inés y Alejandro
A Javi

ABSTRACT

Zero Waste concept aims to minimize the negative effects of the generation and management of waste on human health and the environment, as well as to reduce the use of natural resources.

The novelty of this Thesis comes from the development of a simple procedure to completely transform a hazardous aluminum waste into added-value materials of great industrial interest, as zeolites, which are used later as adsorbents for the removal of heavy metals and ammonium from aqueous effluents. There are not previous works related to the use of the hazardous aluminum waste as a raw material for the synthesis of zeolites.

In this work the following stages were developed:

- i) Characterization of different aluminum wastes to get a representative sample.
- ii) Lab-scale hydrothermal synthesis and characterization of zeolites from aluminum waste to define the optimal experimental conditions.
- iii) Scaling up of the process (bench-scale synthesis) to assess its industrial application.
- iv) Development of a more sustainable synthesis process by alkaline effluents recycling in order to achieve a zero waste and zero effluents process.
- v) Using the zeolites as adsorbents for the removal of heavy metals and ammonium to decontaminate water.

Aluminum waste, due to its high aluminum content ($\text{Al}_2\text{O}_3 \sim 66 \text{ wt.}\%$), was characterized and used as the only aluminum raw material for the lab- and bench-scale synthesis of zeolites in the $\text{Na}_2\text{O}-\text{Al}_2\text{O}_3-\text{SiO}_2-\text{H}_2\text{O}$ system. The synthesized zeolites exhibited high cation exchange capacities (CEC) and suitable adsorption properties, resulting in potential adsorbents for the removal of heavy metals and ammonium from aqueous solutions. The most relevant hazardous features of aluminum waste derive from its mineralogical and chemical composition and very fine granulometry (2.5-93 μm). It exhibits spontaneous and exothermic reactivity because its high contents of metallic aluminum (12.8 wt.%) and aluminum nitride (13.1 wt.%), in contact with water, can generate toxic gases such as ammonia (71 Nm^3 per ton of waste) and/or inflammable and explosive gases like hydrogen (162 Nm^3 per ton of waste). Besides, it contains heavy metals, which can be released by leaching under incorrect management and disposal.

The development of a simple and one-step hydrothermal synthesis process enabled the complete transformation of the waste in zeolite. No other solid residues were generated in the zeolitization process. The lab-scale synthesis process resulted into three types of zeolites: NaP1, Sodalite (SOD), and Analcime (ANA), and led to reaction yields of 2.5 kg of zeolite per kg of waste. The preparation of the zeolites has mainly been designed by selecting temperature and alkalizing agent (NaOH) concentration. The optimal lab-scale synthesis conditions were:

- The NaP1 zeolite was obtained at 120 °C for 6 h, using 1 M NaOH and liquid/solid ratios of 15-25 mL/g, resulting in a Si/Al ratio of 1.85.
- The SOD zeolite was prepared at 120 °C for 6 h, using the highest alkali concentration (5 M NaOH) and a liquid/solid ratio of 25 mL/g, leading to a Si/Al ratio of 1.02.
- The ANA zeolite was synthesized at the highest temperature (200 °C) for 6 h, using 1 M NaOH and a liquid/solid ratio of 25 mL/g, resulting in a Si/Al ratio of 1.73.

The different zeolites (NaP1, SOD, and ANA) were also synthesized via lab-scale synthesis with mother liquor recycling, involving a decrease of the raw materials consumption.

The characterization of the obtained NaP1, SOD, and ANA zeolites revealed that the resulting zeolites showed characteristics and properties similar to those of zeolites prepared from both pure chemical reagents and other waste sources (fly ash, rice husk, kaolin, etc.). From an industrial point of view, NaP1 is the zeolite with most interest in water treatment applications due to its high CEC (2.73 meq NH₄⁺/g).

The scaling up of the synthesis of NaP1 with recycling of alkaline effluents (mother liquor and rinse water) was performed for the optimal conditions to assess the feasibility and reproducibility of the process. It also led to the complete conversion of the waste into highly crystalline zeolite, achieving high reaction yields (2.5 ton of zeolite per ton of waste). The bench-scale zeolitization process involved not only a reduction of the NaOH and water consumptions, but also a significant cost reduction. The resulting NaP1 zeolites obtained in the scaling up with alkaline effluents recycling showed high CEC (2.27-2.37 meq NH₄⁺/g) as well as structural, morphological, textural, and physical-chemical characteristics similar to those synthesized from fresh NaOH solutions.

The removal of Pb^{2+} , Cd^{2+} , and Hg^{2+} from aqueous solutions was studied, evaluating the effects of adsorption parameters on the single- and multi-cation adsorption process. The kinetic of single-cation adsorption process was found to be very rapid, achieving high removal efficiencies: 98.9, 93.3, and 99.3 % for Pb^{2+} , Cd^{2+} , and Hg^{2+} , respectively, in the first 15 min for zeolite doses of 0.5-5 g/L. The experimental maximum removal capacities of the zeolite were: 183.0, 4.37, and 0.23 mg/g for Pb^{2+} , Cd^{2+} , and Hg^{2+} , respectively. The metal cations could be removed by the zeolite through a homogeneous and physical adsorption process. The zeolite showed the greatest affinity for Pb^{2+} , due to its smallest size compared with Cd^{2+} and Hg^{2+} . The multi-cation removal efficiency of Pb^{2+} remained practically unchanged in presence of Hg^{2+} and Cd^{2+} , reaching high removal efficiencies (almost 100 %) both at very low contact times (1 min) and at longer times (30 min) for zeolite doses of 2-10 g/L.

The elimination of NH_4^+ from aqueous solutions was also performed using the zeolite obtained from the waste as adsorbent. The uptake NH_4^+ showed a fast kinetic, leading to removal percentages of 88 % in the first 15 min for a zeolite dose of 5 g/L. The experimental maximum removal capacity of the zeolite was 37.9 mg/g for NH_4^+ , similar to that found for other sorbent materials.

Finally, it can be concluded that the developed zeolitization process would enable to reduce the amount of aluminum waste, which is generally disposed of in secure deposits (involving high treatment cost), preserving natural resources and hence helping the sustainability of environment.

Accordingly, it implies a synergic effect on the environmental protection: firstly, the transformation of the hazardous aluminum waste into a zeolite can contribute to its *end-of-waste* condition, and secondly, the zeolite obtained from aluminum waste can be considered as a promising adsorbent used for the treatment of aqueous effluents contaminated by heavy metals (endocrine disruptors) and other inorganic compounds (ammonium).

LIST OF ABBREVIATIONS

AAS	Atomic Absorption Spectrometry	P1-X	Commercial Zeolite Type NaP1 and X
Alw	Aluminum Waste	PBU	Primary Building Unit
Alw_x	Aluminum Waste Representative Sample	PDF	Power Diffraction File
ANA	Analcime	PRTR	Registro Estatal de Emisiones y Fuentes Contaminantes
CBU	Composite Building Unit	PSD	Particle Size Distribution
CE	Conductivity	PZC	Point of Zero Charge
CEC	Cation-Exchange Capacity	q_e	Adsorption Capacity at Equilibrium
CLO	Cloverite	q_t	Adsorption Capacity at any time
CVAAS	Cold Vapor Atomic Absorption Spectroscopy	q_{max}	Maximum Adsorption Capacity
D_{hkl}	Crystallite size referred to Miller indexes	R²	Coefficient of Determination
DTA	Differential Thermal Analysis	RIR	Reference Intensity Ratio
E	Adsorption Energy	R_L	Separation Factor
EDS	Energy Dispersive Spectrometry	RW	Rinse Water
EWC	European Waste Catalogue	S_{BET}	Specific Surface Area
FA	Fly Ash	SBU	Secondary Building Unit
FAU	Faujasite	SDA	Structure Directing Agent
FD	Framework Density	SEM	Scanning Electron Microscopy
FTIR	Fourier Transform Infrared Spectroscopy	S_{EXT}	External Surface
FWHM	Full Width at Half Maximum	SOD	Sodalite
GIS	Gismondine	TCLP	Toxicity Characteristic Leaching Procedure
hkl	Miller Indexes	TG	Thermogravimetric Analysis
ICDD	International Centre for Diffraction Data	V_{meso}	Mesopore Volume
ICP-OES	Inductively Coupled Plasma Optical Emission Spectrometry	V_{micro}	Micropore Volume
IEP	Isoelectric Point	V_{total}	Total Pore Volume
I_{rel}	Relative Intensity	WFD	Waste Framework Directive
IZA	International Zeolite Association	XRD	X-Ray Diffraction
LCI	Life Cycle Inventory	XRF	X-ray Fluorescence
LOI	Loss of Ignition	ZSM-5	Zeolite Socony Mobil five
LTA	Linde Type A	ζ-potential	Zeta Potential
ML	Mother Liquor	μ-XRF	micro X-ray Fluorescence
MOR	Mordenite	ε	Polanyi Potential

Table of Contents

ABSTRACT	i
LIST OF ABBREVIATIONS	v
1. INTRODUCTION	1
1.1 Aluminum industry: environmental problems and wastes	3
1.2 Zeolites	8
1.2.1 Structure of zeolites	8
1.2.2 Synthesis of zeolites	11
1.2.2.1 Silicon and aluminum sources	12
1.2.2.2 Structure directing and mineralizing agents	13
1.2.3 Synthesis of zeolites from less-common sources	14
1.2.4 Sustainable zeolitization process	17
1.2.5 Applications of zeolites	18
1.3 Water pollution	19
1.3.1 Heavy metals	19
1.3.2 Ammonium.....	19
1.3.3 Water treatment technologies	20
1.3.3.1 Adsorption	21
1.3.4 Zeolites used as adsorbent materials	24
1.4 Motivation and objectives	25
2. MATERIALS AND METHODS	27
2.1 Materials	29
2.1.1 Hazardous aluminum waste.....	29
2.1.2 Reagents for the preparation of zeolites	30
2.2 Methods	31
2.2.1 Lab-scale synthesis of zeolites	31
2.2.1.1 Time	32
2.2.1.2 Temperature.....	33
2.2.1.3 Alkalizing agent concentration	33
2.2.1.4 Stirring.....	33
2.2.1.5 Liquid/solid ratio	33
2.2.2 Lab-scale synthesis of zeolites with alkaline effluent recycling	33
2.2.3 Bench-scale synthesis of zeolites	35
2.2.4 Recovery of zeolites after lab- and bench-scale synthesis	37
2.2.5 Analysis, identification, and characterization techniques	38

2.2.5.1 X-Ray Diffraction	39
2.2.5.2 Chemical characterization	40
2.2.5.3 Fourier transform infrared spectroscopy	41
2.2.5.4 Scanning electron microscopy	42
2.2.5.5 Thermal analysis	42
2.2.5.6 Textural characterization	42
2.2.6 Adsorption study	46
2.2.6.1 Adsorbent.....	46
2.2.6.2 Adsorbates	47
2.2.6.3 Ammonium adsorption procedure.....	48
2.2.6.4 Heavy metals adsorption procedure	50
2.2.6.5 Adsorption efficiency and adsorption capacity	52
2.2.6.6 Kinetic and isotherm modeling.....	52
3. RESULTS AND DISCUSSION.....	57
3.1 Waste characterization	59
3.1.1 Chemical characterization.....	59
3.1.2 Mineralogical characterization	64
3.1.3 Morphological characterization	65
3.1.4 Particle size distribution	68
3.1.5 Leaching behavior	70
3.2 Lab-scale synthesis of zeolites.....	74
3.2.1 Lab-scale synthesis of NaP1, SOD, and ANA zeolites	74
3.2.1.1 Effect of agitation.....	77
3.2.1.2 Effect of time	78
3.2.1.3 Effect of alkalizing agent concentration.....	82
3.2.1.4 Effect of temperature	85
3.2.1.5 Effect of liquid/solid ratio.....	88
3.2.2 Characterization of the zeolites from the waste	90
3.2.2.1 Morphological characterization	90
3.2.2.2 Structural characterization.....	96
3.2.2.3 Thermal behavior.....	99
3.2.2.4 Textural and physical-chemical characterization.....	107
3.2.3 Lab-scale synthesis with mother liquor recycling	113
3.2.3.1 Characterization of NaP1 obtained with recycling.....	114
3.2.3.2 Characterization of SOD and ANA obtained with recycling	120
3.2.4 Comparison of the synthesis conditions using other precursors	123
3.3 Bench-scale synthesis of NaP1 zeolite	126

3.3.1 Effect of effluents recycling	127
3.3.1.1 Crystalline and structural characterization	127
3.3.1.2 Chemical characterization	133
3.3.1.3 Morphological characterization	134
3.3.1.4 Thermal behavior.....	135
3.3.1.5 Textural characterization	139
3.3.1.6 Mother liquor characterization.....	147
3.3.2 Life cycle inventory of the zeolite synthesis	148
3.3.3 Feasibility of industrial-scale zeolitization process.....	150
3.4 Removal of heavy metals from aqueous solutions.....	152
3.4.1 Effect of pH	154
3.4.2 Effect of contact time: adsorption kinetic.....	159
3.4.3 Effect of adsorbent dose	164
3.4.4 Effect of initial adsorbate concentration: equilibrium isotherms	166
3.4.5 Competitive adsorption	170
3.4.6 Removal mechanism	171
3.4.7 Adsorption capacity of NaP1 compared with other adsorbents.....	174
3.5 Removal of ammonium from aqueous solutions	176
3.5.1 Effect of pH	177
3.5.2 Effect of contact time: Adsorption kinetic	179
3.5.3 Effect of adsorbent dose	182
3.5.4 Effect of initial adsorbate concentration: equilibrium isotherms	183
3.5.5 Adsorption capacity of NaP1 compared with other adsorbents.....	185
3.5.6 Removal mechanism	186
4. CONCLUSIONS.....	189
5. REFERENCES.....	195
6. ANNEXES	213
ANNEX I FRAMEWORKS OF ZEOLITES.....	215
ANNEX II PUBLICATIONS.....	219
ANNEX III CONGRESS AND AWARDS	223
ANNEX IV LIST OF TABLES	227
ANNEX V LIST OF FIGURES	231

1. INTRODUCTION

1.1 Aluminum industry: environmental problems and wastes

Aluminum is one of the most widely used metals in majority areas of everyday life (e.g., transport, manufacturing, packaging and construction) due to its remarkable properties (among others lightweight, strength, flexibility, resistance to corrosion, etc.). The world production of aluminum was about 63.4 million tons in 2017 and the global consumption of this metal is estimated to exceed 100 million tons in 2025 [1].

Aluminum production involves the following main stages: mining to extract the aluminum ore (bauxite), refining to recover alumina (Al_2O_3) obtained from bauxite via the Bayer process, and smelting to obtain aluminum.

This metal is obtained from bauxite in the primary industry, and from materials that have reached the end of their life (scraps) in the secondary industry [2].

The primary industry obtains aluminum by electrolytic reduction of alumina dissolved in a cryolite (Na_3AlF_6) bath, constituting an expensive activity due to its high energy and water consumption. It also involves a serious environmental threat due to its harmful emissions, including red mud (highly alkaline waste formed by iron), silicon and titanium oxides, alumina traces, and fluorides released to the atmosphere [3]. After the electrolytic process, the metal is refined to eliminate impurities such as sodium and calcium oxides, and hydrogen. This refining stage generates skimming, which is separated from the molten metal and recycled by the secondary industry [4].

Increased social awareness in recent years, driven by the environmental risks associated with the primary aluminum industry, has given rise to the importance of aluminum recycling. About 75 % of aluminum that has ever been manufactured is still in use today. This metal is easily recycled, keeping the same properties as new [5].

The secondary production of aluminum is carried out by recycling and melting scraps, dross, skimming, and by-products from the primary industry that contain this metal. Depending on the type and quality of these products, different melting technologies are employed, involving the use of salt fluxes (NaCl , KCl , etc.) that facilitate the recovery of the residual aluminum content. Unlike the primary production, the secondary industry requires substantially less energy consumption for aluminum production.

1. INTRODUCTION

Both the primary and secondary industries generate wastes, in particular slag or dross, which are recycled by the tertiary industry [6].

The tertiary aluminum industry recovers aluminum from slag or dross by means of shredding, milling, and sieving processes, and subsequent granulometric classification [7]. Because of these treatments, coarse and fine solid fractions are generated, which are separated according to their granulometry. The coarsest fraction from the tertiary industry is sold to other industries because of its rich-aluminum content. However, the finest fraction, captured by suction systems and treated in sleeve filters, is composed of fine solid powders with very small grain size and is not a marketable product due to its lower aluminum content [4].

In this work, this finest fraction, which represents the main waste from the tertiary industry, constitutes the aluminum waste used as a non-conventional raw material for the preparation of zeolites. To the best of our knowledge, no studies based on zeolites obtained from the Aluminum Waste (which will be referred as Alw hereinafter) have been reported in literature.

Alw is considered as hazardous waste due to its risk to the environment and to human health, according to the European Directive 2008/98/EC on waste (Waste Framework Directive, WFD) [8, 9]. The classification of the different types of hazardous wastes, including those from aluminum metallurgy, is done according to the European Waste Catalogue (EWC hereinafter) (Decision 2000/532/EC). In this EWC, Alw is identified by the six-digit code 100321 [10].

In Spain, the different treatments, including recovery and/or disposal operations, of hazardous wastes from industrial activities are regulated through the Spanish Register of Emissions and Pollutant Sources (i.e. PRTR-España) [11]. According to this register, the majority of hazardous wastes from aluminum metallurgy are represented by primary smelting slag (code 100304), salt slag from secondary smelting (code 100308), black dross from secondary smelting (code 100309), and other particulates and dust (including ball mill dust) containing hazardous substances (code 100321) [8, 10]. The most relevant industrial areas that conduct recovery and/or disposal treatments of hazardous aluminum wastes are mainly located in the north and centre of Spain, which are traditional metallurgical regions (Figure 1.1) [8]. The total amount of Alw, as well as the amount recovered by different recovery and/or disposal operations in Spain during the period 2010-2016, is shown in Figure 1.2.

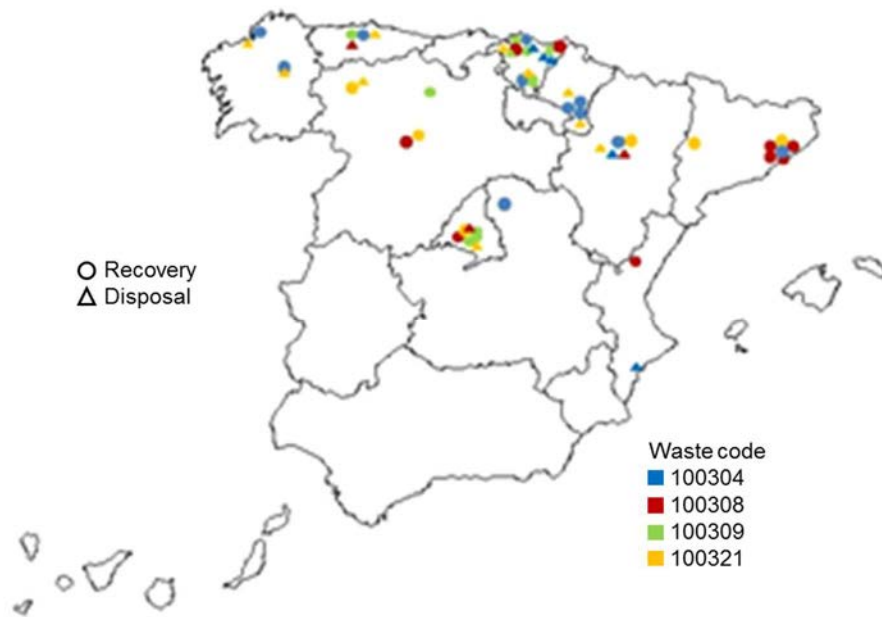


Figure 1.1 Main Spanish industrial areas dedicated to the recovery and/or disposal of aluminum wastes.(Adapted from Galindo et al. [8]).

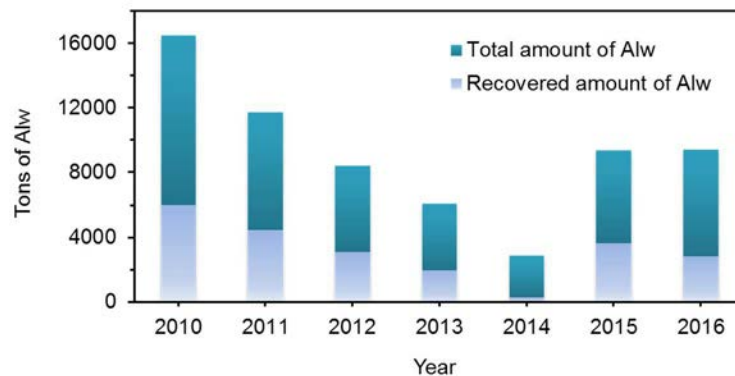


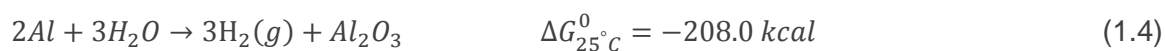
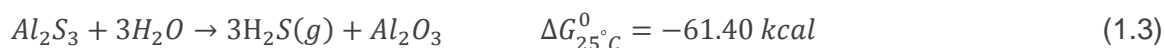
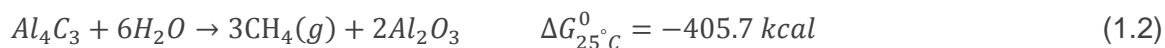
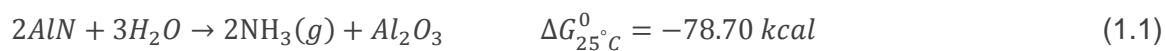
Figure 1.2 Total and recovered amount of hazardous aluminum waste (Alw) from the Spanish tertiary industry during the period 2010-2016 (European Waste Catalogue code: 100321).

In general, the total amount of Alw generated in 2010-2016 evolved accordingly to the national production and demand of aluminum. During the same period, the recovery rate of Alw fluctuated between 58 and 43 %, probably due to the type of recovery treatment employed by the different aluminum sectors. In this context, even though Alw generated by the Spanish tertiary industry is partially recovered, an important amount of it still remains as a waste and is generally disposed into secure landfills [8].

The main negative impacts of Alw come from its very fine grain size (particle size distribution $< 100 \mu\text{m}$) and its heterogeneous chemical and mineralogical composition

1. INTRODUCTION

containing harmful substances such as metallic aluminum, aluminum nitride, aluminum carbide, aluminum sulphide, and heavy metals [8]. Additionally, Alw can react with water or humidity generating certain toxic gases, such as ammonia, methane and hydrogen sulfide, and/or inflammable and explosive gases like hydrogen, according to the following reactions [12]:



According to the regulation on the properties of wastes which render them hazardous [10], Alw may be considered as “highly flammable” (H3-A: “*substances and preparations which, in contact with water or damp air, evolve highly flammable gases in dangerous quantities*”), and even “harmful”: (H5: “*substances and preparations which, if they are inhaled or ingested or if they penetrate the skin, may involve limited health risks*”). As its spontaneous and exothermic reactivity in contact with humidity leads to generate certain toxic gases, Alw may be also defined as H12: “*substances or preparations which release toxic gases in contact with water, air or an acid*”. Alw also presents traces of heavy metals (e.g., copper, zirconium, manganese, lead, or chromium), which are easily leachable elements under incorrect management. Thus, Alw may be also classified as “leachable” (H13: “*substances and preparations capable by any means, after disposal, of yielding another substance, e.g. a leachate*”). Therefore, the inadequate accumulation and disposal of Alw can lead to soil degradation and even to groundwater contamination due to the potential leaching of its harmful elements.

The quantity of Alw generated, its granulometry, and chemical and mineralogical composition varies not only depending on the type and quality of treated scrap, but also according to the classification and collection methods used in the industrial sectors [8]. The estimated amount of Alw is 13 kg per ton of treated scrap, involving a global production of around 300,000-500,000 ton [4]. A proper management of Alw by an authorized waste manager would correspond to approximately 109 € per ton of waste, which would imply a high economic cost.

Political initiatives, based on the *Zero Waste* concept, aim to minimize the negative effects of the generation and management of waste on human health and the environment, as well as to reduce the use of resources. In this sense, the WFD establishes the following hierarchy for waste prevention and management: prevention, preparing for re-use, recycling, another type of recovery (e.g., energy recovery), and lastly, disposal of waste in landfill or secure sites (Figure 1.3) [9].

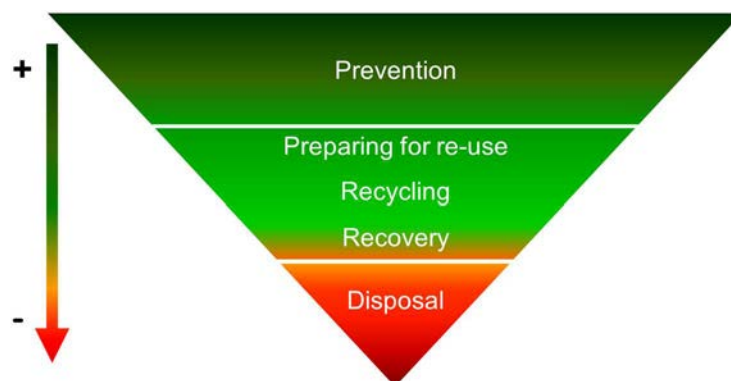


Figure 1.3 Waste prevention and management according to the Waste Framework Directive (WFD) [9].

The content of aluminum (as oxide) in Alw represents about 53-81% in weight, being still potentially valuable [8]. Hence, Alw may be used as a “secondary” raw material for the production of added-value materials.

For example, in prior studies it was successfully developed the conversion of Alw into aluminas and Mg–Al hydrotalcites by extracting the soluble aluminum compounds via acid hydrolysis of the waste and then precipitation of the products using alkalinizing/aging processes [13-15]. However, in those processes only a small fraction of the total aluminum content in Alw was recovered, and a cake which included the non-soluble fractions of Al, Si, and other compounds remained as an inert solid waste.

In the work of the present Thesis, the complete transformation of Alw into zeolites has been envisaged as one of the best ways to recover this waste. In addition, added-value materials like zeolites can be easily obtained by developing a simple one-step hydrothermal synthesis process (described in Chapter 2), and no other solid residues are generated. The developed zeolitization process would enable to reduce the amount of this type of wastes, which are generally disposed of in secure deposits and to preserve natural resources, hence helping the sustainability of environment [16, 17].

1. INTRODUCTION

1.2 Zeolites

Zeolites are crystalline solid materials that present regular porous structure frameworks. The term zeolite was originally described by Axel Fredrik Cronstedt in 1756, who observed that the heating of a natural zeolite (stilbite) resulted in the release of water, which had previously been adsorbed. This particular feature is why such type of materials was called zeolites, based on the Greek words *Zeo* (boiling) and *Lithos* (stone) [18]. These materials occur naturally from volcanic rocks or sedimentary deposits of the earth but can be also synthesized [19]. Natural zeolites (e.g., clinoptilolite, analcime, chabacite, etc.) generally present lower purity than synthetic zeolites due to their compositions containing other minerals, metals, or quartz.

According to the Structure Commission of the International Zeolite Association (IZA), 235 zeolite framework types have been identified, and over 40 natural zeolites were found in 2017. Each zeolite framework type has assigned a three-letter code (e.g., GIS for the gismondine framework) that generally derives from the name of the material type [20]. Some examples of zeolite frameworks are shown in Figure 1.4. The structural characteristics of the main zeolites obtained from Alw are included in Annex I.

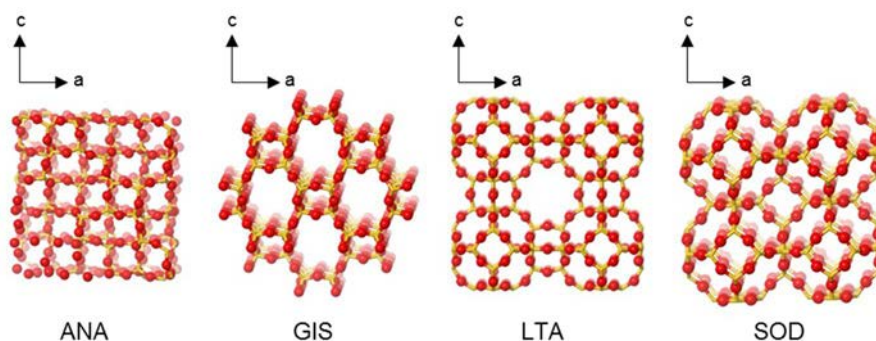


Figure 1.4 Examples of zeolite frameworks: ANA (analcime), GIS (gismondine), LTA (Linde type A), and SOD (sodalite). (Adapted from reference [20]).

1.2.1 Structure of zeolites

Structurally, both natural and synthetic zeolites are characterized by frameworks made up of Primary Building Units (PBUs) of tetrahedra TO_4 (T-atoms = Si, Al, P, Ge, Ti, etc.), as shown in Figure 1.5a. The PBUs are connected through their oxygen atoms in different ways, resulting in a variety of structures that can contain cages, channels, and

cavities [19]. Zeolite frameworks can be thought of as consisting of finite or infinite (chain- or layer-like) component units, where the PBUs are connected together in different ways forming Secondary Building Units (SBUs). The SBUs are defined by the number of T-atoms forming ring-type units that can contain up to 16 T-atoms. Some examples of these units are the single-4-rings and double-4-rings. The arrangement of SBUs leads to more complex polyhedral units, known as Composite Building Units (CBUs), which are some characteristic units in zeolite framework. Thus, different types of zeolite frameworks are built through the same CBUs including cage-type units (Figure 1.5b). For example, sodalite (SOD) and zeolite A (LTA) structures are obtained from the same CBU, sodalite cage, which is a truncated octahedron defined by six 4-rings and eight 6-rings [20] (Figure 1.5c).

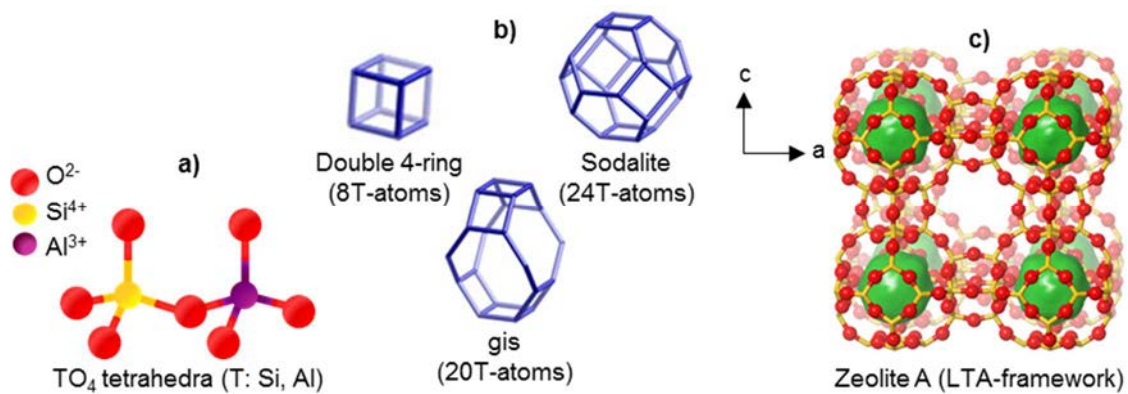


Figure 1.5 a) PBU of zeolites; b) Examples of some CBU; c) LTA-framework formed by sodalite cages represented in green. (Adapted from reference [20]).

In the aluminosilicate-type zeolites, the isomorphous substitution of Si⁴⁺ by Al³⁺ in the tetrahedral units leads to formation of negatively charged structures that are balanced by the introduction of extra-framework cations or counter cations (e.g., Na⁺, K⁺, Ca²⁺). Figure 1.6 shows as an example the structure of an aluminosilicate-type zeolite, in particular NaP1, in which Na⁺ is the main extra-framework cation.

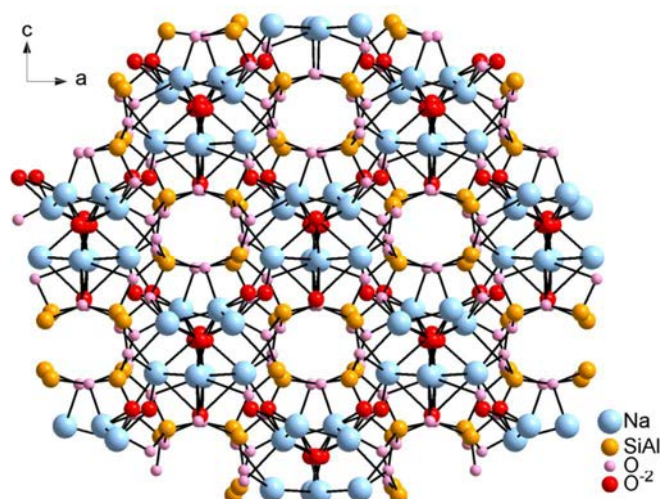
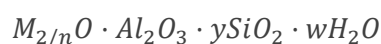


Figure 1.6 NaP1 zeolite (GIS-type framework).

Aluminosilicate zeolites can be described by the following general formula [21]:



where M is a metal cation of valence n, y is a parameter ranging between 2-200 and w is the content of water present in the zeolite structure.

The classification of zeolites can be established according to their Si/Al ratio. In this sense, the type of structure obeys the Löwenstein's rule, which establishes that Al-O-Al linkages are avoided. This is due to the energetic impediment caused by repulsions of charge between two tetrahedral AlO_4 . Following this rule, the limit of composition of a zeolite would be $Si/Al \geq 1$ [22].

Many of the unique properties of zeolites, such as their sorption, molecular sieve, and ion exchange capacities are explained by their structure, in particular, by the presence of their voids or channels that allow the sorption and diffusion of diverse ions and molecules [19]. The channel system of zeolites are delimited by rings formed by T-atoms, and can be one-, two- or three-dimensional leading to interconnected systems or without direct access from one channel system to the other [20]. Figure 1.7 shows some examples of channel systems. The pore sizes of zeolites depends on the size of their rings (i.e., the number of T-atoms that define the pore opening), resulting in small, medium, large, and extra-large pores [22], as shown Table 1.1.

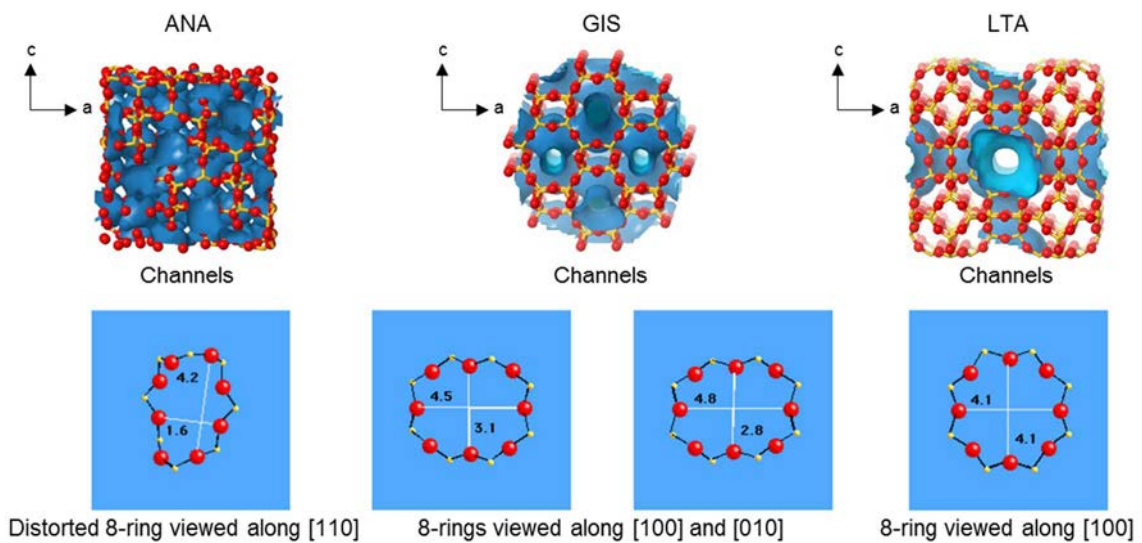


Figure 1.7 Channel systems (represented in blue) and ring sizes (dimensions expressed in Å) of the ANA, GIS, and LTA zeolites. (Adapted from reference [20]).

Table 1.1 Classification of zeolites according to their pore sizes and openings. (Adapted from reference [22]).

Pore size	Pore opening	Pore diameter (Å)	Example of zeolites
Small	8-member ring	4	ANA, GIS, LTA, SOD
Medium	10-member ring	5.5	ZSM-5 (MFI-type framework)
Large	12-member ring	7.5	FAU, MOR
Extra-large	>12-member ring	> 8	CLO, UTL

The number of tetrahedrally coordinated T-atoms per nm^3 , which constitutes the Framework Density (FD) related to the pore volume, ranges approximately from 12 to 21. For example, the SOD and ANA frameworks present FD values of 16.7 and 19.2 T/nm^3 , respectively. Some of the more flexible zeolite structures, such as gismondine (GIS-framework with $\text{FD} = 16.4 \text{ T}/\text{nm}^3$), can present variable FD values. Thus, the flexibility of a framework structure is, to some extent, associated with the possible FD variation [20].

1.2.2 Synthesis of zeolites

Traditionally, the chemistry of zeolites is based on hydrothermal and solvothermal synthesis routes for the preparation and modification of such materials [23, 24]. Nowadays, both the conventional hydrothermal synthesis and other non-conventional methods such as microwave radiation and ultrasound energy have been described in the

1. INTRODUCTION

literature for preparing a wide variety of zeolites. Depending on factors such as the type of precursors (mainly, aluminum and silicon sources), physical-chemical pre-treatment of such precursors, synthesis conditions (e.g., temperature, pressure, time, etc.), and post-synthesis treatment (e.g., calcination, cation exchange, etc.), diverse zeolites can be obtained. In general, the preparation of zeolites can involve a previous activation step by adding and simultaneously stirring of precursors and alkalizing agents (e.g., NaOH, KOH, etc.). Then, the conventional hydrothermal synthesis is carried out at temperatures between 25 and 300 °C and under autogenous pressure or high-pressure conditions for several hours or days to improve the crystallinity of the resulting products.

Depending on the synthesis conditions (e.g., temperature, time, etc.) and on the raw materials used to obtain zeolites, different reaction mechanisms have been proposed in the literature. Thus, during the process of obtaining zeolites, where numerous species soluble in an amorphous and crystalline phase are present, these mechanisms can include reactions of dissolution, polymerization, depolymerization, condensation, precipitation, and crystallization [25]. Therefore, the synthesis of zeolites is significantly susceptible to the modification of any parameter (agitation, temperature, concentration of reactants, etc.) which may cause changes in the resulting products.

1.2.2.1 Silicon and aluminum sources

The preparation of aluminosilicate-type zeolites is based on the $\text{Na}_2\text{O}-\text{Al}_2\text{O}_3-\text{SiO}_2-\text{H}_2\text{O}$ system under basic or strongly basic conditions. For the synthesis of this type of zeolites, a great variety of commercial chemical reagents can be used, including silicon (aqueous sodium silicate or water glass, silica gel, fumed silica, etc.) and aluminum (sodium aluminate, boehmite, aluminum hydroxide, aluminum nitrate, etc.) sources.

Silicate solutions containing alkali metals like sodium or potassium are the most commonly used silicon sources for the preparation of zeolites. The dissolution of silicon and aluminum precursors greatly depends on the pH of the reaction medium. Thus, alkaline media (pH > 10) employed for the synthesis of zeolites generally favor the dissolution of aluminosilicate precursors [26]. Under strong basic conditions, silicon species are presented as polymerized-state polysilicate anions like $[\text{Si}(\text{OH})_2\text{O}]$, while aluminum species are present as $\text{Al}(\text{OH})_4^-$ (main form of aluminate in basic solution).

Likewise, the crystallized zeolitic phases greatly depend on the type of silicon source, since its variation (including its textural and chemical properties) can modify the nucleation and crystal growth of zeolites [22].

1.2.2.2 Structure directing and mineralizing agents

In addition to the main used precursors (i.e., Si and Al sources), different inorganic and organic compounds, including their corresponding cations and anions, are also utilized for the zeolite synthesis. Thus, guest molecules and ions, such as organic compounds (usually quaternary ammonium cations or amines) and/or inorganic salts (NaCl, NaOH, KOH, etc.), are usually added to the reaction media to obtain diverse types of zeolites. The nature and size of these compounds present a great influence on the production of zeolites.

The role of these organic or inorganic compounds, usually known as “templates” or “Structure Directing Agents” (SDAs), is very important because of their charge-balancing, templating or structure-directing effects on the resulting zeolitic products [22, 27].

Compounds containing alkali-metal cations (e.g., NaOH, NaCl), also known as alkalizing agents, stabilize aluminosilicate ions via static electric and steric interactions, playing a remarkable structure-directing role. They also determine their solubility regulating the concentration of aluminum in solution [28] and accordingly helping the pH adjustment of the process [22]. For example, some works have reported that the addition of alkali-metal cations like Na^+ in the reaction medium accelerate the crystallization and facilitate the condensation or rearrangement of the structural units of zeolites [29]. The addition of cations, such as K^+ and/or Na^+ , to the $\text{Na}_2\text{O}-\text{Al}_2\text{O}_3-\text{SiO}_2-\text{H}_2\text{O}$ system may modify the type and structure of zeolite obtained. It could be related to the different templating effect of K^+ compared to the extra-framework Na^+ cation in aluminosilicates zeolites [22]. On other hand, the activation of some precursors of zeolites by the use of KOH solutions could be less effective than with the use of NaOH [30].

Unlike spherical inorganic cations such as Na^+ , diverse organic molecules (e.g., amines) used as SDAs possess more complex shapes and bigger sizes, and are usually employed to tailor the porosity and to obtain high-silica zeolites. After the synthesis of zeolites from organic SDAs, these are usually calcined ($> 400\text{ }^\circ\text{C}$) to remove the contents of SDA, which could block the pores of the resulting materials.

1. INTRODUCTION

In the preparation of zeolites, species like OH^- or F^- anions, known as “mineralizing” agents or “mineralizers”, are also present in the reaction medium. The term mineralizing agent usually describes a source of anions such as OH^- or F^- (e.g., NaOH, HF) with a catalytic role. In this sense, a mineralizing agent or mineralizer converts the starting materials into mobile species and facilitates the breaking and formation of Si-O-Al bonds [25]. The addition of F^- anions through the known fluoride route is employed for the synthesis of all-silica zeolites [31], while the OH^- anion is widely used for the preparation of zeolites with a low Si/Al ratio (e.g., NaP1, ANA).

The basis of laboratory scale experiments is generally applied for industrial production of zeolites. For example, the industrial-scale production of zeolite A (LTA-type framework) is realized via a hydrogel route using water glass and sodium aluminate in aqueous solution. Firstly, an amorphous sodium aluminum silicate is produced, and then crystallized hydrothermally under mild temperature conditions. Finally, after the synthesis process, a powder (i.e., the zeolite) and slurry are obtained and separated by a filtration system [32].

1.2.3 Synthesis of zeolites from less-common sources

In the last years, the use of waste-type precursors for the preparation of zeolites has been increasing, driven by the need to minimize the waste disposal into landfills and to address associated environmental impacts. Among such wastes, fly ash [19, 33, 34] or bottom ash [35], rice husk ash [36], ferrochromium slag [37], steel slag [38], aluminum dross [39], natural clinker [40], etc. have widely been used for the synthesis of different zeolites such as NaP1, SOD, CAN, ANA, Linde F, zeolites A and X, etc.

Fly Ash (FA) from coal combustion plants is one of the most widely wastes used to obtain zeolites or related materials. The production of electricity from coal combustion originates different type of ash, mainly FA, which are considered as industrial wastes. FA consists mainly of spherical vitreous particles (0.2-500 μm) originated in the electrostatic or mechanical precipitation of the dust in suspension present in gases from the coal combustion. The chemical and mineralogical composition of FA can vary depending on the type of coal source. Thus, its major components are usually silica (SiO_2), alumina (Al_2O_3), lime (CaO), and iron oxides. In addition, other minor components, such as SO_3 , alkaline oxides (MgO , Na_2O , K_2O , etc.), and heavy metals (Cr, Pb, Ni, V, As, Mo, etc.), are also present in FA.

In the early 80's, Höller and Wirsching [41] were the pioneers in the synthesis of zeolites from FA because of their similar chemical composition to certain volcanic rocks. Since then, numerous works were developed on the preparation of zeolites from FA and from other waste-type sources.

For instance, Querol et al. [30, 42] and co-workers [26, 43] carried out the hydrothermal alkaline conversion of different FAs into several zeolites (NaP1, zeolite A, SOD, ANA, etc.). The authors studied the characteristics of the resulting products in function of the variation of diverse synthesis parameters. Thus, the type (KOH and NaOH) and concentration (0.1-5 M) of alkaline activation agent, the temperature (60-200 °C) and pressure (~ 5-15 atm) conditions, the time (3-100 h), and the liquid/solid ratio (2-18 mL/g) were evaluated. Maximum conversion efficiencies were achieved using NaOH and a combination of NaOH and KOH solutions. However, the activation of FA with KOH seemed to be less effective. Franus et al. [44] also obtained hydrothermally various Na-type zeolites (NaX, NaP1, and SOD) from FA using 3-5 M NaOH solutions at 75-95 °C for 24 h.

Depending on the type of waste material different treatments, including long aging (about ≥ 1 day), calcination or fusion (600-900 °C), and/or acid treatment (using HCl, H₂SO₄, etc.) can be necessary. These treatments generally improve the reactivity of waste (e.g., rice hush, kaolin, electrolytic manganese residue, etc.) [19, 36, 45-50] used as a "secondary raw material" to obtain zeolites.

For example, Hollman et al. [51] carried out a two-step synthesis to obtain NaP1 and zeolites type A and X from FA. In a first step, an alkaline synthesis (90 °C for 6 h) was performed to obtain a FA residue and a high-Si filtrate. The Si/Al molar ratio of the high-Si filtrate was adjusted by adding an aluminate solution and then heated another 48 h at 90 °C to obtain pure zeolites from the residue as well as a new filtrate. In a second step, the FA residue obtained in the first synthesis of 6 h is mixed with the new filtrate and heated again for 24 h at 90 °C to obtain high FA content zeolites. The results led to 50, 75, and 85 g of zeolites NaP1, zeolite X, and zeolite A, respectively, per kg of FA. Atta et al. [36] synthesized trapezohedral ANA from a mixture of rice husk ash and metakaolin as silica and alumina sources, and NaOH solution ($\text{Na}_2\text{O}/\text{Al}_2\text{O}_3 = 2.6$). Before the synthesis, the rice husk and the kaolin were calcined at 800 and 900 °C, respectively, for 3 h. After calcination, the resulting metakaolin was dissolved in 4 M NaOH followed by refluxing at 90 °C. They carried out an aging step (3 days) followed by a hydrothermal process at 180 °C for 24 h. Bohra et al. [45] also reported the use of rice husk ash

1. INTRODUCTION

(obtained by calcination at 700 °C for 6 h), aluminum foil, and a NaOH solution ($\text{Na}_2\text{O}/\text{Al}_2\text{O}_3 = 2.1$) to obtain zeolites type A and P. They carried out a stirring process of 15 h, followed by a hydrothermal heating at 100 °C of 15 h for zeolite A, and of 72 h for zeolite P.

One of the main drawbacks when working with wastes like FA is some of its phases, among others mullite ($3\text{Al}_2\text{O}_3 \cdot 2\text{SiO}_2$) or quartz (SiO_2), which could be resistant to alkaline treatments. Reutilization of silica-rich precursors with very low alumina contents, such as FA [19, 52], rice husk ash [53, 54], or kaolin-type precursors [55], generally involve heating pre-treatments of these wastes at high temperature to induce their conversion to more reactive products. For example, using FA leads to resulting products with contents of zeolite that can vary between 20 and 65 % depending on the properties of the treated ash and the conditions used to obtain zeolites [26]. The content of the mentioned phases in the resulting zeolitic products are usually decreased after long activation times (24-100 h). There are also other alternatives that can decrease these phases by increasing the temperature or alkaline agent concentration, which would favor the conversion of FA into more pure zeolites for shorter reaction times (15-24 h) [30].

The background on the use of wastes from the aluminum industry to synthesize zeolites is scarce. For example, Dufour et al. [56, 57] obtained zeolites type A and X using alkaline residues from the anodized aluminum industry and commercial sodium hydroxide solutions. The authors studied the effect of the reaction mixture composition, temperature (70-125 °C), and time (3-24 h) on the crystallinity of the products to optimize the process. Belviso et al. [58] used different reaction mixtures of wastes formed by FA and red mud from alumina production to obtain zeolites. The mixtures of both wastes were fused at 600 °C with NaOH/H₂O, and then were incubated at different temperatures (25-40 °C) for 4 days. Depending on the red mud amounts (20-80 %) used in the synthesis, zeolites type A and X and mixtures of both were obtained.

The research group, in which the present work was developed, has great experience in the characterization, re-use, and conversion of aluminum wastes from the secondary and tertiary industries into different valuable materials, such as boehmite, aluminates, glasses, glass-ceramics, and hydrotalcites [4, 6, 8, 15].

In this sense, the aluminum waste (Alw) from the tertiary industry could also be utilized as a “secondary raw material” for the preparation of zeolites.

1.2.4 Sustainable zeolitization process

Synthesis of zeolites processes, both from pure chemical reagents and from waste-type sources, lead to the generation of a solid cake (i.e., the zeolite-type material) and an alkaline effluent or Mother Liquor (ML). This latter may be susceptible to be recycled in order to reduce the water and other reagent consumptions (e.g., NaOH). Additionally, the recycling of ML could also reduce the environmental impacts associated to synthesis processes.

The re-use and recycling of ML produced in the synthesis of zeolites has scarcely been aimed in the literature [51, 59-62]. ML is usually a strongly alkaline solution that can contain valuable elements such as Si, Al and Na, which are the main constituents of aluminosilicate-type zeolites. Although the literature on synthesis of zeolites through the more environmentally sustainable processes has continuously been expanded, only a few studies address issues related to the treatment of MLs, which are usually discarded. For instance, Lin et al. [63] utilized ML to obtain zeolites FAU and LTA from a lithium slag by the traditional hydrothermal method. The use of ML for the preparation of the zeolites showed a great influence on their structures, leading to excellent adsorption calcium and magnesium capacities.

In addition to the generation of ML, other effluents such as Rinse Water (RW) from the cleaning step for the removal of soluble species after the separation of ML and the zeolitic cake are also produced in zeolitization processes. For example, Behin et al. [64] reported a synthesis process of zeolite P from FA under recycling of the effluents from filtration and washing steps. The quality of the resulting products was not modified with the recycling process.

Recycling and reutilization of ML and RW into the synthesis of zeolites could actually be one potential solution to treat such liquid wastes. Indeed, these effluents, in most cases, contain surplus reactants, such as inorganic elements (Si, Al, Ti, Na, etc.) and/or highly toxic organic compounds from SDAs that can be fed again to the synthesis process, thus minimizing the liquid discharge.

1. INTRODUCTION

In this thesis, the feasibility of producing Na-type zeolites from Alw by a zero-waste hydrothermal zeolitization process is performed. The recycling of the effluents (ML and RW) is realized and its influence on the resulting zeolitic products is studied in detail.

The development of a more sustainable synthesis process aims:

- To minimize the consumptions of raw materials and the amount of residual effluents to be treated.
- To reduce the costs associated to the process.
- To minimize the impacts of the process on environment.

1.2.5 Applications of zeolites

Due to the unique properties of zeolites, such as molecular sieve and sorption and ion exchange capacity, these materials are widely used in diverse industrial applications such as water treatment [65-67], catalysis [68], detergents builders [69], gas separation [70], membranes [71, 72], drying processes incorporated into dishwashers [73, 74], etc.

In this work, the zeolites obtained from Alw exhibit appropriate characteristics and properties that make them potential candidates for the removal of different substances such as heavy metals and other inorganic elements like ammonium from waters. Thus, the main application studied for the zeolites synthesized from Alw is focused on the treatment of aqueous effluents contaminated with harmful elements.

1.3 Water pollution

Great efforts are being made to achieve the prevention and reduction of environmental concerns, like water pollution, associated with the rapid global industrialization. Water pollution represents a threat to the aquatic organisms and to the health of human beings. Adequate identification and appropriate management are essential to control anthropogenic emissions of contaminants, such as heavy metals and ammonium, into waters. In this context, different water treatment technologies as well as the use of different sorbent materials to eliminate or reduce harmful substances have been proposed.

1.3.1 Heavy metals

Among the most common pollutants present in aquatic media, heavy metals such as mercury, lead, and cadmium are considered endocrine disruptors due to their bioaccumulation in organisms causing serious health disorders, among others in the endocrine, nervous, and immune systems. Mercury is principally released from different activities, such as battery, thermometer, and chlor-alkali production, paint and color industry, coal combustion, and waste incineration [75, 76]. Anthropogenic sources such as gasoline and water distribution systems like lead-containing pipes contribute to the release of lead [75]. Cadmium is released to industrial effluents from the steel electroplating and nickel-cadmium batteries manufacture [77].

The Directive 2013/39/EU concerning the priority substances in the field of water establishes maximum allowable concentrations in inland surface waters of 0.07 µg/L for mercury, 14 µg/L for lead, and, depending on the hardness of the water, 0.45-1.5 µg/L for cadmium [78].

1.3.2 Ammonium

Excess nitrogen compounds like ammonium (NH_4^+) can cause eutrophication, depriving of oxygen to aquatic organisms in lakes and rivers. In addition, the NH_4^+ ionized form moves much more slowly than other nitrogen compounds, thus persisting in groundwater for long periods of time after it enters the subsurface [79]. Diverse anthropogenic

1. INTRODUCTION

activities, including fossil-fuel combustion, septic systems, sewage sludge, landfill leachate, and agricultural practices (chemical fertilizers or animal manures), can cause an increase of the amount of NH_4^+ in waters [80-82]. Ammonium is also one of the soluble nitrogen species found in airborne particulate matter in urban areas, representing up to approximately 23 % [83].

The Spanish legislation (Real Decreto 817/2015) [84] on the quality of water establishes concentrations of NH_4^+ ranged between 0.2 and 1 mg/L as acceptable limits. However, higher NH_4^+ concentrations can be found in surface waters, generally, exceeding the limits established by water quality standards [85].

1.3.3 Water treatment technologies

Developing more cost effective wastewater treatment techniques by using low-cost sorbents and/or easily handled materials contributes to the environmental sustainability. Various technologies for the treatment of wastewaters have been developed, including electrochemical treatment [86], chemical precipitation [87], adsorption [67], ion exchange [88], advanced oxidation [89], etc. Nowadays, it is very common to use a combination of several techniques to eliminate or minimize the amounts of diverse contaminants present in water.

Table 1.2 shows some technologies used for the treatment of water contaminated with inorganic and/or organic compounds as well as their main advantages and disadvantages. For example, chemical precipitation is widely used, although it usually requires large amounts of chemicals (to pH adjustment) leading to sludge production that needs to be treated, thus increasing process costs and environmental impacts [90].

Although there is no technique that provides the complete removal of all the contaminants from water, adsorption offers several advantages over other techniques, thereby being widely used in many wastewater treatment plants. Adsorption is a simple, efficient, and relatively economic technique to remove different contaminants from waters, including heavy metals and ammonium [19, 91]. It also offers a very versatile design and allows the use of a wide range of sorbents like zeolites. Additionally, diverse types of adsorbent materials, including activated carbons, zeolites, or clays, can be used to remove different contaminants from waters.

Table 1.2 Water treatment technologies. (Adapted from references [92, 93]).

Technology	Contaminant	Advantages	Disadvantages
Precipitation	Inorganic Organic	<ul style="list-style-type: none"> ▪ High efficiency to remove metals and organic compounds ▪ Simple operation 	<ul style="list-style-type: none"> ▪ pH-dependent efficiency ▪ Temperature-dependent efficiency ▪ Sludge generation ▪ Extra operational cost for sludge disposal
Coagulation Flocculation	Suspended solids	<ul style="list-style-type: none"> ▪ Shorter time to settle out suspended solids 	<ul style="list-style-type: none"> ▪ Sludge generation ▪ Extra operational cost for sludge disposal
Filtration	Suspended solids Inorganic Organic	<ul style="list-style-type: none"> ▪ High efficiency ▪ Small space requirement 	<ul style="list-style-type: none"> ▪ High capital
Advanced oxidation	Organic	<ul style="list-style-type: none"> ▪ Organic contaminants are oxidized to CO₂ 	<ul style="list-style-type: none"> ▪ Expensive technique
Ion exchange	Inorganic Organic	<ul style="list-style-type: none"> ▪ High efficiency ▪ Low energy content ▪ No sludge formation 	<ul style="list-style-type: none"> ▪ Expensive ▪ Pre-treatment of water is sometimes required
Adsorption	Inorganic Organic	<ul style="list-style-type: none"> ▪ Low cost technique ▪ Simple operation ▪ Different types of adsorbents (activated carbon, zeolites, clays, etc.) can be used 	<ul style="list-style-type: none"> ▪ Efficiency depends on several factors (pH, temperature, concentration, etc.) ▪ Adsorbent regeneration

Ion exchange can be considered as an adsorption process based on the replacement of ions (cations or anions) in a liquid solution by other ions of the same charge present in a solid material. The solid material (adsorbent) also contains immobile and permanently bound ions of the opposite charge. However, unlike adsorption, ion exchange occurs when one ion (for example Ca²⁺) is exchangeable for other ion (for example Na⁺) with the same charge that is derived from an adsorbent material. The exchange process is governed by a reversible chemical reaction [94], as shown below:



1.3.3.1 Adsorption

Adsorption is a process of separation/concentration of one or more components (known as adsorbates) present in a fluid phase (liquid or gas) on the surface of an insoluble solid phase (adsorbent). The process of adsorption can take place on the external surface

1. INTRODUCTION

and/or internal surface of the adsorbent when the adsorbates penetrate into the interior of the adsorbent pores [94].

The transport processes during the adsorption in solid-liquid systems are commonly characterized by four steps (Figure 1.8) [94, 95]:

External (interphase) mass transfer of the adsorbate from the bulk fluid by convection, through a thin film or boundary layer, to the outer, solid surface of the adsorbent. This step usually occurs quickly.

Internal (intraparticle) mass transfer where the adsorbate is transported from the bulk liquid phase to the active sites on the adsorbent external surface (solid phase), taking place slowly.

Surface diffusion along the porous surface where the adsorbate diffuses slowly from the exterior of the adsorbent to the most internal surface (pores) of the adsorbent.

Adsorption of the adsorbate onto the porous surface. The adsorptive attachment takes place quickly.

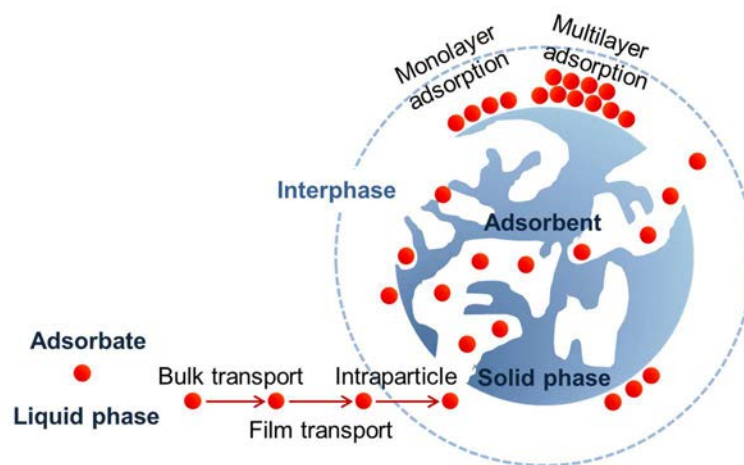


Figure 1.8 Steps that can take place during adsorption between an adsorbate and adsorbent (Adapted from Tran et al. [96]).

Adsorption of contaminants from waters using sorbent materials depends on the following factors, as shown in Figure 1.9:

- The nature and characteristics of the adsorbent.
- Type and amount of the adsorbate.
- The different operating conditions (pH, temperature, time, etc.).

The effects of the different factors on the adsorption process result in different interactions between the solid surface of the adsorbent material and the adsorbed solute. Thus, the process can be characterized by physical adsorption (interaction by van der Waals forces) or chemisorption (stronger interaction through covalent or ionic bonds). Physical adsorption or physisorption is a fast, reversible, and mono or multilayer process characterized by a weak enthalpy. On the other hand, chemisorption, which requires greater binding energies, is usually a slower and non-reversible process involving the formation of monolayer [97]. In general, it is very difficult to distinguish between both types of adsorption.

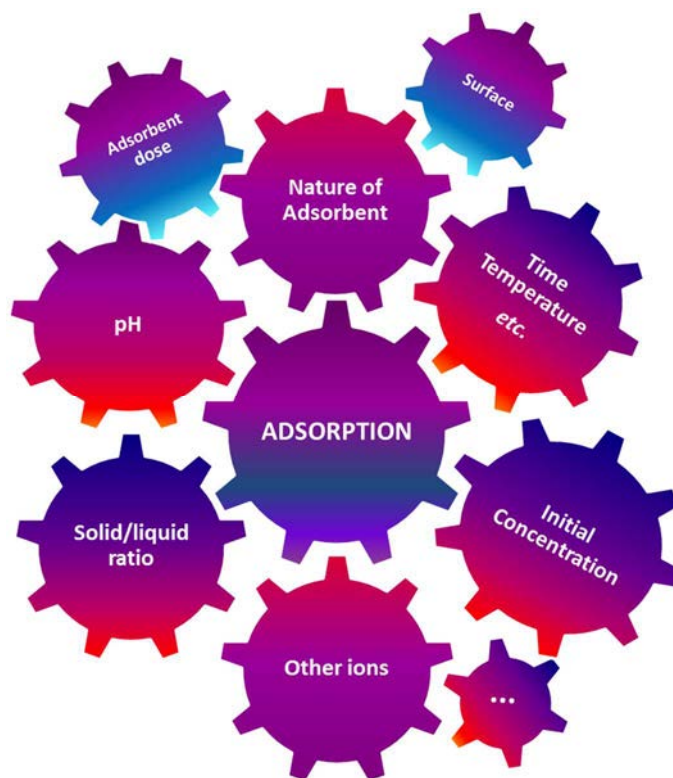


Figure 1.9 Main parameters that influence the adsorption processes.

Traditionally, activated carbons have widely been used as sorbents for the uptake of diverse compounds, specifically organic molecules, from waters. However, such materials must previously be treated by activation methods, which imply high operating temperatures to enhance their porosity and specific surface area [98]. During the last two decades, other potential sorbents like zeolites have also been utilized for the removal of different contaminants, including organic and inorganic contaminants [99]. Unlike the activated carbons, zeolites can be obtained by means of mild synthesis conditions representing a more economically viable alternative. Thus, zeolites can be considered as low-cost sorbents.

1. INTRODUCTION

1.3.4 Zeolites used as adsorbent materials

Zeolites synthesized from different waste sources like FA have widely been studied and used to adsorb heavy metals [100-102] and ammonium [103-106] in waters. Some of the parameters affecting adsorption processes are very important due to their great influence on the adsorption efficiency and capacity of the adsorbent. Among the adsorption parameters, the pH strongly influences on the ionization of the surface groups of the adsorbent, and also affect the speciation of the adsorbates in the solution medium [107].

Generally, the removal of ammonium from water using zeolites is carried out at neutral or basic pH conditions. For example, Jiang et al. [108] studied the removal of ammonium from aqueous solutions at pH 7 and 25 °C using a zeolite type A obtained from FA, reaching an adsorption capacity of 95.4 mg/g. Zhang et al. [109] reported the elimination of ammonium on a zeolite also prepared from FA that showed a adsorption capacity of 37.5 mg/g at pH 8 and 25 °C.

On the contrary, the removal of heavy metals using waste-based adsorbents, including zeolites, is commonly evaluated at different pH conditions (in general, in acid medium). For example, Apiratikul and Pavasant [110] studied the removal of Cu^{2+} , Cd^{2+} , and Pb^{2+} from aqueous solutions at pH 5 by using zeolite X from FA with a CEC of ~ 1.4 meq/g. Asencios and Sun-Kou [111] prepared scrap-based alumina to eliminate Pb^{2+} , Zn^{2+} , and Cd^{2+} from aqueous solutions at pH 3-5 reaching adsorption capacities of 13.1, 7.4, and 8.2 mg/g, respectively. Zhou et al. [112] investigated the adsorption of Pb^{2+} and Zn^{2+} using a biosorbent extracted from waste activate sludge. The authors reported high experimental adsorption capacities (451 and 267 mg/g for Pb^{2+} and Zn^{2+} , respectively) at pH 6 and 25 °C after 30 min.

The investigation on other type of waste-based zeolites could lead to alternative sorbents. In this sense, industrial aluminum waste from tertiary aluminum industry, due to its chemical and mineralogical composition, could be used to obtain zeolites with suitable adsorption properties. Thus, this thesis studies the feasibility of using the zeolites obtained from Alw to remove heavy metals (Pb^{2+} , Cd^{2+} , and Hg^{2+}) and ammonium (NH_4^+) from aqueous solutions.

1.4 Motivation and objectives

This Thesis addresses the resolution in a synergic way of two environmental problems. On the one hand, the generation of hazardous wastes from industrial activities is a problem of great importance, which requires an appropriate management. On the other hand, the contamination of water sources also requires a proper treatment.

The research group Waste for Materials (W4M) of the National Center of Metallurgical Research (CENIM-CSIC), within which this Thesis has been carried out, has focused its main research areas on alternatives to the treatment of wastes from tertiary aluminum industries and on the elimination of contaminants from aqueous effluents using porous materials through the adsorption process.

Thus, the research work developed in this Memory aims at the revalorization of a waste from the aluminum slag milling processes, through its transformation into added-value materials such as zeolites, and the use of these waste-based zeolites for the removal of various contaminants (in particular, ammonium and heavy metals) present in aqueous solutions.

In order to achieve the main objective, the following specific objectives have been proposed:

- Characterization of the different aluminum wastes generated by the tertiary aluminum industry and a representative waste mixture utilized as the main raw material for the preparation of zeolites, in order to obtain a better understanding of the main characteristics and properties of these wastes.
- Development of a simple and low-cost synthesis process on lab-scale that allows the design of different types of zeolites from the representative waste mixture.
- Study and optimization of the operating conditions used for the lab-scale synthesis of zeolites.
- Development of a more sustainable synthesis process through the recycling of liquid effluents generated in the synthesis of the zeolites in order to minimize the environmental impacts.
- Scaling up of the synthesis process of zeolites from the representative waste mixture in order to study the scalability of the process.

1. INTRODUCTION

- Characterization of the resulting zeolites in order to study their main properties and to compare the obtained zeolites with commercial zeolites.
- Selection of those zeolites synthesized that possess the most suitable properties for the further studies of removal of contaminants from aqueous solutions by adsorption.
- Adsorption of heavy metal cations (lead, cadmium, and mercury) and other inorganic cations (ammonium) from aqueous effluents on the waste-based zeolites.
- Study and optimization of mono and multi-cation adsorption processes using the selected zeolites from the waste.

Therefore, the purpose of this work seeks in this way to provide answers to environmental concerns such as the hazardous waste generation and water pollution.

2. MATERIALS AND METHODS

2.1 Materials

The materials used to accomplish the objectives of this Thesis are described in this chapter.

The hazardous aluminum waste, which is the main raw material and the only aluminum source, and other reagents containing silicon, inorganic cations (Na^+), and mineralizing species (OH^-), are the principal materials employed for the synthesis of zeolites.

2.1.1 Hazardous aluminum waste

The main starting material used for the synthesis of zeolites is a hazardous aluminum waste provided by two companies of the Spanish tertiary aluminum industry, namely, *Recuperación y Reciclajes Román S.L.* (Madrid, Spain) and *Metalquex S.L.* (Zaragoza, Spain). As mentioned in Chapter 1, this waste is a gray solid powder with a characteristic odor and very fine granulometry that comes from the sleeve filter suction system of aluminum slag milling processes.

Due to the heterogeneous composition of the waste, different samples of waste were studied to better determine their chemical and mineralogical characteristics. Thus, nine samples of waste from both companies were collected and stored in polyethylene bags. These samples were labeled as Alw_i (i : 1-9). Additionally, a tenth sample (labeled as Alw_x or representative sample) was prepared by mixing all the nine waste samples. Successive quartering steps were made until obtaining around 1 kg of each waste sample. Then, the 1 kg waste samples obtained were divided into eight homogenous fractions through a rotary cone sample divider (Laborette 27, Fritsch), as shown Figure 2.1a. All the samples of waste (Alw_1 - Alw_9), as well as the representative sample (Alw_x), were characterized by using different analytical techniques. Figure 2.1.b shows the macroscopic aspect of the waste sample Alw_x used in the present work for the lab- and bench-scale synthesis of zeolites.

2. MATERIALS AND METHODS

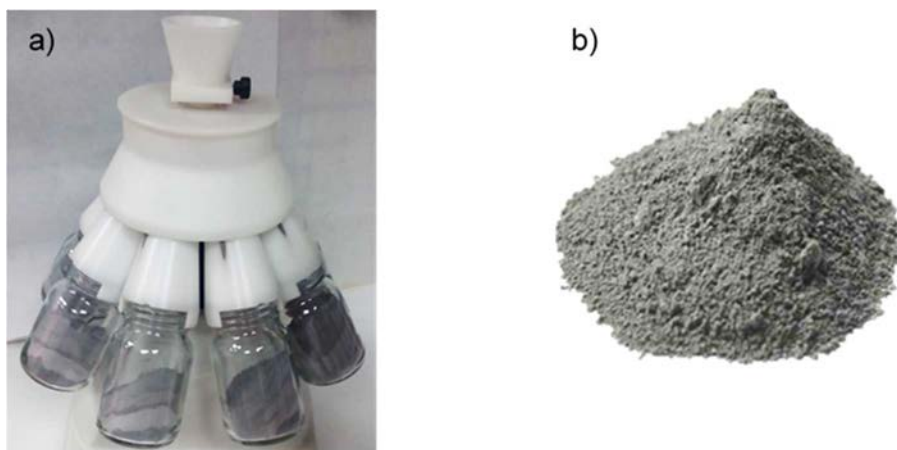


Figure 2.1 a) Homogenization and separation of different aluminum waste fractions. b) Representative sample of the aluminum waste (Alw_x) used for the synthesis of zeolites.

2.1.2 Reagents for the preparation of zeolites

In addition to the use of the aluminum waste, other reagents containing silicon, inorganic cations (Na^+), and mineralizing species (OH^-) were also employed for the synthesis of zeolites.

The required Al^{3+} amount for the preparation of zeolites was totally provided by the waste, which was directly used without any previous treatment.

Due to the low silica content in the waste, the required Si^{4+} amount used to balance the Al/Si ratio was supplied by both the waste and a neutral solution of 11 M Na_2SiO_3 (water glass).

The amounts of Na^+ cation and OH^- anion were mainly provided by 1-5 M NaOH aqueous solutions prepared by dissolving NaOH pellets in distilled water for the lab-scale experiments, and by adding the needed amount of a 50 % (w/w) NaOH aqueous solution for the bench-scale synthesis experiments.

2.2 Methods

The foremost procedures involved in the synthesis of the zeolites are:

- Simple one-step hydrothermal zeolitization process on lab scale and bench scale.
- Recycling of alkaline effluents.
- Separation and recovery of the resulting zeolites.

Additionally, different techniques are employed to characterize the aluminum wastes and the different types of zeolites obtained after the hydrothermal synthesis processes.

Finally, once selected the zeolites with the best adsorption properties, mono- and multi-component adsorption experiments are performed to assess the removal efficiency of some harmful elements, such as heavy metals (lead, cadmium, and mercury) and ammonium, from aqueous solutions. The variation of different adsorption parameters is evaluated for a better understanding of the adsorption process.

2.2.1 Lab-scale synthesis of zeolites

The preparation of zeolites was focused on aluminosilicate zeolites containing sodium as the main extra-framework cation such as zeolites type NaP1, SOD, and ANA due to their diverse industrial applications. The zeolites were synthesized from the representative waste sample (Alw_x) by means of the conventional hydrothermal method based on the $Na_2O-Al_2O_3-SiO_2-H_2O$ system.

The lab-scale hydrothermal synthesis followed to obtain Na-type zeolites (NaP1, SOD, and ANA) from Alw_x consisted of a simple one-step zeolitization process and was carried out in absence of organic templates and without any previous activation process. All reactants, including the aluminum waste (10 g), the Na_2SiO_3 solution, and the NaOH aqueous solution were added into a Teflon-lined autoclave reactor (Parr Instrument Company) with a capacity of 1 L (Figure 2.2).

2. MATERIALS AND METHODS

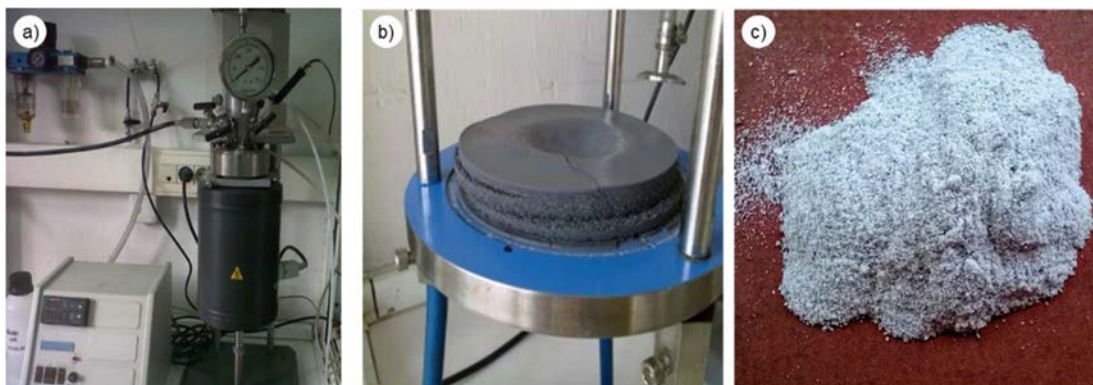


Figure 2.2 a) Reactor used for the lab-scale synthesis experiments of zeolites from aluminum waste. b) Wet zeolite sample obtained after filtration. c) Dry zeolite sample.

All the lab-scale synthesis experiments were performed at a fixed initial Si/Al molar ratio of ~ 2.0 , taking into account the chemical composition of all reactants, and using different liquid/solid ratios (7.5-25 mL/g). They were done with continuous stirring in order to obtain an appropriate homogenization of the initial reaction mixture. In addition, a nitrogen inert atmosphere was applied to maintain the same pressure conditions inside the reactor, approximately 10 bar, during all the synthesis experiments.

For a better determination of the optimal experimental conditions of the synthesis process, the variation of the main synthesis parameters on the properties of the products obtained was studied. Thus, factors such as time, temperature, concentration of alkalizing agent (NaOH), stirring, liquid/solid ratio, and recycling of mother liquor were varied.

The main parameters involved in the synthesis of zeolites from Alw_x and the procedure followed for their study are described below.

2.2.1.1 Time

One of the most important factors to take into account in industrial-scale zeolite synthesis processes is the time of crystallization. Short times are always more favorable due to the economic savings. The effect of the time was studied at 3, 6, and 24 h for a fixed temperature (120 °C) and using a fixed NaOH concentration (1 M).

2.2.1.2 Temperature

Once selected the optimal time conditions for the synthesis of zeolites, the influence of the temperature on the products was evaluated. Thus, this parameter was varied at 80, 90, 100, 120, 140, 160, and 200 °C for a fixed time (6 h) and using a fixed NaOH concentration (1 M).

2.2.1.3 Alkalizing agent concentration

The influence of the alkalizing agent was studied varying the NaOH concentration (1, 3, 4, and 5 M) for a fixed time (6 h) and constant temperature (120 °C).

2.2.1.4 Stirring

As the formation and crystallization of zeolites is very sensitive to the stirring, one synthesis test was performed without stirring to evaluate its influence on the resulting products.

2.2.1.5 Liquid/solid ratio

The variation of the initial liquid/solid ratio used for the synthesis was studied for fixed experimental conditions (6 h; 120 °C; 1 M NaOH) under autogenous pressure and with continuous stirring. The liquid includes the volume of alkalizing agent (NaOH solution), water glass, and distilled water, whereas the solid refers to the amount of the waste (Alw_x) fed into the reaction system. Different liquid/solid ratios (7.5, 15, and 25 mL/g) of the initial reaction suspension were tested in order to evaluate the optimal conditions for a further synthesis process with recycling of alkaline effluents or mother liquors.

2.2.2 Lab-scale synthesis of zeolites with alkaline effluent recycling

The hydrothermal synthesis of the zeolites generates a considerable volume of mother liquor (ML) which is inherent to the process. Even though the ML is usually discarded, it contains elements such as Si, Al, and Na, which are considered as valuable for the zeolite synthesis. For this reason, the recycling of ML was performed in the hydrothermal synthesis process to make it more sustainable. The lab-scale synthesis process with

2. MATERIALS AND METHODS

recycling of ML was developed for the different types of zeolites (NaP1-, SOD-, and ANA-framework) obtained from the waste. Instead of adding the required volume of NaOH solution, a same volume of ML was used to maintain a similar liquid/solid ratio (25 mL/g). The ML was recycled twice and its effect on the resulting products was studied.

All the experimental conditions tested for the lab-scale preparation of zeolites from the representative waste sample (Alw_x) are shown in Table 2.1. For all the lab-scale synthesis experiments, a Si/Al molar initial ratio of 2.0 was fixed while the rest of parameters (time, temperature, etc.) were varied to study their effect on the zeolites obtained from Alw_x .

Table 2.1 Experimental conditions used for the lab-scale synthesis of zeolites from aluminum waste (Alw_x).

Sample	t (h)	Agitation	[NaOH] (mol/L)	T (°C)	l/s ratio ^a (mL/g)	Recycling of mother liquor	
Z1	3	No	1	120	25	No	
Z2							
Z3							
Z4	6	Yes	3	80	25		
Z5							
Z6							
Z7	24	Yes	4	90	25		
Z8							
Z9							
Z10	6	Yes	5	100	25		
Z11							
Z12							
Z13	6	Yes	1	140	25		
Z14							
Z15							
Z16	6	Yes	1	120	15	Yes	0
Z17							
Z18							
Z19	6	Yes	5	120	25	Yes	0
Z20							
Z21							
Z22	6	Yes	1	200	7.5	Yes	1
Z23							
Z24							
Sample	t (h)	Agitation	[NaOH] (mol/L)	T (°C)	l/s ratio (mL/g)	Recycling	Number Cycle
Z16	6	Yes	1	120	25	Yes	0
Z17							
Z18							
Z19	6	Yes	5	120	25	Yes	0
Z20							
Z21							
Z22	6	Yes	1	200	7.5	Yes	1
Z23							
Z24							

^a Liquid/solid ratio.

2.2.3 Bench-scale synthesis of zeolites

The scaling up of the synthesis process was planned not only as a single process to increase the volume of reagents but also a complete process to involve the recycling of liquid effluents generated in that process. In this way, the objective was to develop a more eco-friendly zeolitization process with zero discharge (zero residues and zero effluents). Thus, the ML from the synthesis was recycled up to three times to reduce the raw material consumptions and, accordingly, the environmental impacts of the process. ML can be recycled due to its high basicity (pH ~ 13.6), approximately the same as the alkalizing agent (1 M NaOH solution) utilized for the lab-scale hydrothermal process. Additionally, rinse water (RW), which is generated in the cleaning step of zeolites, was also recycled together with ML.

The bench-scale synthesis experiments under recycling of such effluents (ML and RW) were developed following the same procedure as the previous lab-scale zeolitization process. Once selected the best experimental conditions of the lab-scale synthesis, the feasibility of a scaling up of the zeolite synthesis was assessed under such conditions.

The experimental conditions chosen for the development of the bench-scale synthesis experiments were: initial Si/Al molar ratio = 2.0; 120 °C; 6 h; autogenous pressure; and liquid/solid ratio = 15 mL/g.

The development of the bench-scale synthesis experiments was carried out in the facilities of the company *Archroma S.A.* (Barcelona, Spain).

The required amount of the waste (Alw_x mass = 250 g) and the rest of reactants (NaOH, water glass, ML, and RW) were added into a stainless steel reactor of 5 L volume (E. Bachiller B, S.A.) (Figure 2.3a) which incorporated a control system for temperature, pressure, and agitation (Figure 2.3b). It is also shown the loading of ML and RW in the reactor (Figure 2.3c).

All the experimental conditions studied for the bench-scale zeolitization process using the representative waste sample (Alw_x) are collected in Table 2.2.

2. MATERIALS AND METHODS

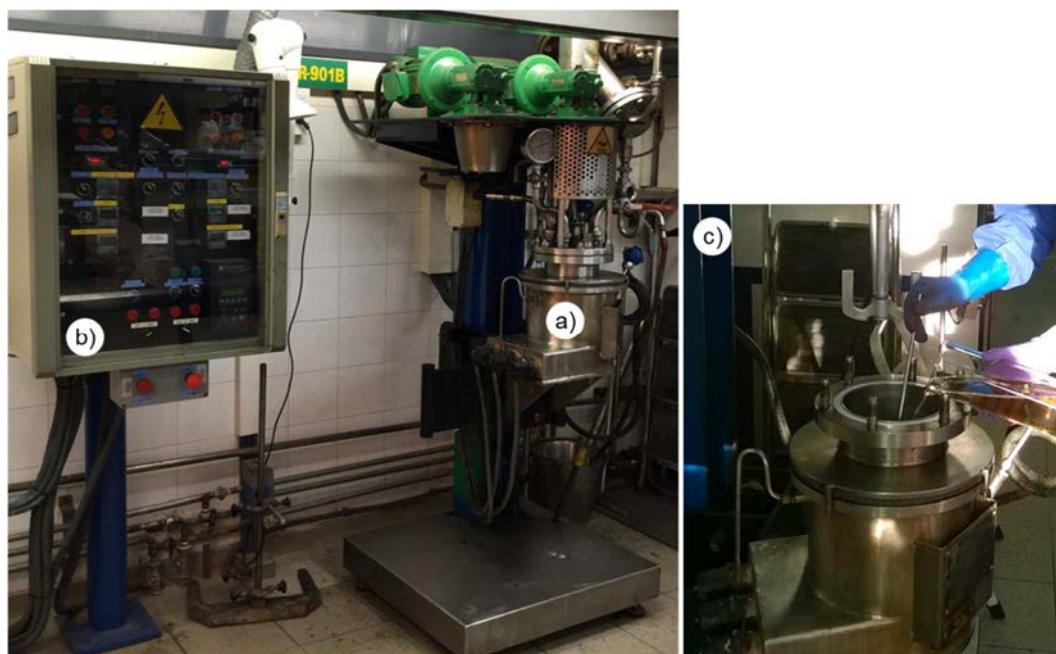


Figure 2.3 Bench-scale synthesis set up (facilities of the company *Archroma S.A.*). a) Reactor and thermal fluid heating and agitation system. b) Control system of synthesis parameters: temperature, pressure, and agitation. c) Loading of mother liquor and rinse water in the reactor.

Table 2.2 Experimental conditions used for the bench-scale synthesis of zeolites from aluminum waste (Alw_x).

Sample	t (h)	Agitation	[NaOH] (mol/L)	T (°C)	l/s ratio ^a (mL/g)	Recycling	Number Cycle
ZB0	6	Yes	1	120	15	Yes	0
ZB1			-				1
ZB2			-				2
ZB3			-				3

^a Liquid/solid ratio.

The Figure 2.4 shows the process of separation of the zeolites and mother liquor by filtration (a), and the appearance of the wet and dry zeolite samples (b and c).

The effect on the products of liquid effluent recycling was studied recycling ML to produce second, third and even fourth generations of zeolites. The recirculated ML alone is not enough to maintain the required alkalinity (1 M NaOH) and liquid/solid ratio (15 mL/g). For this reason, the ML volume that is recirculated (equivalent to 1 M NaOH volume) must be complemented with (i) a small amount of fresh 1 M NaOH (prepared from a 50 wt.% NaOH solution) to balance the alkalinity; and (ii) a small volume of RW to maintain the liquid/solid ratio. The RW pH is very similar to the ML pH, thus allowing even more the reduction in the liquid waste generated in the global process. The pH and

conductivity values of ML and RW were controlled by a multimeter provided with the two corresponding electrodes (MM41, Crison). The main chemical composition of ML was analyzed by means of an Inductively Coupled Plasma Optical Emission Spectrometer, ICP-OES (Spectro Arcos), to determine the Na, Al, and Si contents.



Figure 2.4 a) Separation of the zeolites and mother liquor by filtration. b) Wet zeolite sample. c) Dry zeolite samples.

2.2.4 Recovery of zeolites after lab- and bench-scale synthesis

After all the synthesis experiments, the resulting zeolites were separated from the ML using pressure or vacuum filtration systems. Then, after filtration all the samples were washed with distilled water (up to pH 10-11), and dried in air (at 80 °C for 24 h) for further analysis. Figure 2.5 shows a scheme of the main stages:

- i) Synthesis.
- ii) Filtration.
- iii) Rinsing.
- iv) Drying of the zeolites.
- v) Effluents recycling to prepare the zeolites from the waste on lab and bench scale.

2. MATERIALS AND METHODS

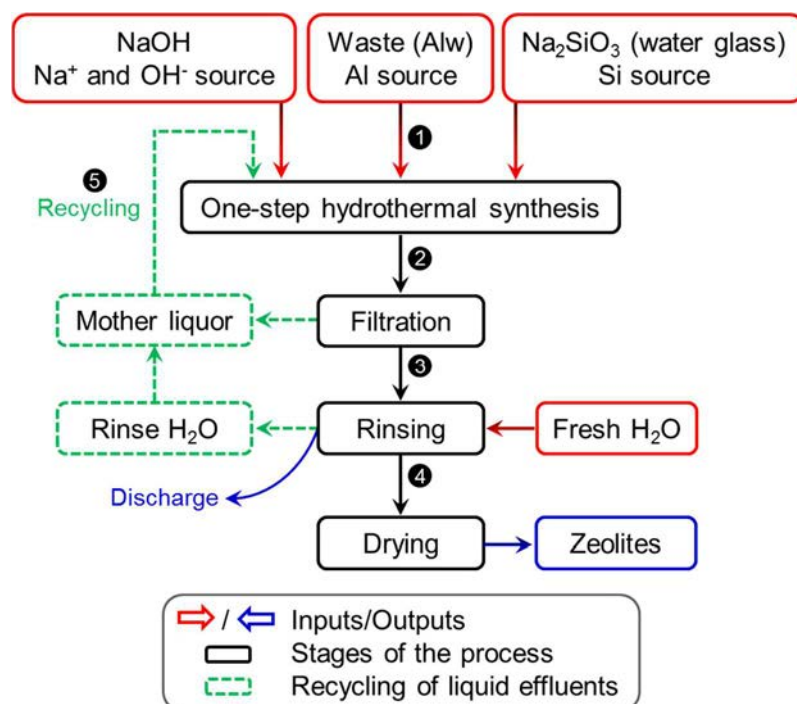


Figure 2.5 Main stages of the synthesis process of zeolites from the aluminum waste.

2.2.5 Analysis, identification, and characterization techniques

The aluminum wastes and the different types of zeolites obtained after the hydrothermal synthesis processes were characterized by using different techniques. Besides, in order to be able to select the most suitable zeolites for the industrial application of interest (i.e. water decontamination), different properties such as crystallinity, morphology, structure, thermal behavior, texture, and surface chemistry were studied.

Figure 2.6 shows a general outline of the different characterization techniques used to study the zeolites obtained from aluminum wastes.

The different characterization techniques are described below, indicating for each of them the equipment and conditions used.

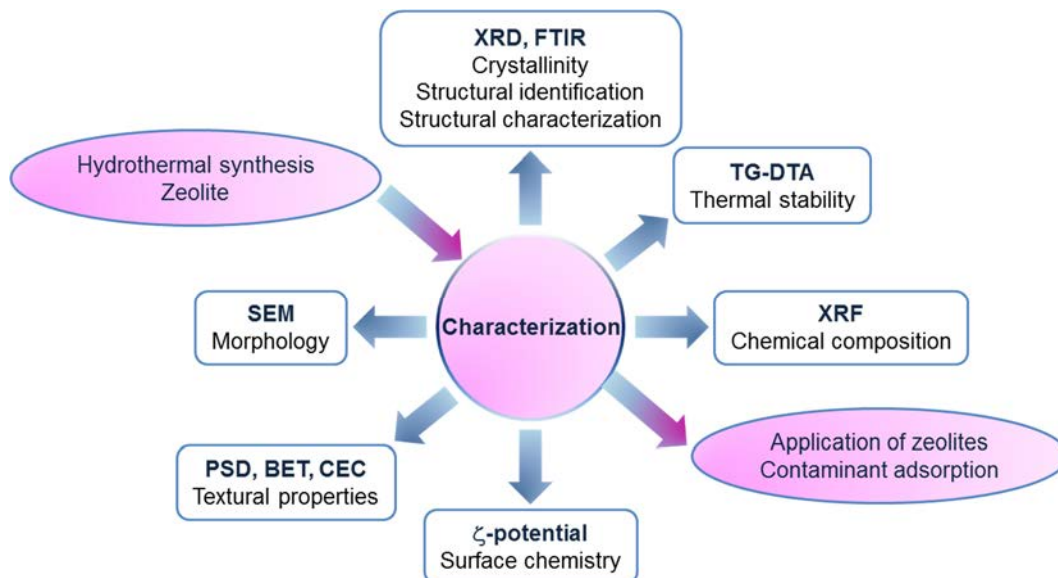


Figure 2.6 Main properties of the zeolites obtained from aluminum wastes analyzed by different characterization techniques.

2.2.5.1 X-Ray Diffraction

The identification of crystalline phases was determined by X-Ray Diffraction (XRD) according to the databases *Powder Diffraction File* (PDF) of the *International Centre for Diffraction Data* (ICDD). The mineralogical composition of the samples was analyzed with $\text{CuK}\alpha$ radiation, from 2° to 65° 2θ , at a scan rate of 0.02° 2θ and 0.07s per step in a Bruker D8 Advance diffractometer. The working conditions were selected to obtain XRD diagrams with sufficient quality, good counting statistics, and well-defined peaks, thus ensuring that the diffraction peaks of the minority phases are visible. The identification of the phases was evaluated according to the reference database PDF-2 and the DIFFRAC plus EVA software.

The crystallite sizes (D_{hkl}) of the crystalline phases were calculated according to the Scherrer equation [113]:

$$D_{hkl} = k \lambda / FWHM \cos \theta \quad (2.1)$$

where k is the Scherrer constant (0.9), λ is the wavelength of X-ray beam (0.15418 nm), FWHM is the Full Width At Half Maximum (in rad), and θ is the experimental Bragg diffraction angle (in rad).

The semi-quantitative analysis of the samples was determined by using the Chung method, also known as the Reference Intensity Ratio (RIR) method. The RIR method

2. MATERIALS AND METHODS

allows the quick and simple calculation of the concentrations of crystalline phases within a sample, based on the integrated intensity of its most intense peaks using the XRD data, and in this case, the EVA software [114, 115]. The relationship between the intensities (I) of diffraction peaks of two phases (α and β) varies linearly with the relationship between the weight fractions (X) of such phases according to the following expression:

$$\frac{I_{\alpha}}{I_{\beta}} = K \frac{X_{\alpha}}{X_{\beta}} \quad (2.2)$$

Where I_{α} and I_{β} , and X_{α} and X_{β} are the intensities of diffraction peaks and the weight fractions of the two phases (α and β); and K is a function of the mass absorption coefficients and the crystalline structure of the phases.

The values of K can be determined from standard samples or from the PDF reference database. The PDF files provide the I/I_{cor} values, where I is the intensity of the peak with the highest number of counts (100 %) of the phase of interest and I_{cor} is the intensity of the most intense peak of the corundum in a mixture 50/50 in weight of both phases [116]. If the relationships between the intensities are known for all the phases present in the sample, the concentration in weight of each phase can be determined.

2.2.5.2 Chemical characterization

The chemical composition of the solid samples of waste was determined by X-Ray Fluorescence (XRF) analysis, using a wavelength dispersive spectrometer (Bruker, S8 Tiger). The sample preparation was performed on 6 mm pellet holders, previously pressing the solid samples for 3 min at a pressure of 10-15 ton using a Specac hydraulic press.

In addition, energy dispersive micro X-ray fluorescence (μ -XRF) analysis (Fischer, Fischerscope XUV 773) was also used for the determination of the elemental chemical composition when working with small quantities of sample.

For the determination of the content of aluminum nitride (AlN) present in the waste samples, the Kjendhal method was used. Thus, solid fractions of waste (0.5-1.0 g) were digested in an alkaline medium (NaOH), in order to reduce the nitrogen content of the samples to ammonia, using the Devarda's alloy. Then, the ammonia content was distilled in an automatic steam distillation unit (UDK 130A, Velp Scientifica), and the

distillate was collected on a 4 % boric acid solution, in which a few drops of Tashiro indicator (methyl red/methylene blue) were previously added. After the distillation, the ammonia content was determined by volumetry using a standardized 0.1 N HCl solution.

The content of metallic aluminum of the waste was determined by keeping in contact solid samples of waste with a 10% HCl solution to obtain soluble compounds of aluminum in the acid medium. After separating the solids from the liquid fractions, the filtrates were analyzed by Atomic Absorption Spectrometry (AAS) in a Varian Spectra model AA-220FS equipment.

Additionally, the leaching behavior of the studied wastes was investigated to know their toxicological characteristics at different pH since the variation of this parameter can affect the mobility of the different elements (metals, minerals, etc.) in the wastes. Thus, the effect of pH on the leaching characteristics of the wastes was studied to assess the potential environmental impacts associated with their disposal in landfills.

The leaching performance of the waste samples was tested following the Toxicity Characteristic Leaching Procedure (TCLP) [117] using aqueous solutions (initial pH ~7.0) and 4 % acetic acid solutions (initial pH ~2.5) as the leaching fluids. The waste samples (10 g), including the representative waste sample (Alw_x), were put in contact with 100 mL TCLP extraction fluid and stirred (30 ± 2 rpm) for 24 h under ambient conditions. After agitation of the waste samples, the leachates were collected using an air filtration system. The concentrations of the different elements present in the leachates were determined using ICP-EOS analysis (Spectro Arcos).

2.2.5.3 Fourier transform infrared spectroscopy

The structural characterization of the samples was analyzed by Fourier Transform Infrared (FTIR) spectroscopy using KBr discs in a Nicolet Nexus 670-870 spectrometer. The sample preparation consisted of mixing 1.0-1.5 mg of sample with approximately 200 mg of KBr, and then pressing the samples at about 10-15 ton in a hydraulic press (Specac) for 5 min. The spectra were recorded in the range of 400-4000 cm^{-1} .

2. MATERIALS AND METHODS

2.2.5.4 Scanning electron microscopy

The morphology and elemental composition of the waste mixture (Alw_x) and zeolites were examined by using Scanning Electron Microscopy (SEM), in a Hitachi S4800 microscope, equipped with an Energy Dispersive X-ray detector (EDS) supplied by Oxford. The samples were previously coated with graphite by using a sputtering procedure, since both the waste and zeolites are not conductive materials.

2.2.5.5 Thermal analysis

The study of the thermal stability of zeolites was carried out by Thermogravimetric (TG) and Differential Thermal Analysis (DTA) in a thermoanalyzer model SDT-Q600, TA Instruments. The samples (approximately 10 mg) were heated up to 1000 °C, at a heating rate of 10 °C/min, in a Pt crucible and under a N_2 flow of 100 mL/min.

The TG analysis provides the mass changes suffered by the sample as the temperature increases, while the DTA analysis measures the heat absorbed or emitted by the sample as a function of the temperature difference between the sample and a standard material, which shows no phase changes during the test.

2.2.5.6 Textural characterization

In order to perform textural characterization of zeolites, the particle size distribution, the porosity, the cation-exchange capacity, the zeta potential, and the point of zero charge were measured.

Particle size distribution

The measurement of Particle Size Distribution (PSD) and the determination of the characteristic parameters d_{10} , d_{50} and d_{90} (i.e., the maximum particle diameters below which 10 %, 50 %, and 90 % of the sample volume exists) for both the waste and zeolite samples were carried out by means of laser diffraction analysis.

Laser diffraction provides the PSD by measuring the angular variation in intensity of light scattered as a laser beam passes through a dispersed particulate sample. The angular scattering intensity data is then analyzed to calculate the size of the particles responsible for creating the scattering pattern, using the Mie theory of light scattering [118].

Concerning the different samples of waste, their granulometry were determined in a Sympatec Helos 12LA equipment with a particle size range from 0.1 μ m to 1750 μ m. The samples of waste were dispersed by means of an ultrasonic system in isopropyl alcohol in order to avoid the dissolution of the soluble phases of the waste and particle agglomerates.

The PSD of the zeolites was also measured by laser scattering analysis in a Mastersizer S, Malvern analyzer with a particle size range from 10 nm to 10 mm. The sample preparation consisted of aqueous suspensions of zeolite with a solid/liquid ratio of approximately 0.001 g/mL, which were sonicated in ultrasounds (at least for 1 h) prior to the measurements. The measurement of PSD was done in triplicate considering the obscuration within an acceptable range (10-30 %) for a proper dispersion of the sample.

Nitrogen adsorption/desorption analysis

Physical gas adsorption is commonly used for the characterization of micro (pore width < 2 nm), meso (2-50 nm) and macroporous (> 50 nm) materials [119], including zeolites. This technique determines the amount of nitrogen adsorbed on a solid material that is associated to the porous properties and structure. Parameters such as surface area, pore volume, pore diameter, and pore size distribution of a porous material depend on the isotherm type obtained from the nitrogen adsorption/desorption analysis [120, 121].

The textural characterization of the zeolites obtained from the waste was performed by determination of nitrogen adsorption/desorption isotherms at 77 K in an ASAP 2010 Micromeritics equipment. Before the measurements, the samples (200-400 mg) were outgassed at 60-350 °C in vacuum for 24 h.

The BET specific surface area (S_{BET} , expressed in m²/g) was calculated by the BET method [122] in the relative pressure (P/P_0) range of 0.003-0.3, according to:

$$S_{BET} = \frac{q_m \rho N_A A_{CS}}{M} \quad (2.3)$$

where q_m is the monolayer capacity, ρ is the density of nitrogen at standard temperature and pressure ($P = 1$ atm; $T = 273$ K), N_A is the Avogadro's constant, A_{CS} (0.162 nm²) is the cross sectional area of a nitrogen molecule, and M (28 g/mol) is the nitrogen molar mass.

2. MATERIALS AND METHODS

The external area (S_{EXT} , in m^2/g), i.e. the area of those pores which are not micropores (mesopores, macropores, and exterior surface of the particle), was calculated by the t-plot method from the slope (s) of the linear fit in the thickness range (t) of 0.35-0.5 nm, according to the Harkins-Jura expression [123]:

$$S_{EXT} = s_{t-plot} 15.47 \quad (2.4)$$

The total pore volume (V_{total}) was estimated for the nitrogen amount adsorbed at the P/P_0 of 0.99, according to the following equation:

$$V_{total} = \frac{PV_{0.99}}{\frac{RT}{\rho}} M \quad (2.5)$$

Where $P = 1$ atm; $R = 0.082$ atm dm^3/mol K; $T = 273$ K; $M = 28$ g/mol; and $\rho = 0.0818$ g/cm³.

The micropore volume (V_{micro}) was calculated from the intercept (i) of the t-plot method, while the mesopore volume (V_{meso}) was calculated as the difference between V_{total} and V_{micro} :

$$V_{micro} = i_{t-plot} 1.547 \cdot 10^{-3} \quad (2.6)$$

$$V_{meso} = V_{total} - V_{micro} \quad (2.7)$$

The pore size distribution was calculated using the Barrett-Joyner-Halenda (BJH) method [124] in the adsorption branches.

Cation-exchange capacity

The Cation-Exchange Capacity (CEC) of the zeolites was determined by the NH_4^+ cation exchange method with a 1 M NH_4Cl solution (pH ~7) following the procedure described in [125]. The measures of CEC were done in triplicate and consisted of samples of zeolite (2.5 g) which were put in contact with 100 mL of NH_4Cl solution (1 M) at pH 7. The mixture was stirred for 1 h and left for 24 h, and then separated by filtration. Next, aliquots of the filtrate (50 mL) and 2 drops of methyl orange solution were put together until neutralization. Then, 5 mL of formaldehyde and 2 drops of phenolphthalein were added to the sample, and titrated with NaOH solution until the solution had a purplish red color. The values of CEC for the zeolites were calculated using the next expression:

$$CEC = \frac{(V_1 - V_2)C_{NaOH} \cdot 200}{M} k \quad (2.8)$$

where V_1 and V_2 are the NaOH volumes consumed during the titration of blank and zeolite samples, respectively; C is the NaOH concentration; k is a coefficient that varies between 1 and 10 depending on the moisture content of the sample; and M is the sample mass.

Zeta potential and point of zero charge

The zeta potential (ζ -potential) is a parameter related to the external surface charge of materials, including zeolites [126], and reveals the type of charge of a material as a function of pH. The point where the ζ -potential is zero, known as Isoelectric Point (IEP), represents the point where the material is least stable.

The ζ -potential of samples was determined by the electrophoretic mobility of zeolite particles in aqueous solutions at different pH (ZetaSizer Nano, Malvern), following the Smoluchowski approximation. The measurement of ζ -potential was prepared using 0.05 g of zeolite per 100 mL of aqueous solution. Zeolite suspensions were previously stirred in an ultrasonic bath (60 min) and kept in contact for a long time (24 h) to achieve the suspensions homogenization and stabilization. Absolute ζ -potential values > 20 mV can be considered electrically stable, resulting in a suitable separation of low charged surfaces from highly charged surfaces [127, 128].

The Point of Zero Charge (PZC) is associated with the total surface charge (i.e. the external and internal surface charge) and indicates that the surface charge density of a material is zero for a value/s of pH.

The PZC analysis was determined by preparing zeolite aqueous suspensions adjusted at different pH values using dilute HNO_3 or NaOH. The suspensions were agitated for 24 h until an equilibrium pH was reached.

2. MATERIALS AND METHODS

2.2.6 Adsorption study

One the aims of this thesis is the evaluation of the adsorption properties of the zeolites obtained from the waste. For this purpose, the resulting zeolites were tested as adsorbent materials to remove different compounds such as heavy metals (lead, cadmium, and mercury) and ammonium due to their harmful effects in aquatic media. As commented in Chapter 1, heavy metals, such as lead, cadmium, and mercury, can act as endocrine disruptors because of their bioaccumulation in organisms causing severe health problems. On the other hand, an excess of nitrogen compounds including ammonium in lakes and rivers can cause eutrophication, resulting in oxygen depletion of such aquatic media.

The removal of the adsorbates (ammonium, lead, cadmium, and mercury) from aqueous solutions using the zeolites synthesized from the aluminum waste was studied by developing batch adsorption experiments. The effects of the most relevant adsorption parameters, such as pH, contact time, adsorbent dose, and initial concentration, on the removal efficiency and adsorption capacity of the zeolites were evaluated.

The adsorption kinetics were evaluated using different kinetic models, among others: the pseudo-first-order [129] and pseudo-second-order [130] models and intra-particle diffusion model [131]. Adsorption equilibrium was studied applying isotherms with two parameters (Langmuir [132], Freundlich [133], Dubinin-Radushkevich [134], and Temkin [135]) and with three parameters (Sips [136], Toth [137], and Redlich-Peterson [138]), widely reported in the literature [96, 139]. These models are widely used in the literature related to the removal of contaminants from water providing useful information about the type of adsorption process (homogeneous or heterogeneous). In addition, some of these models can also estimate the energy related to the adsorption process. Depending on the value of adsorption energy, the process can take place via physical or chemical adsorption [97].

2.2.6.1 Adsorbent

The adsorbent materials used for the removal of the different adsorbates were the zeolites synthesized from the waste by the eco-friendly bench-scale process. Once selected the zeolites with the best adsorption properties, the adsorption process of ammonium and heavy metals from aqueous effluents was evaluated.

In particular, the zeolite adsorbent chosen for the adsorption experiments was the NaP1 zeolite, whose theoretical formula is $\text{Na}_6\text{Al}_6\text{Si}_{10}\text{O}_{32}\cdot 12\text{H}_2\text{O}$, due to its high CEC compared with the other types of zeolites (SOD and ANA) obtained from the same waste.

2.2.6.2 Adsorbates

Due to the high ammonium CEC of the zeolite NaP1 obtained from the waste in the synthesis, different adsorbates such as ammonium and various heavy metals (lead, cadmium, and mercury) were selected to study their adsorption onto the zeolite.

All chemicals used for the adsorption tests were analytical reagents of high purity. Aqueous solutions containing the adsorbates were prepared using deionized water with a resistivity of 18.2 M Ω ·cm.

The initial concentrations of the adsorbates tested in the adsorption experiments are above the maximum allowable concentrations in inland surface waters: 0.07 $\mu\text{g/L}$ for mercury, 14 $\mu\text{g/L}$ for lead, 0.45-1.5 $\mu\text{g/L}$ for cadmium (depending on the hardness of the water), and 0.2-1 mg/L for ammonium, according to the environmental legislation on the quality of water [78, 84].

Ammonium

Aqueous solutions containing the ammonium cation (NH_4^+) were prepared by dissolving a certain amount of a 1000 mg/L stock solution of ammonium chloride (99.5 % purity, Panreac) in deionized water.

The concentrations of NH_4^+ before and after the adsorption experiments were determined colorimetrically with Nessler reagent by UV-Vis spectroscopy (Varian, Cari 1E), monitoring the absorbance at a wavelength of maximum absorbance (420 nm). The pH values of all experiments were adjusted by adding aqueous solutions of dilute NaOH or HCl, using a pH meter (Crison, MM41).

One of the most important parameters in adsorption processes is the pH of the solution where the removal of the contaminants takes place. As a first approximation for the study of the effect of pH on the adsorption efficiency and capacity of the zeolites, the chemical equilibrium diagram of NH_4^+ in aqueous solution was obtained to better understand the behavior of this cation under different pH conditions. The chemical equilibrium diagram

2. MATERIALS AND METHODS

of NH_4^+ for the initial concentration of 50 ppm was obtained by using the software MEDUSA (Make Equilibrium Diagrams Using Sophisticated Algorithms).

Heavy metals

Lead: A stock solution (1000 mg/L) of the Pb^{2+} cation was prepared by dissolving the required amount of pure lead metal (99.9 % purity, Merck) in ultra-pure water containing 4-5 % HNO_3 (69 % v/v, Panreac).

Cadmium: A stock solution (1000 mg/L) of the Cd^{2+} cation was prepared by dissolving the needed amount of cadmium chloride (99.995 % purity, Sigma-Aldrich) in ultra-pure water containing 4-5 % HNO_3 (69 % v/v, Panreac).

Mercury: A commercial standard solution (Hg 1000 mg/L in 2-5 % v/v HNO_3 , Panreac) was used to study the Hg^{2+} cation. To avoid the precipitation of the metal cations, in particular Pb^{2+} which tends to form PbCl_2 in contact with HCl, the pH values required for the adsorption experiments were adjusted by adding dilute NaOH or HNO_3 aqueous solutions (both from Panreac).

The concentrations of the Pb^{2+} and Cd^{2+} cations were determined using ICP-OES (Perkin Elmer, Optima 3300 DV). The concentration of the Hg^{2+} cation was analyzed using Cold Vapor Atomic Absorption Spectrometry (CVAAS) (PS Analytical, 10.025 Millennium Merlin) at wavelength of 235 nm. The variation of the solution pH was controlled using a pH meter (Crison, MM41).

The chemical equilibrium diagrams of Pb^{2+} , Cd^{2+} , and Hg^{2+} in aqueous solution were also obtained by applying the software MEDUSA for the initial concentrations: 20 ppm for Pb^{2+} , 20 ppm for Cd^{2+} , and 0.2 ppm for Hg^{2+} .

After reaching adsorption equilibrium, all the samples were collected by filtration. All the adsorption tests were duplicate, representing the error bars and average values.

2.2.6.3 Ammonium adsorption procedure

The adsorption of the NH_4^+ cation by the zeolite was performed through the batch experiments under ambient conditions (28 ± 2 °C) using aqueous solutions of the adsorbate with a fixed volume (100 mL). The adsorption ability of the zeolite was only studied under ambient conditions, since the increase of temperature can lead to the

decrease of the NH_4^+ adsorption capacity [140]. Before adsorption, blank tests were prepared in order to discard possible contamination resulting from the adsorbent, the reagents or the equipment used during sample processing including filtration. All samples were placed in 150 mL glass conical flasks, which were kept covered and stirred at constant speed (125 rpm) using an orbital and horizontal shaker (Selecta, Rotabit) with speed and time control. The solution pH was maintained constant during each adsorption experiment by adding small volumes of dilute NaOH or HCl aqueous solutions. The effect of pH, contact time, and adsorbent dose on the ammonium removal efficiency and on the adsorption capacity was studied using fixed initial concentrations (50 mg/L). The variation of the initial NH_4^+ concentration was evaluated in a concentration range of 10-1500 mg/L.

Effect of pH

As the pH influences both the ionization of surface groups of an adsorbent and the speciation of the different species in the adsorption system, the effect of this factor on the ammonium uptake was studied. Thus, the influence of pH on the NH_4^+ cation adsorption by the zeolite was studied in a pH range of 6-8, simulating pH conditions similar to leachates from landfills, which contain high concentrations of ammonium [81]. For the pH experiments, an adsorbent dose of 5 g/L (0.5 g of zeolite per 100 mL of NH_4^+ aqueous solution) and an initial adsorbate concentration of 50 mg/L were selected for a fixed contact time (15 min).

Effect of contact time

The contact time required for reaching the adsorption equilibrium was determined at the optimal pH value. The effect of the contact time on the NH_4^+ adsorption efficiency of the zeolite was studied varying the time (1, 2, 5, 10, 15, 30, 60, 120, and 360 min) and using 0.5 g of zeolite per 100 mL of adsorbate aqueous solution with an initial NH_4^+ concentration of 50 mg/L at pH 7.5. The adsorption kinetic was studied using the pseudo-first- [129] and pseudo-second-order [130] models.

Effect of adsorbent dose

Once selected the optimal conditions of pH (7.5) and contact time (15 min) for the NH_4^+ removal on the zeolite, the adsorbent dose was evaluated by varying the zeolite mass (0.1, 0.25, 0.5, 0.75, 1, 1.25, and 1.5 g) in contact with 100 mL aqueous solutions of NH_4^+ , with an initial adsorbate concentration of 50 mg/L.

2. MATERIALS AND METHODS

Effect of initial adsorbate concentration

The effect of the initial ammonium concentration was studied for the optimal adsorption conditions (i.e., pH 7.5; 15 min; 10 g/L). The adsorption equilibrium experiments were performed varying the initial adsorbate concentration between 10 and 1500 mg/L, and evaluating different isotherms models (Langmuir [132], Freundlich [133], Temkin [135], Sips [136], Toth [137], and Redlich-Peterson [138]).

All conditions studied in the ammonium adsorption experiments using the zeolite type NaP1 obtained from the waste are summarized in Chapter 3, Section 3.5 (see Table 3.50).

2.2.6.4 Heavy metals adsorption procedure

The adsorption of the heavy metals (Pb^{2+} , Cd^{2+} , and Hg^{2+}) using the zeolite NaP1 was carried out at room temperature ($25\text{ }^{\circ}\text{C} \pm 2$) through the batch experiments. In addition to the evaluation of single-cation adsorption, the multi-cation adsorption process was also studied. All the aqueous solutions of the metal cations were placed in 150 mL Erlenmeyer flasks with adsorbate solution volumes of 100 mL, and were stirred at 125 rpm using an orbital and horizontal shaker (Selecta, Rotabit). The influence of adsorption parameters such as the pH, contact time, adsorbent dose, and initial concentration on the removal of each metal cation (single adsorption) was evaluated as detailed for the ammonium adsorption.

Besides, the multi-cation adsorption was also studied. For the competitive adsorption experiments, the effect of the coexisting metal cations, i.e., Pb^{2+} , Cd^{2+} , and Hg^{2+} , in the solution medium on the removal ability of the zeolite was also studied.

Single-cation adsorption

Effect of pH

In order to determine the optimal operating conditions for the adsorption process, the effect of pH on the metal cations and on the adsorbent was studied. The speciation of lead, cadmium, and mercury in aqueous medium was evaluated using fixed initial concentrations (20 mg/L for Pb^{2+} and Cd^{2+} , and 0.2 mg/L for Hg^{2+}) in a pH range of 2-12. The influence of the pH on the crystalline and morphological properties of the zeolite was studied. For this, a fixed zeolite mass (5 g) was measured before and after placing the

adsorbent in contact with a fixed aqueous solution volume (250 mL) at different pH values.

Unlike the Pb^{2+} and Cd^{2+} cations, the Hg^{2+} specie is more strongly influenced by the solution pH. Therefore, the effect of the pH on the Hg^{2+} adsorption was evaluated at pH 2-6 using an initial Hg^{2+} concentration of 0.2 mg/L and an adsorbent dose of 10 g/L to select the best conditions. Further adsorption tests for all the metal cations were performed under the pH selected as optimal.

Effect of contact time

The effect of the contact time on the adsorption efficiency of the zeolite was evaluated from 1 to 120 min using the initial concentrations studied (20 mg/L for Pb^{2+} and for Cd^{2+} , and 0.2 mg/L for Hg^{2+}) and the optimal adsorbent dose for each cation at pH 4.5. The adsorption kinetics of all the cations were also evaluated applying the pseudo-first- [129] and pseudo-second-order [130] models, as well as the intra-particle diffusion model [131].

Effect of adsorbent dose

The effect of the zeolite dose (0.125-10 g/L) on the removal efficiency and adsorption capacity was studied using fixed initial concentrations (20 mg/L for Pb^{2+} and Cd^{2+} , and 0.2 mg/L for Hg^{2+}) at pH 4.5 for 30 min to ensure sufficient equilibrium time.

Effect of initial concentration

The adsorption equilibrium experiments were developed at pH 4.5, using the optimal adsorbent dose and contact time: 0.5 g/L and 30 min for Pb^{2+} , 5 g/L and 30 min for Cd^{2+} , and 5 g/L and 60 min for Hg^{2+} . The effect of the initial concentration of each metal cation on the adsorption ability of the adsorbent was evaluated using the following isotherm models: Langmuir [132], Freundlich [133], Dubinin-Radushkevich [134], Sips [136], Toth [137], and Redlich-Peterson [138]. The isotherms were evaluated for different initial concentrations of the metal cations: 5-100 mg/L for Pb^{2+} , 1-40 mg/L for Cd^{2+} , and 0.02-1.5 mg/L for Hg^{2+} .

Effect of competitive adsorption of Pb^{2+} , Cd^{2+} , and Hg^{2+}

In order to simulate more realistic conditions, the competitive adsorption of Pb^{2+} , Cd^{2+} , and Hg^{2+} on the zeolite was studied in the adsorbent dose range of 2- 10 g/L at pH 4.5, for contact times ranged from 1 to 30 min under ambient conditions (25 ± 2 °C).

2. MATERIALS AND METHODS

All conditions studied in the in the single- and multi-metal cation adsorption experiments using the zeolite type NaP1 obtained from the waste are summarized in Chapter 3, Section 3.4 (see Table 3.42).

2.2.6.5 Adsorption efficiency and adsorption capacity

The adsorption or removal efficiency of the adsorbent (expressed in %) was determined according to the following equation:

$$\text{Removal (\%)} = \left(\frac{C_o - C_t}{C_o} \right) \cdot 100 \quad (2.9)$$

The adsorption capacity of the adsorbent corresponds to the amounts of the NH_4^+ , Pb^{2+} , Cd^{2+} , and Hg^{2+} cations adsorbed by the zeolite at any time (q_t , expressed in mg/g) and at equilibrium (q_e , in mg/g). They were calculated according to the next equations:

$$q_t = \frac{(C_o - C_t)}{m} \cdot V \quad (2.10)$$

$$q_e = \frac{(C_o - C_e)}{m} \cdot V \quad (2.11)$$

where C_o (mg/L) is the initial adsorbate concentration, C_t and C_e (mg/L) are the adsorbate concentration at contact time t and at equilibrium, respectively, m (g) is the mass of zeolite, and V (L) the volume of adsorbate solution.

2.2.6.6 Kinetic and isotherm modeling

Adsorption kinetics

The pseudo-first- [129] and pseudo-second-order [130] models, and intra-particle diffusion model [131] were applied to the experimental data according to the next equations:

$$q_t = q_e (1 - e^{-k_1 t}) \quad (2.12)$$

$$q_t = \frac{k_2 q_e^2 t}{1 + k_2 q_e t} \quad (2.13)$$

$$q_t = k_p t^{0.5} + C \quad (2.14)$$

where q_e (mg/g) and q_t (mg/g) are the amount of adsorbate adsorbed per mass of adsorbent at equilibrium and at any time t (min), respectively; k_1 (1/min) and k_2 (g/mg min) are the rate constants for the pseudo-first- and pseudo-second-order models; k_p (mg/g min^{0.5}) is the rate constant of the intra-particle diffusion model, and C (mg/g) is a constant related to the thickness of the boundary layer.

Unlike the pseudo-second- and pseudo-first-order kinetic models, the intra-particle diffusion model provides information about the reaction pathways and adsorption mechanisms, predicting the rate-controlling step. The internal surface and pore diffusion of an adsorbate inside an adsorbent may represent the rate-limiting steps. When this model represents a straight line that passes through the origin, adsorption process is mainly governed by intra-particle diffusion; on the contrary, a multi-step adsorption process is given by multiple linear regions [96]. The intra-particle diffusion model was evaluated following the piecewise linear regression proposed by Malash et al. [141].

Adsorption isotherms

The effect of the adsorbate concentration on the adsorption ability of the adsorbent was evaluated using the following isotherm models: Langmuir [132], Freundlich [133], Dubinin-Radushkevich [134], Temkin [135], Sips [136], Toth [137], and Redlich-Peterson [138].

The Langmuir isotherm describes homogeneous adsorption systems [132] and is commonly expressed in terms of the separation factor (R_L) [142]:

$$q_e = \frac{q_{max}k_L C_e}{1+k_L C_e} \quad (2.15)$$

$$R_L = \frac{1}{1+k_L C_o} \quad (2.16)$$

where q_e (mg/g) is the amount of adsorbate adsorbed at equilibrium, q_{max} (mg/g) is the maximum monolayer adsorption capacity of the adsorbent, C_o and C_e (mg/L) are the initial and equilibrium adsorbate concentrations, respectively, and k_L (L/mg) is a constant related to the affinity between the adsorbent and adsorbate.

The Freundlich isotherm is usually applied to heterogeneous adsorption processes [133]:

$$q_e = k_F C_e^n \quad (2.17)$$

2. MATERIALS AND METHODS

where q_e (mg/g) is the amount of adsorbate adsorbed at equilibrium, C_e (mg/L) is the adsorbate concentration at equilibrium, k_F (mg/g)/(mg/L)ⁿ is the Freundlich constant, and n (dimensionless) is the Freundlich intensity parameter, which indicates the magnitude of the adsorption driving force or the surface heterogeneity.

The Dubinin-Radushkevich isotherm is related to the porosity of the adsorbent [134] and is represented by the next equations:

$$q_e = q_{DR} e^{-k_{DR} \varepsilon^2} \quad (2.18)$$

$$\varepsilon = \left[RT \ln \left(1 + \frac{1}{C_e} \right) \right]^2 \quad (2.19)$$

where q_{RD} (mg/g) is the adsorption capacity, k_{RD} (mol²/kJ²) is a constant associated with the sorption energy, ε is the Polanyi potential, R is the gas constant (8.341 J/mol K), and T (Kelvin) is the temperature.

The Dubinin-Radushkevich model can provide the value of the mean adsorption energy (E , expressed in kJ/mol) associated with the type of process (physical or chemical adsorption) [96, 139]:

$$E = \frac{1}{\sqrt{2k_{DR}}} = \frac{RT}{\sqrt{-2slope}} \quad (2.20)$$

The Temkin model [135] is related to the effects of indirect interactions between adsorbent and adsorbate, and is characterized by a uniform distribution of binding energies according to the following expression:

$$q_e = \frac{RT}{b} \ln(AC_e) \quad (2.21)$$

where A is the equilibrium binding constant (L/g), b is related to the heat of adsorption (J/mol), R is the gas constant (8.314 J/K mol), and T is the temperature (K).

The Redlich-Peterson isotherm [138] is used for both homogeneous and heterogeneous adsorption in a wide concentration range:

$$q_e = \frac{k_{RP} C_e}{1 + a_{RP} C_e^\beta} \quad (2.22)$$

where k_{RP} (L/g) and a_{RP} (mg/L)^{- β} are the Redlich-Peterson constants, and β (dimensionless) is an exponent whose value must lie between 0 and 1. This model tends

to the Langmuir isotherm when the exponent $\beta = 1$, while it is described by the Freundlich isotherm when K_{RP} and a_{KP} are higher than 1 and β is 1 [96].

The Sips isotherm [136] combines the Langmuir and Freundlich models and is usually described as follows:

$$q_e = \frac{q_{max}(k_S C_e)^n}{1+(k_S C_e)^n} \quad (2.23)$$

where q_{max} (mg/g) is the maximum adsorption capacity, k_S (L/mg) is the Sips constants, C_e (mg/L) is the adsorbate concentration at equilibrium, and n (dimensionless) is an exponent.

The Sips model tends to the Freundlich isotherm at low adsorbate concentrations, while it approaches the Langmuir isotherm at high concentrations.

The Toth isotherm [137] improves the Langmuir and Freundlich models:

$$q_e = \frac{q_{max} k_T C_e}{[1+(k_T C_e)^n]^{1/n}} \quad (2.24)$$

where q_{max} (mg/g) is the maximum adsorption capacity, C_e (mg/L) is the adsorbate concentration at equilibrium, k_T (L/mg) is the Toth isotherm constant, and n (dimensionless) is the Toth exponent [143].

Non-linear optimization method

Besides, a non-linear optimization method using Microsoft Excel Solver was applied for the evaluation of the goodness of fit of the different models. All the parameters and constants of the studied kinetic and isotherm models were determined by maximizing the coefficient of determination (R^2) [144]:

$$R^2 = 1 - \left[\frac{\sum_{i=1}^n (q_{i,exp} - q_{i,model})^2}{\sum_{i=1}^n (q_{i,exp} - \bar{q}_{i,exp})^2} \right] \quad (2.25)$$

where n is the number of experimental values in a dataset, and $q_{i,exp}$ and $q_{i,model}$ are the experimental and calculated adsorption capacities.

2. MATERIALS AND METHODS

3. RESULTS AND DISCUSSION

3.1 Waste characterization

In this thesis, as previously commented, nine samples of waste from the tertiary aluminum industry were selected evaluating their chemical and mineralogical characteristics. The characterization of the different aluminum wastes (samples Alw₁-Alw₉) and representative waste (sample Alw_x) used for the synthesis of zeolites is described in this section for a better understanding of their main physical-chemical properties.

The complete characterization of the waste samples was performed using different techniques. Thus:

- Chemical and mineralogical compositions were determined by XRF and XRD.
- Morphology was analyzed by SEM.
- PSD was obtained by laser diffraction analysis.
- Leaching character was evaluated using the TCLP and ICP-OES.

Most results included in Section 3.1 were previously published in a publication [8].

3.1.1 Chemical characterization

The chemical composition (expressed as oxides) of the waste samples is shown in Table 3.1, according to the results obtained by XRF. The statistical values, average value (\bar{x}) and standard deviation (σ), are also included. The fluctuations in the composition of the waste samples derive from their heterogeneity associated with the type of starting scraps and processes followed for the treatment of the scraps in the aluminum industry.

As can be seen, all the waste samples presented high contents in aluminum compounds, expressed as Al₂O₃, oscillating between and 53 and 81 wt.%. The content of SiO₂ varied between 3 and 18 wt.%. It is noticeable that the Alw₅ sample showed the highest amounts of SiO₂ (17.8 wt.%) and Na₂O (11.0 wt.%). The high content of sodium present in this sample was associated with the use of flux salts in the melting processes in order to recover the maximum aluminum content. In fact, this sample had the lowest amount of aluminum (53.4 wt.%). According to the literature, saline slags, which are generated from the secondary aluminum melting processes, show high contents of inorganic salts, such

3. RESULTS AND DISCUSSION

as NaCl (30-55 wt.%) and KCl (15-30 wt.%), but lower contents of aluminum oxide (15-30 wt.%) and silica (3-8 wt.%) [145, 146].

Table 3.1 Chemical composition of the different waste samples (Alw₁-Alw₉) and the representative waste sample (Alw_x) determined by X-ray fluorescence (XRF).

Waste sample	XRF (wt.%)									
	Al ₂ O ₃	MgO	Fe ₂ O ₃	TiO ₂	SiO ₂	CaO	K ₂ O	Na ₂ O	Cl	Others
Alw ₁	79.3	4.7	0.6	2.7	2.9	2.2	1.0	2.5	2.0	2.3
Alw ₂	79.6	4.3	0.7	3.5	2.8	2.2	0.2	1.8	0.7	4.1
Alw ₃	80.9	3.4	0.7	3.4	2.7	2.1	0.3	1.7	0.9	4.0
Alw ₄	71.6	4.5	1.9	5.6	6.2	6.0	0.3	-	-	4.1
Alw ₅	53.4	6.8	1.2	0.5	17.8	2.9	1.1	11.0	3.5	2.4
Alw ₆	80.5	1.3	0.9	8.3	2.9	1.6	3.0	0.4	-	1.0
Alw ₇	77.9	3.8	1.3	0.4	7.6	2.5	1.1	2.8	0.9	1.7
Alw ₈	76.7	4.3	3.4	2.0	5.2	3.5	0.7	1.0	0.8	2.5
Alw ₉	76.9	4.1	0.4	3.2	2.6	2.0	0.6	3.2	3.4	3.7
\bar{x}	75.2	4.1	1.2	3.3	5.6	2.8	0.9	3.0	1.5	2.9
σ	8.6	1.4	0.9	2.5	4.9	1.3	0.8	3.2	1.3	1.2
Waste mixture	XRF (wt.%)									
	Al ₂ O ₃	MgO	Fe ₂ O ₃	TiO ₂	SiO ₂	CaO	K ₂ O	Na ₂ O	Cl	Others
Alw _x	65.9	4.8	1.1	3.5	5.3	3.4	1.7	3.8	8.1	2.4

The higher amounts of other components, such as TiO₂, in some of the wastes (as for example samples Alw₄ and Alw₆) may be related to different types of scrap utilized for the secondary aluminum production. The same may happen for other components like diverse metallic elements (e.g., Fe, Cr, Cu...) also present in the wastes. Additionally, other minor components or traces (collected in the column "others"), including copper, zirconium, manganese, lead, and chromium, can appear in all the wastes.

The variable nature of the samples that come from the aluminum production processes in the secondary industry resulted in a high standard deviation associated with the average chemical composition. Due to this fact, it is necessary to get a representative sample to be used as a raw material for the synthesis of zeolites.

The representative waste sample (Alw_x) included mainly Al₂O₃ 65.9 wt.%, chloride 8.1wt.%, SiO₂ 5.3 wt.%, and small quantities of other oxides, such as MgO, TiO₂, CaO, Na₂O, and Fe₂O₃. The total content of aluminum (34.9 wt.%) is distributed in different aluminum compounds such as: (i) metallic aluminum (Al); (ii) aluminum nitride (AlN); (iii) corundum (Al₂O₃); and (iv) spinel (Al₂MgO₄).

3. RESULTS AND DISCUSSION

Although some of the samples such as Alw₁, Alw₂, and Alw₃ showed very similar chemical compositions, it is not clearly attributable to the fact of their origin company being the same, because the wastes Alw₄-Alw₉, which come from the same company, present some variations in their compositions, in particular for Alw₅ and Alw₆. Then, compositional variations can mostly be attributable to the raw materials and to the manufacture processes.

Therefore, the wastes from the tertiary aluminum production are composed of similar compounds, whose quantities depend mainly on: (i) the type of treated aluminum scraps; (ii) the equipment and conditions used in the scrap treatment; and (iii) the type and amount of inorganic salts/oxides used in the scrap melting processes to recover the aluminum content in such scraps [8]. All these factors contribute to the heterogeneity of these wastes, which require appropriate characterization prior to their use as raw material for the synthesis of zeolites.

Among all the aluminum components in the wastes, only aluminum nitride (AlN) and metallic aluminum (Al) are species soluble in acidic medium. Quantitative analyses of total aluminum, soluble aluminum, and aluminum nitride were determined by wet analytical techniques described in Chapter 2. Table 3.2 collects the content of AlN determined by the Kjeldhal method and the content of Al analyzed by Atomic Absorption Spectroscopy (AAS).

Table 3.2 Aluminum nitride (AlN) and metallic aluminum (Al) contents present in the waste samples determined by the Kjeldhal method and AAS, respectively.

Waste Sample	AlN (wt.%)	Al (wt.%)
Alw ₁	11.8	15.6
Alw ₂	15.3	7.7
Alw ₃	13.7	17.6
Alw ₄	13.7	5.4
Alw ₅	1.4	17.4
Alw ₆	23.6	7.4
Alw ₇	12.6	11.9
Alw ₈	12.7	7.4
Alw ₉	16.0	8.7
\bar{x}	13.3	11.8
σ	5.4	7.5
Alw _x	13.1	12.8

3. RESULTS AND DISCUSSION

As can be observed, the content of these compounds in the wastes varied around 1.4-24 wt.% for AlN and 5-18 wt.% for Al, showing average values (13.3 wt.% and 11.8 wt.%, respectively) very close to those of the representative sample Alw_x (AlN 13.1 wt.% and Al 12.8 wt.%).

Concerning the metallic aluminum content in the waste samples, it was determined as the difference between the content of soluble aluminum and aluminum from AlN. Thus, for sample Alw_x the soluble aluminum content was approximately 21.4 wt.%, while the content of aluminum from AlN was about 8.6 wt.%, leading to a content of metallic aluminum of 12.8 wt.%. The rest (13.5 wt.%) corresponded to the aluminum contained in the insoluble phases such as corundum (7.04 wt.%) and spinel (6.4 wt.%). Table 3.3 summarizes the content of all the aluminum phases present in the representative waste sample Alw_x.

Table 3.3 Content of aluminum in the different aluminum phases of the waste sample Alw_x.

Aluminum from aluminum phases	Aluminum content (wt.%)
Metallic aluminum (Al)	12.84
Aluminum nitride (AlN)	8.60
Corundum (Al ₂ O ₃)	7.04
Spinel (MgAl ₂ O ₄)	6.43
Total aluminum content	34.90

As mentioned in Chapter 1, the main environmental drawbacks of the wastes are derived from their high reactivity with humidity or water leading to the release of certain gases, such as ammonia (NH₃) and hydrogen (H₂).

The volumes of NH₃ and H₂ (expressed as Nm³ per ton of waste) released by the waste samples are shown in Figure 3.1. The NH₃ volume generated by the wastes was determined from the calculated aluminum nitride content (according to reaction (1.1) described in Chapter 1). The volume of H₂ was obtained from the metallic aluminum content (following the reaction (1.4), see Chapter 1). The results indicate that the volume of NH₃ released to atmosphere from these wastes varied between 8 and 129 Nm³ per ton of waste, while the volume of H₂ oscillated from 67 to 219 Nm³ per ton of waste.

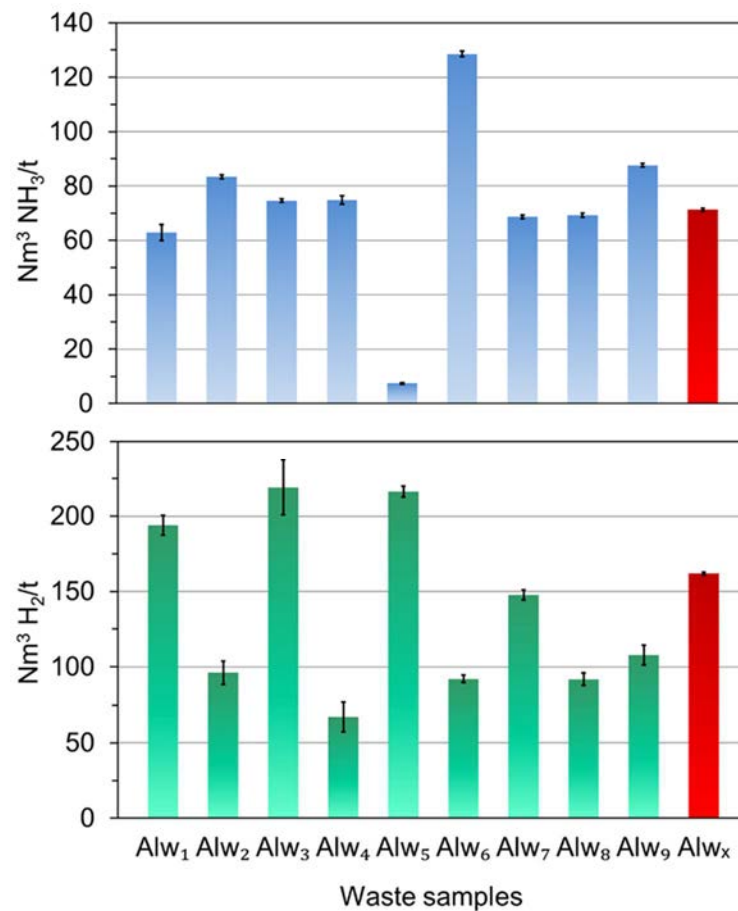


Figure 3.1 Volumes of NH_3 and H_2 released by the wastes.

The highest volume of NH_3 ($129 \text{ Nm}^3/\text{ton}$) was obtained for the sample Alw_6 which was associated with its highest AlN amount (23.6 wt.%). The sample Alw_3 led to the highest volume of H_2 ($219 \text{ Nm}^3/\text{ton}$), determining by its highest Al content (17.6 wt.%). The representative waste sample led to approximately 71 and 162 Nm^3 of NH_3 and H_2 per ton of Alw_x .

Unlike slags from the secondary industry (contents of $\text{AlN} < 5\%$) [147], the wastes from the tertiary aluminum production have higher AlN contents. This is attributable to the phases distribution according to the granulometries in the slag milling treatments developed by the tertiary industry, leading to finest fractions enriched in aluminum nitride and salts.

In relation to other wastes widely used for the synthesis of zeolites such as FA from combustion processes, the wastes from the tertiary aluminum industry possess higher aluminum amount but lower silicon content. Thus, FA presents $\text{Al}_2\text{O}_3/\text{SiO}_2$ ratios ranged 1.2-3.8 [26, 43] while the ratio for Alw_x is 12.4.

3. RESULTS AND DISCUSSION

3.1.2 Mineralogical characterization

The XRD pattern of the representative waste sample is presented in Figure 3.2 along with the corresponding entry numbers (shown in brackets) for each phase, according to the ICDD.

Alw_x mainly consists of different aluminum phases such as corundum (Al₂O₃), aluminum nitride (AlN), and metallic aluminum (Al). In addition, Alw_x also presents other phases, including quartz (SiO₂), spinel (MgAl₂O₄), and metal chlorides such as halite (NaCl) and sylvite (KCl), which derived from inorganic salts in the fluxes used to smelt aluminum scraps. The XRD data confirmed the results from the chemical composition analysis obtained by XRF for the sample Alw_x. Due to the high background of the XRD profile and the number of low intensity reflections, a more complete and accurate identification of phases was not feasible. This XRD background may indicate the presence of non-well crystallized or amorphous phases, including various components such as Fe and Cu oxides.

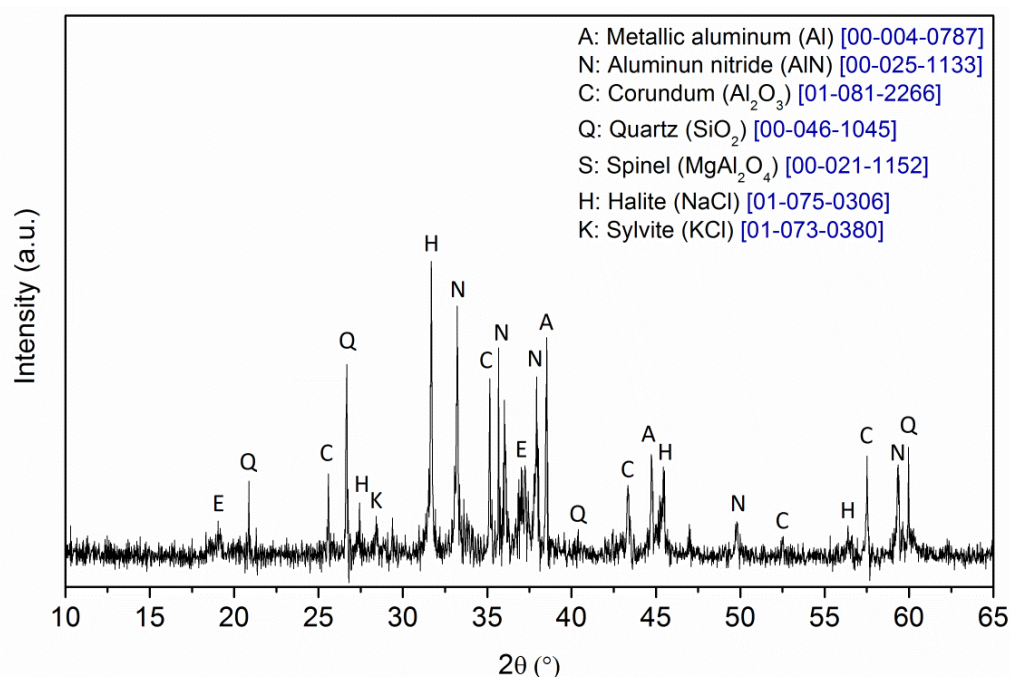


Figure 3.2 XRD pattern of the representative waste sample Alw_x used for the synthesis of zeolites.

From the data of the XRD analysis, a semi-quantitative analysis of crystalline phases was determined by applying the Chung method [114, 115], previously described in

Chapter 2. The quantification of the different mineralogical phases present in Alw_x is collected in Table 3.4.

Table 3.4 Semi-quantitative analysis of crystalline phases in Alw_x determined by the Chung method [114, 115].

Crystalline phase	(%)
Aluminum nitride (AlN)	28.9
Corundum (Al ₂ O ₃)	23.7
Metallic aluminum (Al)	12.6
Halite (NaCl)	12.2
Quartz (SiO ₂)	11.2
Spinel (MgAl ₂ O ₄)	10.0
Sylvite (KCl)	1.4

According to the results obtained by the XRF characterization of Alw_x, the total aluminum content in this sample corresponded to 34.9 wt.%, which was distributed in the following crystalline phases: metallic aluminum (12.8 wt.%), aluminum nitride (8.6 wt.%), corundum (7.0 wt.%), and spinel (6.4 wt.%).

The differences found between the results obtained from the two techniques (XRF and XRD) could be due to the existence of amorphous phases, preferred orientations, etc.

3.1.3 Morphological characterization

In addition to the XRD analysis, the main crystalline phases of Alw_x were identified by means of SEM-EDS elemental analysis. The global morphology of Alw_x was also significantly heterogeneous, presenting fine particles with irregular shapes and with variable sizes, as shown Figure 3.3. The waste was mainly comprised of very fine particles (< 50 μm) and agglomerated particles (< 450 μm) formed by different elements such as Al, Na, Mg, Cl, K, Ca, O, etc., as showed the chemical composition (expressed as atomic %) obtained for Alw_x (Table 3.5).

Among the phases present in the waste, corundum, metallic aluminum, spinel, quartz, halite, and amorphous aluminosilicates were well identified, as showed the SEM images obtained at different magnifications and their microchemical analysis (Figure 3.4 and Table 3.6).

3. RESULTS AND DISCUSSION

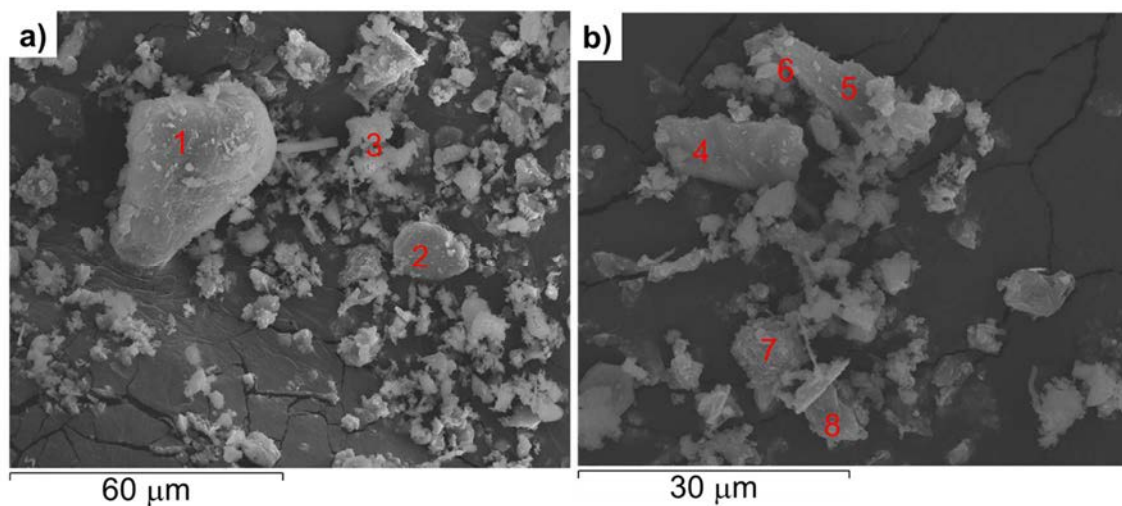


Figure 3.3 General morphology of the representative waste sample Alw_x used for the synthesis of zeolites. SEM images at magnification $\times 1,000$ (a) and $\times 2,000$ (b).

Table 3.5 Microchemical point analyses of the representative waste sample Alw_x (according to Figure 3.3).

Spectrum	Atomic %							Total
	Na	Mg	Al	Cl	K	Ca	O	
1			38.58	6.01			44.24	100
2			40				47.07	100
3	4.4	1.92	32.92	4.86	1.59		54.3	100
4		7.45	34.04				58.51	100
5			38.49	3.77			57.74	100
6	2.7		36.27	5.28			55.75	100
7			40				60	100
8			9.89			37.64	52.47	100

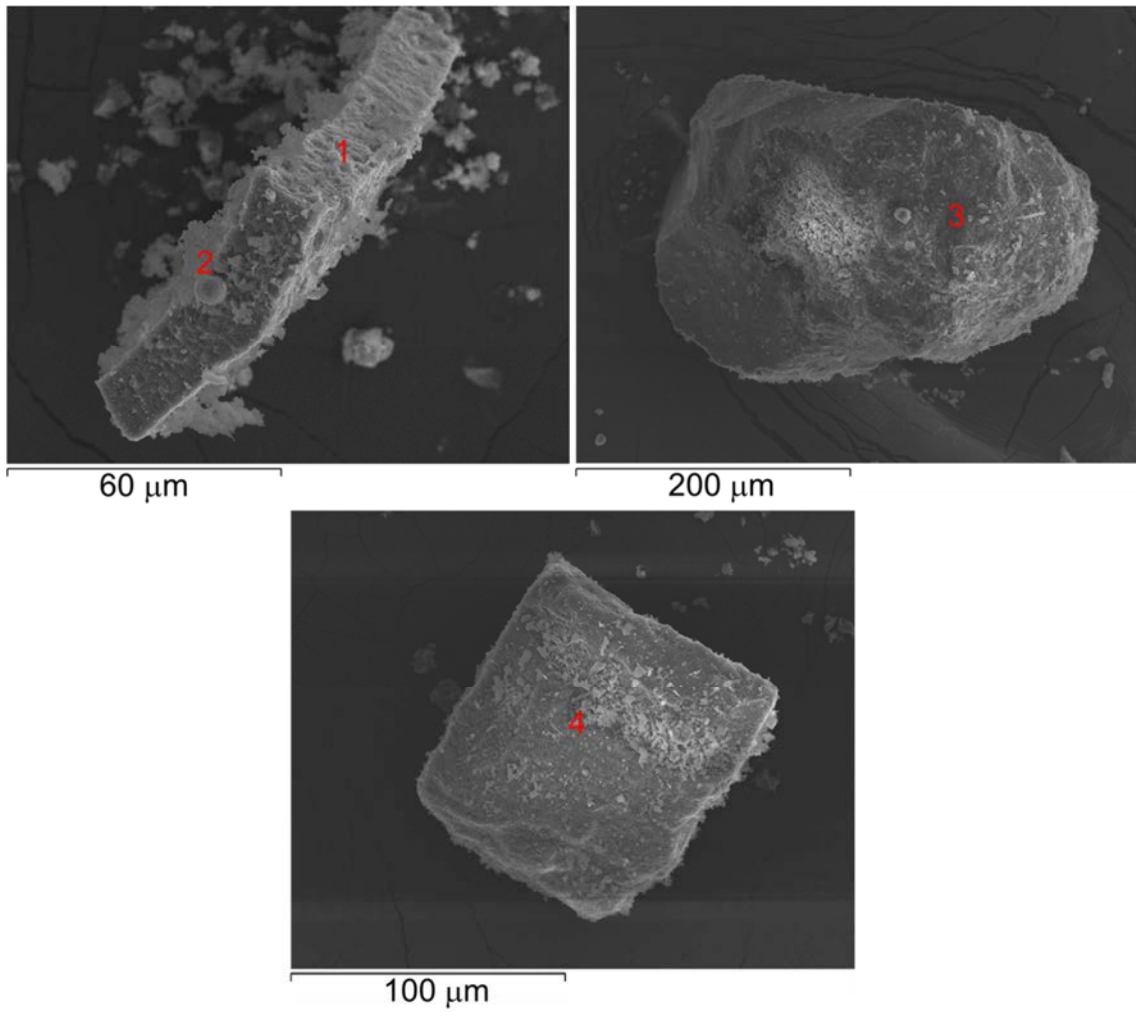


Figure 3.4 Characteristic phases of Alw: Spinel (1) and metallic aluminum (2), SEM image at magnification x1,000; quartz (3), SEM image at magnification x250; and halite (4), SEM image at magnification x400.

Table 3.6 Microchemical point analyses of the representative waste sample Alw (according to Figure 3.4).

Spectrum	Atomic %						
	Na	Mg	Al	Cl	Si	O	Total
1		7.38	34.1			58.52	100
2			40			60	100
3					33.33	66.67	100
4	37.97			43.05		18.98	100

3. RESULTS AND DISCUSSION

All these phases are characteristic of this kind of wastes from the tertiary industry, showing their typical morphologies [3]. For example, spinel (point 1 in Figure 3.4) shows a tabular crystal habit and metallic aluminum (point 2 in Figure 3.4) appears as spherical particles with sizes between 5 and 10 μm , in general, hardly crushed in the slag milling processes in comparison with the other phases and inorganic salts. Among all the components, quartz (point 3 in Figure 3.4) with an irregular shape ($\sim 390 \mu\text{m}$) and halite (point 4 in Figure 3.4) showing a typical cubic morphology (150 μm), were the largest particles found in the waste. The results obtained by SEM also revealed that Alw_x is largely composed of aluminum and other minor elements such as silicon and sodium, that is, the main elements that make up the structure of aluminosilicate zeolites.

3.1.4 Particle size distribution

Table 3.7 collects the PSD based on the particle diameters d_{10} , d_{50} , and d_{90} for the waste samples (Alw_1 - Alw_9). As shown, all the wastes except the sample Alw_5 contain mainly very fine particles with diameters smaller than 30 μm , according to the cumulative size distribution calculated at 50 % (i.e., particle diameter d_{50}).

Table 3.7 Particle size distribution of the waste samples according to their particle diameters d_{10} , d_{50} and d_{90} .

Sample	Particle diameter (μm)		
	d_{10}	d_{50}	d_{90}
Alw_1	2.4	29.0	81.1
Alw_2	2.1	17.8	81.9
Alw_3	0.9	5.1	40.4
Alw_4	1.0	6.0	43.7
Alw_5	7.1	47.4	154.7
Alw_6	2.2	28.0	119.0
Alw_7	3.2	27.4	80.7
Alw_8	2.4	25.9	99.7
Alw_9	2.3	27.9	89.9
\bar{x}	2.5	22.8	92.8
σ	1.7	11.8	39.9

The very fine granulometry of the waste samples comes from the high efficiencies reached in the shredding, milling, and sieving processes for the recovery of aluminum

from slags as well as the suction systems and sleeve filters used to capture the solid aluminum powders (i.e., the finest fraction).

In addition to the release of gases such as NH_3 and H_2 from the wastes, as commented above, this very fine granulometry also contributes to the hazardousness of the wastes. Due to the small size of these waste particles with d_{10} values around $2.5 \mu\text{m}$ (except for Alw_5), their inhalation or penetration into the alveolar region may occur easily [148].

The PSD curves determined by laser diffraction are shown in Figure 3.5. As can be seen, all the waste samples except the sample Alw_5 seem to exhibit a trimodal tendency. The waste samples could be classified in several groups according to their PSD curves which could be associated with their similar chemical composition.

The waste samples Alw_1 , Alw_2 , Alw_7 , Alw_8 , and Alw_9 exhibited diameters d_{10} , d_{50} , and d_{90} ranged between 2 and $100 \mu\text{m}$ that were very similar to the average values ($3\text{-}93 \mu\text{m}$).

The samples Alw_3 and Alw_4 showed values oscillating between 1 and $44 \mu\text{m}$, which were lower than the average diameter values.

The samples Alw_5 and Alw_6 presented the highest diameters d_{90} (155 and $119 \mu\text{m}$, respectively) that could come from coarse particles such as quartz or salt fluxes (NaCl and KCl). In fact, it could be attributable to the sample Alw_5 which showed the highest amounts in SiO_2 and Na_2O , as showed the chemical analysis obtained by XRF.

3. RESULTS AND DISCUSSION

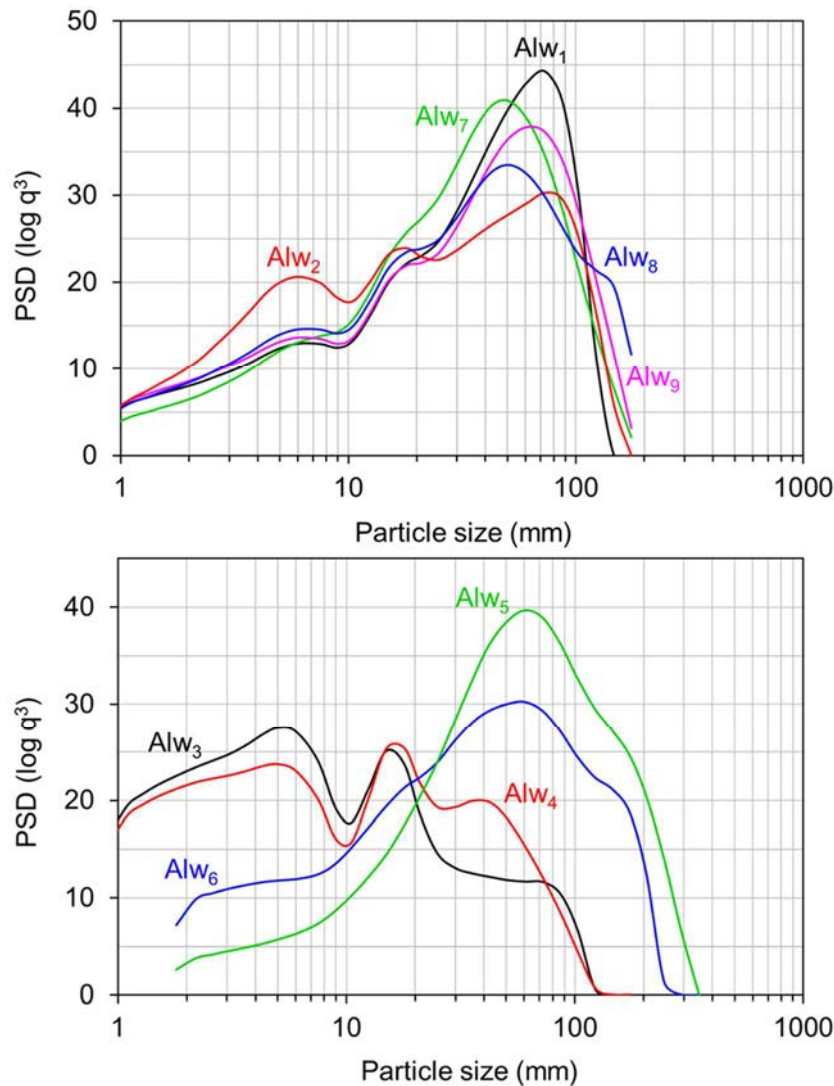


Figure 3.5 Particle size distribution (PSD) of the waste samples.

The PSD has a great influence on the reactivity of the wastes, and accordingly on the synthesis of zeolites. The finer the grain size distribution, the greater the waste reactivity is. In addition, fine waste particles containing essential elements such as aluminum and silicon are more easily dissolved in alkaline conditions during the synthesis of zeolites.

3.1.5 Leaching behavior

As mentioned in Chapter 1, the incorrect accumulation and disposal of the wastes can lead to soil degradation and even to groundwater contamination because of the potential leaching of its harmful elements. To provide a better insight of the leaching characteristics of the wastes, their leaching behavior was evaluated using aqueous

3. RESULTS AND DISCUSSION

solutions and 4 % acetic acid solutions with an initial pH of approximately 7 and 2.5, respectively, as leaching fluids following the methodology TCLP [117].

Table 3.8 and Table 3.9 collect the concentrations analyzed by ICP-OES for the elements leached from the wastes after the acid and aqueous treatments. As can be seen, after the acidic extraction (initial pH ~ 2.5), the major elements leached from the wastes were Al, Na, K, Ca, Mg, Fe, Si, and Zn. The highest amounts of aluminum and silicon leached from the wastes were found at acidic pH conditions. The elements leached from the wastes could be directly related to their chemical composition. Thus, the highest concentrations of Si, Na, and Mg in acid conditions were found for the sample Alw₅ due to its high contents in these elements compared with the other waste samples. The acid treatment of Alw₄ led to the highest concentration of Ca leached as indicated the highest amount of this element in this waste sample.

Table 3.8 Concentrations of elements present in the leachates after acid treatment.

Element (µg/mL)	Leaching fluid: 4 % acetic acid solution									
	Alw ₁	Alw ₂	Alw ₃	Alw ₄	Alw ₅	Alw ₆	Alw ₇	Alw ₈	Alw ₉	Alw _x
Ca	796	553	454	2546	467	457	461	1428	864	780
K	398	430	374	146	1110	1214	945	765	528	790
Na	3682	2604	3001	210	6052	72	2694	918	2763	2273
Mg	435	350	284	527	1270	329	374	439	358	460
Si	110	121	90	208	450	79	216	222	107	162
Fe	65	10	31	108	30	122	76	215	65	99
Al	3529	1720	2228	1330	3557	2612	3772	2574	1931	2328
Mn	12	5	16	12	46	44	14	15	45	13
P	6.4	0.65	0.84	2.5	0.56	5.9	5.9	9.8	5.5	1.7
Ti	1.1	1.4	1	0.9	0.97	1.7	0.8	0.9	0.6	0.704
Ni	5	1.8	1.2	1.4	0.52	3	1.4	3	4	1.6
Cu	0.11	<0.05	<0.05	<0.05	0.71	0.19	0.08	<0.05	<0.05	0.08
Co	0.14	0.09	<0.07	0.12	<0.05	0.07	<0.05	0.20	0.14	0.07
Cr	1.5	0.27	0.24	0.84	0.26	0.93	1.1	2.4	0.56	1.8
Ba	0.52	0.43	0.3	0.31	0.34	6.7	1.2	1.1	0.69	0.32
Cd	0.05	<0.05	<0.05	<0.05	<0.05	0.084	0.06	0.13	0.06	<0.01
Sr	5	3.5	2.9	8.3	19	9	3	9.5	8	5.5
Li	0.08	0.45	0.45	0.58	0.86	0.38	0.18	0.34	0.10	0.18
Zn	11	5.8	9.4	32	33	25	364	157	10	53
As	<0.1	<0.05	<0.05	<0.05	<0.05	<0.1	<0.1	<0.1	<0.1	<0.05
Pb	0.08	1.3	1.7	0.46	1.1	1.4	<0.05	1.2	0.18	0.13

3. RESULTS AND DISCUSSION

Table 3.9 Concentrations of elements present in the leachates after aqueous treatment.

Element ($\mu\text{g/mL}$)	Leaching fluid: aqueous solution									
	Alw ₁	Alw ₂	Alw ₃	Alw ₄	Alw ₅	Alw ₆	Alw ₇	Alw ₈	Alw ₉	Alw _x
Ca	123	95	85	215	91	16	<0.5	186	128	31
K	336	345	275	89	777	304	623	556	396	284
Na	3917	2433	2700	235	4819	28	2268	893	2707	2640
Mg	0.5	6	7	2	1	24	<0.5	<0.5	<0.5	14
Si	6	1	2	2	0.12	5	6	5.8	6	4
Fe	<0.1	<0.05	<0.05	<0.05	<0.05	<0.1	<0.1	<0.1	<0.1	<0.01
Al	3.6	33	48	32	102	3.8	8.5	6.8	5.6	17
Mn	<0.1	<0.05	<0.05	<0.05	<0.05	0.25	<0.1	<0.1	<0.1	<0.005
P	0.46	0.25	0.26	0.1	0.06	0.18	0.23	1.2	0.46	0.12
Ti	<0.1	<0.10	<0.10	<0.10	<0.10	<0.1	<0.1	<0.1	<0.1	<0.03
Ni	<0.1	<0.05	<0.05	<0.05	<0.05	<0.1	<0.1	<0.1	<0.1	<0.01
Cu	<0.05	<0.05	<0.05	<0.05	<0.05	<0.05	0.23	<0.05	<0.05	0.02
Co	<0.05	<0.05	<0.05	<0.05	<0.05	<0.05	<0.05	<0.05	<0.05	<0.010
Cr	<0.05	<0.05	<0.05	<0.05	<0.05	<0.05	<0.05	<0.05	<0.05	<0.010
Ba	0.28	0.16	0.18	0.06	<0.05	0.06	<0.05	0.25	0.31	0.29
Cd	<0.05	<0.05	<0.05	<0.05	<0.05	<0.05	<0.05	<0.05	<0.05	<0.01
Sr	3	1.5	1.7	2.2	0.25	0.4	0.05	2.5	3	0.3
Li	<0.02	0.42	0.42	0.42	0.42	0.03	<0.02	0.02	<0.02	0.01
Zn	<0.05	<0.05	0.06	<0.05	<0.05	<0.05	<0.05	<0.05	<0.05	0.01
As	<0.1	<0.05	<0.05	<0.05	<0.05	<0.1	<0.1	<0.1	<0.1	<0.05
Pb	<0.05	<0.1	<0.100	<0.100	<0.100	<0.05	0.06	<0.05	<0.05	<0.05
V	<0.05	<0.05	<0.05	<0.05	0.4	0.125	0.07	<0.05	0.07	0.1

Additionally, minor elements such as Sr, Cr, P, Ni, Ti, V, Ba, Li, and Pb were also identified in the leachates analyzed at both acid and aqueous conditions. Thus, some of the elements present in the tertiary aluminum wastes seem to show a pH-dependent leaching behavior.

Some investigations on the characterization of other wastes such as FA analyze the leaching behavior of this waste as a function of the pH [149, 150]. For example, Gitari et al. [150] studied the leaching characteristics of different soluble species (Ca, Mg, Na, K, Li, Si, Al, etc.) in FA under alkaline and acid conditions. The authors reported that elements such as aluminum and silicon were easily leached at acidic pH, while their concentrations were minimal as the pH increased. At neutral and slightly alkaline conditions (pH = 6–9), aluminum seems to hardly leach from FA due to its precipitation as $\text{Al}(\text{OH})_3$ amorphous, and to increase again around pH = 11. On the contrary,

elements such as sodium and potassium present in FA could show a pH-independent behavior.

The main hazardous characteristics and properties of the aluminum wastes from the tertiary industry are associated with their heterogeneous chemical and mineralogical composition, spontaneous and high reactivity with water or humidity, very fine granulometry, and leaching behavior when they are exposed specifically to acid pH conditions. Moreover, some of the harmful elements, such as heavy metals (Pb, Ni, Cd, etc.), leached from the wastes can involve concentrations above the concentration limits established in the environmental legislation [78]. Therefore, a correct management of these wastes is needed since their inappropriate disposal can entail serious environmental risks.

In this thesis, the re-use of the wastes from the tertiary industry as raw materials for the preparation of zeolites, added-value materials of industrial interest, is proposed in order to minimize the environmental impacts associated with these wastes.

3. RESULTS AND DISCUSSION

3.2 Lab-scale synthesis of zeolites

Aluminosilicate-type zeolites are commonly formed in the $\text{Na}_2\text{O}-\text{Al}_2\text{O}_3-\text{SiO}_2-\text{H}_2\text{O}$ reaction system where aluminum and silicon are the essential elements in their tetrahedral units and sodium acts as the main extra-framework cation to balance their charge. In this thesis, the waste from the tertiary aluminum industry is used as the main source for the zeolite synthesis, due to its high aluminum content, but it needs an extra contribution of sodium and silicon.

The zeolitization process developed to transform completely an aluminum waste into a zeolite was firstly studied on laboratory scale to investigate the influence of some experimental factors, such as agitation, time, alkalizing agent concentration, temperature, liquid/solid ratio, and recycling of mother liquor (ML), on the synthesis and resulting products.

According to the characterization of the wastes (Section 3.1), the representative waste sample (Alw_x) was selected to develop the zeolitization experiments. Working with a representative sample is the usual way of operating in the industry to avoid the fluctuations in the chemical and mineralogical composition, especially when the raw materials are wastes.

Most results presented in Section 3.2 were previously published in a peer-reviewed publication [16] and a patent [151].

3.2.1 Lab-scale synthesis of NaP1, SOD, and ANA zeolites

The results obtained for the different laboratory conditions tested to synthesize zeolites from Alw_x are summarized in Table 3.10 which includes the type of zeolitic phase as well as the reaction yield (expressed as mass of product per mass of waste) obtained after the synthesis tests.

The formation of different types of zeolite depended on parameters such as the NaOH concentration and temperature. Thus, three different types of zeolites, NaP1, sodalite (SOD), and analcime (ANA), were achieved from the waste via the simple and one-step hydrothermal process. For a short synthesis time (6 h), the best conditions to obtain NaP1 as the only crystalline phase were 120 °C and 1 M NaOH. SOD was also obtained

3. RESULTS AND DISCUSSION

at 120 °C but using the highest NaOH concentration (5 M) tested, while ANA was synthesized at the highest temperatures (160 and 200 °C) using 1 M NaOH.

Table 3.10 Experimental lab-scale synthesis conditions used to obtain zeolites from the waste, zeolitic phases and reaction yields obtained.

Sample	t (h)	NaOH (M)	T (°C)	Liquid/solid ratio (mL/g)	Phase	Yield (kg _{zeolite} /kg _{waste})	
Z1	3	1	120	25	NaP1+amorphous	2.25	
Z2					NaP1	2.38	
Z3	6				NaP1	2.39	
Z4					NaP1	2.35	
Z5	6	3	80		NaP1+SOD	2.15	
Z6		4			NaP1+SOD	2.13	
Z7		5	90		SOD	2.17	
Z8		1			120	Amorphous	1.80
Z9						NaP1	1.86
Z10						100	NaP1
Z11				140		NaP1+ANA	2.38
Z12				160		ANA	2.34
Z13				200		ANA	2.39
Z14				120		15	NaP1
Z15	7.5		NaP1				2.29

As observed, most experimental conditions studied were suitable for the formation of zeolitic phases due to the high solubility of some aluminum compounds, such as metallic aluminum and aluminum nitride, from Al_w and the presence of dissolved silicon in alkaline medium.

The experimental conditions tested allowed the complete hydrothermal conversion of the waste into zeolite via a simple one-step synthesis process, even without using a previous activation step of the waste or any organic template.

It is noticeable that the high reaction yields were obtained, which ranged between 2.2 and 2.5 kg of zeolite per kg of waste. In addition, the synthesis process developed did not generate new solid residues.

As the initial molar ratio of silicon/aluminum (Si/Al) was the same for all the synthesis tests, the formation, crystal growth, and type of zeolite depended on the rest of experimental factors (agitation, time, alkalizing agent concentration, temperature, and

3. RESULTS AND DISCUSSION

liquid/solid ratio). This was confirmed from the results of XRD, SEM, FTIR, TG-DTA, and textural analysis, as will be shown below.

Different types of zeolites such as NaP1, SOD, and ANA were achieved from the same waste (Alw_x) by means of varying the synthesis conditions, in particular the alkalizing agent concentration and temperature.

The effects of the different synthesis parameters on the zeolitization process and resulting products are described in detail below.

The values of the diffraction angle (2θ), full width at half maximum (FWHM), and crystallite size (D_{hkl}) measured by the Scherrer equation [113] for the most intense diffraction peak of each sample are shown in Table 3.11.

Table 3.11 Peak parameters (2θ and FWHM) and crystallite sizes (D_{hkl}) calculated for the samples obtained from the waste via the lab-scale synthesis.

Sample	Phase	hkl	2θ (°)	FWHM (°)	D_{hkl} (nm)
Z1	NaP1+amorphous	301	28.09	0.31	27
Z2	NaP1	301	28.11	0.33	25
Z3	NaP1	301	28.07	0.31	26
Z4	NaP1	301	28.06	0.26	32
Z5	NaP1 (43 %)	301	28.02	0.32	26
	SOD (57 %)	211	24.38	0.24	34
Z6	NaP1 (30 %)	301	28.12	0.22	23
	SOD (70 %)	211	24.43	0.36	38
Z7	SOD	211	24.43	0.25	32
Z8	Amorphous	-	-	-	-
Z9	NaP1	301	28.17	0.67	12
Z10	NaP1	301	28.06	0.27	31
Z11	NaP1 (66 %)	301	28.06	0.29	28
	ANA (34 %)	400	25.86	0.15	54
Z12	ANA	400	25.86	0.12	68
Z13	ANA	400	25.88	0.11	73
Z14	NaP1	301	28.11	0.27	31
Z15	NaP1	301	28.06	0.27	30

3.2.1.1 Effect of agitation

The effect of agitation on the resulting products was investigated using 1 M NaOH at 120 °C and for 3 h. The stirring speed used for the zeolite synthesis was fixed at 900 rpm. Figure 3.6 shows the XRD patterns of the samples synthesized without and with agitation (Z1 and Z2, respectively).

Both conditions led to obtain the same zeolitic phase that was characterized by the zeolite NaP1 (ICDD PDF 01-071-0962) based on the framework type gismondine (its crystallographic properties can be found in Annex I). The most intense 301 basal reflection of NaP1 was identified at very similar 2θ values in both samples: 28.09 and 28.11° for Z1 and Z2, respectively (Table 3.11).

However, the sample Z1 obtained via the synthesis without agitation showed a lower crystallinity. It could be related to the incomplete synthesis reaction caused by the partial dissolution of the aluminum and silicon sources, in particular corundum and quartz, present in Alw_x . In addition, the background signal obtained in the XRD pattern of this sample would indicate the presence of amorphous phase.

The sample Z2 prepared under homogeneous stirring conditions showed a better crystallinity and a higher reaction yield (2.4 kg of zeolite per kg of waste).

These results demonstrated that the crystallization of zeolites like NaP1 from Alw_x is very sensitive to agitation, which would favor the reagents dissolution, homogeneous reaction suspension, and uniform temperature in the reaction system [152].

As the formation of zeolites from Alw_x was found to be positively favored by using agitation, the following experiments were carried out under homogeneous stirring conditions (900 rpm).

3. RESULTS AND DISCUSSION

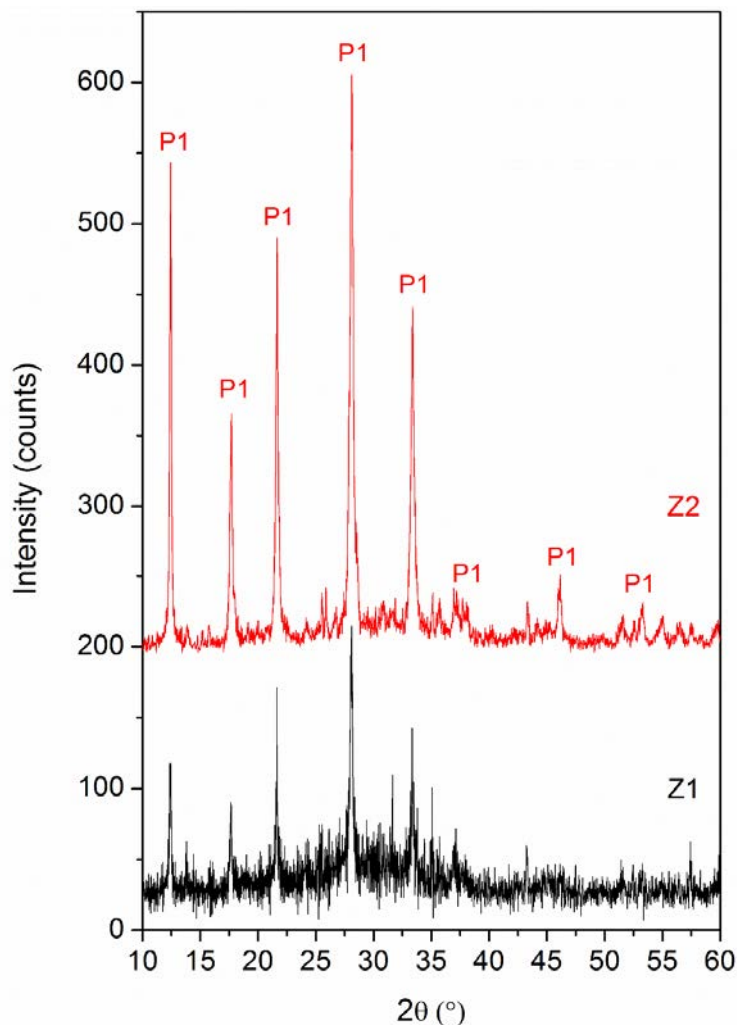


Figure 3.6 XRD patterns of zeolite NaP1 obtained from the waste at 120 °C for 3 h using 1 M NaOH without (Z1) and with (Z2) agitation. P1 = NaP1 (ICDD PDF 01-071-0962).

3.2.1.2 Effect of time

The synthesis time is another important factor mainly affecting the formation and crystal growth of zeolites. The XRD patterns of the samples obtained at 3, 6, and 24 h for a fixed temperature (120 °C) and using a fixed NaOH concentration (1 M) are shown in Figure 3.7.

In all the samples, NaP1-type zeolite was identified (ICDD PDF 01-071-0962) as the only zeolite phase. Well-defined diffraction profiles were obtained and no shifts of the 2θ values were observed for the samples prepared at 3, 6, and 24 h (Z2, Z3, and Z4, respectively).

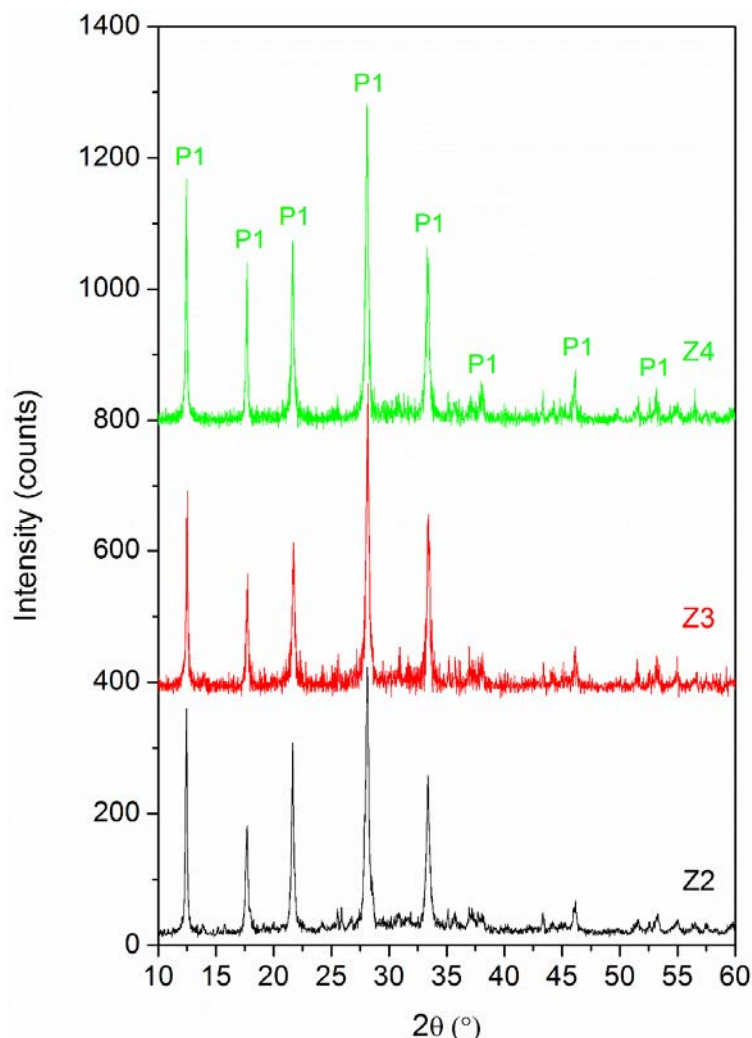


Figure 3.7 XRD patterns of zeolite NaP1 obtained from the waste at 120 °C and with 1 M NaOH for 3 h (Z2), 6 h (Z3), and 24 h (Z4) with stirring. P1 = NaP1 (ICDD PDF 01-071-0962).

Table 3.12 shows as examples the Miller indices (*hkl*), peak parameters (2θ and FWHM), and relative intensities corresponded to the samples Z3 and Z4.

The 301 basal reflections of the samples were centered at 28.11, 28.07, and 28.06° for Z2, Z3, and Z4, respectively (Table 3.11), which are almost identical to the NaP1 value (28.10°) reported in the literature [153].

The crystal growth of the zeolites depended on the time used during the synthesis process. The crystallinity of the samples increased as the reaction time increased, as can be seen from the sharpness of the peaks (Figure 3.7). The most crystalline NaP1 was obtained for 24 h (Z4). An increase of the time from 6 to 24 h seems to increase the crystallite size of the zeolite from 26 to 32 nm (sample Z3 and Z4, respectively).

3. RESULTS AND DISCUSSION

Table 3.12 Miller indices (hkl), peak parameters (2θ and FWHM), and relative intensities (I_{rel}) for NaP1 obtained for 6 h (sample Z3) and 24 h (sample Z4).

hkl	Z3			Z4		
	2θ (°)	FWHM (°)	I_{rel} (%)	2θ (°)	FWHM (°)	I_{rel} (%)
101	12.39	0.17	67.23	12.42	0.16	78.09
200	17.64	0.23	40.22	17.66	0.21	47.60
112	21.63	0.24	50.71	21.63	0.21	59.01
301	28.07	0.31	100.00	28.08	0.31	100.00
312	33.34	0.31	57.04	33.37	0.36	50.69

Additionally, the SEM analysis performed to characterize the morphology of the zeolitic phases also demonstrated that as the time increases from 6 h (Figure 3.8a-b) to 24 h (Figure 3.8c-e) the crystal size of NaP1 obtained from Alw_x also increases. The samples Z3 and Z4 obtained after 6 and 24 h exhibited an identical morphology formed by both spherical primary and smaller secondary aggregates containing nano-size cubic crystals, which are typical of NaP1. However, the sample prepared for 24 h showed nanocrystals with edges (277-364 nm) bigger than those ones obtained for 6 h (150-345 nm).

The results are in agreement with those reported in the literature. For example, Sharma et al. [154] studied the influence of time on the synthesis of NaP1 prepared at 100 °C from the use of commercial reagents (sodium aluminate, water glass, sodium hydroxide, and water). The authors obtained amorphous phases after short crystallization times (≤ 2 h), while times ≥ 3 h favored the formation and crystal growth of NaP1.

The amount of zeolite NaP1 synthesized from Alw_x was approximately 2.4 kg per kg of waste (Table 3.10) for the different periods of time tested (3, 6, and 24 h).

Generally, reaction times as long as 24 h are not profitable industrially, being more convenient the use of shorter times to improve the productivity of the synthesis process.

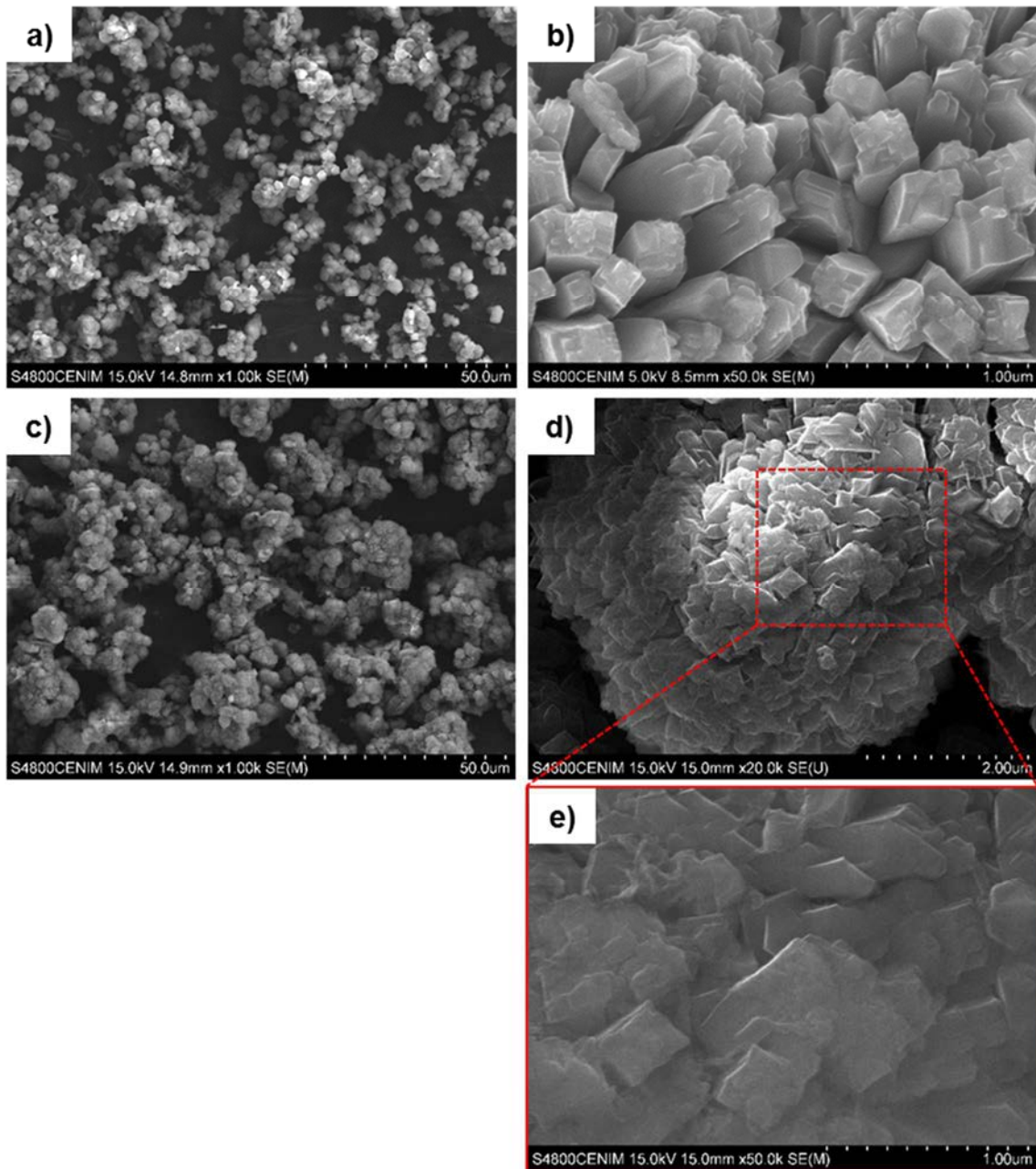


Figure 3.8 SEM images of the zeolite NaP1 obtained at 120 °C with 1 M NaOH and a liquid/solid ratio of 25 mL/g for different times: (a-b) 6 h (sample Z3) and (c-e) 24 h (sample Z4).

As a reaction time of 6 h was suitable to obtain a high reaction yield as well as well-crystallized products from the use of Alw_x , it was selected to perform the following synthesis tests studying the effect of other factors (alkalizing agent concentration, temperature, liquid/solid ratio, and ML recycling) on the resulting materials.

3. RESULTS AND DISCUSSION

3.2.1.3 Effect of alkalinizing agent concentration

The concentration of the alkalinizing agent (NaOH) strongly influences the type of zeolite synthesized due to the presence of sodium cations (Na^+) in the reaction system.

Figure 3.9 shows the XRD patterns of the samples synthesized varying the NaOH concentration (1, 3, 4, and 5 M, samples Z3, Z5, Z6, and Z7, respectively) for a fixed time (6 h) and constant temperature (120 °C).

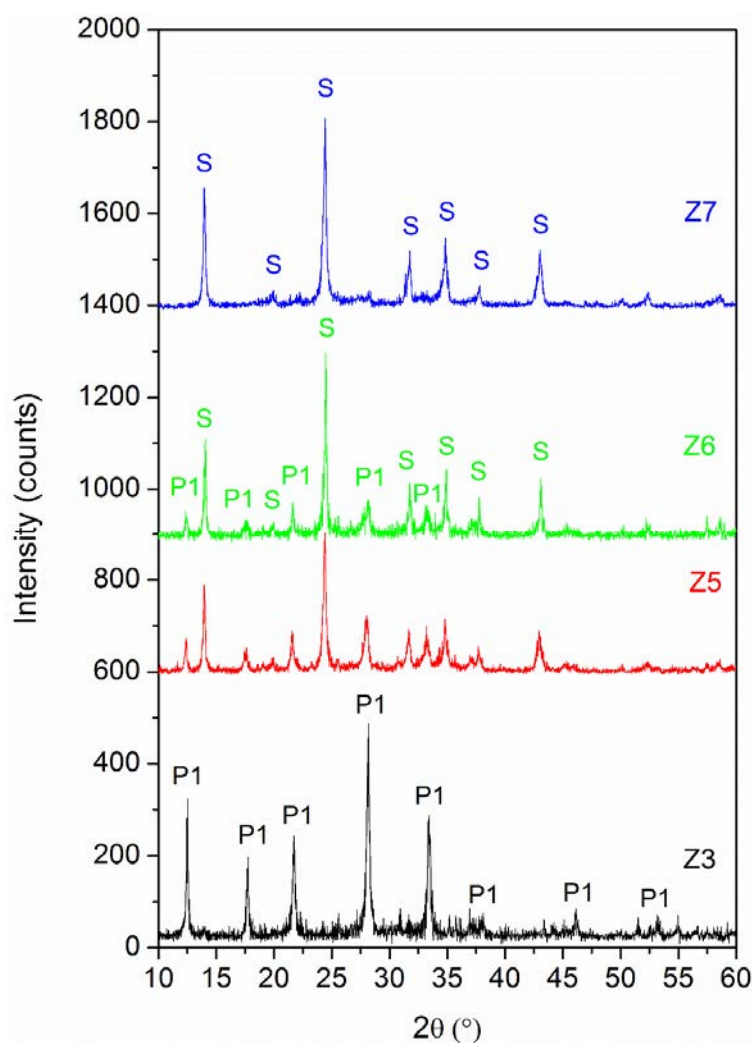


Figure 3.9 XRD patterns of the samples obtained from the waste at 120 °C for 6 h with a NaOH concentration of 1 M (Z3), 3 M (Z5), 4 M (Z6), and 5 M (Z7). P1 = NaP1 (ICDD PDF 01-071-0962) and S = hydroxy-sodalite (ICDD PDF 01-076-1639) and/or chloride-sodalite (ICDD PDF 01-086-1844).

When the alkali concentration increased, from 1 to 5 M, both the peak intensity and the crystallite size corresponding to the NaP1 phase gradually decreased due to the

formation of a new phase identified by the SOD zeolite (crystal structure described in Annex I). Due to the coincidence of the XRD patterns of hydroxy-sodalite (ICDD PDF 01-076-1639) and chloride-sodalite (ICDD PDF 01-086-1844), it was not possible to decide between both phases unambiguously.

For the samples Z5 and Z6, as the NaOH concentration was increased from 3 to 4 M, the crystallite size of the NaP1 phase slightly diminished, and the percentage of this phase varied from 43 to 30 %, respectively (Table 3.11). Concerning the crystallite size of the SOD phase, it did not vary significantly in the samples Z5 and Z6.

SOD was obtained as the only crystalline phase characterized by its most intense 211 basal reflection centered at 24.43° in the sample Z7, which corresponds to the highest NaOH concentration (5 M). The amount of SOD obtained per kg of waste was 2.2 kg.

The Miller indices (hkl), peak parameters (2θ and FWHM), and relative intensities that characterize to the SOD zeolite (sample Z7) are summarized in Table 3.13.

Table 3.13 Miller indices (hkl), peak parameters (2θ and FWHM), and relative intensities (I_{rel}) for SOD (sample Z7).

hkl	2θ (°)	FWHM (°)	I_{rel} (%)
110	13.98	0.23	64.43
211	24.43	0.29	100.00
310	31.75	0.35	27.79
222	34.83	0.32	35.89
330	43.02	0.39	30.32

In the case of the samples obtained with 3 and 4 M NaOH concentration, no shift of the 2θ value of the diffraction maximum peak was observed (Table 3.11).

The crystallinity as well as the morphology of the zeolitic phases from Alw_x were found to be dependent on the NaOH concentration used during the zeolitization process. It was confirmed from the SEM characterization (Figure 3.10) showing that an increase of the NaOH concentration from 3 to 5 M (sample Z5 and Z7, respectively) results in an increase of the crystal size of the SOD zeolite. Although both samples exhibited the typical SOD morphology, which is composed of spherical aggregates with hexagonal tabular crystals, bigger crystal sizes were obtained when using the highest NaOH concentration (5 M).

3. RESULTS AND DISCUSSION

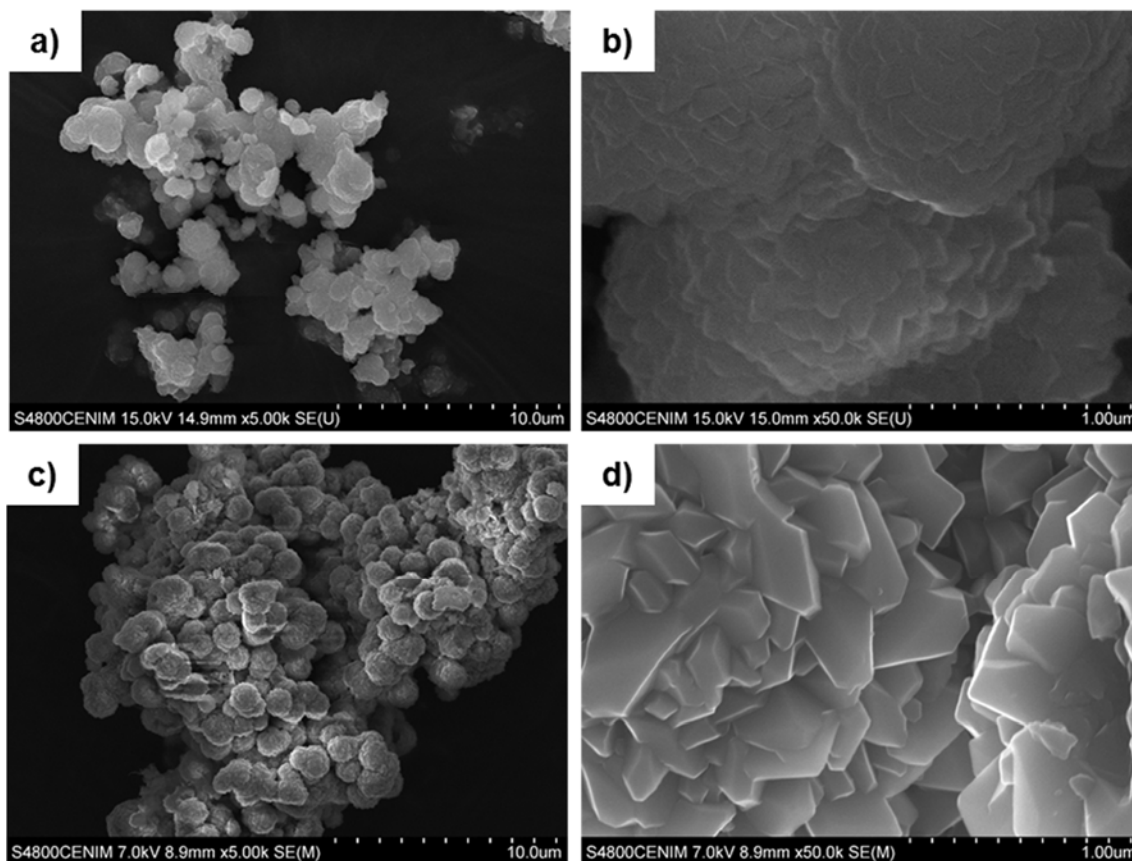


Figure 3.10 SEM images of the SOD zeolite obtained at 120 °C for 6 h with a liquid/solid ratio of 25 mL/g and different NaOH concentrations: (a-b) 3 M (sample Z5) and (c-d) 5 M (sample Z7).

During the zeolite synthesis, the interactions between the negatively charged aluminosilicates and cations in the reaction suspension are extremely important in determining the final zeolite structure.

The reviewed literature reports the influence of the Na^+ cations on the crystallization of Na-type zeolites as NaP1 [155]. For instance, Murayama et al. [155] studied the role of the Na^+ and K^+ cations on the synthesis of zeolites from FA varying the type and concentration of the alkali solution. The authors reported that the crystal structure of the products changes from zeolite P to hydroxy-sodalite via co-crystallization. Wang et al. [156] also observed the transformation of zeolite A obtained from FA into hydroxy-sodalite by increasing the NaOH concentration. The authors established that it is attributable to an extinction effect of the small crystallites of zeolite A, instead of the reduction in crystallinity of this phase. In our case, the decrease of the crystallite size as the NaOH concentration increased supports this last statement.

3.2.1.4 Effect of temperature

The XRD patterns of the samples prepared at different temperatures 80, 90, 100, 120, 140, 160, and 200 °C (samples Z8, Z9, Z10, Z3, Z11, Z12, and Z13, respectively) for a fixed crystallization time (6 h) and using a fixed NaOH concentration (1 M) are shown in Figure 3.11.

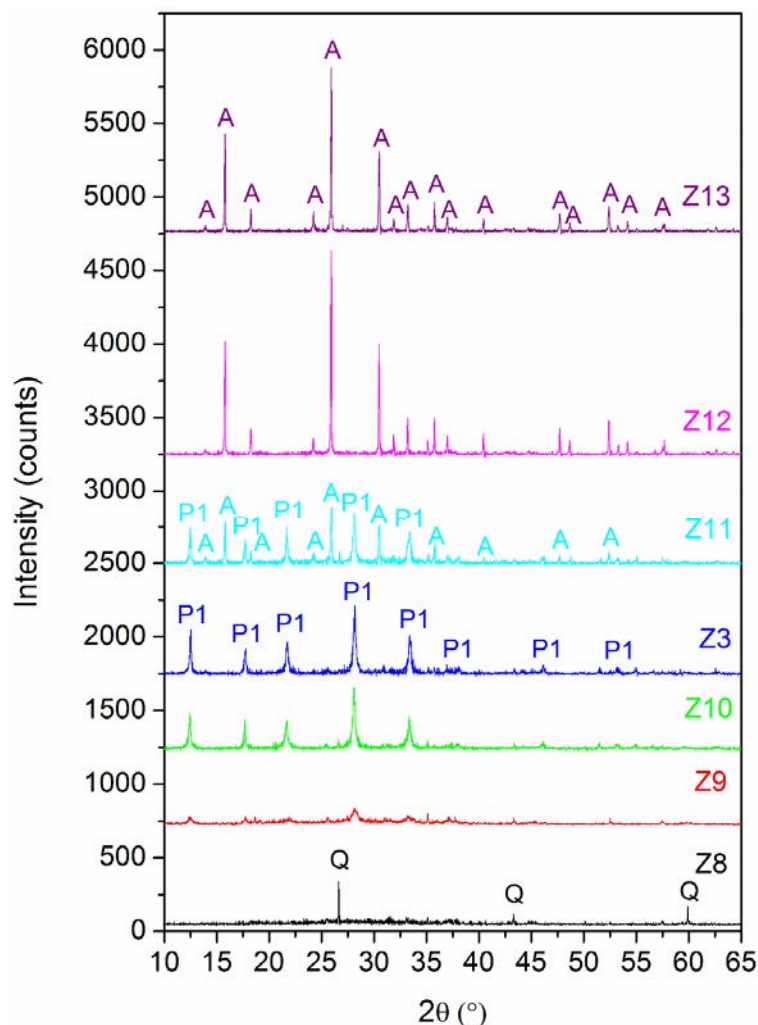


Figure 3.11 XRD patterns of the samples synthesized with 1 M NaOH for 6 h at 80 °C (Z8), 90 °C (Z9), 100 °C (Z10), 120 °C (Z3), 140 °C (Z11), 160 °C (Z12), and 200 °C (Z13). P1 = NaP1 (ICDD PDF 01-071-0962), A = analcime (ICDD PDF 00-041-1478), and Q = quartz (ICDD PDF 00-046-1045).

For the samples Z9, Z10, and Z3 obtained at 90, 100, and 120 °C, respectively, all their diffraction peaks were attributable to zeolite NaP1. The XRD profiles of these samples indicate the increase of both their crystallite sizes (Table 3.11) and crystallinities as the temperature increases.

3. RESULTS AND DISCUSSION

The amount of zeolite NaP1 per kg of waste also increased with the temperature, showing values higher than 2.0 kg at temperatures above 100 °C.

The tests developed at both 160 and 200 °C (Z12 and Z13, respectively) led to the formation of ANA as the only zeolite phase (ICDD PDF 00-041-1478). Both sample Z12 and Z13 showed diffraction profiles composed of well-defined and narrow peaks that are characteristic of highly crystalline samples. The most intense 400 reflection of ANA was centered at 25.86 and 25.88° for Z12 and Z13, respectively, which is quite similar to the ANA value (25.96°) found in the literature [153]. The crystallographic properties of this zeolite can be found in Annex I.

Table 3.14 shows as an example the Miller indices (hkl), peak parameters (2θ and FWHM), and relative intensities corresponding to ANA (sample Z13).

Table 3.14 Miller indices (hkl), peak parameters (2θ and FWHM), and relative intensities (I_{rel}) for ANA (sample Z13).

hkl	2θ (°)	FWHM (°)	I_{rel} (%)
211	15.75	0.09	72.37
400	25.88	0.12	100.00
332	30.46	0.15	49.15
431	33.18	0.18	15.71
651	52.34	0.21	13.64

The increase of temperature from 160 to 200 °C involved the increase of crystallite size of the ANA phase (Table 3.11).

As occurred with the time and NaOH concentration, the temperature also affects the formation and crystal growth as well as the morphology of the zeolites from Alw_x. The influence of this parameter on the morphology of the zeolitic phases is shown in Figure 3.12. The samples obtained at 160 and 200 °C (sample Z12 and Z13, respectively) showed the same morphology formed by trapezohedron crystals, which are characteristic of ANA [157]. The crystal size of the ANA zeolite increases when the temperature increases from 160 to 200 °C. Thus, bigger trapezohedron crystals with sizes ranged between 5 and 11 μm (Figure 3.12a-b) were achieved at the highest temperature tested (200 °C) compared with those crystals (2-8 μm) obtained at lower temperature (160 °C) (Figure 3.12c-d).

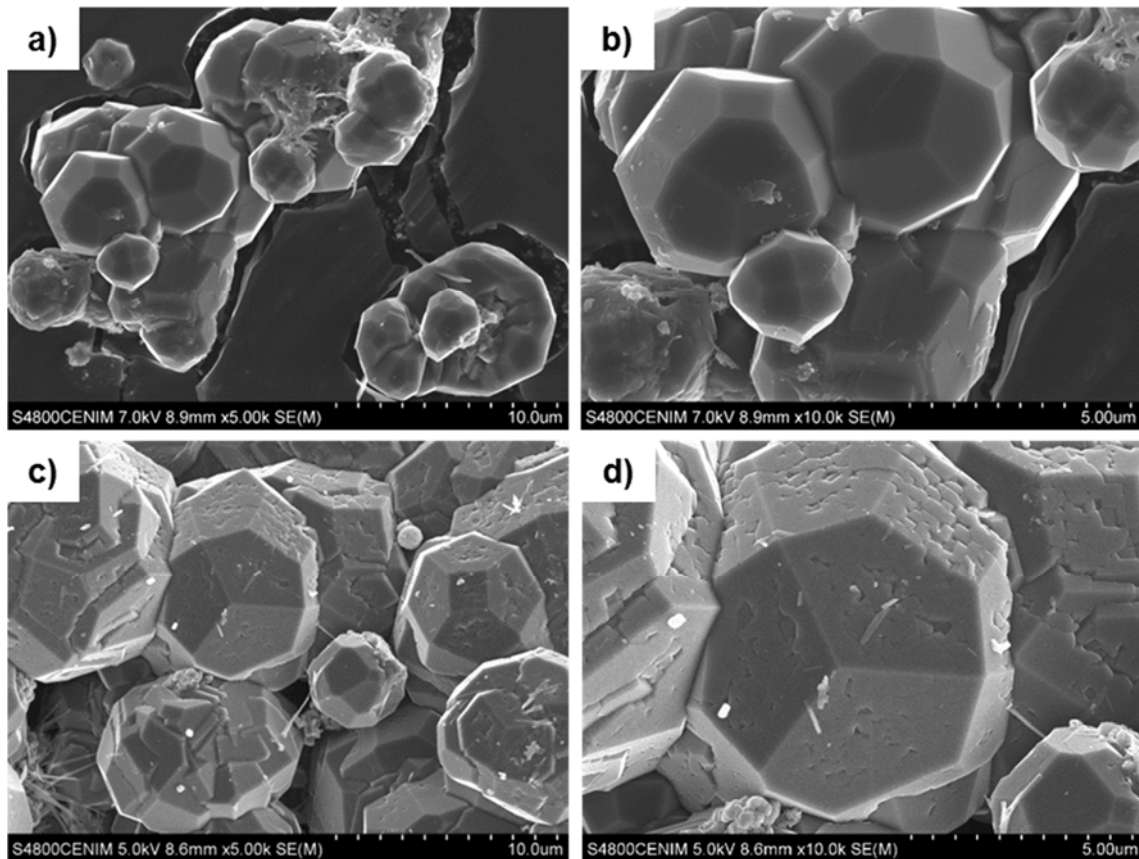


Figure 3.12 SEM images of the zeolite ANA obtained with 1 M NaOH and a liquid/solid ratio of 25 mL/g for 6 h at different temperatures: (a-b) 160 °C (sample Z12) and (c-d) 200 °C (sample Z13).

The ANA zeolite can be also obtained from other types of waste at high temperature for longer reaction times (> 24 h) [36, 40, 157]. In our case, ANA was synthesized directly from the transformation of Alw_x in a very much short one-step process (6 h).

Concerning the sample Z11 prepared at the intermediate temperature (140 °C), it resulted in a combination of zeolitic phases, NaP1 (66 %) and ANA (34 %), as showed the results obtained by XRD (Figure 3.11).

For the lowest temperature tested, 80 °C, (sample Z8), the XRD profile corresponds to an amorphous phase, and only three diffraction peaks of quartz were observed. This could be associated with the incomplete dissolution of silicon sources from the waste at temperatures < 90 °C.

The yield obtained for ANA was of 2.3-2.4 kg per kg of waste. Like the other zeolites (NaP1 and SOD), the reaction yield reached in the lab-scale synthesis of ANA was very high, and Alw_x was completely transformed into a zeolitic material by a direct process and without any previous treatment of the waste.

3. RESULTS AND DISCUSSION

3.2.1.5 Effect of liquid/solid ratio

The effect of the volume of liquid per amount of solid (liquid/solid ratio) in the reaction system on the crystallinity of the resulting products was studied to assess the best synthesis conditions and to develop the scaling up of a more eco-friendly process.

Liquid/solid ratios of 7.5, 15, and 25 mL/g were used in the synthesis tests using at fixed time (6 h), temperature (120 °C), and NaOH concentration (1 M).

The XRD patterns of the samples synthesized at the different liquid/solid ratios (7.5, 15, and 25 mL/g, samples Z15, Z14, and Z3, respectively) are shown in Figure 3.13.

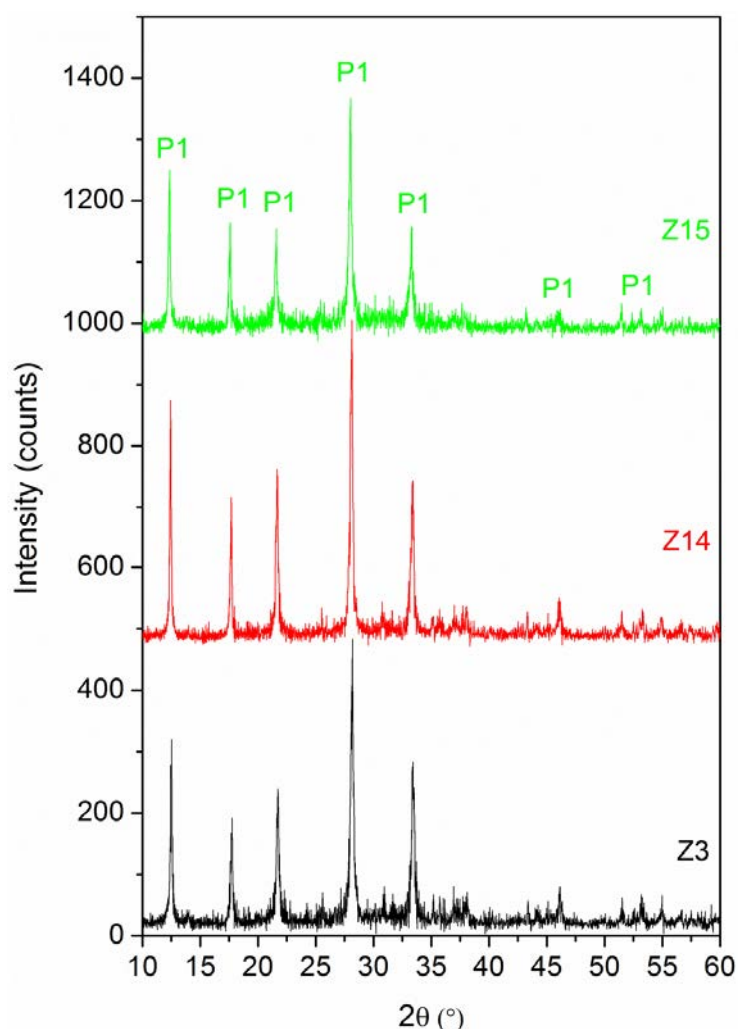


Figure 3.13 XRD patterns of zeolite NaP1 obtained at 120 °C for 6 h with different liquid/solid ratios of the reaction suspension: 25 mL/g (Z3), 15 mL/g (Z14), and 7.5 mL/g (Z15). P1 = NaP1 (ICDD PDF 01-071-0962).

The different liquid/solid ratios tested led to the formation of NaP1 as the only crystalline phase (ICDD PDF 01-071-0962), identifying its most intense 301 reflection at approximately 28.1° for the samples Z3, Z14, and Z15. The samples showed well-defined XRD profiles, and shifts in the peak parameters such as 2θ and FWHM were not observed (Table 3.11). In addition, the crystallite sizes obtained at the different liquid/solid ratios tested were very similar. It could indicate that the liquid/solid ratio in the reaction medium does not seem to modify the crystallite size.

Table 3.15 shows the values of intensity for the main diffraction peaks (d_{101} , d_{200} , d_{112} , d_{301} , and d_{312}) of the samples prepared at the different liquid/solid ratios. The most crystalline NaP1 was obtained for a liquid/solid ratio of 15 mL/g (sample Z14), as showed its diffraction profile composed of well-defined and narrower peaks, resulting in the highest intensity values for the main reflections (d_{101} , d_{112} , and d_{301}).

Table 3.15 Influence of the initial liquid/solid ratio on the crystallinity of NaP1 from the waste.

Sample	Liquid/solid ratio (mL/g)	Phase	hkl				
			101	200	112	301	312
Z3	25	NaP1	335	249	219	464	277
Z14	15		396	236	282	525	264
Z15	7.5		268	182	172	385	175

In general, a high liquid/solid ratio favors the complete dissolution of aluminosilicate phases, improving the reaction yield. On the other hand, a low liquid/solid ratio is always more favorable in synthesis processes on industrial scale since the time as well as the alkali and water consumptions can considerably be reduced.

The hydrothermal conversion of Alw_x into NaP1 led to reaction yields of 2.4 and 2.5 kg of zeolite per kg of waste for the liquid/solid ratios of 25 and 15 mL/g, samples Z3 and Z14, respectively (Table 3.10). As can be concluded, very similar amounts of zeolite per kg of treated waste are achieved using both 25 and 15 mL/g.

On the contrary, the lowest zeolite amount was obtained using the lowest liquid/solid ratio of 7.5 mL/g (sample Z15). It could be related to the lowest liquid volume used in the reaction medium, leading to the poorest homogenization of all the reactants during the synthesis as well as the lowest formation of crystal nuclei. One of the main drawbacks of using a low ratio is the generation of dense slurry that is hardly mixed and homogenized.

3. RESULTS AND DISCUSSION

The ML volumes generated after the zeolitization processes were ranged between 1.3 and 8.9 L per kg of zeolite obtained, which corresponded to the lowest (7.5 mL/g) and highest (25 mL/g) liquid/solid ratio, respectively. The synthesis test using the intermediate liquid/solid ratio (15 mL/g) resulted in 4.4 L of ML per kg of zeolite.

In order to develop a more sustainable zeolitization process, the liquid/solid ratio of 15 mL/g was selected as optimal to perform the further bench-scale synthesis experiments with recovery and recycling of effluents (mother liquor and rinse water). This liquid/solid ratio not only would allow the production of well-crystallized NaP1, but also the reduction in the waste effluent generation, resulting in 4.4 L of ML per kg of zeolite.

3.2.2 Characterization of the zeolites from the waste

A more exhaustive characterization of the different types of zeolites obtained from the waste was performed to determine their properties and characteristics.

The samples Z3, Z7, and Z13, which correspond to pure NaP1, SOD, and ANA, were subjected to further studies. The reaction yields for these samples involved the maximum amounts of zeolite obtained per kg of waste for each group of zeolite (NaP1, SOD, and ANA) under the same conditions of time (6 h) and liquid/solid ratio (25 mL/g).

3.2.2.1 Morphological characterization

The morphologies obtained for the three zeolites (NaP1, SOD, and ANA) are shown in the following SEM images at different magnifications (Figure 3.14, Figure 3.15, and Figure 3.16).

NaP1 (Z3) exhibited a homogenous morphology composed of “cauliflower-like” primary aggregates of around 15-45 μm (Figure 3.14a-b). These primary aggregates consist of smaller secondary aggregates with an average diameter of 4 μm (Figure 3.14c), which are formed by cubic nanocrystals with well-defined edges (150-345 nm) and an anisotropic growth of crystals (Figure 3.14d-f).

Some authors also reported the same morphology characteristic of zeolites with a gismondine-type structure obtained from chemical reagents [158] and wastes such as FA [51, 59, 155]. However, other authors have obtained NaP zeolites with variable

3. RESULTS AND DISCUSSION

morphologies depending on the synthesis conditions used. For instance, Huo et al. [159] prepared NaP from chemicals via hydrothermal synthesis at 100 °C for 48 h, resulting in different morphologies, such as diamond, cactus, and wool ball, as a function of the initial $\text{SiO}_2/\text{Al}_2\text{O}_3$ ratio (varied from 3.8 to 10).

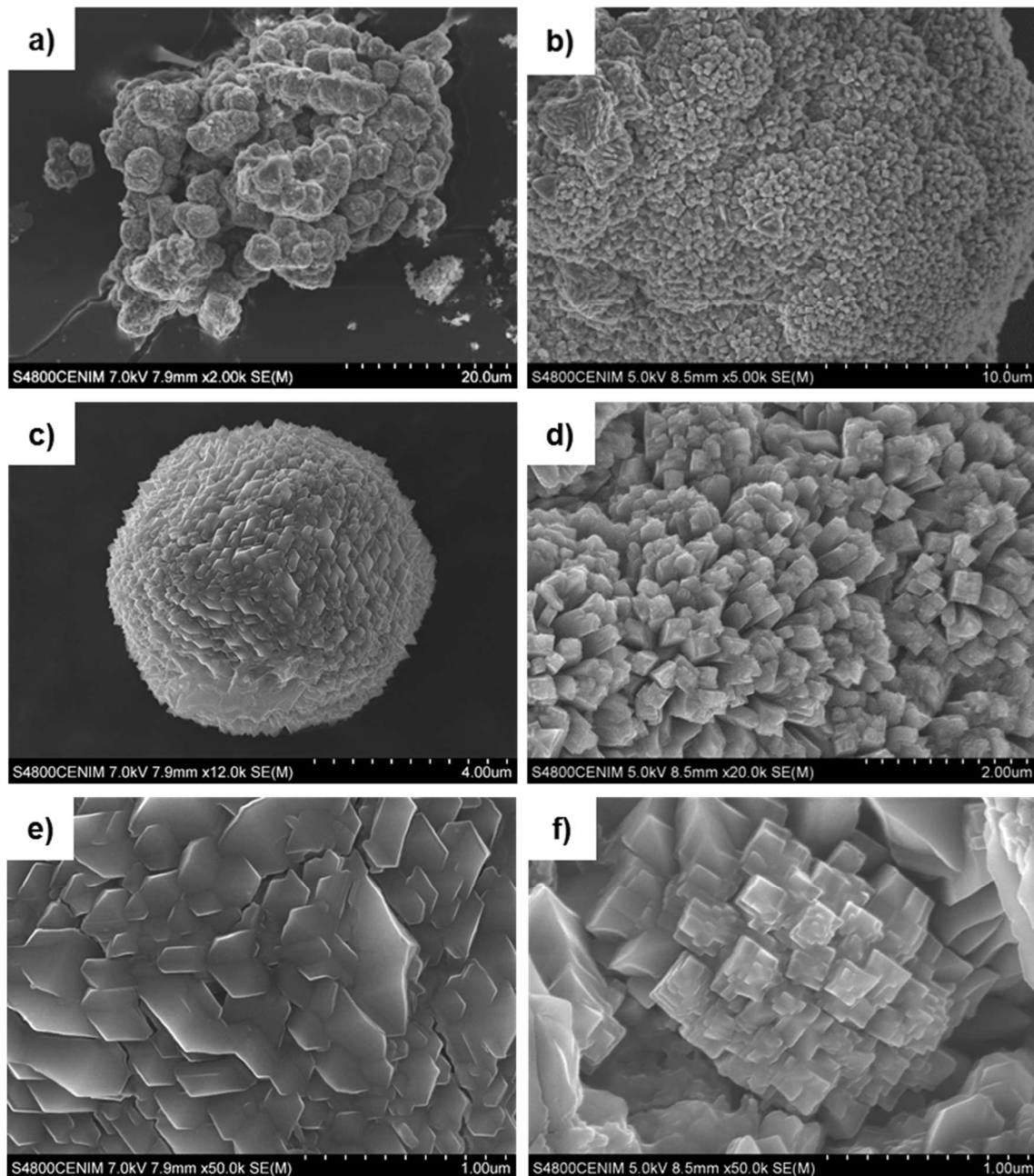


Figure 3.14 SEM images at different magnifications of the zeolite NaP1 (sample Z3) obtained from the waste at 120 °C for 6 h using 1 M NaOH and a liquid/solid ratio of 25 mL/g.

3. RESULTS AND DISCUSSION

SOD (Z7) showed a morphology similar to that reported in the literature [71, 160] that is characterized by highly densified agglomerates composed of “raspberry-like” balls with sizes around 1.3-1.9 μm (Figure 3.15a-c). It was observed that a certain number of these microballs consisted of hollow balls as those showed in Figure 3.15d. At higher magnification (Figure 3.15e-f), intergrowth of distorted hexagonal tabular crystals with edges that ranged around 40-350 nm was observed.

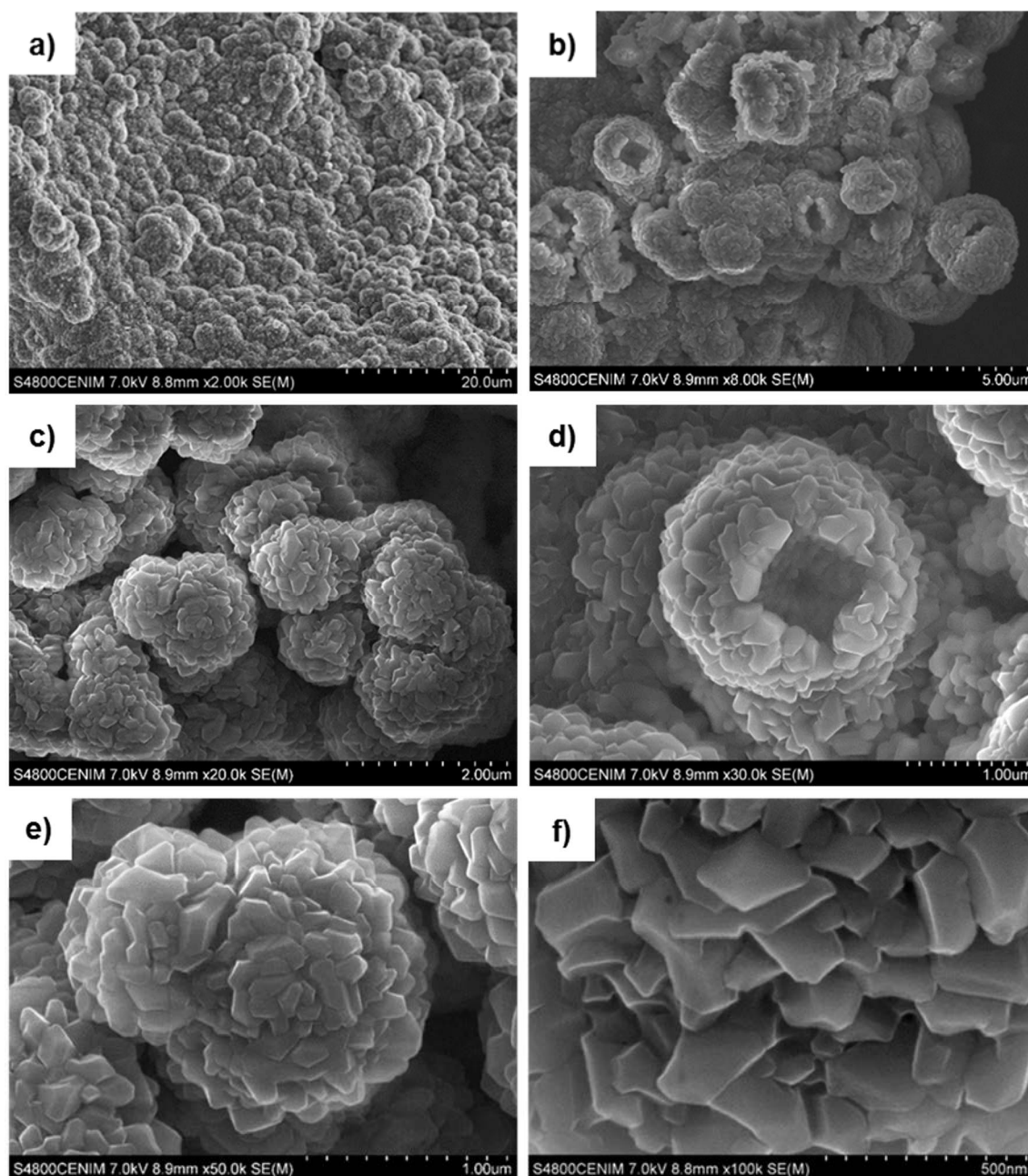


Figure 3.15 SEM images at different magnifications of the zeolite SOD (sample Z7) obtained from the waste at 120 $^{\circ}\text{C}$ for 6 h using 5 M NaOH and a liquid/solid ratio of 25 mL/g.

As mentioned, the type of morphology obtained can vary depending on the reaction medium, synthesis process, and conditions (temperature, time, etc.). Huang et al. [161] reported several morphologies for SOD obtained from chemical reagents (sodium hydroxide, sodium aluminate, and ethanol). The authors studied the effects of ethanol and synthesis time on the morphology of the zeolite showing different structures such as thread-ball and core-shell particles obtained for low and high ethanol contents, respectively. On the other hand, they obtained hollow SOD after a long time (67 h) compared with the shorter time (6 h) required to synthesize SOD from Alw_x with a similar morphology.

The morphology of ANA (Z13) consisted of agglomerates with sizes ranged between 4.6 and 11.2 μm (Figure 3.16a-c). At high magnification (Figure 3.16d-f), euhedral crystals can be observed, forming trapezohedra with highly faceted crystals and well defined edges, most of the crystals exhibit intergrowths.

Some investigations have showed a direct correlation between the composition of the reagents and the resulting products. For example, Ghobarkar and Schäf [162] obtained ANA from artificial glasses via hydrothermal synthesis for a very long time (6 weeks), resulting in different morphologies of the zeolite as a function of the temperature: orthorhombic (160 °C), tetragonal (230-270°), or cubic (300-450 °C) morphology. Although the ANA morphology is found to be very sensitive to the experimental conditions, a similar trapezohedron-type morphology was also described for zeolites obtained from both quartz syenite [163] and FA [36, 59, 164].

3. RESULTS AND DISCUSSION

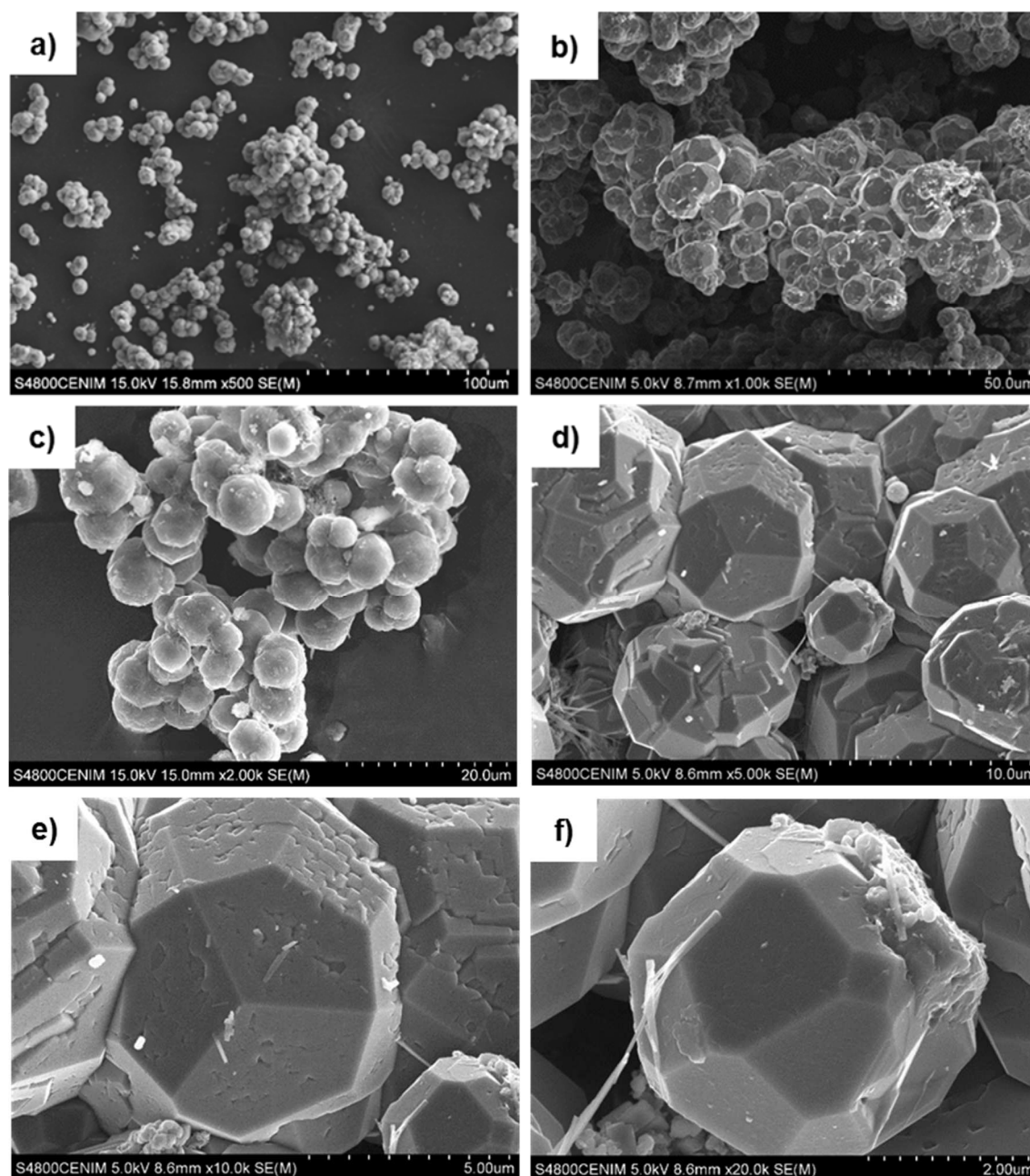


Figure 3.16 SEM images at different magnifications of the zeolite ANA (sample Z13) obtained from the waste at 200 °C for 6 h using 1 M NaOH and a liquid/solid ratio of 25 mL/g.

The EDS spectra as well as the average chemical composition determined by microchemical point analysis (selecting ten points per sample) for the three zeolites (samples Z3, Z7, and Z13) are shown in Figure 3.17.

The results obtained from the EDS analyses showed that Na^+ is the main exchange cation in the structure of the three zeolites.

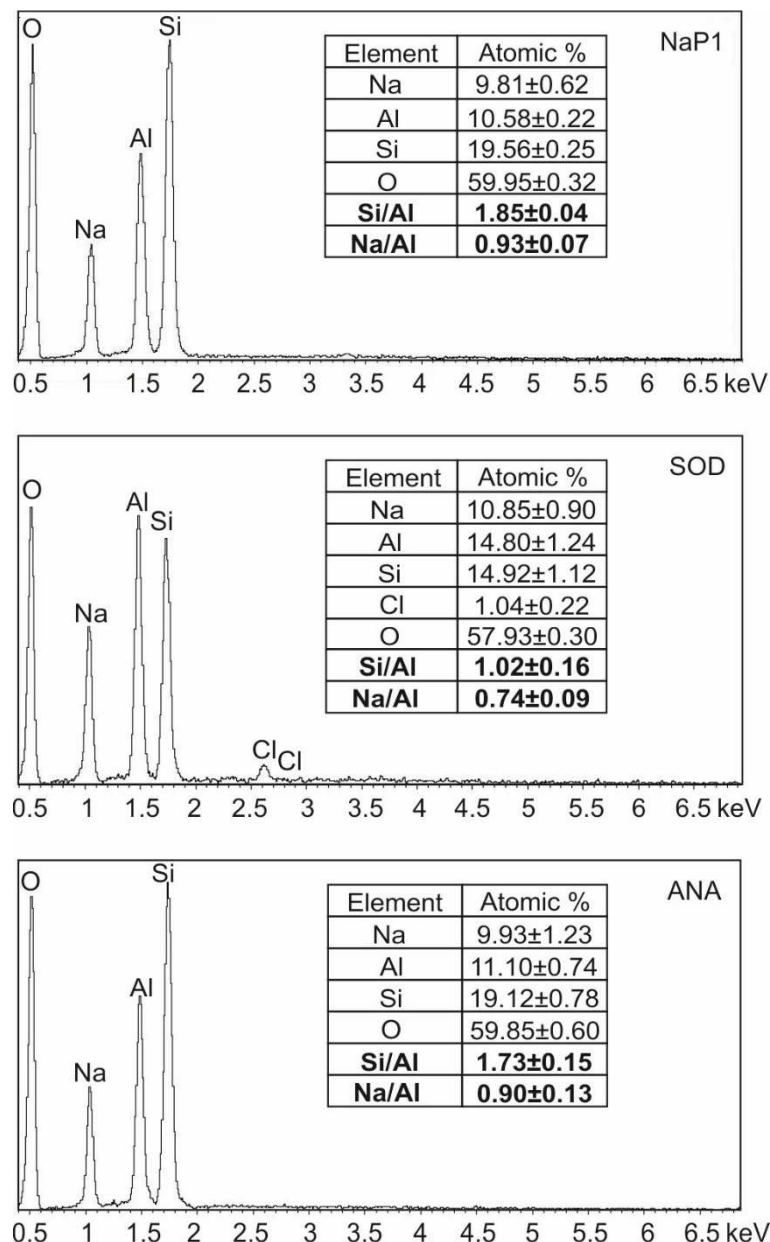


Figure 3.17 EDS spectra and microchemical point analyses of NaP1 (Z3), SOD (Z7), and ANA (Z13) obtained from the waste.

For NaP1 (Z3), the average Si/Al ratio obtained as an average of ten microchemical points analysis was of 1.85 ± 0.04 . Although this value is slightly higher than the stoichiometric value (~ 1.67) of NaP1 ($\text{Na}_6\text{Al}_6\text{Si}_{10}\text{O}_{32} \cdot 12\text{H}_2\text{O}$), variable Si/Al ratios (1.9-3.0) were reported in the literature depending on the synthesis conditions (temperature, time, and type and concentration of raw materials) [158, 159]. For example, Zubowa et al. [158] obtained NaP with 2-2.6 Si/Al ratios by applying a microwave treatment at 150 °C for 5 h and using chemical reagents (silica sol, sodium aluminate, NaOH, and

3. RESULTS AND DISCUSSION

hexamethyleneimine as organic template). Huo et al. [159] also synthesized NaP zeolites with variable Si/Al ratios (1.9-3) from commercial reagents (sodium silicate, sodium aluminate, and NaOH) via the conventional hydrothermal synthesis at 100 °C for 48 h. An average Na/Al ratio of 0.93 ± 0.04 was obtained and, in general, other exchange cations were not observed, but scarcely, minor content of K^+ and Ca^{2+} cations were detected in the microchemical point analysis of several crystals with very low K/Na and Ca/Na ratios (~ 0.02). Some works also reported the presence of K^+ and even other cations such as Ca^{2+} , Mg^{2+} , and Fe^{2+} for the NaP1, SOD, and ANA zeolites obtained from FA [44, 59].

For SOD (Z7), the average Si/Al ratio was of 1.02 ± 0.16 and the average Na/Al ratio of 0.74 ± 0.09 (Figure 3.17), which are values similar to the theoretical of both hydroxy-sodalite ($Na_8Al_6Si_6O_{24}(OH)_2 \cdot 2H_2O$) and chloride-sodalite ($Na_4Al_3Si_3O_{12}Cl$). Chloride peaks were observed in most of the microchemical point analysis as shown in the EDS spectrum (Figure 3.17). This seems to indicate the partial replacement of OH^- by Cl^- and accordingly the formation of chloride-sodalite. The presence of Ca^{2+} cations was also detected in some of the analyzed points showing a very low Ca/Na ratio (0.07).

In the case of ANA (Z13), the average Si/Al ratio was of 1.73 ± 0.15 (Figure 3.17), which fits well with the theoretical value (2) for the stoichiometry of ANA ($NaAlSi_2O_6 \cdot H_2O$). Only Na^+ was detected as exchange cation to balance the ANA structure, resulting in a Na/Al ratio of 0.90 ± 0.13 , which is very similar to that Na/Al ratio (0.7-0.9) reported in the synthesis of ANA from coal by-products like natural clinker with a 2.1-2.6 Si/Al ratio [40].

3.2.2.2 Structural characterization

Due to the direct relation between the properties of zeolites and their structures, FTIR analysis is used to determine the main absorption bands associated to the typical vibration modes of the TO_4 tetrahedra (T = Si or Al) that form their frameworks.

The hydroxyl groups (band at around 3600 cm^{-1}) as well as the content of water (around 1645 cm^{-1}) present in the structures of zeolites can be also easily detectable by FTIR analysis. The assignments of the main IR bands and vibration modes of zeolites are shown in Table 3.16.

Table 3.16 Characteristic IR bands of zeolites [165].

Wave number (cm ⁻¹)	Vibration mode	T-atom: Si or Al
3700-3600	Hydroxyl stretching (ν_{OH})	T-(OH)-T
1645	Water adsorbed	
1250-950	Asymmetrical stretching (ν_{as})	$\leftarrow OT \rightarrow \leftarrow O$
790-650	Symmetrical stretching (ν_s)	$\leftarrow OTO \rightarrow$
500-420	Bending (δ)	T-O
420-300	Pore opening	

The XRD and SEM analyses revealed that the obtained NaP1, SOD, and ANA zeolites (samples Z3, Z7, and Z13, respectively) show different crystallinities and crystal habits, as mentioned above. In relation to their structural characterization by FTIR, the assignments of their characteristics vibrational modes are summarized in Table 3.17 in which values reported in the literature are also included.

The typical bands attributed to the presence of hydroxyl (OH) groups (very broad band around 3400 cm⁻¹), structural water (~1650 cm⁻¹), and internal Si-O-Al bond vibrations of tetrahedra (1200-400 cm⁻¹) were identified in all the samples.

The FTIR spectra recorded in the region of the “finger-print” (1200-400 cm⁻¹) for each zeolite are shown in Figure 3.18.

The NaP1, SOD, and ANA zeolites from Alw_x showed spectra with absorption bands corresponding to aluminosilicate-type materials. The very strong and broad band at approximately 1000 cm⁻¹ assigned to the asymmetric stretching of internal Si-O or Al-O tetrahedra [46, 166] was observed for each zeolite. This asymmetric stretching mode appeared with a shoulder at 1075 cm⁻¹ in the NaP1 and SOD zeolites (samples Z3 and Z7). This is in agreement with the FTIR results reported for NaP1 and hydroxysodalite obtained from diatomite showing asymmetric stretching bands at 1003 and 985 cm⁻¹ with shoulders at 1111 and 1113 cm⁻¹, respectively [166].

3. RESULTS AND DISCUSSION

Table 3.17 Assignments of bands observed by FTIR for NaP1 (Z3), SOD (Z7), and ANA (Z13) synthesized from the waste.

Vibration mode	Wavenumber (cm ⁻¹)								
	NaP1			SOD			ANA		
	This thesis	Ref. [154]	Ref. [166]	This thesis	Ref. [167]	Ref. [166]	This thesis	Ref. [163]	Ref. [166]
v(OH) ^a	3448	3434	-	3448	-	-	3432	3617	-
H ₂ O	1654 (m)	1641	-	1637 (m) 1459 (vw)	1650 1479	-	1654 (m)	1637	-
v _{as} (SiAlO) ^b	1075 (sh) 1000 (s)	998	1111 1003	1075 (sh) 988 (s)	995 (s)	1113 985	1016 (s)	1027	1000
v _s (SiAlO) ^b	743 (w) 679 (w) 604 (m)	605	774 739 675 603	732 (m) 704 (w) 669 (m) 623 (w) 565 (vw)	725 700 662 624 566	736 708 666 567	872 (vw) 700 (m) 591 (w)	739 645 587 543 444	740 687 622
δ(T-O) ^c	433 (m)	435	435	461 (m) 433 (m)	461 431	463 435	448 (m)	444	450

^a v(OH): hydroxyl stretching.

^b v_{as}(SiAlO) and v_s(SiAlO): asymmetric and symmetric stretching.

^c δ(T-O): bending of SiO₄ or AlO₄ tetrahedron.

Absorption band intensity: s = strong; sh = shoulder; m = medium; w = weak; and vw = very weak.

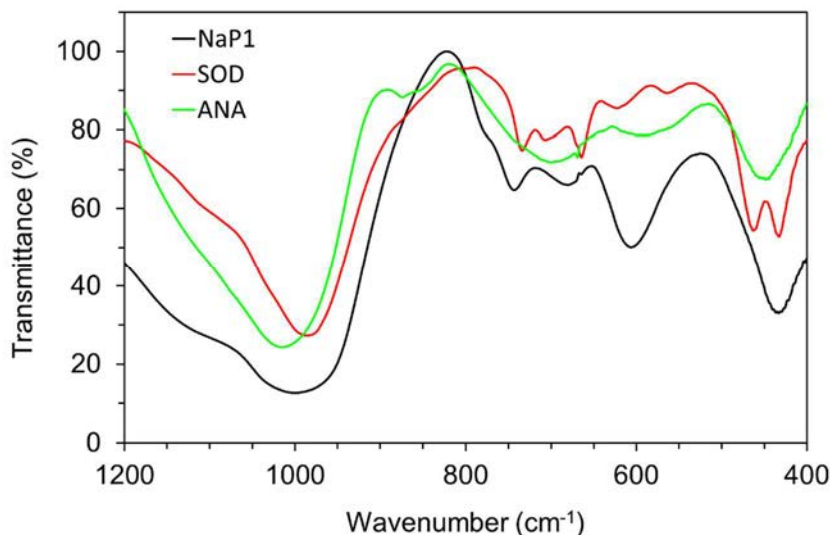


Figure 3.18 FTIR spectra (“finger print” region) of NaP1 (Z3), SOD (Z7), and ANA (Z13) synthesized from the waste.

The sample Z3 showed a FTIR spectrum characteristic of NaP1: three bands centered at 743, 679, and 604 cm⁻¹ attributable to the symmetric stretching vibrational mode of internal tetrahedron, and the band at 433 cm⁻¹ assigned to tetrahedron bending mode,

which fits well with the spectrum reported by Huo et al. [159] for NaP1 obtained from pure reagents. This indicates the high purity of the zeolite obtained from the Alw_x.

Concerning the sample Z7, it is remarkable the typical triplet of SOD, in the region of the “finger-print” (symmetric stretching mode), at 732, 704, and 669 cm⁻¹ and the two bands corresponding to the octahedron bending modes at 461 and 433 cm⁻¹ [168]. These results are in good agreement with those reported by Kròl et al. [167] for SOD hydrothermally synthesized from expanded perlite.

The sample Z13 exhibited a FTIR spectrum that fit well with those previously reported in the literature for ANA from other waste sources such as kaolin and rice husk, and quartz syenite [36, 163]. Thus, the ANA spectrum showed the asymmetric stretching modes of tetrahedron at 1014 cm⁻¹, the bands corresponding to symmetric modes at 872, 700, and 591 cm⁻¹, and the bending mode at 448 cm⁻¹.

3.2.2.3 Thermal behavior

The main structural changes including dehydration, dihydroxylation, or transformation of the zeolitic phases into other more metastable phases (e.g., nepheline) can be determined by the combination of TG and DTA analysis.

The TG-DTA curves from 25 to 1000 °C in nitrogen atmosphere of NaP1, SOD, and ANA (samples Z3, Z7, and Z13, respectively) are plotted in Figure 3.19.

Table 3.18 collects the results obtained from TG-DTA curves that include the mass losses and integrate peak analyses with their corresponding temperature intervals.

3. RESULTS AND DISCUSSION

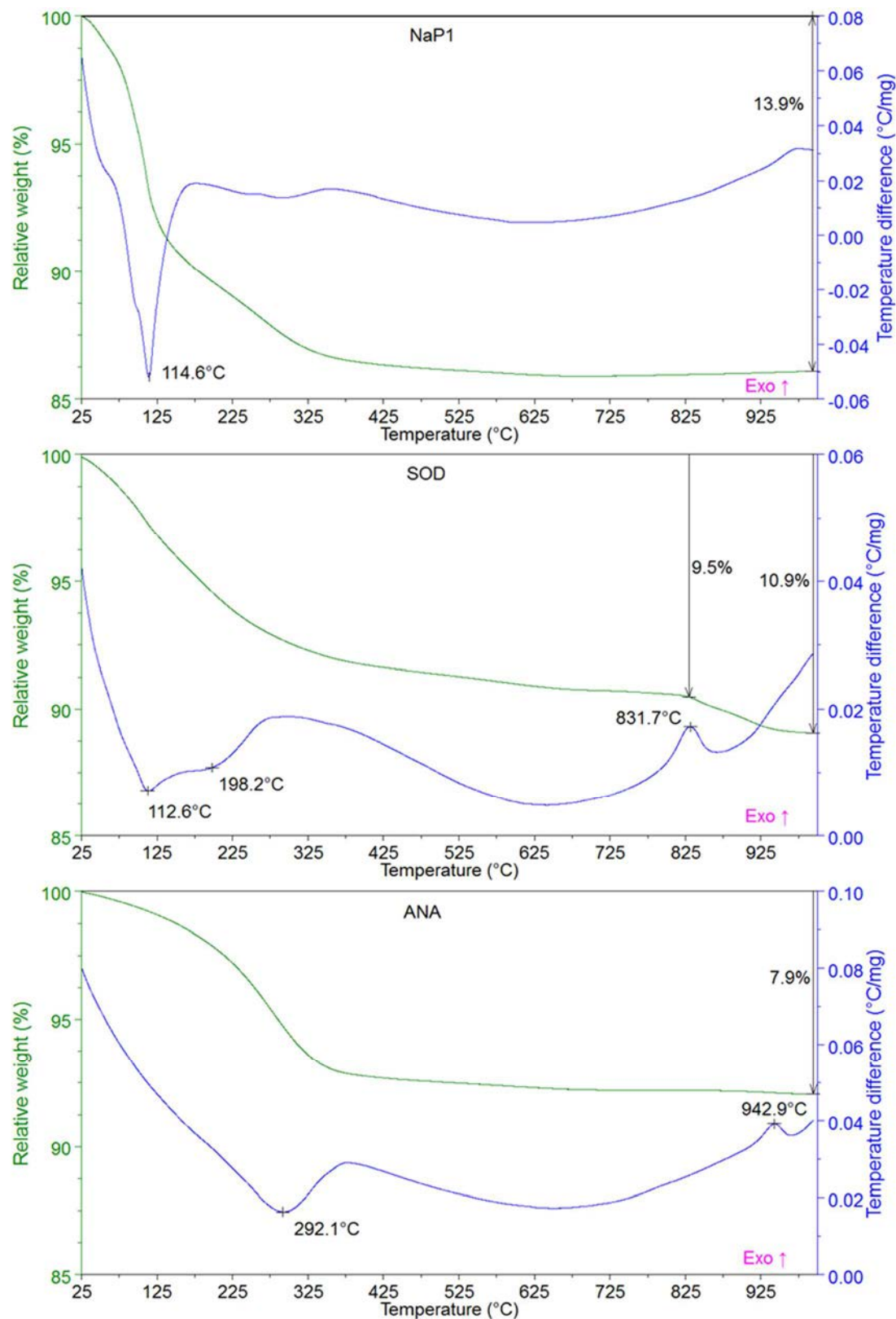


Figure 3.19 TG-DTA curves of NaP1 (Z3), SOD (Z7), and ANA (Z13) obtained from the waste. (TG (relative mass loss, %): green curve. DTA analysis (°C/mg): blue curve).

3. RESULTS AND DISCUSSION

Table 3.18 TG-DTA analyses of the NaP1 (Z3), SOD (Z7), and ANA (Z13) zeolites obtained from the waste.

Effect	DTA			TG	
	Temperature interval (°C)	Peak temperature (°C)	Integrate peak ($\mu\text{V}\cdot\text{min}/\text{mg}$)	Temperature interval (°C)	Mass loss (%)
NaP1 (sample Z3)					
1 Endo	71-160	115	3.7	25-115	7.6
2	-	-	-	115-339	5.6
3	-	-	-	339-1000	0.7
SOD (sample Z7)					
1 Endo	54-240	113	1.2	25-280	7.1
2	-	-	-	280-832	2.4
3 Exo	808-864	832	0.2	832-1000	1.4
ANA (sample Z13)					
1 Endo	118-375	292	4.0	25-395	7.2
2	-	-	-	395-1000	0.7
3 Exo	922-962	943	0.1	-	-

The NaP1 zeolite (Z3) suffered a total mass loss of 13.9 wt.%. This value fit well with the LOI (13.3 wt.%) and corresponds to the release of 10 water molecules. Although the theoretical mass loss for the stoichiometry $\text{Na}_6\text{Al}_6\text{Si}_{10}\text{O}_{32}\cdot 12\text{H}_2\text{O}$ is higher (around 16.5 %), even lower values of mass loss (12 wt.%) were reported by Kazemian et al. [46] for NaP1 obtained from FA. The maximum water losing rate took place at 115 °C, according to the endothermic peak in DTA curve. Nevertheless, the water release occurred in several steps, as shown for both TG and DTA curves.

For the SOD zeolite (Z7), the total mass loss occurred in three steps and was of 10.9 wt.%, quite similar to the LOI value (10.2 wt.%). The obtained results are corroborated with the mass loss of 10 % for hydroxy-sodalite ($\text{Na}_8\text{Al}_6\text{Si}_6\text{O}_{24}(\text{OH})_2\cdot 2\text{H}_2\text{O}$) synthesized from pure reagents by Günther et al. [169]. DTA curve indicated that water is lost in the first two steps: a first endothermic peak at 113 °C with a shoulder at 198 °C. Thus, it resulted in a mass loss of 9.5 wt.%, that is, the corresponding water content (5 molecules) in the structure of SOD.

The last step of mass loss (around 1.4 wt. %) was associated to an exothermic peak at 832 °C. This effect could be attributable to the release of chloride and accordingly to the collapse of the SOD structure. Some authors associate this exothermic peak with the thermal transformation of SOD into nepheline or carnegieite ($\text{NaAlSi}_3\text{O}_8$) [169, 170]. This was confirmed from the results obtained by the XRD analysis, concluding that SOD from

3. RESULTS AND DISCUSSION

Alw_x was thermally transformed into a new phase (nepheline) at 800 °C, as will be discussed below.

The profiles of both TG and DTA curves for ANA (sample Z13) indicate that the water molecules were released at a lower rate than those corresponding to samples Z3 and Z7. This profile is characteristic of ANA composed of smooth faceted high size crystals, which provokes a retarded dehydration [157]. For Z13 the dehydration occurred from room temperature up to ~ 400 °C, with an associated endothermic peak centered at 292 °C. The mass loss of 7.9 wt.% (quite similar to the LOI value of 8.2 wt.%) fit well with the theoretical value for the stoichiometry of NaAlSi₂O₆·H₂O. The exothermic peak observed in DTA curve at 943 °C without associated mass loss could be attributable to the collapse of the ANA framework [40] or to the formation of other more thermally stable phase like nepheline. As will be discussed below, it was demonstrated that ANA from Alw_x was thermally transformed into nepheline at approximately 1000 °C.

From the results of the elemental composition obtained by the EDS analysis and the zeolitic water content determined by the TG analysis, the approximate formulae of the studied zeolites were estimated as follows (Table 3.19):

Table 3.19 Chemical formula of NaP1, SOD, and ANA obtained from the waste via direct synthesis on lab scale.

Sample	Zeolite phase	Estimated formula	Theoretical formula
Z3	NaP1	Na _{5.6} Al ₆ Si _{11.1} O ₃₄ ·10H ₂ O	Na ₆ Al ₆ Si ₁₀ O ₃₂ ·12H ₂ O
Z7	SOD	Na _{2.2} Al ₃ Si _{3.1} Cl _{0.2} O _{11.9} ·5H ₂ O	Na ₄ Al ₃ Si ₃ O ₁₂ Cl
Z13	ANA	Na _{0.9} AlSi _{1.7} O _{5.4} ·H ₂ O	NaAlSi ₂ O ₆ ·H ₂ O

As mentioned above, SOD (sample Z7) showed the presence of chloride what could indicate the formation of chloride-sodalite (Na₄Al₃Si₃O₁₂Cl), instead of hydroxy-sodalite (Na₈Al₆Si₆O₂₄(OH)₂·2H₂O), from Alw_x, which was supported by the microchemical analysis.

To provide a better insight on the influence of temperature, the thermal stability of each zeolite was evaluated at different temperature conditions. Thus, the samples Z3, Z7, and Z13 were subjected to thermal treatments at temperatures ranged between 400 and 1000 °C for 4 h in air atmosphere. After these thermal treatments, the crystallinities of the samples were evaluated by XRD analysis to elucidate the possible formation of new phases like nepheline.

The resulting XRD profiles of NaP1, ANA, and SOD after their thermal treatments at temperatures ranged between 400 and 1000 °C are shown in Figure 3.20, Figure 3.21, and Figure 3.22. As can be seen, the three zeolites were found to be thermally stable up to around 400 °C. At higher temperature (above 800 °C), the zeolites were transformed into nepheline (ICDD PDF 00-035-0424), which is characterized by its 201 and 202 basal reflections at 23.11 and 29.70° [171].

Nepheline (NaAlSiO_4) is a feldspathoid with a framework formed by regular and flattened hexagonal rings and is characterized by its high chemical and mechanical strength and impact resistance, being used in different industrial applications (microwaves ovens, dental applications, or in Ag-composites with antibacterial properties) [172, 173].

Previous works reported the crystallization of nepheline derived from zeolitic-type precursors such as zeolites LTA, FAU, and GIS [174-177]. Depending on the chemical composition and framework topology of the starting zeolite, different ceramic phases such as nepheline (NaAlSiO_4), carnegite (NaAlSiO_4), albite ($\text{NaAlSi}_3\text{O}_8$), jadeite ($\text{NaAlSi}_2\text{O}_6$), and/or silica phases (cristobalite, tridymite, etc.) can be obtained after a thermal transformation treatment. For example, the initial Si/Al ratio of the zeolite, the type and amount of exchangeable cations in the zeolite structure, and the water content adsorbed on the zeolite can modify both the thermal transformation rate and path, and accordingly, the formation of new phases.

The phase transformation of a zeolite into a ceramic phase as nepheline is a complex process that can involve different mineralogical, chemical, and structural changes. These changes can principally be caused by migration and/or ejection of atoms from the crystal lattice of the zeolite, causing chemical stoichiometry variations as well as expansion or contraction of the material [176].

In the case of NaP1 (Z3), its framework collapsed forming an amorphous phase after heating at 800 °C. This amorphous phase may remain stable in a narrow temperature range. A further heating up to 1000 °C led to the formation of nepheline from such amorphous phase (Figure 3.20). The formation of an amorphous phase at temperatures above 700 °C using the GIS-type zeolite (initial Si/Al ratio = 1.5) as precursor of nepheline was also reported by Dimitrijevic et al. [174].

Compared to SOD and ANA, NaP1 was the least stable zeolitic phase at a temperature > 400 °C, involving a thermal conversion of this zeolite (tetragonal crystal) into nepheline (hexagonal crystal) quicker than SOD (cubic crystal) and ANA (cubic crystal).

3. RESULTS AND DISCUSSION

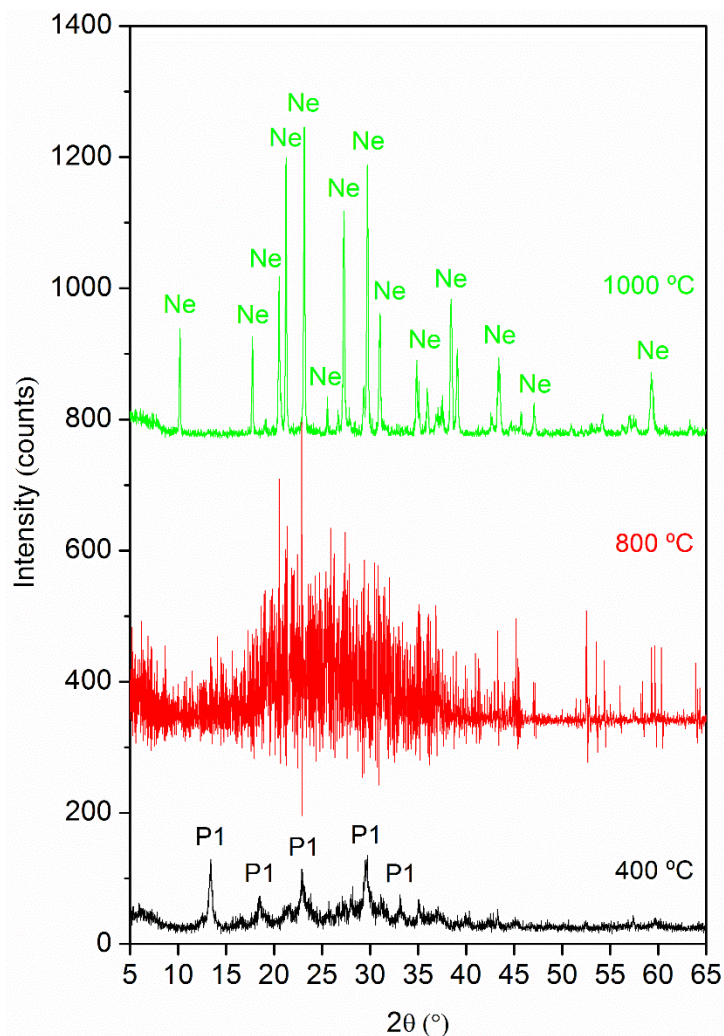
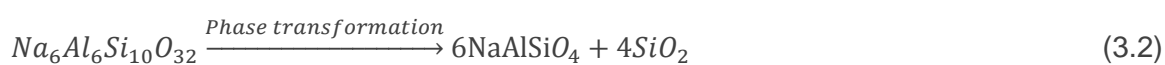
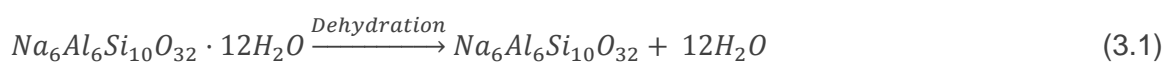


Figure 3.20 XRD patterns obtained after the thermal treatment of NaP1 (Z3) at 400, 800, and 1000 °C for 4 h in air atmosphere. P1 = NaP1 (ICDD PDF 01-071-0962) and Ne = nepheline (ICDD PDF 00-035-0424).

The thermal conversion of NaP1 into nepheline would require a readjustment of atoms because of its excess of silica, resulting in an amorphization prior to the transformation into nepheline. The sequences of the dehydration and thermal transformation processes that undergo the NaP1 zeolite are shown in reactions (3.1) and (3.2), respectively.



On the contrary, ANA (Z13) appeared to be thermally stable up to 800 °C and it was totally transformed into nepheline at 1000 °C as shown in Figure 3.21. The conversion of ANA into nepheline would also involve the formation of a silica-type phase which is highly stable at high temperature, according to the sequence of reactions (3.3) and (3.4).

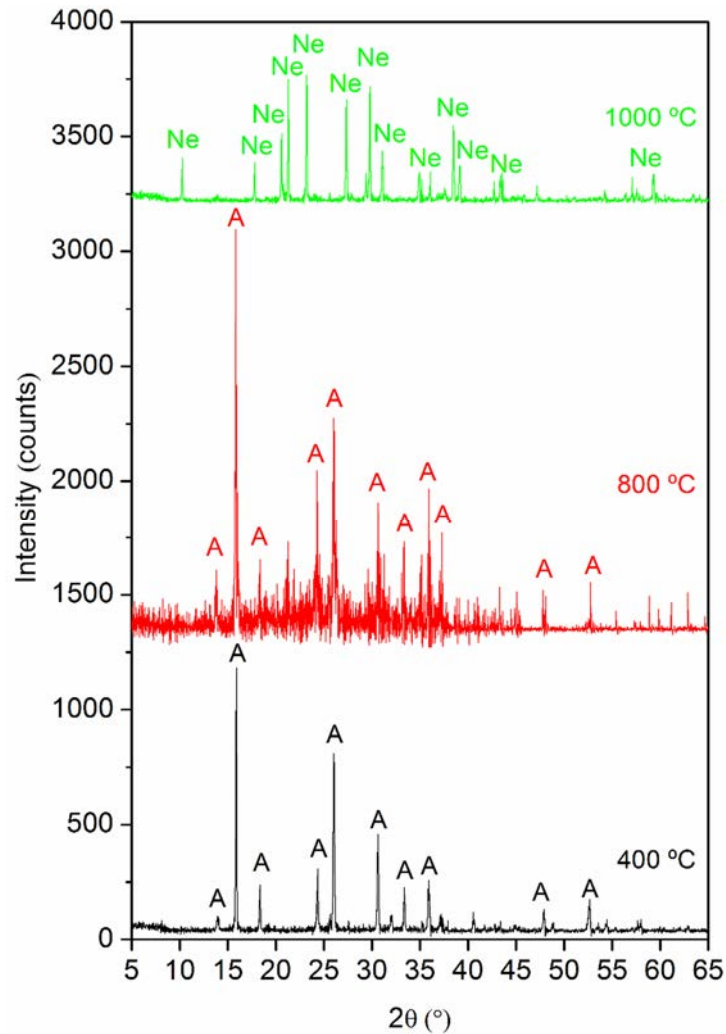
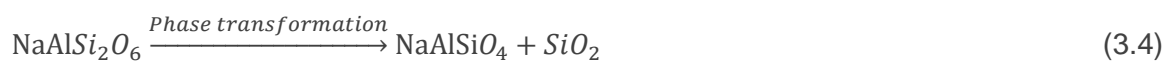
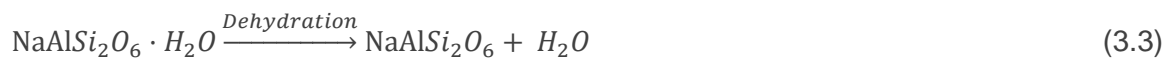


Figure 3.21 XRD patterns obtained after the thermal treatment of ANA (Z13) at 400, 800, and 1000 °C for 4 h in air atmosphere. A = analcime (ICDD PDF 00-041-1478) and Ne = nepheline (ICDD PDF 00-035-0424).



3. RESULTS AND DISCUSSION

Concerning SOD (Z7), the conversion of this phase into nepheline took place at a lower temperature (800 °C) than that used for the thermal treatment of NaP1 and ANA (1000 °C). After the treatment at 1000 °C, nepheline was found along with small traces of SOD (Figure 3.22). SOD could be more easily transformed into nepheline due to its chemical composition and crystal structure. Additionally, other phases such as NaOH or NaCl are also formed during this thermal transformation depending on the starting SOD zeolite (i.e., hydroxy-sodalite or chloride-sodalite, respectively), as indicates the reactions (3.5) and (3.6).

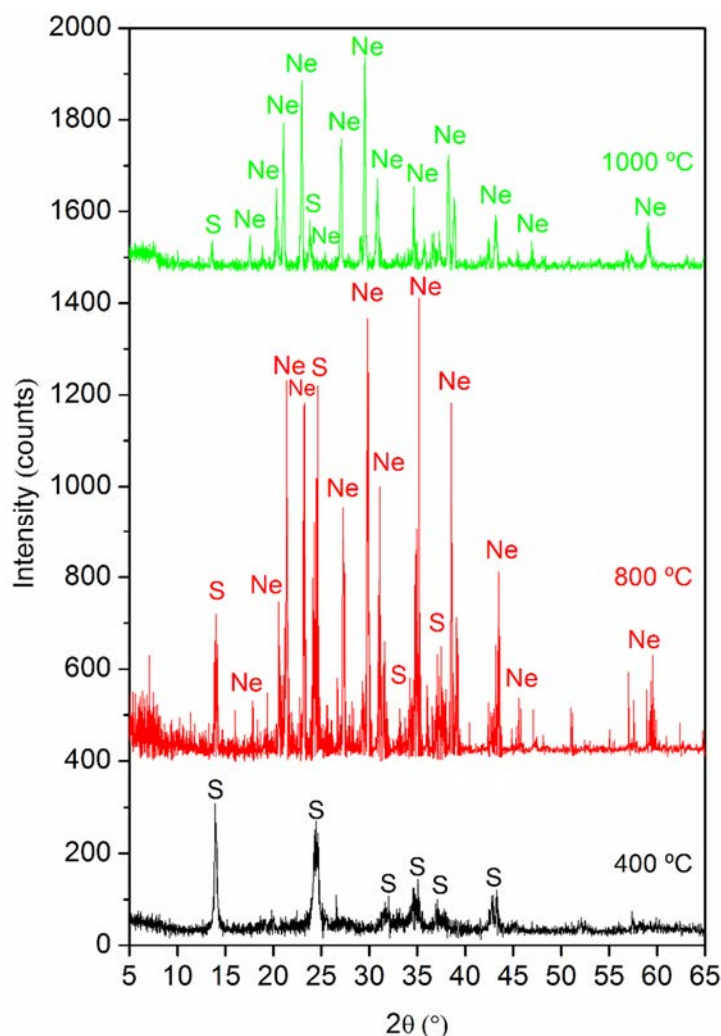
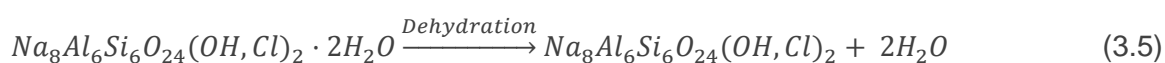


Figure 3.22 XRD patterns obtained after the thermal treatment of SOD (Z7) at 400, 800, and 1000 °C for 4 h in air atmosphere. S = hydroxy-sodalite (ICDD PDF 01-076-1639) and/or chloride-sodalite (ICDD PDF 01-086-1844), and Ne = nepheline (ICDD PDF 00-035-0424).



From the XRD analysis, any crystalline phases of silica were not detected, but it is believed that the zeolites have aluminosilicate-type structures close to those of polymorphs of the silica such as tridymite. Nepheline has structure of tridymite which is stable from 870-1470 °C and could also be formed during the thermal transformation of the zeolites into nepheline. Both nepheline and tridymite have some diffraction peaks in common in the 2θ interval of ~ 20 - 24° , in particular the d-spacing (\AA) of 4.107 [178]. Earlier works reported the formation of nepheline through a stuffed derivative structure of silica such as tridymite [172].

These results demonstrate NaP1, SOD, and ANA obtained from Alw_x can be used as precursors of ceramic-type material (nepheline) with interesting applications in the industry by thermal transformation.

3.2.2.4 Textural and physical-chemical characterization

The study of textural characteristics and some physical-chemical properties, such as the particle size distribution (PSD), the zeta potential (ζ -potential), and the cation-exchange capacity (CEC), of NaP1, SOD, and ANA is shown below.

Nitrogen adsorption/desorption analysis

Physical adsorption of the nitrogen molecule is a standard tool widely used to analyze textural characteristics, such as BET specific surface area (S_{BET}), external area (S_{EXT}), and pore size, of sorbent materials.

The nitrogen adsorption/desorption isotherms of NaP1, SOD, and ANA are exhibited in Figure 3.23a. The three zeolites showed a similar isotherm shape corresponding to type IV [121]. This shape of isotherm is typical of mesoporous materials showing a hysteresis loop associated with the occurrence of pore condensation. The hysteresis loop for all the samples was H3-type (observed at relative pressure range of 0.45-0.99), which is characteristic of systems with a distribution of “bottle shape” pores [179, 180].

3. RESULTS AND DISCUSSION

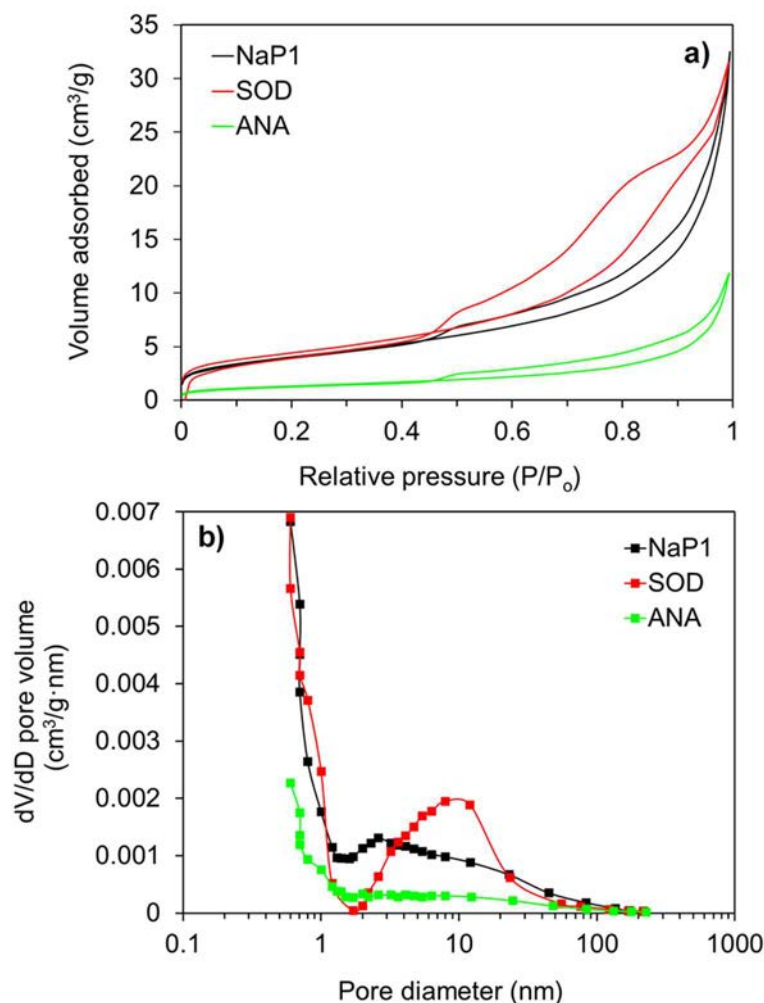


Figure 3.23 a) Nitrogen adsorption/desorption isotherms, and b) distribution of pore diameter of NaP1 (Z3), SOD (Z7), and ANA (Z13) obtained from the waste.

Concerning the pore size distribution (dV/dD curves) obtained by the BJH method (Figure 3.23b), the studied zeolites showed mesoporous distributions. The highest porosity found was for Z3 and Z7, where the pore size was around 2.6 nm and 8 nm, respectively, while Z13 exhibited a wide pore size distribution from 1.7 to 48 nm due to its smallest pore size.

The results from the textural and PSD characterization of the three zeolites from Alw_x are summarized in Table 3.20, including the values corresponding to S_{BET} , S_{EXT} , and parameters d_{10} , d_{50} , and d_{90} .

Table 3.20 Specific surface area (S_{BET}), external area (S_{EXT}), and particle size distribution (PSD) of NaP1, SOD, and ANA synthesized from the waste.

Sample	Phase	S_{BET} (m^2/g)	S_{EXT} (m^2/g)	PSD		
				d_{10}	d_{50}	d_{90}
Z3	NaP1	14.2 ± 0.09	14.5	1.51 ± 0.57	10.52 ± 0.15	23.12 ± 0.33
Z7	SOD	15.5 ± 0.06	14.6	2.42 ± 0.25	16.74 ± 0.52	41.46 ± 2.28
Z13	ANA	4.6 ± 0.03	4.5	0.41 ± 0.06	9.0 ± 0.04	17.51 ± 0.15

As can be seen, S_{EXT} , i.e. the area not involved with the filling of the micropores, was almost the same as that calculated by the BET method (S_{BET}), as shown Table 3.20. It indicates that the obtained zeolites are practically no microporous materials. The NaP1 and SOD zeolites, whose crystallite sizes (26 and 32 nm, respectively) were smaller than ANA (73 nm), exhibited higher S_{BET} values.

The low microporosity of the samples estimated by the physical nitrogen adsorption could be associated with diffusion restrictions of the N_2 molecule. The size of this molecule could limit its complete adsorption on the pores of the NaP1, SOD, and ANA zeolites. In some cases, the nitrogen adsorption/desorption analysis can provide unreliable results in the evaluation of materials containing small pore openings. The pore filling depends on the accessibility of the pores for the gas molecules (i.e., nitrogen) which is determined by the molecule size as well as the experimental conditions used in the analysis. The kinetic diameter of the N_2 molecule is estimated to be 3.6 Å which could not enter into all pores, in particular into the narrowest ones (< 4.5 Å), due to diffusion limitations [121].

Structurally NaP1 contains an interconnected channel system with sizes of 3.1 x 4.5 Å and 2.8 x 4.8 Å formed by 8-membered rings, while ANA has irregular channels formed by highly distorted 8-rings with 1.6 x 4.2 Å sizes [20]. The lowest S_{BET} value obtained for ANA (sample Z13) could be related to the small pore opening, as reported in the literature [157]. In the case of SOD, this zeolite has a smaller pore size (2.3 Å) [19] determined by its channel system containing apertures formed by 6-membered rings only.

Previous investigations have been proposed several alternatives to improve the porous characteristics of zeolites, in particular S_{BET} . For example, the variation of the initial Si/Al ratio from 5 to 11 in the reaction mixture of NaP1 can increase the value of S_{BET} from 29 to 47 m^2/g [181]. The synthesis of SOD from chemicals including different templates (mainly organic compounds) can lead to S_{BET} values of up to 266 m^2/g compared with

3. RESULTS AND DISCUSSION

that (11 m²/g) obtained without using templates [27]. The S_{BET} of ANA can be improved by using an acid and thermal treatment prior to the synthesis process, increasing the porosity from 16 to 424 m²/g when the concentration of acid (HCl) increases up to 4 M [157].

Particle size distribution

The PSD and parameters d₁₀, d₅₀ and d₉₀ for the zeolite samples were carried out using laser diffraction analysis and aqueous suspensions of each zeolite, as explained in Chapter 2.

The results obtained for the PSD and d₁₀, d₅₀, and d₉₀ of the three synthesized zeolites are shown in Figure 3.24 and Table 3.20.

Both NaP1 and SOD exhibited a quasi-unimodal population centered at 17 and 40 μm, respectively. The SOD zeolite presented the narrowest size particle profile. This was caused by the increase of the alkalinity in the reaction medium, resulting in an increase of the rate of nucleation and polymerization between silicate and aluminate anions, and thus, in the narrowest particle size distribution [182].

On the contrary, a bimodal distribution with two maxima centered at 0.3 and 12 μm was observed for the ANA zeolite.

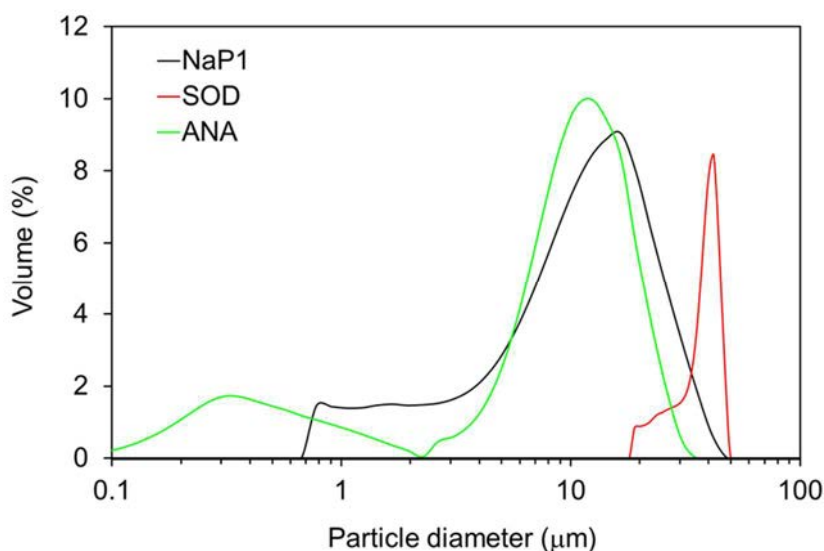


Figure 3.24 Particle size distribution of NaP1 (Z3), SOD (Z7), and ANA (Z13) synthesized from the waste.

Zeta potential

In adsorption processes, the electrostatic forces between adsorbent and adsorbates play an important role, favoring or limiting the adsorption on the adsorbent. For this reason, it is important to properly characterize physical-chemical properties such as ζ -potential of the adsorbent. ζ -potential can provide useful information about the surface charge of the zeolites in aqueous solution and interactions between the zeolites and pollutants (heavy metals and ammonium).

The ζ -potentials of the zeolites were determined in aqueous solutions at pH 7. According to the literature, absolute ζ -potential values > 20 mV are attributed to electrically stable materials [127, 128].

The results from the physical-chemical characterization of the three zeolites from Alw_x are summarized in Table 3.21, including the values of ζ -potential and CEC.

Table 3.21 Zeta-potential (ζ -potential) and cation-exchange capacity (CEC) of NaP1, SOD, and ANA obtained from the waste. Aqueous suspensions of zeolite prepared at initial pH 7 and 25 °C.

Sample	Phase	ζ -potential (mV)	CEC (meq NH ₄ ⁺ /g)
Z3	NaP1	-76.6	2.73 ± 0.02
Z7	SOD	-82.4	0.71 ± 0.03
Z13	ANA	-49.2	0.57 ± 0.04

The three zeolites exhibited negative ζ -potential values ranged between -50 and -82 mV, according to the kind of materials, aluminosilicates, which are based on a three-dimensional framework of AlO₄ and SiO₄ tetrahedra with a negatively charged surface [183].

The results revealed that more negative charges could be available in NaP1 and SOD than in ANA, and hence, the highest electrostatic attraction between the active sites of such zeolites and positively charged particles (or cations) could be expected. Thus, the studied zeolites can be used as adsorbents in adsorption processes of cations present in aqueous effluents.

The lowest ζ -potential (-82.4 mV) corresponded to SOD compared with the values obtained for NaP1 and ANA (-76.6 and -49.2 mV, respectively). It could be related to the excess of NaOH (5 M) used in the synthesis of SOD what could cause particle

3. RESULTS AND DISCUSSION

aggregation, as indicated its highest particle diameters, ranged between 2 and 42 μm (Table 3.20), resulting from the interaction between Na^+ and negative charges of the SOD framework.

Cation-exchange capacity (CEC)

The CEC of the zeolites were obtained by exchange between the NH_4^+ cations from a commercial salt (NH_4Cl) and mainly the Na^+ cations from the structure of the zeolites in aqueous medium, as indicated in Chapter 2.

The CEC values of NaP1, SOD, and ANA are also collected in Table 3.21.

NaP1 (sample Z3) showed the highest CEC (2.73 meq NH_4^+ /g), which is in agreement with the values reported in the literature (0.72-3.7 meq/g) [19, 44, 59]. It could be associated with the low alkali concentration (1 M NaOH) as well as the mild temperature conditions (120 $^\circ\text{C}$) used during its hydrothermal synthesis. Thus, these conditions lead to the formation of the GIS-framework, which would allow ions and/or molecules to diffuse more easily through its interconnected channel system.

On the contrary, low-CEC zeolites such as SOD and ANA (samples Z7 and Z13) were obtained when using higher alkali concentration (5 M NaOH) and/or higher temperature (200 $^\circ\text{C}$) in the synthesis.

Previous investigations have reported CEC values ranged between 0.36 and 3.7 meq/g for the same types of studied zeolites prepared from different precursors via hydrothermal synthesis processes [19, 59, 166]. For instance, Querol et al. [19] developed the alkaline conversion of FA into NaP1 and ANA with CEC values (2.7 and 0.6 meq/g, respectively) quite similar to our results, but SOD from FA showed a lower CEC (0.3 meq/g). Chaisena and Rangsrivatananon [166] obtained NaP1, SOD, and ANA with CEC of 1.73, 0.87, and 0.36 meq/g, respectively, using diatomite as precursor.

The high-CEC of NaP1 obtained from Alw_x makes it susceptible to be used in the wastewater treatment as potential adsorbent of heavy metals and ammonium.

3.2.3 Lab-scale synthesis with mother liquor recycling

In order to minimize the generation of the effluents generated in the zeolitization process, and accordingly, its impact on the environment, the synthesis of zeolites from Alw_x was developed with ML recycling. Thus, the effects of two consecutive recycling cycles on the three types of zeolites (NaP1, SOD, and ANA) obtained from Alw_x were evaluated.

The synthesis experiments with ML recycling were performed using a fixed same liquid/solid ratio (25 mL/g) and the synthesis conditions required to obtain each type of zeolite. The ML volume used for the synthesis with recycling was approximately the same as the volume of the 1 M NaOH solution employed for the preparation of each type of zeolite.

The results obtained for the different laboratory conditions used to synthesize zeolites from Alw_x with ML recycling are summarized in Table 3.22.

Table 3.22 Experimental lab-scale synthesis conditions to obtain zeolites from the waste with mother liquor recycling, zeolitic phases, and reaction yields obtained.

Sample	t (h)	NaOH (M)	T (°C)	Liquid/solid ratio (mL/g)	Cycle	Phase	Yield (kg _{zeolite} /kg _{waste})
Z16	6	1	120	25	0	NaP1	2.30
Z17		-			1		2.45
Z18		-			2		2.19
Z19		5			0	SOD	2.05
Z20		-			1		2.05
Z21		-			2	SOD+NaP1	2.10
Z22		1	200		0	ANA	2.32
Z23		-			1		2.33
Z24		-			2		2.33

As observed, most experimental conditions allowed the formation of the three types of zeolite, specifically NaP1 and ANA, from Alw_x and ML recycling.

The yields achieved in the synthesis of NaP1, SOD, and ANA after the first ML recycling cycle were quite similar to those obtained without recycling.

After developing the second ML recycling, lower amount of NaP1 per kg of waste was obtained. The SOD zeolite was only obtained after the first ML recycling cycle, while a mixture of phases (SOD and NaP1) was obtained after the second ML recycling. These

3. RESULTS AND DISCUSSION

findings could be attributed to a lower alkalinity of ML in the reaction medium compared with the initial (1 and 5 M for NaP1 and SOD, respectively) needed for the proper growth and formation of these zeolites.

On the contrary, the synthesis of ANA after two ML recycling cycles led to identical yield values. It could be explained because of the greater dependency of ANA to the temperature rather than to the alkalinity of ML.

3.2.3.1 Characterization of NaP1 obtained with recycling

The samples obtained from Alw_x via the one-step NaP1 synthesis process under ML recycling were characterized to determine their crystalline, morphological, and textural properties using XRD, SEM, and nitrogen adsorption/desorption analysis.

Crystalline characterization

The XRD patterns of the samples obtained at 120 °C for 6 h after the first (Z17) and second (Z18) ML recycling cycle compared with the original NaP1 zeolite (Z16) are shown in Figure 3.25. Their corresponding peak parameters (2θ and FWHM) and crystallite sizes (D_{hkl}) for the most intense diffraction peak are shown in Table 3.23.

The results revealed the presence of NaP1 (ICDD PDF 01-071-0962) as the only zeolitic phase before and after the ML recycling. The samples obtained after the ML recycling exhibited well-defined diffraction profiles with the 301 reflection centered at around 28°, and no shifts of the 2θ and FWHM values were observed (Table 3.23). The zeolitization process developed with ML recycling seems not to modify the crystallite sizes (25-31 nm) of the zeolites compared with that obtained from the initial synthesis using 1 M NaOH and without recycling (29 nm).

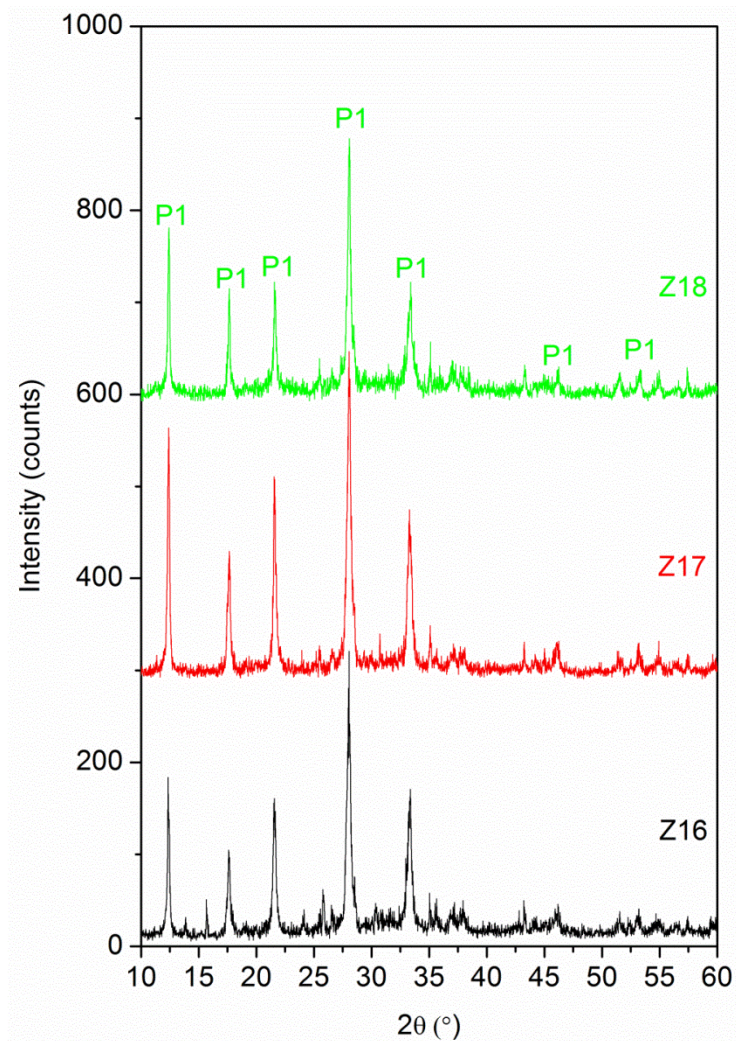


Figure 3.25 XRD patterns of NaP1 synthesized at 120 °C for 6 h after the first (Z17) and second (Z18) mother liquor recycling compared with the initial NaP1 zeolite (Z16) obtained with 1 M NaOH. P1 = NaP1 (ICDD PDF 01-071-0962).

Table 3.23 Peak parameters (2θ and FWHM) and crystallite sizes (D_{hkl}) calculated for the samples obtained from the waste via the lab-scale synthesis of NaP1 with mother liquor recycling.

Sample	Phase	2θ (°)	FWHM	D_{301} (nm)
Z16	NaP1	28.04	0.28	29
Z17		28.07	0.33	25
Z18		28.07	0.27	31

A diffraction profile of narrow peaks and high intensity was observed for Z17, probably due to the beneficial effect of the small quantities of NaP1 seeds present in the first ML. These crystal seeds favor the nucleation and crystal growth of the zeolite as described by Cardoso et al. [59] for zeolite NaP1 from coal fly ash.

3. RESULTS AND DISCUSSION

The sample Z18 obtained after the second ML recycling cycle led to a profile of slightly lower intensity where the peak centered at 33.3° was broader. This could be ascribed to the presence of K^+ cations in the reaction medium. The successive ML recycling cycles can lead to the enrichment in salts (sodium and potassium chlorides, etc.) from the Alw_x . This would involve a potential competition between Na^+ and K^+ cations. Unlike the Na^+ cation, K^+ has a larger size that could originate a broadening of the XRD profile of the sample Z18.

As the amount of Na^+ cations from the second ML could be deficient compared with the required amount for the synthesis of high-crystalline NaP1 (sample Z16), probably it would be necessary to accurately adjust the amount of Na^+ adding a small volume of fresh 1 M NaOH to obtain the theoretical Na/Al ratio of the NaP1 framework.

The amount of NaP1 achieved in the first recycling (Z17) per kg of waste was 2.5 kg (Table 3.22), while a somewhat lower yield (2.2 kg of NaP1 per kg of waste) was obtained after the second ML recycling (Z18).

Morphological characterization

The results obtained by SEM revealed the characteristic structure of NaP1 for Z17 and Z18. Both samples exhibited a homogenous morphology similar to the sample prepared without ML recycling (Z16). Thus, the synthesis developed under ML recycling does not seem to modify the morphology of the samples.

As an example, Figure 3.26 shows the SEM images, EDS spectrum, and microchemical point analysis (average of ten zones selected) of the sample Z18 obtained after the second ML recycling.

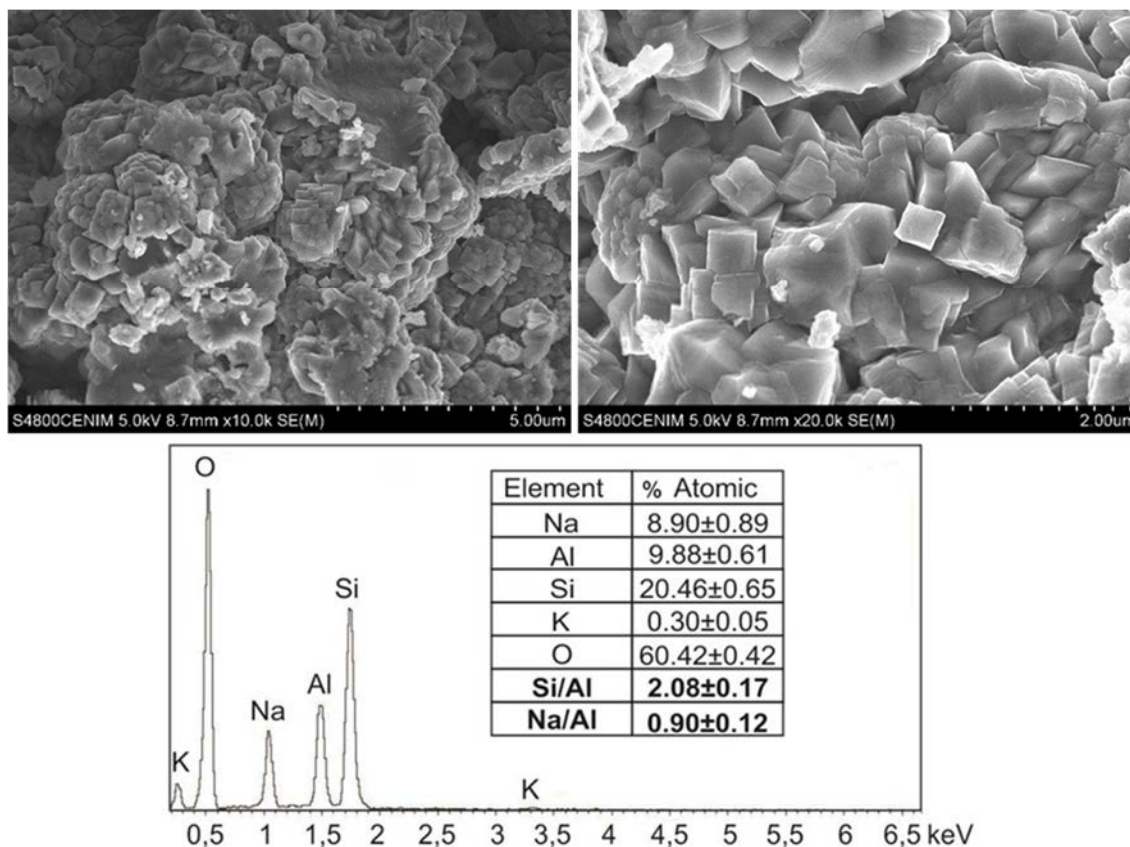


Figure 3.26 SEM images and EDS spectrum and microchemical point analysis of NaP1 obtained from the second mother liquor recycling (sample Z18).

The EDS analysis showed that sodium is the main exchange cation in the structure of NaP1, along with minor quantities of potassium detected in the microchemical point analysis of several crystals with a low K /Na ratio (0.03) but slightly higher than the original zeolite (Z16). For Z18, the average Si/Al ratio obtained was of 2.08 ± 0.17 , slightly higher than the value of Z16 (Si/Al = 1.85), while a similar average Na/Al ratio (0.90 ± 0.12) was obtained.

Nitrogen adsorption/desorption analysis

The nitrogen adsorption/desorption isotherms and the pore size distributions in the mesopore and low macropore range of the samples Z17 and Z18 compared with the initial zeolite synthesized without ML recycling (Z16) are shown in Figure 3.27.

The two samples obtained after the ML recycling (Z17 and Z18) exhibited the same type of isotherm (type IV) as the initial zeolite (Z16), and also showed a hysteresis loop at relative pressure (P/P_0) range of 0.45-0.99. It indicates that the samples obtained were mesoporous and practically no microporous zeolites (Figure 3.27a).

3. RESULTS AND DISCUSSION

Concerning the pore size distribution, the samples Z17 and Z18 exhibited a similar average pore diameter (around 2.6 nm), which was similar to that obtained for Z16 (Figure 3.27b).

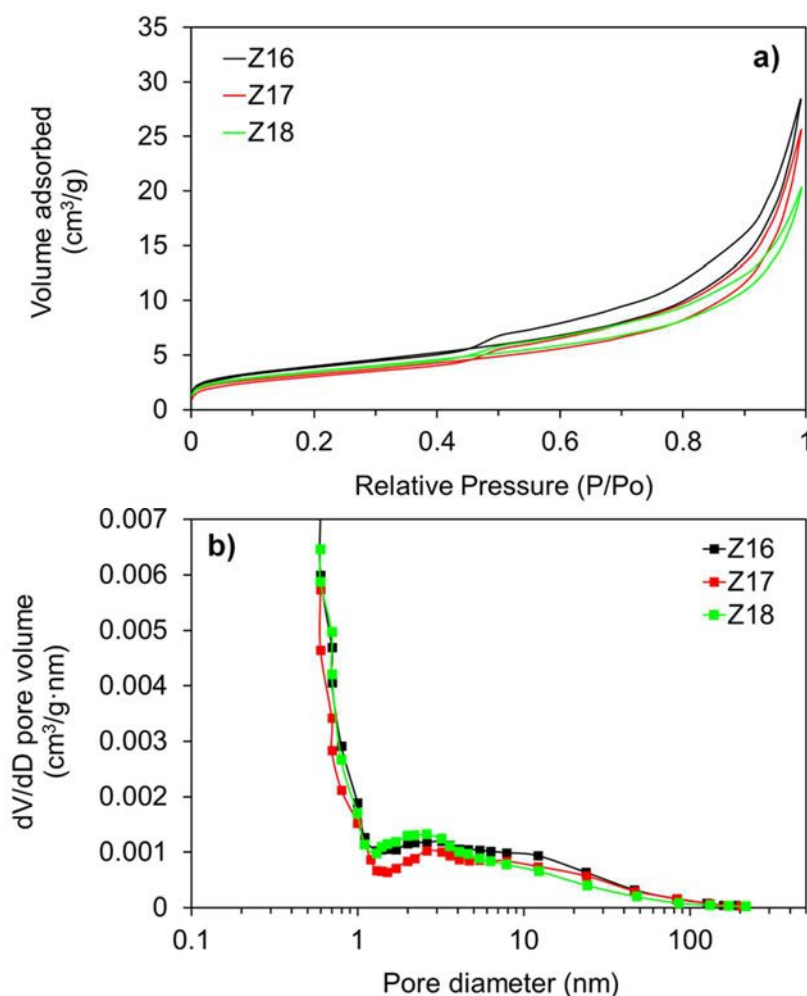


Figure 3.27 a) Nitrogen adsorption/desorption isotherms and b) pore diameter distribution of NaP1 obtained without recycling (Z16) and after the first (Z17) and second recycling cycle (Z18).

Both the sample obtained after the first and second recycling showed very similar values of S_{BET} and S_{EXT} , but slightly lower than sample Z16, as shown in Table 3.24. Thus, the ML recycling seems to maintain the textural properties of the samples when it is compared with the synthesis process developed without recycling.

Table 3.24 Specific surface area (S_{BET}) and external area (S_{EXT}) of NaP1 obtained without mother liquor recycling (Z16) and after the first (Z17) and second recycling cycle (Z18).

Sample		S_{BET} (m ² /g)	S_{EXT} (m ² /g)
Z16	Initial zeolite (without recycling)	14.2	14.5
Z17	First ML recycling	11.5	11.6
Z18	Second ML recycling	12.5	12.7

Chemical analysis of mother liquor

The mother liquors generated after the zeolitization process were analyzed to evaluate their chemical composition, pH, and conductivity and compared with the fresh alkali solution (1 M NaOH).

Table 3.25 shows the chemical composition (expressed as $\mu\text{g/mL}$) of the first and second recycled mother liquor (ML1 and ML2, respectively) used for the synthesis of the samples Z17 and Z18, respectively, as well as their pH and conductivity.

Table 3.25 Chemical composition determined by ICP-OES, pH, and conductivity (CE) of the mother liquors obtained in the synthesis of NaP1 after the first (ML1) and second (ML2) recycling.

Mother liquor	Composition ($\mu\text{g/mL}$)				Molar Si/Al ratio	pH	CE (mS/cm)
	Na	K	Si	Al			
ML1	17000	224	1048	65	15.5	12.98	136.7
ML2	13700	170	326	145	2.2	13.56	106.3

According to the ICP-OES analysis of ML1 and ML2, the main elements detected were Na, Si, K, and Al. As these elements form the frameworks of zeolitic materials, then ML would be a favorable medium to take into account in the synthesis of zeolites. Other elements such as Zn, P, Li, As, and Ti with lower concentrations (2.0-0.1 $\mu\text{g/mL}$) and traces of Cu, Ni, Co, Pb, Mn, Ca, and Mg (< 0.06 $\mu\text{g/mL}$) were also detected in ML1 and ML2. All these elements come from the waste because of its variable composition, as discussed in Section 3.1.

Moreover, both the pH and conductivity of the ML1 and ML2 were very similar to the 1 M NaOH solution (pH = 13.26 and CE = 175 mS/cm), thus confirming that ML can be used in the zeolite synthesis instead of the fresh alkali solution.

3. RESULTS AND DISCUSSION

On the other hand, a significant decrease of the Na⁺ cation content was observed in ML2. It would mean that for the next recycling cycle, a certain amount of fresh alkaline solution (i.e., 1 M NaOH) should be added to adjust the required Na⁺ content.

3.2.3.2 Characterization of SOD and ANA obtained with recycling

The effect of two consecutive cycles of ML recycling (without adding extra fresh alkalizing agent) was also evaluated to synthesize SOD and ANA in the experimental conditions collected in Table 3.22.

In the case of SOD zeolite, it was achieved as the only crystalline phase (ICDD PDF 01-086-1844) after the first ML recycling cycle (Z20), while NaP1 (ICDD PDF 01-071-0962) and small traces of SOD (Z21) were obtained after the second ML recycling (Figure 3.28). It can be associated with the decrease of the ML molarity in the second recycling cycle. The addition of a certain amount of fresh alkalizing agent should be necessary to properly synthesize SOD after a second recycling cycle.

The initial sample (Z19) and that obtained after the first ML recycling (Z20) exhibited the 211 reflection centered at around 24.4° typical of SOD, and no significant shifts of the 2 θ and FWHM values were found (Table 3.26).

Table 3.26 Peak parameters (2 θ and FWHM) and crystallite sizes (D_{hkl}) calculated for the samples obtained from the waste via the lab-scale synthesis of SOD and ANA with mother liquor recycling.

Sample	Phase	2 θ (°)	FWHM	D_{hkl} (nm)
Z19	SOD	24.43	0.31	26
Z20		24.40	0.36	23
Z21	SOD (4 %)	24.29	0.35	23
	NaP1 (96 %)	28.08	0.29	28
Z22	ANA	25.85	0.15	54
Z23		25.87	0.15	54
Z24		25.91	0.17	48

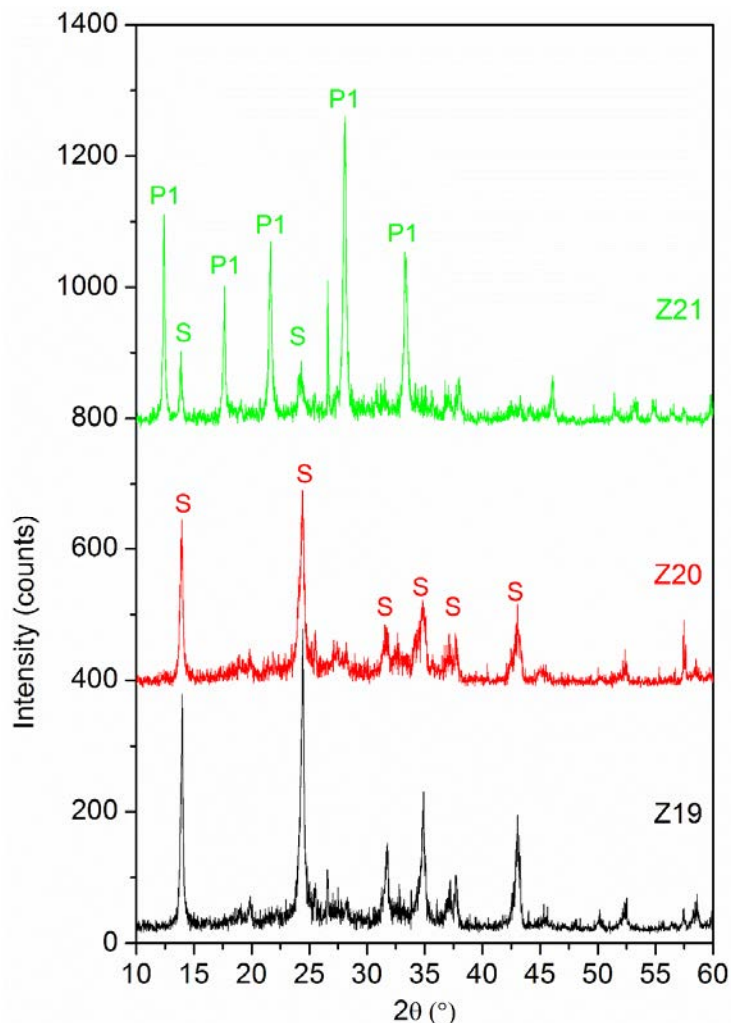


Figure 3.28 XRD patterns of SOD synthesized at 120 °C for 6 h after the first (Z20) and second (Z21) mother liquor recycling compared with the initial SOD zeolite (Z19) obtained with 5 M NaOH. S = hydroxy-sodalite (ICDD PDF 01-076-1639) and/or chloride-sodalite (ICDD PDF 01-086-1844) and P1 = NaP1 (ICDD PDF 01-071-0962).

Concerning the synthesis of ANA, both the first and second ML recycling cycle (samples Z23 and Z24, respectively) led to obtain this zeolite as the only crystalline phase (ICDD PDF 00-041-1478), as shown in Figure 3.29. The samples synthesized under ML recycling showed crystallinities similar to the initial ANA zeolite obtained without recycling (Z22) and the characteristic 400 reflection of ANA centered at around 25.9°.

Therefore, after ML recycling, no significant variations of the peak parameters and crystalline sizes of the SOD and ANA samples were appreciated (Table 3.26).

3. RESULTS AND DISCUSSION

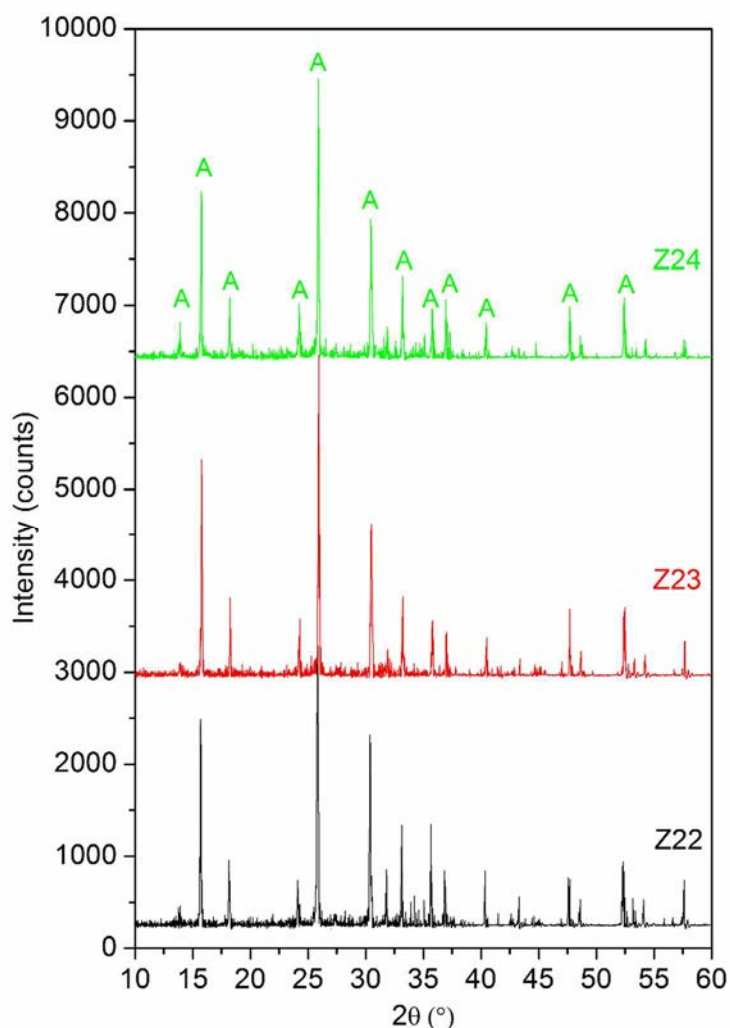


Figure 3.29 XRD patterns of ANA synthesized at 200 °C for 6 h after the first (Z23) and second (Z24) mother liquor recycling compared with the initial ANA zeolite (Z22) obtained with 1 M NaOH. A = analcime (ICDD PDF 00-041-1478).

The results obtained from the ML recycling in the synthesis demonstrates that the recycling of mother liquors seems to maintain the same crystalline, morphological, and textural properties of the zeolites as those obtained from the synthesis without recycling. It was due to the alkalinity and pH of ML which are similar to the fresh alkali solution (NaOH) used to synthesize the zeolites.

Therefore, the ML recycling not only allows reducing the economical impact of the synthesis process (the consumption of water and alkalizing agent is reduced), but also palliating the environmental impact (the effluent discharge is reduced).

3.2.4 Comparison of the synthesis conditions using other precursors

The experimental conditions used in the one-step synthesis process to obtain NaP1, SOD, and ANA from the aluminum waste were compared with those used to synthesize these zeolites from other types of precursors using the conventional hydrothermal processes.

Table 3.27 shows some examples of different sources employed, the conditions used, and the type of zeolite obtained. As can be seen, different synthesis conditions (time, temperature, and alkali concentration) can be employed for the preparation of zeolites depending on the type of precursor used.

Table 3.27 Zeolites obtained from different precursors by conventional hydrothermal processes.

Waste	t (h)	NaOH (M)	T (°C)	Zeolite	Reference
Diatomite	144	2.5	100	NaP1	[166]
	132	2.5	140	ANA	
	96	7.5	100	SOD	
Fly ash	24	1	150	NaP1	[59]
Natural clinker	24	3	150	ANA	[11]
Rice husk + kaolin	24	-	180	ANA	[36]
Fly ash	24	1	200	ANA	[184]
	24	3	150	SOD	
	9	3	125	NaP1	
Perlite	24	3	90	NaP1	[167]
	24	5	90	SOD	
Fly ash	24	3	95	NaP1	[44]
	24	5	95	SOD	
Quartz syenite	4	4	240	ANA	[163]
Aluminum waste (Alw _x)	6	1	120	NaP1	This Thesis
	6	1	160	ANA	
	6	5	120	SOD	

The valorization of the aluminum waste (Alw_x) into highly crystalline zeolites was developed through a direct and very short (6 h) zeolitization process due to chemical and mineralogical compositions of Alw_x, which are easily dissolved in alkali medium.

When zeolites are obtained from other types of precursors, such as diatomite [166], rice husk [36] and kaolin [36, 185] or FA [51, 186], previous activation and/or calcination treatments are normally needed to remove impurities from such sources. These

3. RESULTS AND DISCUSSION

treatments can prolong the zeolitization procedure (> 24 h), and accordingly they can raise the costs of the synthesis process.

Moreover, FA contains elements such as glass, quartz, and mullite that are hardly dissolved in the reaction medium. In most cases, the synthesis processes using FA can result in zeolitic products along with quantities of non-reactive quartz and/or mullite ($3\text{Al}_2\text{O}_3 \cdot 2\text{SiO}_2$) [59, 164, 187, 188].

In our case, secondary phases such as mullite and/or quartz were not observed in the results obtained by the XRD and SEM analyses. Only traces of quartz were detected at the lowest temperature tested (80 °C). It indicates that Alw_x could contain highly reactive elements what favors their complete dissolution in the alkaline reaction medium, favoring the growth and formation of the zeolites.

Generally, conversion processes of FA into zeolitic materials involve yields between 85 and 250 g of zeolite per kg of FA [51, 186], which are very much lower than using the aluminum waste (around 2.5 kg of zeolite per kg of Alw_x).

The synthesis process of zeolites from Alw_x seems to occur through the same stages described to prepare zeolites from FA, according to the literature [189]:

- Firstly, dissolution of the aluminum and silicon contents from the waste in alkaline conditions.
- Then, condensation of aluminum and silicon polymers on the surface of waste particles.
- Finally, nucleation and crystal growth of zeolites.

The most relevant findings derived from the lab-scale synthesis of zeolites using the aluminum waste are summarized in Figure 3.30, including the influence of the NaOH concentration and temperature for the optimal time (6 h) on the type of zeolite and crystalline size (expressed in nm).

As mentioned, the variation of the NaOH concentration from 1 to 5 M at the same temperature (120 °) leads to the phase transformation of the NaP1 zeolite into SOD, which is the most stable zeolitic phase at the highest alkali concentration. On the other hand, when the temperature increases up to 200 °C for the same NaOH concentration (1 M), the most thermally stable phase is formed corresponding to the ANA zeolite.

These results indicate that NaP1 is a metastable zeolite that tends to convert it into SOD or ANA zeolites which have lower CEC (0.71 and 0.57 meq/g), as the alkalinizing agent concentration or temperature increases.

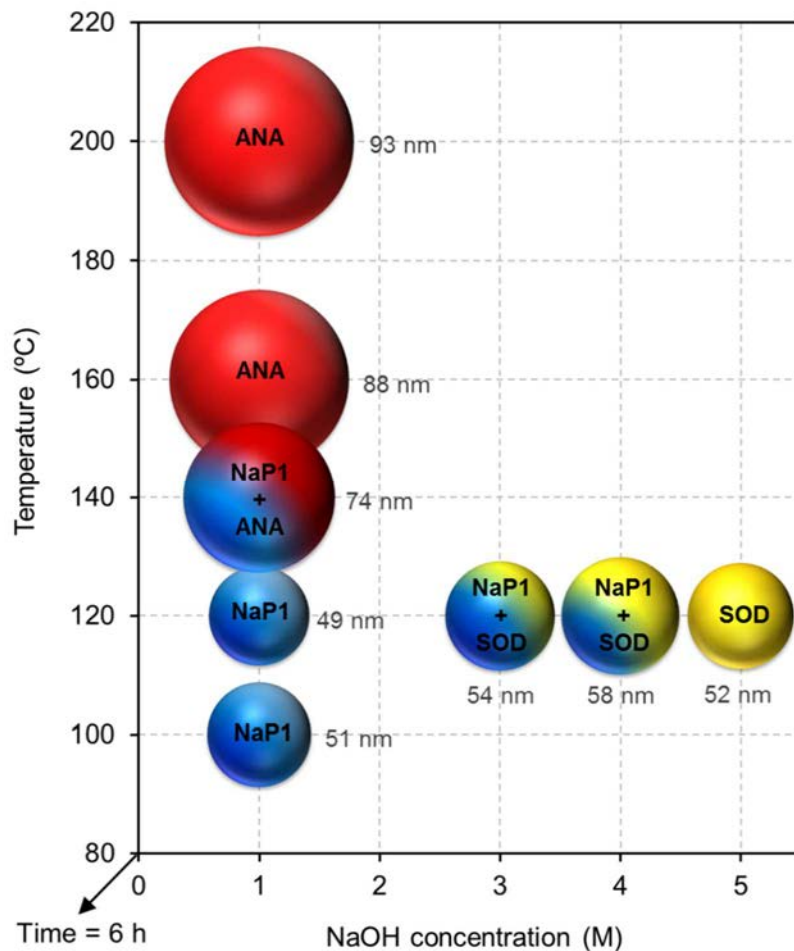


Figure 3.30 Zeolitic phases and their corresponding crystalline sizes as a function of the temperature and NaOH concentration tested to obtain the NaP1, SOD, and ANA zeolites from the waste through the simple one-step zeolitization process.

From an industrial point of view, NaP1 is the zeolite with most interest in water treatment applications due to its high CEC (2.7 meq/g) derived from its GIS-type framework. This zeolite is obtained from the aluminum waste at the mildest synthesis conditions (1 M and 120 °C) what would involve a considerable reduction in the cost of the zeolitization process compared with the other types of zeolites (SOD and ANA).

The developed zeolitization process led to successfully obtain different types of zeolites using the same type of waste precursor (Alw_x).

3. RESULTS AND DISCUSSION

3.3 Bench-scale synthesis of NaP1 zeolite

Bench-scale synthesis experiments to obtain the NaP1 zeolite from the representative waste (Alw_x) were performed in order to scale up the process for future industrial applications. The synthesis experiments were focused on this type of zeolite since NaP1 has greater industrial interest due to its higher cation-exchange capacity compared with the other zeolites (SOD and ANA) previously synthesized by the lab-scale zeolitization process (see Section 3.2).

As commented in Chapter 1, alkaline effluents such as mother liquor (ML) and rinse water (RW) generated in synthesis processes of zeolites are generally discarded. However, such effluents can contain valuable elements (Si, Al, and Na) that are the main constituents of zeolites, and besides saving process cost can be get by the recycling of the effluents. ML is the alkaline effluent produced during the zeolite synthesis process, while RW is the water generated after the cleaning step used to remove soluble species in the separation of ML and the zeolitic cake.

The main advantages derived from the re-use and recycling of ML and RW are the minimization of the consumptions of raw materials (water and NaOH) and the reduction of the amounts of residual effluents to be treated.

According to the results from the one-step synthesis process developed on lab scale (Section 3.2), the NaP1 zeolite was synthesized from Alw_x using a low alkalizing agent concentration (1 M NaOH) and mild synthesis conditions (120 °C for 6 h). In addition, the lab-scale synthesis process performed with ML recycling led to zeolitic phases with characteristics similar to those obtained without recycling.

In order to develop an environmentally-friendly synthesis process, the bench-scale synthesis tests were conducted under recycling of ML and RW at 120 °C for 6 h. To minimize the consumptions of both NaOH and water, an intermediate liquid/solid ratio (15 mL/g) was used in all the bench-scale synthesis tests.

The possibility to extrapolate the lab-scale synthesis conditions to the bench-scale zeolitization process under recycling was demonstrated. The effluents recycling allowed obtaining zeolites with properties similar to commercial zeolites and those reported in the literature. In addition, the recycling of the effluents (ML and RW) allowed reducing the

consumptions of raw materials and the generation of liquid residues to be treated, minimizing the impacts on the environment.

It is noteworthy that the recycling of the effluents in the bench-scale synthesis process led to the complete dissolution of the silica and alumina amounts present in Alw_x , resulting in highly pure NaP1.

Most results presented in Section 3.3 were previously published in a peer-reviewed publication [17].

3.3.1 Effect of effluents recycling

The effect of the recycling of effluents (ML and RW) on the bench-scale zeolitization process and products was evaluated according to the optimal conditions of the lab-scale synthesis experiments (initial Si/Al ratio = 2; $T = 120\text{ }^\circ\text{C}$; $t = 6\text{ h}$; and liquid/solid ratio = 15 mL/g).

The resulting samples were characterized by XRD, μ -XRF, SEM, FTIR, TG-DTA, and textural analysis, as shown below.

Additionally, the main properties of the samples obtained were compared with a commercial zeolite used for water treatment.

3.3.1.1 Crystalline and structural characterization

The influence of the effluents recycling on the structural characteristics of the samples was studied by XRD and FTIR analysis.

Figure 3.31 compares the XRD patterns of the reference sample synthesized using fresh 1 M NaOH solution without recycling (sample ZB0) with those obtained with ML and RW recycling, resulting in the second, third, and fourth zeolite generation (samples ZB1, ZB2, and ZB3, respectively).

The NaP1 zeolite was obtained in all the bench-scale experiments, being this zeolite identified as the only phase (ICDD PDF 01-071-0962). The samples showed well-defined XRD profiles that are identical to the sample Z14 obtained from Alw_x via the lab-scale synthesis process developed at the same conditions (Section 3.2).

3. RESULTS AND DISCUSSION

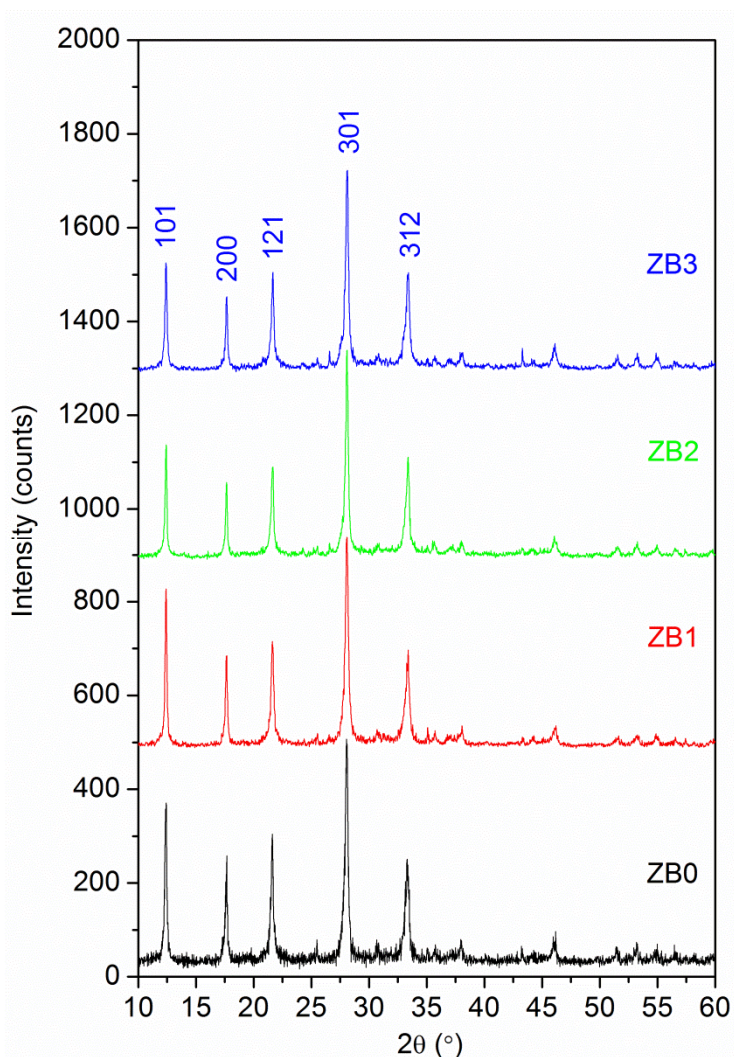


Figure 3.31 XRD patterns of NaP1 synthesized from the waste by bench-scale synthesis with fresh NaOH solution (ZB0) and with effluents re-used: first (ZB1), second (ZB2), and third (ZB3) recycling cycle. All peaks were identified with NaP1 (ICDD PDF 01-071-0962).

The yield (expressed as tons of zeolite per ton of waste), relative crystallinity, peak parameters (2θ and FWHM), and crystalline sizes (D_{hkl}) obtained in the bench-scale synthesis process with and without ML and RW recycling are shown in Table 3.28. The relative crystallinity was calculated from the sum of intensities of each diffraction peak of NaP1 (d_{101} , d_{200} , d_{112} , d_{301} , and d_{312}), designating the zeolite obtained in the synthesis without recycling as the reference (100 % crystallinity) [190]. The values of 2θ , FWHM, and D_{hkl} were only determined for to the most intense reflection of the zeolite (d_{301}).

Table 3.28 Zeolitic phase, yield (expressed as tons of zeolite per ton of waste), crystallinity, peak parameters (2θ and FWHM), and crystalline sizes (D_{hkl}) obtained in the bench-scale synthesis process with and without ML and RW recycling.

Sample	Phase	Yield ($t_{zeolite}/t_{waste}$)	Σ Intensity (counts)	Crystallinity (%)	2θ ($^\circ$)	FWHM ($^\circ$)	D_{301} (nm)
ZB0	NaP1	2.45	1580	100	28.07	0.33	25
ZB1		2.49	1464	92.6	28.07	0.30	27
ZB2		2.46	1312	83.0	28.09	0.28	29
ZB3		2.52	1322	83.6	28.09	0.29	28

Both the reference sample (ZB0) and the samples obtained with recycling (ZB1, ZB2, and ZB3) showed no shifts in their peak parameters (2θ and FWHM). The most intense 301 reflection was centered around 28° for ZB0 prepared with a fresh 1 M NaOH solution, and identical results were obtained for ZB1, ZB2, and ZB3 prepared from the ML and RW recycling.

As observed in the XRD profiles (Figure 3.31), the crystallinity as well as crystallite sizes, which ranged between 25 and 29 nm, (Table 3.28) of the samples did not vary significantly. It could be associated to the small quantities of NaP1 crystals present in the ML that act as seeds, thus favoring the nucleation and crystal growth of the zeolite.

The reached reaction yields were quite similar for all the samples, achieving approximately 2.5 ton of NaP1 per ton of waste after three consecutive recycling cycles. These values are in agreement with the yield reached for the sample Z14 (2.46 kg/kg) obtained in the lab-scale synthesis (Section 3.2). Although the zeolitization process with effluents recycling seems to slightly decrease the crystallinity (Table 3.28), this parameter was maintained after each recycling cycle between 93 and 83 % for the recycled samples (ZB1, ZB2, and ZB3), compared with the reference sample (ZB0).

The decrease of crystallinity could be related to the incorporation of other cations (e.g., K, Ca, etc.), which come from the liquid mixture of ML and RW, to the framework. It could slightly distort the zeolitic structure as a result of the difference of cation sizes compared with Na^+ .

The NaP1 zeolite obtained in these conditions was compared with a commercial zeolite used in water treatment applications. Figure 3.32 shows the diffraction pattern of the commercial zeolite analyzed using the same operating conditions of the XRD analysis. The XRD pattern of the commercial zeolite was characterized by the presence of NaP1

3. RESULTS AND DISCUSSION

zeolite as the main phase (ICDD PDF 01-071-0962), and zeolite X as the minor phase (ICDD PDF 00-038-0237) were also found, as can be observed in Figure 3.32.

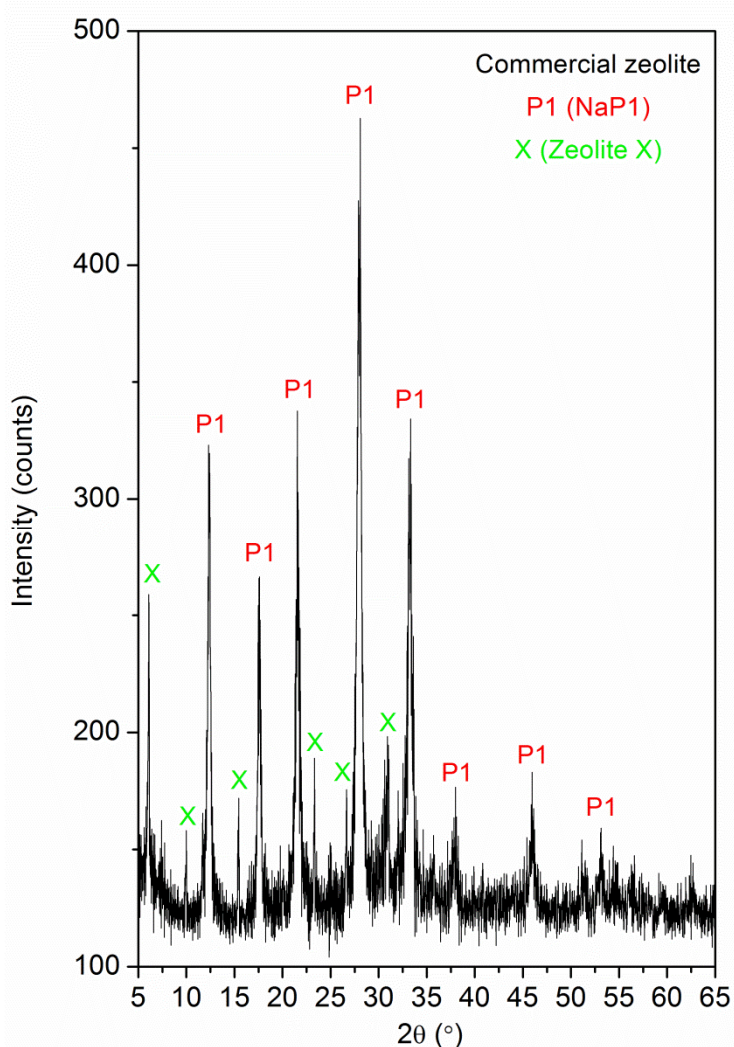


Figure 3.32 XRD pattern of a commercial zeolite (P1-X) characterized by NaP1 zeolite along with traces of zeolite X. All peaks were identified with NaP1 (ICDD PDF 01-071-0962) and zeolite X (ICDD PDF 00-038-0237).

The peak parameters and crystalline sizes (Table 3.29) of this commercial zeolite were evaluated for the most intense reflections of NaP1 (d_{301}) and the zeolite X (d_{111}). It exhibited the intense 301 reflection of the NaP1 phase at 28.07° , which is in good agreement with the 2θ values obtained (28.07 - 28.09°) for the samples synthesized from the waste without (ZB0) and with (ZB1, ZB2, and ZB3) effluents recycling.

Table 3.29 Peak parameters of a commercial zeolite (P1-X) characterized by NaP1 and traces of X zeolite.

Commercial zeolite P1-X	Phase	hkl	2 θ (°)	FWHM (°)	D _{hkl} (nm)
	NaP1	301	28.07	0.56	15
X	111	6.10	0.12	66	

The commercial zeolite (hereinafter, P1-X,) showed a crystallite size of around 15 nm determined for its main zeolitic phase (NaP1), which is smaller than the crystallite sizes (25-29 nm) obtained for ZB0, ZB1, ZB2, and ZB3 (Table 3.28). It could be attributed to the different synthesis process and conditions used to prepare P1-X from only pure chemical reagents what would lead to smaller crystals of zeolite.

Concerning the structural characterization of the samples, the FTIR spectra of ZB0, ZB1, ZB2, and ZB3 compared with the commercial zeolite (P1-X) are shown in Figure 3.33, in which the assignments of the IR absorption bands related to P1-X are included.

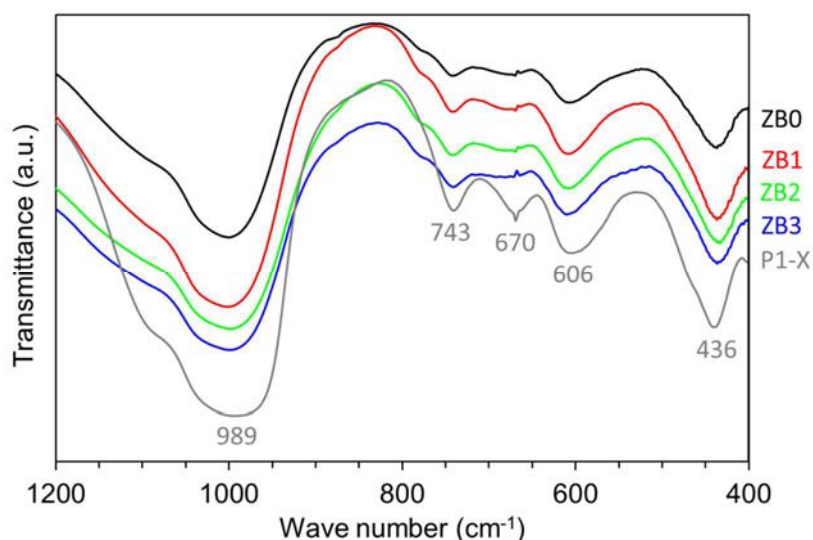


Figure 3.33 FTIR spectra of NaP1 obtained from the waste by bench-scale synthesis with liquid discharge (ZB0) and under the first (ZB1), second (ZB2), and third (ZB3) effluent recycling cycle. Wave number values shown for the commercial zeolite (P1-X).

The samples prepared without and with effluents recycling exhibited the spectrum characteristic of the NaP1 zeolite resulting in very similar assignments of the FTIR bands of each sample (Table 3.30).

3. RESULTS AND DISCUSSION

The samples obtained from Alw_x showed a very strong and broad band at 1000 cm⁻¹ with a shoulder at 1072 cm⁻¹ corresponding to the asymmetric stretching mode. The symmetric stretching mode of internal tetrahedron was associated with a medium band centered at 607 cm⁻¹, a weak band at 742 cm⁻¹, and a very weak band at 670 cm⁻¹, while the tetrahedron bending mode was observed at 437 cm⁻¹.

The absorption bands of the samples synthesized on bench scale coincide with the samples obtained from Alw_x through the lab-scale synthesis of NaP1. In addition, the assignments of the absorption bands of ZB0, ZB1, ZB2, and ZB3 were almost identical to those identified in the commercial zeolite (P1-X).

Table 3.30 Assignments of bands observed by FTIR for the NaP1 zeolites obtained from the waste by the bench-scale synthesis without recycling (ZB0) and with effluents recycling (ZB1, ZB2, and ZB3) compared with a commercial zeolite (P1-X).

Vibration mode	Wave number (cm ⁻¹)				
	ZB0	ZB1	ZB2	ZB3	P1-X
v(OH) ^a	3448	3448	3448	3448	3442
H ₂ O	1637 (m)	1637 (m)	1654 (m)	1637 (m)	1637 (m)
v _{as} (SiAlO) ^b	1072 (sh) 1000 (s)	1072 (sh) 1000 (s)	1077 (sh) 1000 (s)	1068 (sh) 1000 (s)	1084 (sh) 993 (s)
v _s (SiAlO) ^b	742 (w) 670 (w) 607 (m)	742 (w) 669 (w) 607 (m)	742 (w) 670 (w) 607 (m)	742 (w) 675 (w) 610 (m)	741 (w) 669 (w) 604 (m)
δ(T-O) ^c	437 (m)	437 (m)	433 (m)	437 (m)	440 (m)

^a v(OH): hydroxyl stretching.

^b v_{as}(SiAlO) and v_s(SiAlO): asymmetric and symmetric stretching.

^c δ(T-O): bending of SiO₄ or AlO₄ tetrahedron.

Absorption band intensity: s = strong; sh = shoulder; m = medium; w = weak; and vw = very weak.

These findings are in good agreement with the FTIR results found in the literature for NaP1 synthesized from pure chemical reagents, including water glass and NaOH, by hydrothermal methods [154, 191]. Similar FTIR bands were reported for NaP from other precursors like kaolin treated by means of a hydrothermal route at 100 °C for 48 h [55].

3.3.1.2 Chemical characterization

The determination of the elemental chemical composition of the zeolites obtained was determined by using μ -XRF analysis.

As an example, the chemical compositions of the reference sample (ZB0) obtained from Alw_x after the bench-scale zeolitization process without ML and RW recycling and the commercial zeolite are shown in Table 3.31.

Table 3.31 Chemical composition (determined by μ -XRF) of NaP1 synthesized from the waste by bench-scale synthesis without recycling (ZB0) compared with a commercial zeolite (P1-X). Standard deviation = ± 0.1 .

Element	ZB0 (wt.%)	P1-X (wt.%)
SiO ₂	55.16	63.25
Al ₂ O ₃	26.74	28.04
Na ₂ O	7.62	7.49
CaO	2.88	0.16
TiO ₂	2.77	0.22
K ₂ O	2.02	0.70
Fe ₂ O ₃	1.18	0.15
MgO	0.96	-
ZnO	0.41	-
CuO	0.26	-
Total	100	100
Molar SiO ₂ /Al ₂ O ₃ ratio	3.5	3.8

As can be seen, the main elements (Si, Al, and Na) that constitute the structure of the NaP1 zeolite were detected in the sample synthesized from Alw_x after the bench-scale synthesis without effluents recycling (ZB0).

In addition to sodium (the main exchange cation detected), small quantities of other cationic metals, including calcium, titanium, potassium, and iron, and traces of magnesium, zinc, and copper were also found in ZB0. Some of such cationic metals (calcium, titanium, potassium, and iron) were also present in the commercial zeolite.

The zeolite ZB0 showed a molar SiO₂/Al₂O₃ ratio of 3.5, which is very close to the theoretical value (SiO₂/Al₂O₃ = 3.3) for NaP1 and is similar to commercial P1-X zeolite.

3. RESULTS AND DISCUSSION

3.3.1.3 Morphological characterization

The zeolitization process using both the fresh NaOH solution and the recycled effluents (ML and RW) resulted in highly crystalline zeolitic products with the same morphology, as shown in Figure 3.34. This morphology, which is characteristic of the NaP1 zeolite, consisted of “cauliflower-like” primary aggregates with well-defined cubic nanocrystals (ranged between 200 and 500 nm).

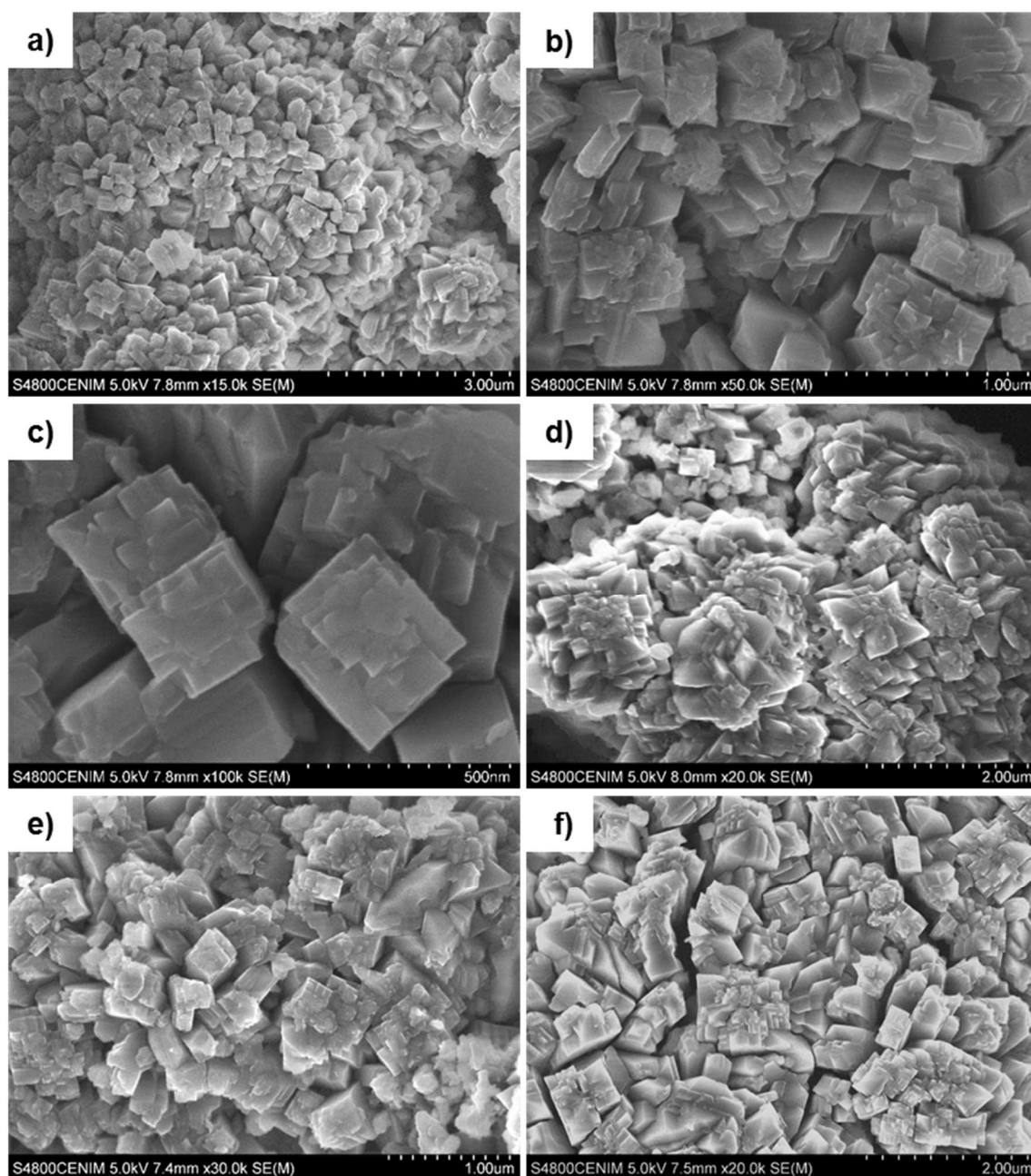


Figure 3.34 SEM images at different magnifications of NaP1 from the waste via bench-scale synthesis. Sample ZB0 obtained using fresh alkalizing agent (a-c) and samples ZB1, ZB2, and ZB3 prepared after the first (d), second (e), and third (f) effluent recycling cycle, respectively.

The reviewed literature shows identical morphologies for NaP obtained from chemical reagents by a hydrothermal method [191] and by other methods like microwave radiation [158]. The hydrothermal conversion of FA into NaP with 2 M NaOH at 100 °C for 24 h also showed this morphology [192]. However, traces of unreacted quartz and mullite from FA are frequently observed in the resulting zeolitic phases due to the lower solubility of these minerals in alkali solution [19, 52, 193, 194].

According to the EDS analyses (Table 3.32), the average molar Si/Al ratio ranged between 1.65 and 1.80 for ZB0, ZB1, ZB2, and ZB3. These values are in accordance with the corresponding stoichiometric ratio (~1.67) of the NaP1 zeolite ($\text{Na}_6\text{Al}_6\text{Si}_{10}\text{O}_{32}\cdot 12\text{H}_2\text{O}$).

Table 3.32 EDS analysis of the NaP1 zeolite synthesized from the waste by the bench-scale zeolitization process without (ZB0) and with effluent recycling (ZB1, ZB2, and ZB3).

Sample	Atomic %				Si/Al ratio
	Na	Al	Si	O	
ZB0	9.40 ± 0.99	11.63 ± 0.54	18.78 ± 0.44	59.91 ± 0.47	1.65 ± 0.06
ZB1	9.71 ± 0.56	11.25 ± 0.05	18.95 ± 0.26	59.82 ± 0.24	1.69 ± 0.03
ZB2	7.72 ± 2.04	11.54 ± 0.48	19.64 ± 0.61	60.68 ± 0.78	1.70 ± 0.07
ZB3	8.67 ± 1.23	10.95 ± 0.05	19.71 ± 0.59	60.34 ± 0.57	1.80 ± 0.06

Sodium was the main exchange cation in the structure of the obtained zeolites. Thus, for all the samples, Na/Al ratios between 0.8 and 0.9 were obtained. In general, other exchange cations were not observed, but scarcely, minor potassium content (with K/Na ratio < 0.03) was detected.

The NaP1 morphology arising from the bench-scale synthesis process developed without and with recycling was found to be identical to that obtained from the lab-scale synthesis.

3.3.1.4 Thermal behavior

The thermal behavior of all samples was studied from room temperature to 1000 °C. The TG-DTA curves recorded between 25 and 400 °C for the reference sample (Figure 3.35) and samples obtained after the effluents recycling (Figure 3.36, Figure 3.37, and Figure 3.38) are shown below.

3. RESULTS AND DISCUSSION

All the samples followed the same profile showing identical TG-DTA curves. The total mass loss, up to 1000 °C, was related to the content of water released from the zeolite structure taking place in several steps for each sample.

The reference sample ZB0 involved a total mass loss of 13.4 wt.% up to 1000 °C, being almost similar to that obtained in the lab-scale synthesis of NaP1 (sample Z3) from Alw_x at 120 °C for 6 h (13.9 wt.%).

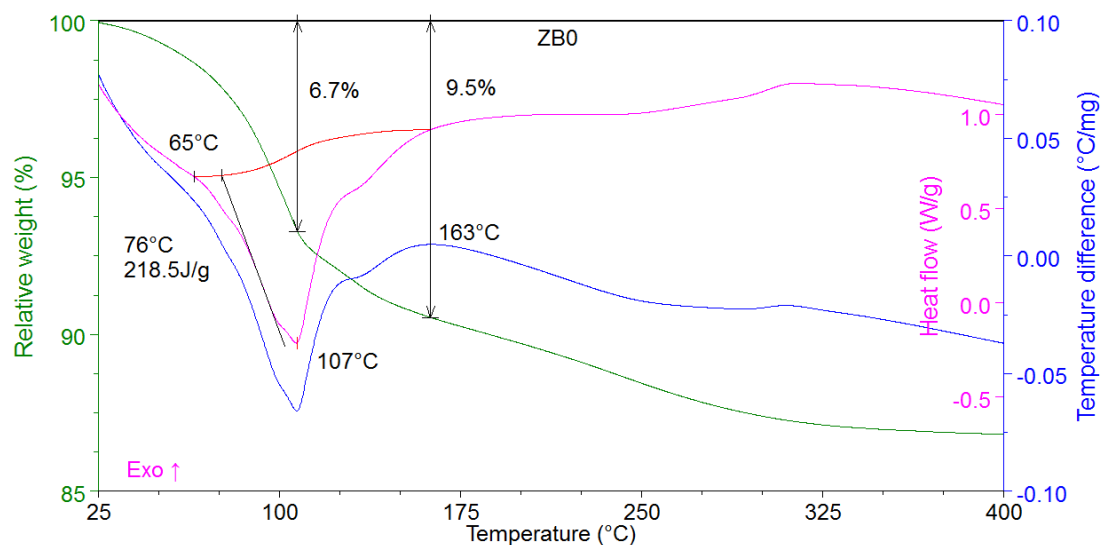


Figure 3.35 TG-DTA curve of the initial NaP1 zeolite (ZB0) obtained from the waste by the bench-scale synthesis.

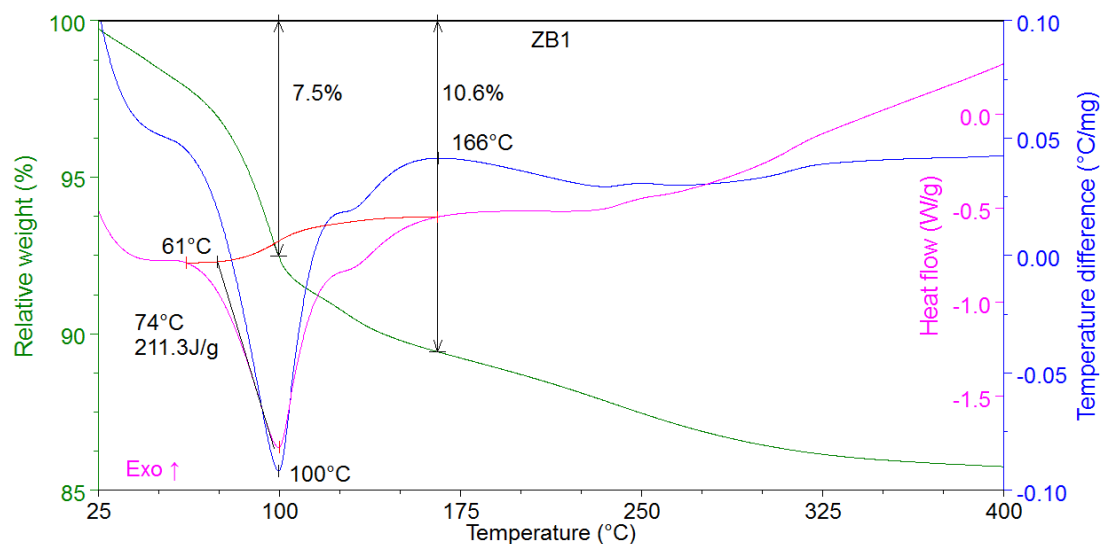


Figure 3.36 TG-DTA curve of the NaP1 zeolite obtained after the first mother liquor recycling (ZB1) by the bench-scale synthesis.

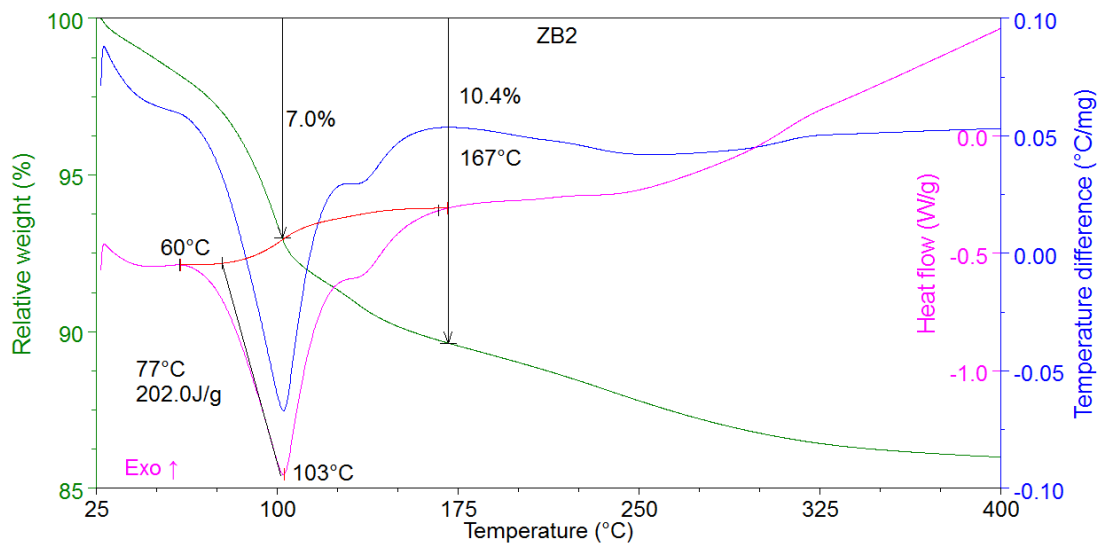


Figure 3.37 TG-DTA curve of the NaP1 zeolite obtained after the second mother liquor recycling (ZB2) by the bench-scale synthesis.

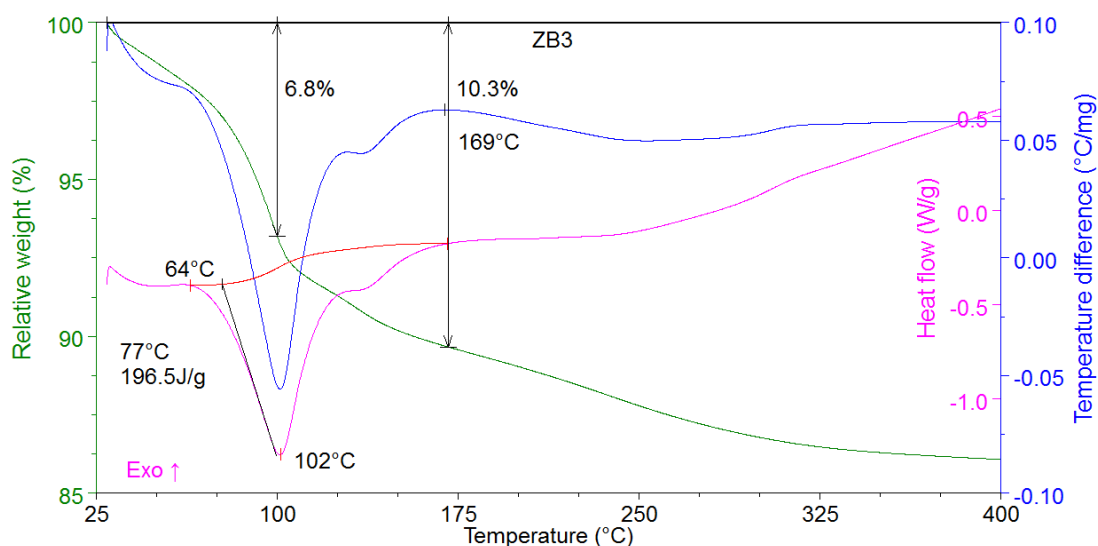


Figure 3.38 TG-DTA curve of the NaP1 zeolite obtained after the third mother liquor recycling (ZB3) by the bench-scale synthesis.

The samples ZB1, ZB2, and ZB3 showed slightly higher total mass losses of 15.1, 14.8, and 14.9 wt.%, respectively.

As commented above, the mass losses are associated with the content of water molecules present in the zeolite. It would involve 10 water molecules for ZB0 and 11 water molecules for ZB1, ZB2, and ZB3. These values are quite similar to the theoretical water content of NaP1 corresponding to 12 water molecules [195].

3. RESULTS AND DISCUSSION

Compared to the mass losses values obtained, the literature shows both lower and higher values, between 12.5 and 18.0 wt.%, for NaP obtained from chemicals by a hydrothermal method at 100 °C for 4 days [191] and from gels of MCM-22 zeolite with framework type MWW (Mobil Composition of Matter-twenty-two [20]) via microwave heating at 140 °C for 3 h [158].

The strongest endothermic peak of NaP1 was determined at 107 °C for the reference sample (ZB0), due to the highest heat flow (218.5 J/g) from the release of water strongly adsorbed in the channels of NaP1 (Figure 3.35).

The sample ZB1 showed the maximum water loss at 100 °C resulting in water evaporation energy of 211.1 J/g (Figure 3.36), while ZB2 and ZB3 showed this water release with heat flows of 202.0 and 196.5 J/g at similar temperature values, 102 and 102 °C, respectively (Figure 3.37 and Figure 3.38).

The results obtained from the TG-DTA curves are collected in Table 3.33 including the mass losses and integrate peak analyses.

Table 3.33 TG-DTA analyses of the initial NaP1 zeolite (ZB0), and the recycled zeolites (ZB1, ZB2, and ZB3) from the waste.

Effect	DTA			TG	
	Temperature interval (°C)	Peak temperature (°C)	Integrate peak ($\mu\text{V}\cdot\text{min}/\text{mg}$)	Temperature interval (°C)	Mass loss (%)
Initial NaP1 (ZB0)					
1 Endo	65-163	107	3.7	25-107	6.7
2	-	-	-	107-163	2.8
3	-	-	-	163-1000	3.9
First recycling (ZB1)					
1 Endo	61-166	100	3.6	25-100	7.5
2	-	-	-	100-166	3.1
3	-	-	-	166-1000	4.5
Second recycling (ZB2)					
1 Endo	60-167	103	2.5	25-103	7.0
2	-	-	-	103-167	3.4
3	-	-	-	167-1000	4.4
Third recycling (ZB3)					
1 Endo	64-169	102	3.1	25-102	6.8
2	-	-	-	102-169	3.5
3	-	-	-	169-1000	4.6

One explanation for this is that the cations from the recycled effluents (ML and RW) could occupy the most internal voids to balance the zeolite charge, leading to lowest temperatures for the release of water from the zeolitic structure.

The thermal behavior of the NaP1 zeolites obtained via bench-scale synthesis is assumed exactly equivalent to that of NaP1 prepared on lab scale (sample Z3).

Similarly, the samples obtained through the bench-scale synthesis were transformed into a more stable phase, nepheline, after heating up to 1000 °C.

3.3.1.5 Textural characterization

The textural properties such as the specific surface area (S_{BET}) and external area (S_{EXT}), characteristic values (d_{10} , d_{50} and d_{90}) of particle size distribution (PSD), zeta potential (ζ -potential), and cation-exchange capacity (CEC) of ZB0, ZB1, ZB2, and ZB3 are studied and compared with the commercial zeolite (P1-X).

Nitrogen adsorption/desorption analysis

The nitrogen adsorption/desorption isotherms as well as the S_{BET} and S_{EXT} values for ZB0, ZB1, ZB2, and ZB3 compared with P1-X are shown in Figure 3.39 and Table 3.34.

All samples exhibited isotherms type IV with a hysteresis loop type H3 [121] at a relative pressure range between 0.45 and 0.99 (Figure 3.39), indicating meso and macroporous behavior.

Similar results to those from lab-scale synthesis using Alw_x were obtained. Low S_{BET} values, which were close to the S_{EXT} values, were obtained for both the reference sample and samples synthesized with ML and RW recycling (Table 3.34).

These low S_{BET} results obtained for the samples from Alw_x could be related to the low outgassing conditions (60 °C for 24) used prior to nitrogen adsorption/desorption analysis.

3. RESULTS AND DISCUSSION

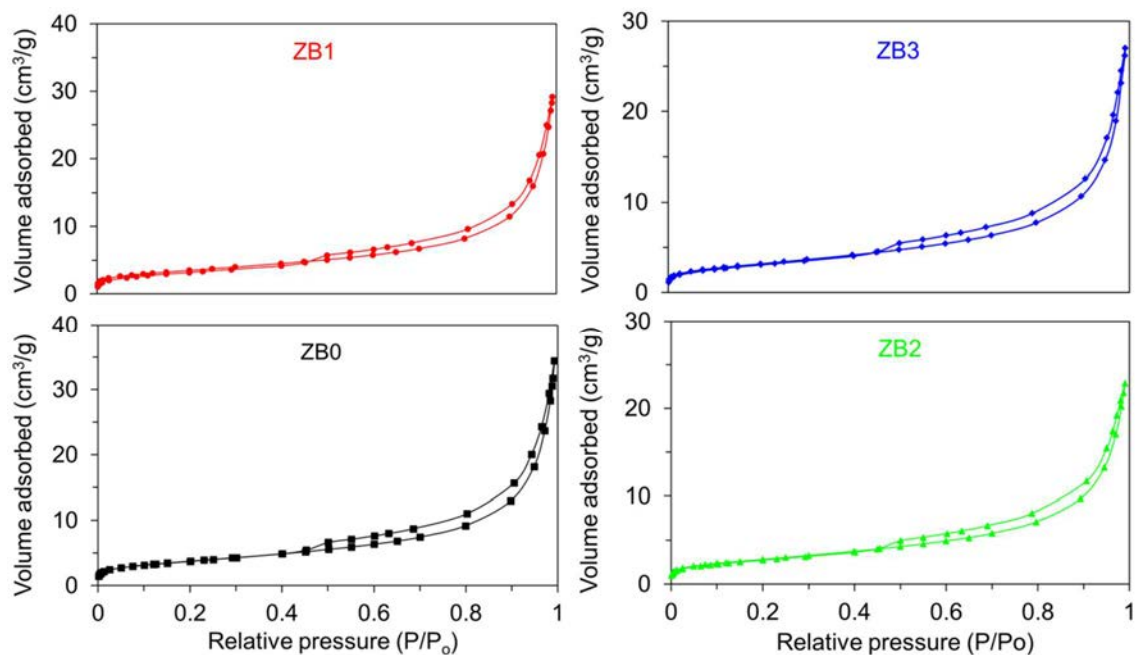


Figure 3.39 Nitrogen adsorption/desorption isotherms of NaP1 synthesized from the waste by bench-scale synthesis using fresh NaOH solution (ZB0) and after effluent recycling (ZB1, ZB2, and ZB3). Outgassing conditions: 60 °C for 24 h.

Table 3.34 Specific surface area (S_{BET}) and external area (S_{EXT}) values of the NaP1 zeolites from the waste through the bench-scale synthesis without (ZB0) and with (ZB1, ZB2, and ZB3) recycling. Outgassing conditions: 60 °C for 24 h.

Sample	S_{BET} (m ² /g)	S_{EXT} (m ² /g)
ZB0	13.21 ± 0.08	13.38
ZB1	12.27 ± 0.06	11.93
ZB2	10.05 ± 0.08	10.39
ZB3	11.24 ± 0.07	11.21

According to the literature, different S_{BET} values are found for different outgassing conditions for NaP1 obtained from chemicals and waste sources. For example, Cama et al. [196] obtained NaP1 from FA by an alkaline treatment. The authors found higher S_{BET} values (18 ± 2 m²/g) than a commercial zeolite (10 ± 1 m²/g), and enhanced its porosity by an acid treatment that showed the highest S_{BET} (63 ± 3 m²/g). Prior to nitrogen adsorption experiments, the samples were outgassed at 140 °C for 24 h. Bandura et al. [197] reported higher area values (S_{BET} around 95 m²/g) when using higher outgassing temperature conditions (250 °C for 24 h) for NaP1 synthesized from FA at 75 °C for 24 h.

It seems that the higher outgassing temperature, the higher S_{BET} is achieved after the nitrogen isotherm analysis.

However, some works that use high outgassing temperatures (200-250 °C) report low S_{BET} values for the same type of zeolite (NaP1) prepared from conventional chemical reagents. For example, Ali et al. [191] obtained NaP1 at lower temperature (100 °C) and for a longer time (4 days), leading to low porosity, 6 - 14 m²/g (samples outgassed at 200 °C). Huang et al. [198] reported even lower values than 5 m²/g (outgassing conditions: 250 °C, 10 h) for NaP. The authors stated that these results were related to the high crystallization of NaP and its small pores.

In order to elucidate the effect of the outgassing temperature on the microporosity of the samples, some nitrogen adsorption/desorption analyses were conducted at higher temperature (350 °C for 24 h), as shown in Table 3.35.

Table 3.35 Specific surface area (S_{BET}), external area (S_{EXT}), total, meso and micropore volume values (V_{total} , V_{meso} , and V_{micro}) of NaP1 from the waste through the bench-scale synthesis without recycling (ZB0) and after three recycling cycles (ZB3) compared with a commercial zeolite (P1-X).
Outgassing conditions: 350 ° for 24 h.

Sample	S_{BET} (m ² /g)	S_{EXT} (m ² /g)	V_{total} (cm ³ /g)	V_{meso} (cm ³ /g)	V_{micro} (cm ³ /g)
ZB0	15.93 ± 0.08	15.08	0.04773	0.04729	0.00044
ZB3	12.78 ± 0.06	11.92	0.03871	0.03827	0.00044
P1-X	56.17 ± 1.50	8.63	0.04863	0.02556	0.02307

After outgassing the zeolites at higher temperature (350 °C), the S_{BET} values were slightly improved and higher than the S_{EXT} values, but the micropore volumes (V_{micro}) were very low for ZB0 and ZB3. The commercial zeolite (P1-X) showed higher S_{BET} and V_{micro} values and lower S_{EXT} because of its synthesis from the use of chemical reagents instead of waste sources like Alw_x.

Concerning microporosity, the low values obtained for the samples from Alw_x could be more influenced by the synthesis conditions used than the outgassing temperature used in the nitrogen adsorption/desorption analysis.

3. RESULTS AND DISCUSSION

Some works evaluate the influence of synthesis parameters like Si/Al ratio on the porosity of zeolites. For instance, Sharma et al. [181] obtained different S_{BET} values (outgassing conditions: 250 °C, 6 h) depending on the reaction mixture Si/Al ratio used for the synthesis of NaP1 microspheres from chemicals. The authors achieved the lowest area ($S_{\text{BET}} = 29 \text{ m}^2/\text{g}$) for the lowest reaction ratio (Si/Al = 5), while the highest ratio (Si/Al = 11) seems to favor the microporosity ($S_{\text{BET}} = 47 \text{ m}^2/\text{g}$) of the zeolite.

As commented in Chapter 2, the initial Si/Al ratio (Si/Al = 2) was maintained in all lab-scale and bench-scale experiments without and with ML and RW recycling. Although this Si/Al ratio was low compared to the literature [181], it led to highly-crystalline NaP1 whose microporosity could be improved through the use of “templates” in the synthesis process.

The nitrogen adsorption/desorption is usually considered as a standard textural analysis, but this technique could lead to inaccurate values for the assessment of materials with relatively small micropores as is the case of GIS-type zeolite with 8 membered-rings [159, 181, 191].

Particle size distribution

The PSD and characteristic parameters d_{10} , d_{50} , and d_{90} for the samples were determined by means of laser diffraction analysis.

The PSD from 0.1 to 100 μm of the samples showed a quasi-unimodal and narrow distribution centered at 16.57, 22.49, 26.20, and 22.49 μm of particle diameter for ZB0, ZB1, ZB2, and ZB3, respectively, as can be seen in Figure 3.40. These results fit well to those found in the literature for NaP1 obtained from FA [197].

The characteristic parameters of PSD (Table 3.36) for the sample prepared using fresh solution of NaOH (ZB0) oscillated between 1 and 24 μm , while the first, second, and third recycling (samples ZB1, ZB2 and ZB3, respectively) led to higher values (1-41 μm). It could be related to a particle aggregative behavior as a consequence of the effluents recycling.

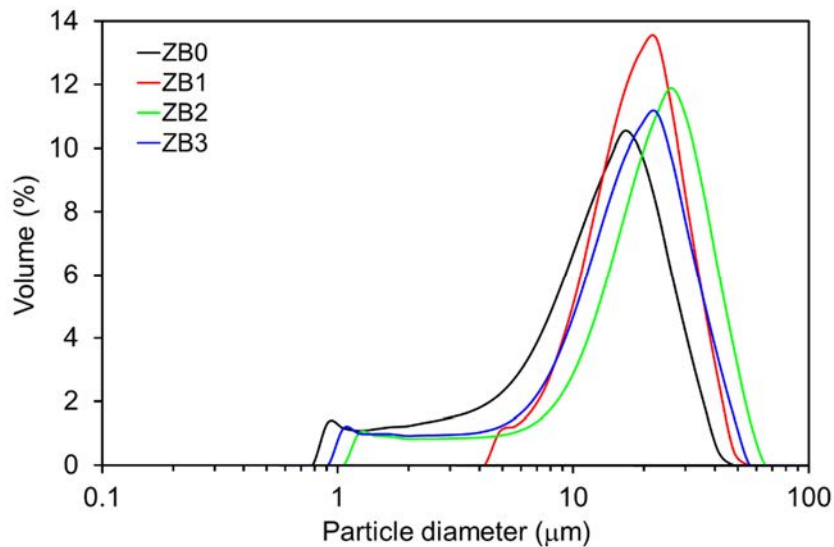


Figure 3.40 Particle size distribution of the NaP1 zeolite synthesized with fresh alkalizing agent (Z0) and with effluent recycling (Z1, Z2, and Z3) on bench scale.

Table 3.36 Characteristic parameters (d_{10} , d_{50} , and d_{90}) of the particle size distribution (PSD) for the NaP1 zeolite synthesized with fresh alkalizing agent (Z0) and with effluent recycling (Z1, Z2, and Z3) on bench scale.

Sample	PSD (μm)		
	d_{10}	d_{50}	d_{90}
ZB0	0.85 ± 0.06	12.36 ± 0.03	23.95 ± 0.18
ZB1	0.99 ± 0.03	17.09 ± 0.25	29.12 ± 0.22
ZB2	1.78 ± 0.07	21.62 ± 0.90	40.54 ± 0.46
ZB3	4.15 ± 0.06	16.29 ± 0.04	30.47 ± 0.09

Zeta potential and point of zero charge

Table 3.37 shows the ζ -potential values of the reference (ZB0) and samples obtained after the effluents recycling compared with the commercial zeolite. The measures of ζ -potential were determined using aqueous suspensions at fixed pH conditions (initial pH = 7 and final pH = 9 -10). As can be seen, all samples presented negative ζ -potentials at the studied pH conditions, resulting in materials with negatively charged surfaces.

The results indicate that slightly more negative charges were available in the samples obtained from the zeolitization process under effluents recycling (ZB1, ZB2, and ZB3), and hence, a higher electrostatic attraction between positive charges and the active sites of NaP1 can be found. However, these differences are scarcely significant.

3. RESULTS AND DISCUSSION

Table 3.37 Zeta-potential (ζ -potential) of NaP1 from the waste through the bench-scale synthesis without (ZB0) and with (ZB1, ZB2, and ZB3) recycling compared with a commercial zeolite (P1-X). Aqueous suspensions of zeolite prepared at initial pH 7 and 25 °C.

Sample	ζ -potential (mV)
ZB0	-70.9
ZB1	-77.5
ZB2	-79.2
ZB3	-76.2
P1-X	-78.7

Therefore, the samples prepared by the synthesis with recycling of effluents present the same textural characteristic as the sample obtained with fresh solution, and all of them might be used in water remediation applications to adsorb different contaminants such as heavy metals and ammonium.

In order to better study the ζ -potential of the samples at different pH, this parameter was measured in a wide pH range at room temperature (25 °C), as shown in Figure 3.41.

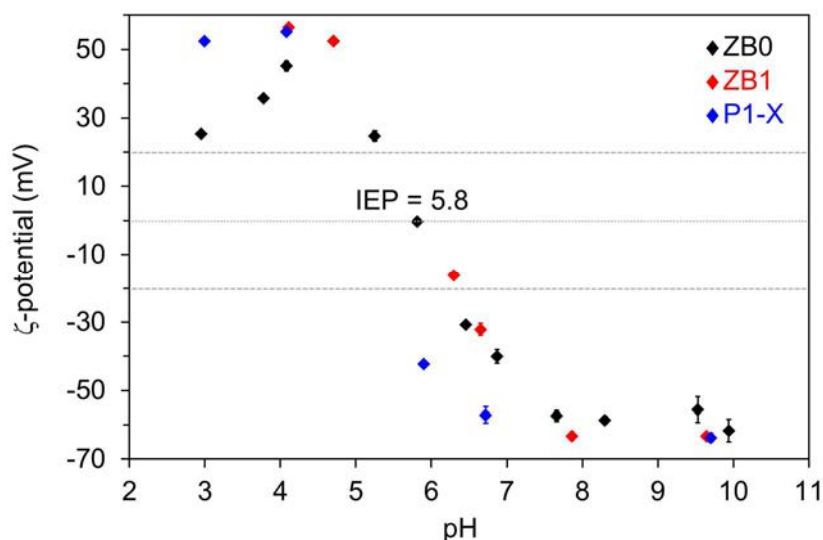


Figure 3.41 ζ -potentials for NaP1 from the waste through the bench-scale synthesis without (ZB0) recycling and after the first recycling (ZB1) compared with a commercial zeolite (P1-X).

IEP = isoelectric point.

The ζ -potential, which is related to the external surface charge of each sample [126], revealed that it is positively charged at pH 3-5 and negatively charged above pH ~ 6 for each sample.

Most measures obtained for ZB0, ZB1, and P1-X showed absolute values of ζ -potential above 20 mV, which indicates a good electrical stability [127, 128].

The point where the ζ -potential is zero, called the isoelectric point (IEP), represents the point where the system is least stable. The IEP of the reference sample (ZB0) was reached at approximately pH 5.8. Despite not detecting the IEP values for the rest of studied samples (ZB1 and P1-X), it is believed that they could show similar behavior, in particular the sample obtained after the first recycling (ZB1).

Although the reviewed literature reports many zeolites with IEP obtained at lower pH conditions [199], there are some exceptions including IEP values close to the results obtained for NaP1 from Alw_x. For example, Arancibia-Miranda et al. [200] reported a similar ζ -potential curve, where the IEP was reached at pH = 6, for a natural zeolite that exhibited good affinity for the uptake of heavy metals like Pb²⁺ at pH 3-6.

As occurred with the porosity, in particular with S_{BET}, the surface charge of zeolites could depend on their Si/Al ratio.

Previous works have stated that zeolites with high Al-content (Si/Al ratios < 2) can present IEP values at neutral pH conditions [126]. This behavior could be associated to materials with particle surfaces dominated mainly by aluminol groups. Compounds like aluminas show similar behavior, presenting positive ζ -potential values at acid conditions (ζ -potential close to 30 mV at pH ~ 4.5, according to [201]).

The point of zero charge (PZC), which is associated with the total surface charge (i.e. the external and internal surface charge), was also determined. As an example, the variation of this parameter for ZB0 in function of the pH is shown in Figure 3.42. This zeolite reached the PZC at approximately pH 10.0. It indicates that the surface charge density of ZB0 is zero at this value of pH.

According to the literature [202], if the difference between PZC and IEP is higher than one (i.e., pH_{PZC}-pH_{IEP} >1), the external surface of the NaP1 zeolite obtained from the waste could be more negatively charged than the internal one.

3. RESULTS AND DISCUSSION

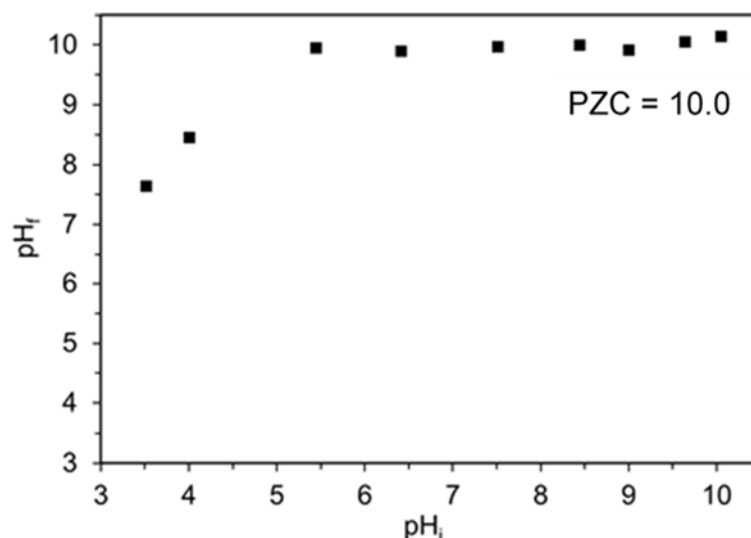


Figure 3.42 Point of zero charge (PZC) for ZB0 obtained from the waste through the bench-scale synthesis without effluents.

Cation-exchange capacity (CEC)

The mild conditions employed in the synthesis under recycling of ML and RW effluents led to high-CEC zeolites, resulting in 2.3-2.4 meq NH₄⁺/g (Table 3.38).

These results coincide with those obtained for the sample ZB0 as well as with that CEC (2.73 meq NH₄⁺/g) for NaP1 prepared from Alw_x by the lab-scale zeolitization process. Similar results were also found in the literature for NaP1 (2.7 meq/g) obtained from FA using 3 M NaOH at 125 °C for 8 h via hydrothermal synthesis on pilot scale [26].

Table 3.38 Cation-exchange capacity (CEC) values of the NaP1 zeolites from the waste via the bench-scale synthesis without (ZB0) and with (ZB1, ZB2, and ZB3) recycling compared with a commercial zeolite (P1-X).

Sample	CEC (meq/g)
ZB0	2.37 ± 0.12
ZB1	2.37 ± 0.15
ZB2	2.25 ± 0.06
ZB3	2.27 ± 0.20
P1-X	2.70 ± 0.01

Therefore, after three consecutive effluent recycling cycles, the resulting zeolites retained high crystallinity as well as morphological, textural, and adsorption properties,

as compared to the zeolite obtained in the initial experiments where a fresh 1 M NaOH solution was used as the alkalizing agent.

Thus, the scaling up of the synthesis showed quite similar results compared with those found in the lab-scale synthesis of NaP1 from the aluminum waste (Alw_x). This means that the process has a good reproducibility to be up-scale to an industrial process.

3.3.1.6 Mother liquor characterization

The main alkaline effluent (ML) generated in the zeolitization process was analyzed by ICP-OES to determine its chemical composition.

In addition to the chemical composition, pH and conductivity of the ML recycled during the hydrothermal synthesis of ZB1, ZB2, and ZB3 were also determined, as shown in Table 3.39.

Table 3.39 Chemical composition, pH, and conductivity (CE) of the mother liquors (ML) obtained after the synthesis from fresh NaOH solution (MLZB0) and from the first (MLZB1) and second (MLZB2) recycling.

Mother liquor	Chemical composition				pH	CE (mS/cm)
	Na (mg/mL)	K (mg/mL)	Si (mg/mL)	Al (μ g/mL)		
MLZB0	20.21	0.32	0.98	25	13.6	134
MLZB1	24.33	0.30	0.89	20	13.7	126
MLZB2	24.79	0.31	0.64	25	13.7	127

The main elements detected in the different ML were Na, Si, K, and Al. All these elements constituent the zeolite frameworks, and therefore, ML could have a profitable effect on the synthesis of zeolites.

Likewise, the pH and conductivity values of ML are very similar to the 1 M NaOH solution [16], thus confirming that ML can be recovered and fed into zeolitization processes, and saving NaOH and water consumptions.

3. RESULTS AND DISCUSSION

3.3.2 Life cycle inventory of the zeolite synthesis

A preliminary Life Cycle Inventory (LCI) analysis of the NaP1 production (based on 1 ton of zeolite) through the bench-scale process with and without effluent discharge was performed. The results obtained in this preliminary LCI analysis are shown in Table 3.40.

Table 3.40 LCI of the production of 1 ton of NaP1 through the bench-scale synthesis process with and without discharge of effluents (ML and RW).

Sample	Input (kg/t _{zeolite})					Recycled effluent ^a (kg/t _{zeolite})		Output (kg/t _{zeolite})
	Waste Alw _x	Water glass	NaOH 50 wt.%	H ₂ O synthesis	H ₂ O cleaning	ML	RW	Discharged effluent
ZB0	408	1470	390	4898	2449	4080	816	1633
ZB1	402	1450	80	-	2410	4110	804	1606
ZB2	407	1460	100	-	2439	4030	813	1626
ZB3	397	1430	120	-	2381	-	-	6281

^a Mixture formed by ML 83 wt.% and RW 17 wt.%, where the total amount of ML and a certain amount of RW are recycled. The amount of recycled effluent for the synthesis of Z1, Z2, and Z3 is equivalent to the amount of fresh water used for the preparation of Z0.

LCI provides the data of inputs (sources of Na, Al, and Si as well as synthesis process and cleaning water), recycled effluent, and outputs (discharged RW after the zeolite cleaning) of the analyzed synthesis system. Due to the lack of data related to the industrial-scale production of zeolites, the LCI assessment was based on the mass flows from the lab and bench-scale experiments. The energy flow, not evaluated in this thesis, may oscillate between 21400 and 25200 MJ/t, according to the LCI for the production of zeolite A [32].

The bench-scale synthesis involved similar yields and the generation of the same volume of ML per kg of zeolite (~ 4 L/kg) in all the recycling cycles compared with the sample Z14 obtained in the lab-scale synthesis (Section 3.2).

Both the lab and bench-scale synthesis process of NaP1 allowed getting materials with very similar crystallinities and equivalent reaction yields.

These findings help emphasize the feasibility of the scaling up of the zeolitization process using an aluminum waste and under effluents recycling. It demonstrates the good reproducibility of the lab-scale synthesis conditions to higher scale.

As all the synthesis conditions (Si/Al ratio, temperature, time, and liquid/solid ratio) remain unchanged in each recycling cycle, the type of zeolite obtained, i.e., the formation and crystal growth of the zeolitic products would depend on the reactant composition of the initial solution.

As commented in Chapter 1, aluminosilicate zeolites are generally obtained under basic conditions in the $\text{Na}_2\text{O}-\text{Al}_2\text{O}_3-\text{SiO}_2-\text{H}_2\text{O}$ system, where the alkalinity, defined as the concentration of base ($\text{H}_2\text{O}/\text{Na}_2\text{O}$), plays an important role in the zeolite crystallization [22].

The alkalinity would significantly affect the nucleation and crystal growth of zeolites. The amount of Na^+ cations and mineralizing agent (OH^-) in the initial reaction solution would play an important role in the zeolite formation. The OH^- anions affect dissolution and polymerization/depolymerization reactions of aluminosilicates [22]. Cations like Na^+ stabilize aluminosilicate ions via static electric and steric interactions, playing a remarkable structure-directing role, and determine their solubility regulating the concentration of aluminum in solution [28] and accordingly helping the pH adjustment of the process [22].

Some works reported that additions of alkali-metal cations like Na^+ in the initial solution involved an acceleration effect for the crystallization, facilitating the condensation or rearrangement of the structural building units of zeolites [29]. Thus, the increase of the alkalinity by increasing the pH leads to a higher solubility of silicon and aluminum sources, favoring the crystallization of zeolites [22, 25, 203]. As the alkalinity of the reaction medium of the synthesis process under recycling of effluents must be adjusted, the pH and molarity values in each cycle were controlled.

The molarity of recycled liquid mixture, ranged 0.86-0.80 M for ML and 0.54-0.37 M for RW, is somewhat insufficient for an adequate synthesis of NaP1, being necessary to add a certain amount of fresh 50 wt.% NaOH solution to reach 1 M, and accordingly to get the required alkalinity.

Consumption savings of such fresh 50 wt.% NaOH solution of 80, 74 and 69 % were obtained in the first, second and third recycling cycle (ZB1, ZB2 and ZB3, respectively), as shown Table 3.40. The amount of 50 wt.% fresh alkali solution should be increased only 5 % in each recycling cycle, thus saving costs in the preparation of NaP1. The volume of the recycled effluent mixture in each cycle contained ca. 83 wt.% of ML and 17 wt.% of RW. The process allows recovering the total volume of ML generated in each

3. RESULTS AND DISCUSSION

synthesis, and also around 33 % of the total water amount employed for the rinsing step to remove traces of soluble species in the zeolitic cake.

3.3.3 Feasibility of industrial-scale zeolitization process

To assess the feasibility of industrial-scale production, a preliminary cost estimation (Table 3.41) was determined according to the LCI analysis, showing the production of one ton of NaP1 from Alw_x by the process using fresh NaOH solution (ZB0) and by the improved process after three consecutive recycling cycles (ZB3).

Table 3.41 Cost estimation based on the production of one ton of NaP1 obtained from the waste by the zeolitization process with and without liquid effluents recycling.

Inputs ^a	Developed process with recycling (€ ₂₀₁₆ /ton _{zeolite}) ^b	Developed process without recycling (€ ₂₀₁₆ /ton _{zeolite}) ^c	Conventional process without recycling (€ ₂₀₁₆ /ton _{zeolite})
Al ₂ O ₃	-	-	2430
Water glass	1329	1367	1367
NaOH 50 wt. %	75	252	252
Fresh H ₂ O	1	4	4
Total	1405	1624	4054

a Chemical reagent prices based on Manuel Riesgo, S.A. Spanish supplier: 9.01 €₂₀₁₆ per kg of commercial aluminum source (Al₂O₃) used for the conventional synthesis of NaP1, 158.45 €₂₀₁₆ per 125 L of water glass, and 63.50 €₂₀₁₆ per 50 kg of NaOH pellets; 0.5486 €₂₀₁₆ per m³ of water (Madrid, Spain).

b The consumption of water only involves the fresh water used in the rinsing step of the zeolite Z3.

c The consumption of fresh water involves the fresh water fed to the synthesis process and used in the rinsing step of the zeolite ZB0.

Moreover, the conventional synthesis process (without recycling) of NaP1 from commercial aluminum sources like Al₂O₃ was evaluated, considering the same amount of aluminum oxide present in the waste (ca. 66 wt.%).

The price of commercial NaP1 depends on the manufacturer and may be ranged 600-1325 €/ton of zeolite, according to data provided by some members of the European Zeolites Producers Association.

The lifetime of NaP1 varies according to the pH, being of 2 years at near neutral pH and less than 10 days at below pH 3 [196].

As commented above, the process under effluents recycling led to a considerable decrease in the amount of fresh 50 wt.% NaOH of 80, 74 and 69 % for ZB1, ZB2, and ZB3, respectively, compared with the synthesis of ZB0.

Concerning the total water amount required for the synthesis of ZB3, only RW was required since all the ML volume from the synthesis of ZB2 together with a certain amount of RW were recycled for the preparation of ZB3. It involved a water consumption saving of 67 % when it is related to the total water amount (i.e., fresh water for the synthesis and RW for the rinsing step) used for the synthesis of ZB0.

The effluent recycling process represented a cost reduction of 68 and 70 % for water and NaOH, respectively. In addition, the re-use of Alw_x would involve a significant cost reduction when it is compared with the cost of the aluminum sources commonly used in the zeolite synthesis, such as sodium aluminate, pseudo-boehmite, aluminum hydroxide and aluminum isopropoxide [22].

The use of the waste in the synthesis process can also save the costs of deposit authorized landfill (around 109 € per ton of waste).

Thus, the zero liquid discharge process implies not only an economical opportunity respect to the process without re-using of effluents (ML and RW), but also an environmental improvement. It would help to handle and reduce the generation of effluents from the zeolitization process, saving the raw materials consumption, especially the saving of water which is one of the most natural resources to the life conservation on the Earth.

3. RESULTS AND DISCUSSION

3.4 Removal of heavy metals from aqueous solutions

Nowadays, one of the most relevant environmental concerns is water pollution. Global industrialization is causing massive releases of harmful elements such as heavy metals in water sources. Heavy metals such as lead, cadmium, and mercury are endocrine disruptors due to their bioaccumulation in organisms causing important health problems. In this context, appropriate management is needed to control emissions of pollutants into waters.

Among the different water treatment technologies, adsorption is a simple, efficient, and economic technique for the removal of different pollutants in water, including heavy metals. Zeolites can be used as adsorbents due to their main properties: structure as well as adsorption and ion exchange capacities.

The removal of heavy metal cations (Pb^{2+} , Cd^{2+} , and Hg^{2+}) in aqueous solutions on the synthesized zeolites from the waste as adsorbent materials was evaluated, showing the most relevant results in this section.

The NaP1 zeolite (sample ZB0) obtained from the waste (Alw_x) through the bench-scale zeolitization process was selected to perform batch adsorption experiments at room temperature ($25\text{ }^\circ\text{C} \pm 2$). As commented in Section 3.3, this zeolite could show appropriate properties for the adsorption of contaminants from water due to its high cation-exchange capacity (2.37 meq/g).

Single- and multi-cation adsorption experiments were performed, evaluating the effects of parameters such as pH, contact time, adsorbent dose, initial cation concentration, and coexisting-cations on the adsorption efficiency and capacity of the zeolitic adsorbent. Table 3.42 summarizes all adsorption parameters studied in the single- and multi-cation adsorption experiments using ZB0 as zeolitic adsorbent.

Different kinetic and isotherm models were applied by means of a non-linear optimization method in order to study the behavior of the zeolite in the adsorption process.

3. RESULTS AND DISCUSSION

Table 3.42 Conditions studied in the single- and multi-metal cation adsorption experiments using the zeolite NaP1 (sample ZB0) synthesized from the waste.

Conditions	pH	Adsorbent dose (g/L)	Time (min)	Initial concentration (mg/L)
Lead (Pb²⁺) adsorption				
Contact time	4.5	0.5	1-120	20
Adsorbent dose		0.125-1	30	
Initial concentration		0.5		5-100
Cadmium (Cd²⁺) adsorption				
Contact time	4.5	5	1-120	20
Adsorbent dose		1-10	30	
Initial concentration		5		1-40
Mercury (Hg²⁺) adsorption				
pH	2-6	10	1-120	0.2
Contact time	4.5	5		
Adsorbent dose		1-10	30	
Initial concentration		5	60	0.02-1.5
Multi-cation adsorption: Pb²⁺, Cd²⁺, and Hg²⁺				
Conditions	4.5	2 and 10	1-30	20, Pb ²⁺ 20, Cd ²⁺ 0.2, Hg ²⁺

In addition, the morphological, structural, and chemical properties of the zeolite ZB0 were analyzed before and after the competitive adsorption of Pb²⁺, Cd²⁺, and Hg²⁺ to better understand the studied adsorption system.

Single-cation adsorption was found to be a fast process where adsorption equilibrium was reached in the first 15 min achieving high removal efficiencies, which were near 100 %. The removal of the metal cations could occur via a homogeneous and physical adsorption process.

In multi-cation adsorption, the zeolite presented the greatest affinity for Pb²⁺ (due to its smallest cationic size) compared with Cd²⁺ and Hg²⁺. The Pb²⁺ removal efficiency remained practically constant in presence of Hg²⁺ and Cd²⁺, reaching efficiencies near 100 % at very low contact times (< 5 min).

3. RESULTS AND DISCUSSION

Thus, this studied zeolite (ZB0), which was previously obtained from Alw_x by a direct bench-scale synthesis process, could become an alternative adsorbent to eliminate heavy metals from aqueous effluents.

A synergic effect on the environmental protection could be achieved: the *end-of-waste* condition of a hazardous waste as well as the water decontamination.

3.4.1 Effect of pH

Among all the influencing parameters, pH can affect the solubility and speciation of metal ions, and it can also affect the properties of sorbent materials [107]. Several works in the literature have shown that the pH plays a key role, affecting the sorption of diverse contaminants like heavy metals by different sorbents, including zeolites [200, 204-206].

The effect of pH on the concentration of the studied metal cations, referred to their initial concentration (20 mg/L for Pb^{2+} and Cd^{2+} , and 0.2 mg/L for Hg^{2+}), was evaluated, as shown Figure 3.43. As the pH increased up to pH 8 for Pb^{2+} and Hg^{2+} and up to pH 10 for Cd^{2+} approximately, the stability of the cations in the aqueous solution decreased due to their hydrolysis.

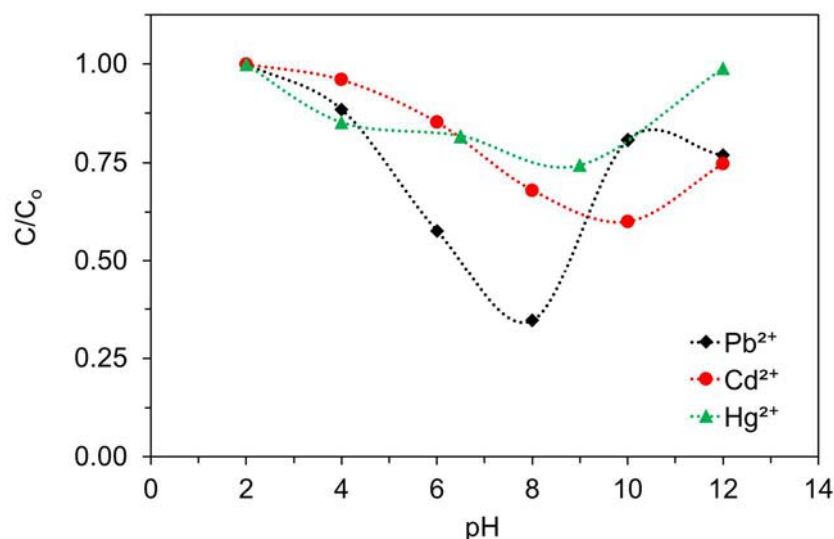


Figure 3.43 Effect of the solution pH on the stability of Pb^{2+} , Cd^{2+} , and Hg^{2+} in aqueous medium at $25\text{ }^\circ\text{C} \pm 2$. C/C_0 : final concentration referred to the initial cation concentration (20 mg/L for Pb^{2+} and Cd^{2+} , and 0.2 mg/L for Hg^{2+}).

3. RESULTS AND DISCUSSION

In order to better evaluate the behavior of each metal cation at different pH, their corresponding chemical equilibrium diagrams in aqueous solution were determined. The chemical equilibrium diagrams of the Pb^{2+} , Cd^{2+} , and Hg^{2+} cations (Log cation concentration versus pH) determined for the same initial concentrations are shown in Figure 3.44. The obtained logarithmic diagrams show the distribution of hydrolysis products of the metal cations as a function of pH.

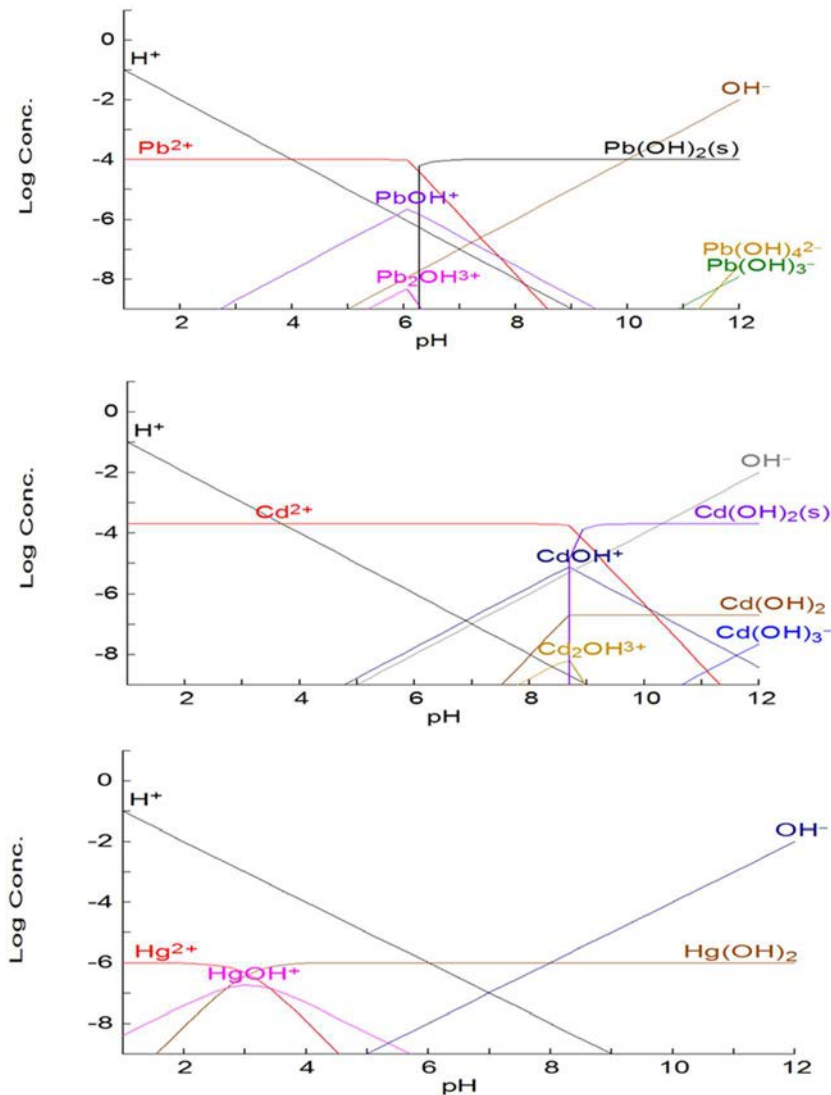


Figure 3.44 Chemical equilibrium diagrams of Pb^{2+} , Cd^{2+} , and Hg^{2+} in aqueous solution determined for the next initial concentrations: 20 mg/L for Pb^{2+} and Cd^{2+} , and 0.2 mg/L for Hg^{2+} .

As can be seen, the Pb^{2+} cation is stable in aqueous medium until $\text{pH} \sim 6$, partially hydrolyzing to form PbOH^+ and Pb(OH)_2 as pH increases. The Cd^{2+} cation is very stable up to around $\text{pH} 9$. As the basicity of the aqueous medium increases, the formation of cadmium species such as CdOH^+ , Cd(OH)_2 , and Cd(OH)_3^- is favored.

3. RESULTS AND DISCUSSION

On the contrary, the Hg^{2+} cation is stable in very acid medium (until $\text{pH} \sim 4$). An increase of the pH leads to the hydrolysis of mercury to form HgOH^+ and subsequently $\text{Hg}(\text{OH})_2$, coexisting these mercury species at $\text{pH} < 6$.

Thus, the formation of soluble and/or precipitated species of each metal strongly depends on the solution pH used to remove them.

As the removal of Hg^{2+} is highly dependent on the solution pH , the effect of this parameter was studied in a pH range of 2-6 (Figure 3.45) to select the optimal pH conditions for the single- and multi- cation uptake.

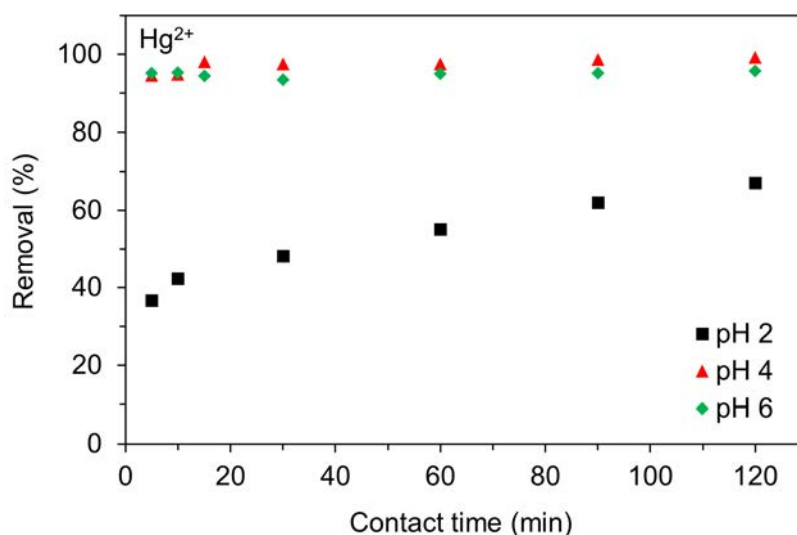


Figure 3.45 Influence of the solution pH on the removal efficiency of Hg^{2+} by ZB0. Conditions: zeolite dose = 10 g/L; $C_0 = 0.2$ mg/L; $T = 25 \pm 2$ °C.

The removal ability of the obtained zeolite (sample ZB0) was found to be practically unchanged at pH values above 2, in particular at pH ranged between 4 and 6.

The adsorption efficiency of ZB0 decreased at low pH . It can be associated to the potential competition between the H^+ and Hg^{2+} ions at acid pH . The higher affinity of H^+ toward the active sites of adsorption under low pH conditions during removal processes of different heavy metals has also been reported [207, 208].

For example, Fernández-Nava et al. [208] studied the removal of the same heavy metals from aqueous solutions at pH 2-7 using bentonite as adsorbent (dose: 2 g/L for Pb^{2+} and Cd^{2+} , and 10 g/L for Hg^{2+}). The authors observed precipitation of the studied metals at pH 7 for Cd^{2+} and Hg^{2+} and at pH 6.5 for Pb^{2+} and reported that the adsorption efficiency

of Pb^{2+} , Cd^{2+} , and Hg^{2+} increased up to 82, 70, and 15 %, respectively, when the initial pH increased up to approximately 6. The decrease in the adsorption capacity of bentonite at acidic pH conditions was explained because of the protonation of the aluminol and silanol groups (Al-OH and Si-OH) of the adsorbent.

Additionally, the lower adsorption ability of ZB0 at acid pH could be related to the loss of active sites because of the partial dissolution of the zeolite.

In order to select the most adequate conditions for the removal of all the heavy metals, the influence of the pH on the crystallinity of the zeolite was also evaluated by XRD analysis. It should be noted that the initial zeolite (sample ZB0) presents a $\text{pH} = 10 \pm 0.5$ when put in contact with aqueous solutions (due to its alkaline character derived from the zeolite synthesis process [17]). It was considered that acid pH could favor the adsorption of the metal cations.

Figure 3.46 compares the XRD patterns of the initial zeolite (Figure 3.46a) as well as those of the zeolite when it was put in contact with acid aqueous solutions for at least 1 h at pH 4 (Figure 3.46b) and pH 6 (Figure 3.46c).

The results revealed that the zeolite exhibited well-defined XRD profiles at the different pH showing the NaP1 phase (ICDD PDF 01-071-0962).

Table 3.43 shows the values estimated for the relative crystallinity, peak parameters (2θ and FWHM), and crystalline sizes (D_{hkl}) of the initial zeolite (sample ZB0 at $\text{pH} 10 \pm 0.5$) and at the different pH (pH 4 and 6). The relative crystallinities of the samples were estimated from the sum of intensities of each diffraction peak of the NaP1 zeolite (d_{101} , d_{200} , d_{112} , d_{301} , and d_{312}), designating the initial zeolite as the reference (100 % crystallinity).

The variation of the solution pH seems to slightly modify the peak parameters and crystallite sizes of the zeolite samples at pH 4 and pH 6. As shown in Section 3.3, the sample ZB0 exhibited the most intense 301 reflection at 28.07° and a FWHM value of 0.33° , resulting in a crystallite size of 25 nm.

3. RESULTS AND DISCUSSION

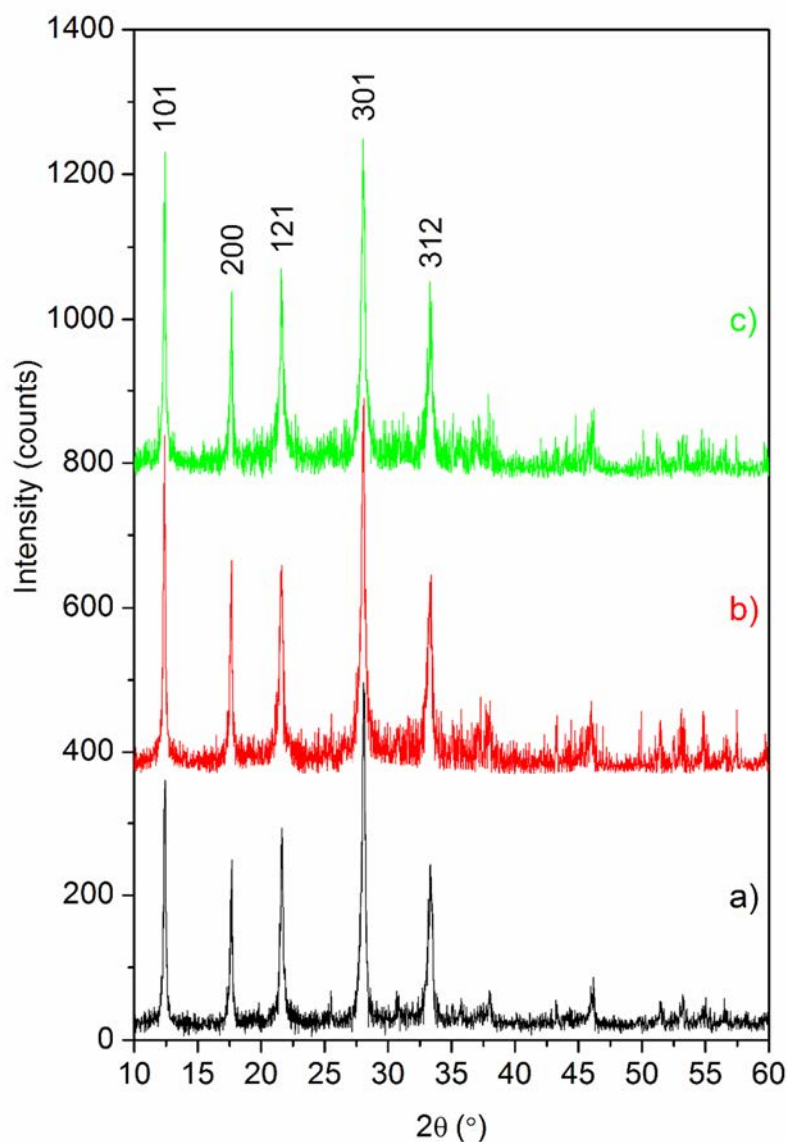


Figure 3.46. Comparison of the XRD patterns of the sample ZB0 at different pH: initial sample of zeolite (ZB0) at pH 10 ± 0.5 (a); ZB0 samples in aqueous solutions at pH 4 (b) and at pH 6 (c). All diffraction peaks were identified by the NaP1 zeolite (ICDD PDF 01-071-0962).

Table 3.43 Crystallinity, peak parameters (2θ and FWHM), and crystalline sizes (D_{hkl}) obtained for the initial NaP1 zeolite (sample ZB0 at pH 10 ± 0.5) compared with NaP1 in aqueous solution at pH 6 and 4.

Zeolite	pH	Σ Intensity (counts)	Crystallinity (%)	2θ (°)	FWHM (°)	D_{301} (nm)
NaP1	10	1580	100	28.07	0.33	25
	6	1579	99.9	28.08	0.34	24
	4	1458	92.3	28.08	0.37	22

Although the samples b and c at pH 4 and pH 6, respectively, also showed the 301 reflection centered at very similar 2θ angle (28.08°), slight changes in FWHM (0.37 and 0.34°) were found, leading to slightly smaller crystallite sizes (22 and 24 nm for samples b and c, respectively).

The mass of the zeolite remained unchanged for the studied pH range of 4-6. On the contrary, pH < 4 led to significant zeolite mass losses, between 48 and 86 % for pH 3 and pH 2, respectively, as a consequence of the partial dissolution and dealumination of the zeolite [25].

Therefore, the solution pH should be controlled and kept constant in order to properly study the removal of the heavy metals by ZB0. Thus, the further removal experiments of the metal cations by ZB0 were performed at a fixed pH 4.5 to avoid zeolite mass losses caused by dissolution and dealumination and also to avoid the precipitation of the metal cations.

3.4.2 Effect of contact time: adsorption kinetic

The single-cation adsorption as a function of the contact time for Pb^{2+} , Cd^{2+} , and Hg^{2+} is shown in Figure 3.47. As can be seen, the removal of each metal cation by ZB0 followed a very similar trend. The corresponding removal of three cations was a very fast process; the equilibrium was reached in less than 30 min, leading to high adsorption efficiencies (98.9, 93.3, and 99.3 % for Pb^{2+} , Cd^{2+} , and Hg^{2+} , respectively, in 15 min). These results were related to the fast diffusion of the metal cations from the solution to the interface and to the zeolite structure which is accessible to the cations through its tridimensional channel system.

The experiments were controlled up to 24 h in order to ensure no significant changes in the adsorption system. A contact time of 30 min was established as sufficient to achieve equilibrium conditions for all cations, leading to the following experimental removal capacities (q_t): 41.6, 3.8, and 0.045 mg/g for Pb^{2+} , Cd^{2+} , and Hg^{2+} , respectively.

Adsorption kinetic for each metal cation was evaluated applying the pseudo-first [129] and pseudo-second-order [130] models, as well as the intra-particle diffusion model [131], previously described in Chapter 2. A non-linear optimization method was applied for the evaluation of the goodness of fit of the different kinetic models. The parameters of the studied were determined by maximizing the coefficient of determination (R^2).

3. RESULTS AND DISCUSSION

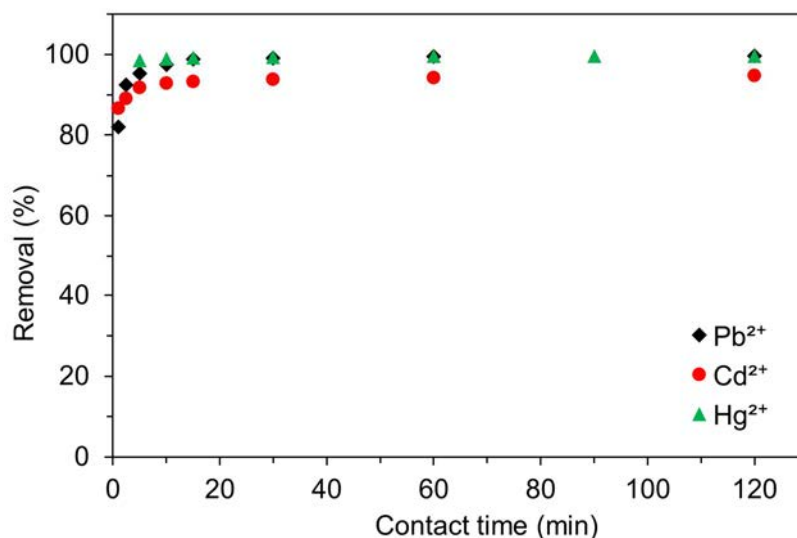


Figure 3.47. Effect of the contact time for the single-cation adsorption of Pb²⁺, Cd²⁺, and Hg²⁺ onto ZB0. Conditions: pH = 4.5; adsorbent dose = 5 g/L for Cd²⁺, and Hg²⁺, and 0.5 g/L for Pb²⁺; C₀ = 20 mg/L for Pb²⁺ and Cd²⁺, and 0.2 mg/L for Hg²⁺; T = 25 ± 2 °C.

Table 3.44 and Figure 3.48 show the results obtained in the evaluation of the pseudo-first-order and pseudo-second-order models for the removal of Pb²⁺, Cd²⁺, and Hg²⁺ by ZB0.

Table 3.44. Kinetic model parameters and error function values calculated for the single adsorption of the Pb²⁺, Cd²⁺, and Hg²⁺ cations onto ZB0.

Kinetic model	Parameters	Pb ²⁺	Cd ²⁺	Hg ²⁺
Pseudo-first-order [129]	q _{t,model} (mg/g)	41.10	3.72	0.0445
$q_t = q_e(1 - e^{-k_1 t})$	k ₁ (1/min)	1.77	2.61	0.96
	R ²	0.819	0.668	0.568
Pseudo-second-order [130]	q _{t,model} (mg/g)	42.09	3.76	0.0446
$q_t = \frac{k_2 q_e^2 t}{1 + k_2 q_e t}$	k ₂ (g/mg min)	0.10	2.86	0.38
	R ²	0.988	0.964	0.945
Experimental data	q _{t,experimental} (mg/g)	42.27	3.79	0.0446

The results indicated that the pseudo-second-order model provided a significantly better correlation with the experimental data for the adsorption of all metal cations. Several studies also found that the pseudo-second-order model tends to describe satisfactorily the removal of diverse metals using sorbents from both chemicals and waste-based sources [209-211].

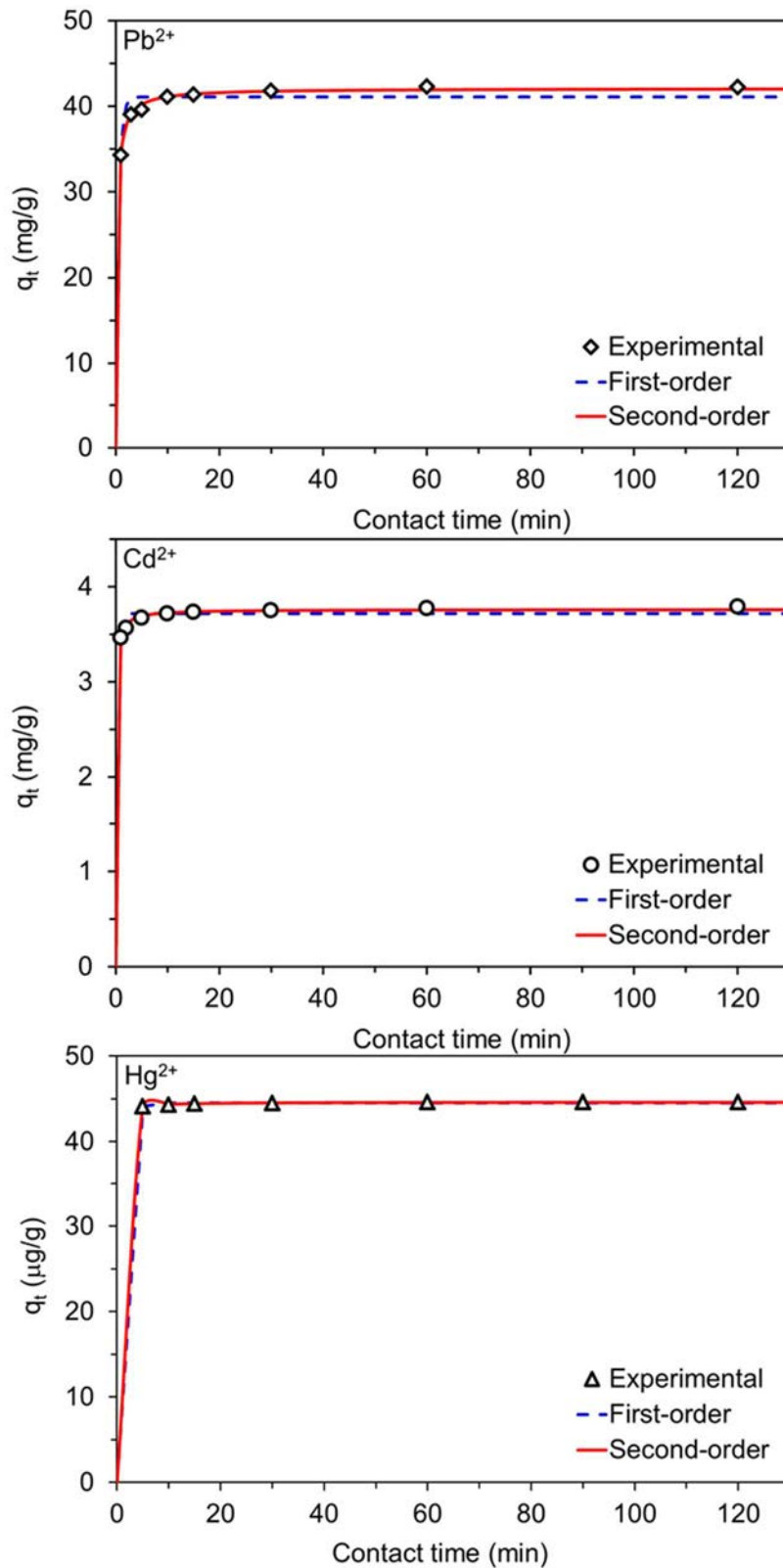


Figure 3.48 Pseudo-first-order and pseudo-second-order models for the single-cation adsorption of Pb^{2+} , Cd^{2+} , and Hg^{2+} onto ZBO. Conditions: pH = 4.5; adsorbent dose = 5 g/L for Cd^{2+} , and Hg^{2+} , and 0.5 g/L for Pb^{2+} ; $C_0 = 20$ mg/L for Pb^{2+} and Cd^{2+} , and 0.2 mg/L for Hg^{2+} ; $T = 25 \pm 2$ °C.

3. RESULTS AND DISCUSSION

As commented in Chapter 2, the intra-particle diffusion model can provide information about the reaction pathways and adsorption mechanisms.

Table 3.45 and Figure 3.49 show the results obtained from the evaluation of the Pb^{2+} , Cd^{2+} , and Hg^{2+} uptake on ZB0 by the intra-particle diffusion model in order to determine the rate-limiting steps of the adsorption.

Table 3.45. Parameters obtained from the intra-particle diffusion model applied to the adsorption of Pb^{2+} , Cd^{2+} , and Hg^{2+} using ZB0.

Cation	Step	Intra-particle diffusion model [131]		
		$q_t = k_p t^{0.5} + C$		
		k_p (mg/g min ^{0.5})	C (mg/g)	R ²
Pb^{2+}	1	5.18	29.43	0.99
	2	1.11	37.60	0.99
	3	0.046	41.38	0.73
Cd^{2+}	1	0.160	3.31	0.98
	2	0.015	3.67	0.99
	3	0.004	3.74	0.93
Hg^{2+}	1	$1.78 \cdot 10^{-4}$	$4.38 \cdot 10^{-2}$	0.99
	2	$3.30 \cdot 10^{-5}$	$4.43 \cdot 10^{-2}$	0.94

As can be seen, the trend lines of the representation plots did not pass through the origin, it meaning that the intra-particle diffusion was not the only rate-controlling step [96].

Thus, the overall adsorption process of Pb^{2+} , Cd^{2+} , and Hg^{2+} on ZB0 could be explained by a combination of fast bulk transport followed by film and intra-particle diffusion.

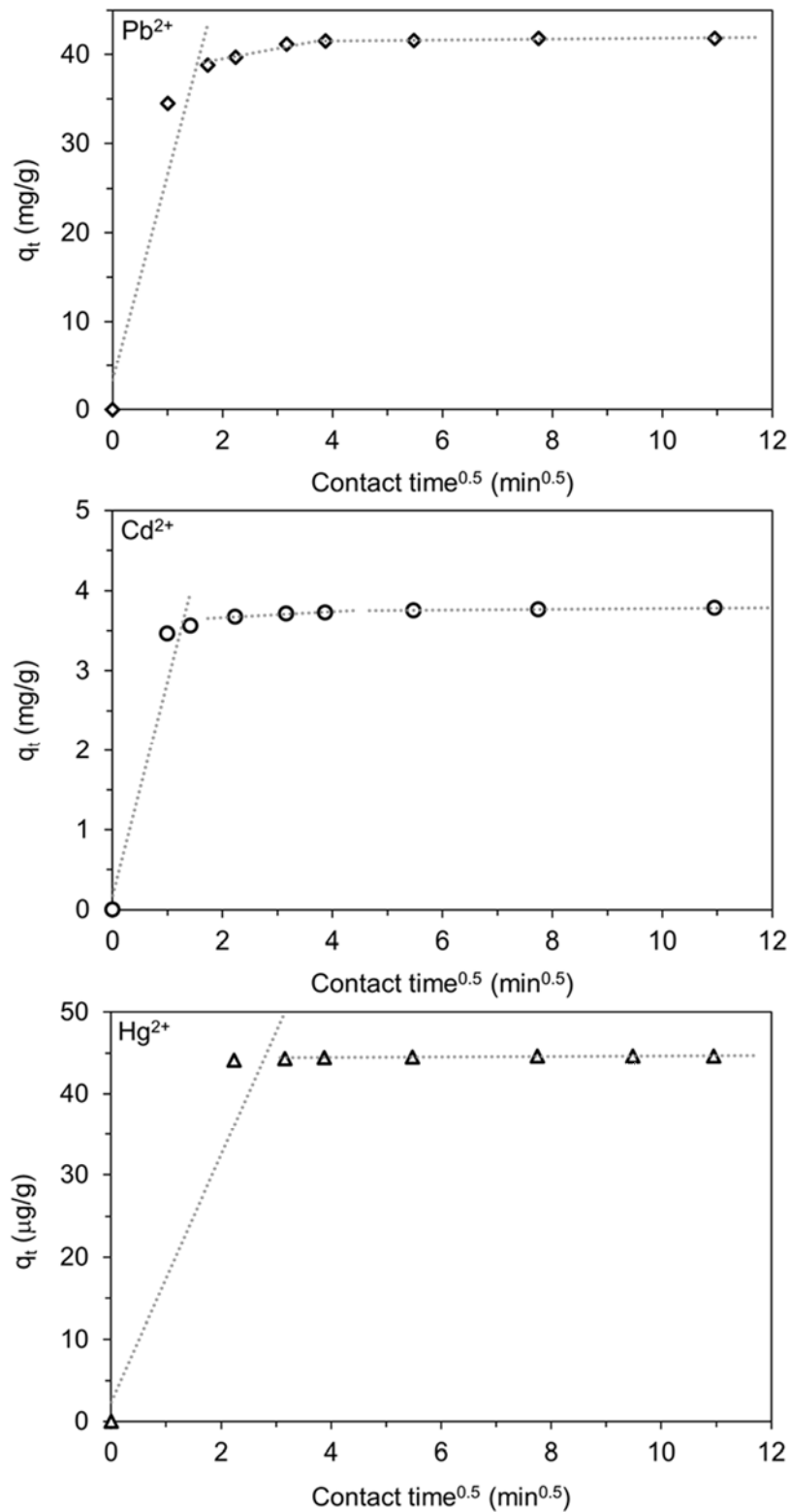


Figure 3.49. Intra-particle diffusion models of the adsorption of Pb²⁺, Cd²⁺, and Hg²⁺ onto ZB0. Conditions: pH = 4.5; adsorbent dose = 5 g/L for Cd²⁺ and Hg²⁺, and 0.5 g/L for Pb²⁺; C₀ = 20 mg/L for Pb²⁺ and Cd²⁺, and 0.2 mg/L for Hg²⁺; T = 25 ± 2 °C.

3. RESULTS AND DISCUSSION

3.4.3 Effect of adsorbent dose

The influence of the solid-liquid ratio (i.e., ratio of zeolite mass referred to solution volume) or adsorbent dose for each metal cation was studied. Figure 3.50 shows the effect of the zeolite dose on the Pb^{2+} , Cd^{2+} , and Hg^{2+} adsorption efficiency and capacity of ZB0.

The metal cations adsorption efficiency increased along with the solid-liquid ratio or dose. In this sense, an increase in the mass of zeolite leads to an increase of the active sites on the adsorbent surface, thus favoring the adsorption process. Thus, Pb^{2+} , Cd^{2+} , and Hg^{2+} would diffuse from the aqueous solution toward the surface of ZB0, tending to occupy the available adsorption sites.

The increase of adsorbent dose, involving larger amounts of zeolite available for the adsorbates, led to the decrease in the adsorption capacity of the metal cations. The elimination of the Pb^{2+} cation involved the smallest doses of the zeolite, ranged between 0.125 and 1 g/L, compared with the Cd^{2+} and Hg^{2+} uptake under the tested operating conditions.

These results indicate that the adsorption ability of ZB0 seems to remain practically constant from an intermediate amount of zeolite, particularly for the Pb^{2+} and Cd^{2+} cations. Thus, an adsorbent dose of 0.5 g/L was fixed for the further Pb^{2+} removal experiments, while doses of 5 g/L were selected for both the Cd^{2+} and Hg^{2+} uptake.

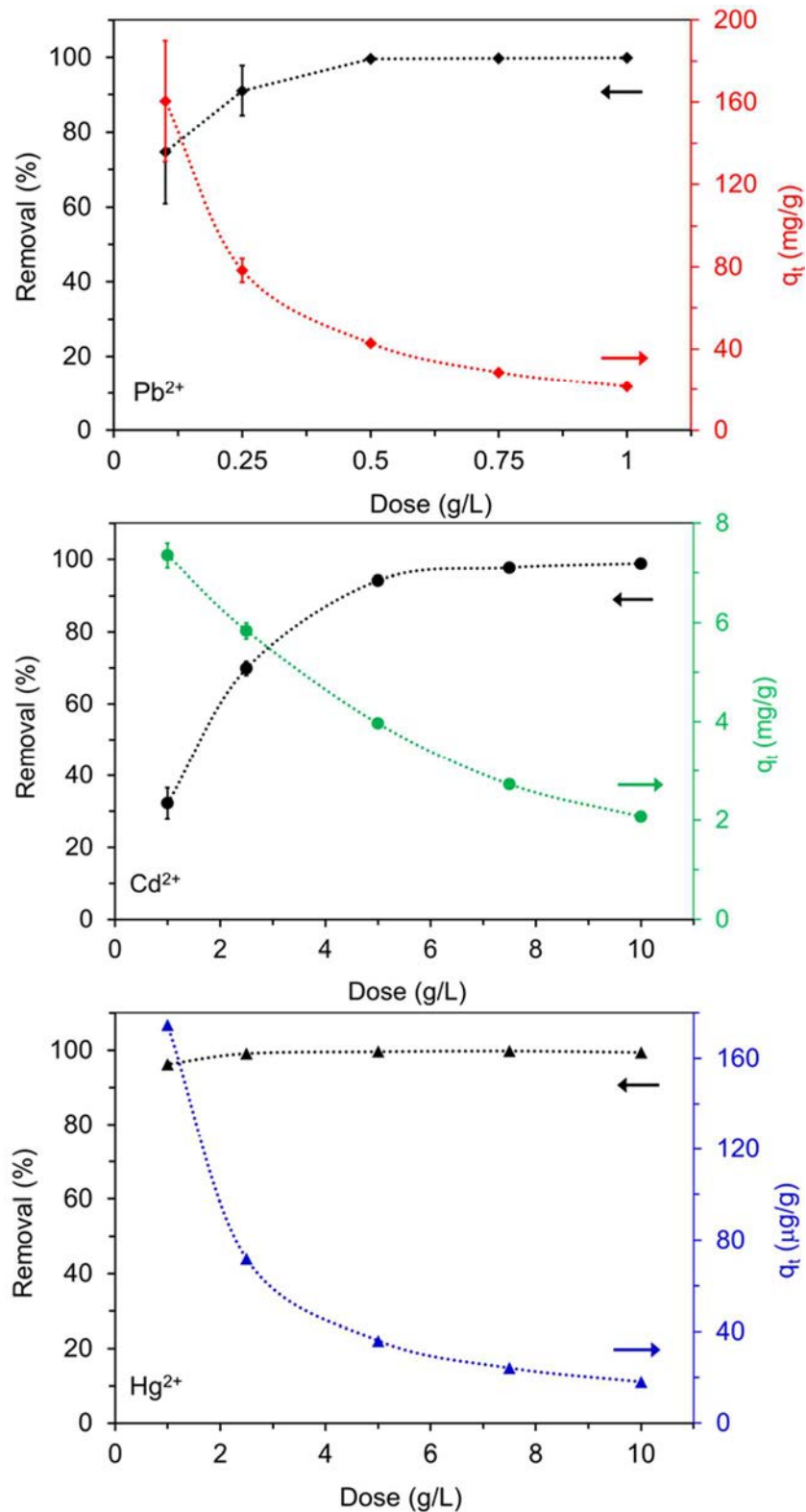


Figure 3.50. Effect of the zeolite dose on the single-cation adsorption efficiency and uptake capacity of Pb²⁺, Cd²⁺, and Hg²⁺ onto ZB0. Conditions: pH = 4.5; contact time = 30 min; C₀ = 20 mg/L for Pb²⁺ and Cd²⁺, and 0.2 mg/L for Hg²⁺; T = 25 ± 2 °C.

3. RESULTS AND DISCUSSION

3.4.4 Effect of initial adsorbate concentration: equilibrium isotherms

The effect of the initial concentration of each metal cation on the adsorption capacity of ZB0 was evaluated applying the best conditions.

The amount of Pb^{2+} , Cd^{2+} , and Hg^{2+} removed by the zeolite increased progressively as the initial concentration of each heavy metal increased up to reach the saturation of the adsorbent (ZB0).

Adsorption equilibrium of the metal cations uptake by ZB0 was evaluated according to the following two- and three-parameter models (described in Chapter 2): Langmuir [132], Freundlich [133], Dubinin-Radushkevich [134], Redlich-Peterson [138], Toth [137], and Sips [136].

The evaluation of the different isotherm models was performed by a non-linear optimization method. All the parameters and constants of the isotherm models were determined by maximizing the coefficient of determination (R^2).

The two-parameter (Figure 3.51) and three-parameter (Figure 3.52) isotherms and their derived-parameters for each metal cation are shown below and collected in Table 3.46.

The experimental data were better described by the isotherm models based on three parameters compared with the two-parameter isotherms.

In particular, the Sips and Toth models provided the highest R^2 values. The experimental maximum removal capacity of the zeolite was 183, 4.37, and 0.23 mg/g for Pb^{2+} , Cd^{2+} , and Hg^{2+} , respectively. The maximum adsorption capacities obtained from the Sips isotherm model were 245.75, 4.43, and 0.22 mg/g for Pb^{2+} , Cd^{2+} , and Hg^{2+} , respectively.

The Langmuir isotherm was the only two-parameter model that provided a good fit to the data in the whole range of initial concentrations. The nature of the adsorption process can be described through the Langmuir separation factor ($R_L = \frac{1}{1+k_L C_0}$), indicating if the adsorption is irreversible ($R_L = 0$), favourable ($0 < R_L < 1$), or unfavorable ($R_L > 1$) [212]. The experimental data led to R_L ranged 0.93-0.99, 0.96-0.99, and 0.84-0.99 for Pb^{2+} , Cd^{2+} , and Hg^{2+} , respectively.

3. RESULTS AND DISCUSSION

Table 3.46. Isotherm models: parameters and error function (R^2) values obtained for the removal of the Pb^{2+} , Cd^{2+} , and Hg^{2+} cations onto ZB0.

Two-parameter isotherm model				
Isotherm	Parameters	Pb^{2+}	Cd^{2+}	Hg^{2+}
Langmuir [132]	q_{max} (mg/g)	198.18	5.08	0.24
$q_e = \frac{q_{max}k_L C_e}{1 + k_L C_e}$	k_L (L/mg)	0.78	1.11	1.47×10^{-4}
	R^2	0.967	0.819	0.954
Freundlich [133]	k_F (mg/g)/(mg/L) ⁿ	82.15	2.52	50.19
$q_e = k_F C_e^n$	n	0.35	0.25	0.33
	R^2	0.950	0.680	0.870
Dubinin-Radushkevich [134]	q_{max} (mg/g)	158.55	4.53	0.22
$q_e = q_{DR} e^{-k_{DR} \epsilon^2}$	k_{DR} (mol ² /kJ ²)	1.36×10^{-7}	9.23×10^{-8}	2.37×10^{-6}
	R^2	0.926	0.792	0.958
Three-parameter isotherm model				
Isotherm	Parameters	Pb^{2+}	Cd^{2+}	Hg^{2+}
Sips [136]	q_{max} (mg/g)	245.75	4.43	0.22
$q_e = \frac{q_{max}(k_S C_e)^n}{1 + (k_S C_e)^n}$	k_S (L/mg)	0.41	1.62	2.23×10^{-4}
	n	0.70	2.81	1.83
	R^2	0.975	0.997	0.966
Toth [137]	q_{max} (mg/g)	233.13	4.41	0.22
$q_e = \frac{q_{max} k_T C_e}{[1 + (k_T C_e)^n]^{1/n}}$	k_T (L/mg)	0.76	0.74	0.11
	n	0.75	6.97	3.0
	R^2	0.977	0.986	0.965
Redlich-Peterson [138]	k_{RP} (L/g)	211.29	6.01	30.93
$q_e = \frac{k_{RP} C_e}{1 + a_{RP} C_e^\beta}$	a_{RP} (mg/L) ^{-β}	1.41	1.27	9.09×10^{-5}
	β	0.89	0.97	1.08
	R^2	0.971	0.810	0.957

So, the removal of the metal cations using ZB0 from the waste could be explained by homogeneous adsorption on the active sites of the zeolite.

In addition, the estimation of the sorption energy (1.9, 2.3, and 0.5 kJ/mol for Pb^{2+} , Cd^{2+} , and Hg^{2+} , respectively) using the Dubinin-Radushkevich model, revealed values of $E < 8$ kJ/mol, indicating that the metal cations uptake by ZB0 could take place by physical adsorption [110].

3. RESULTS AND DISCUSSION

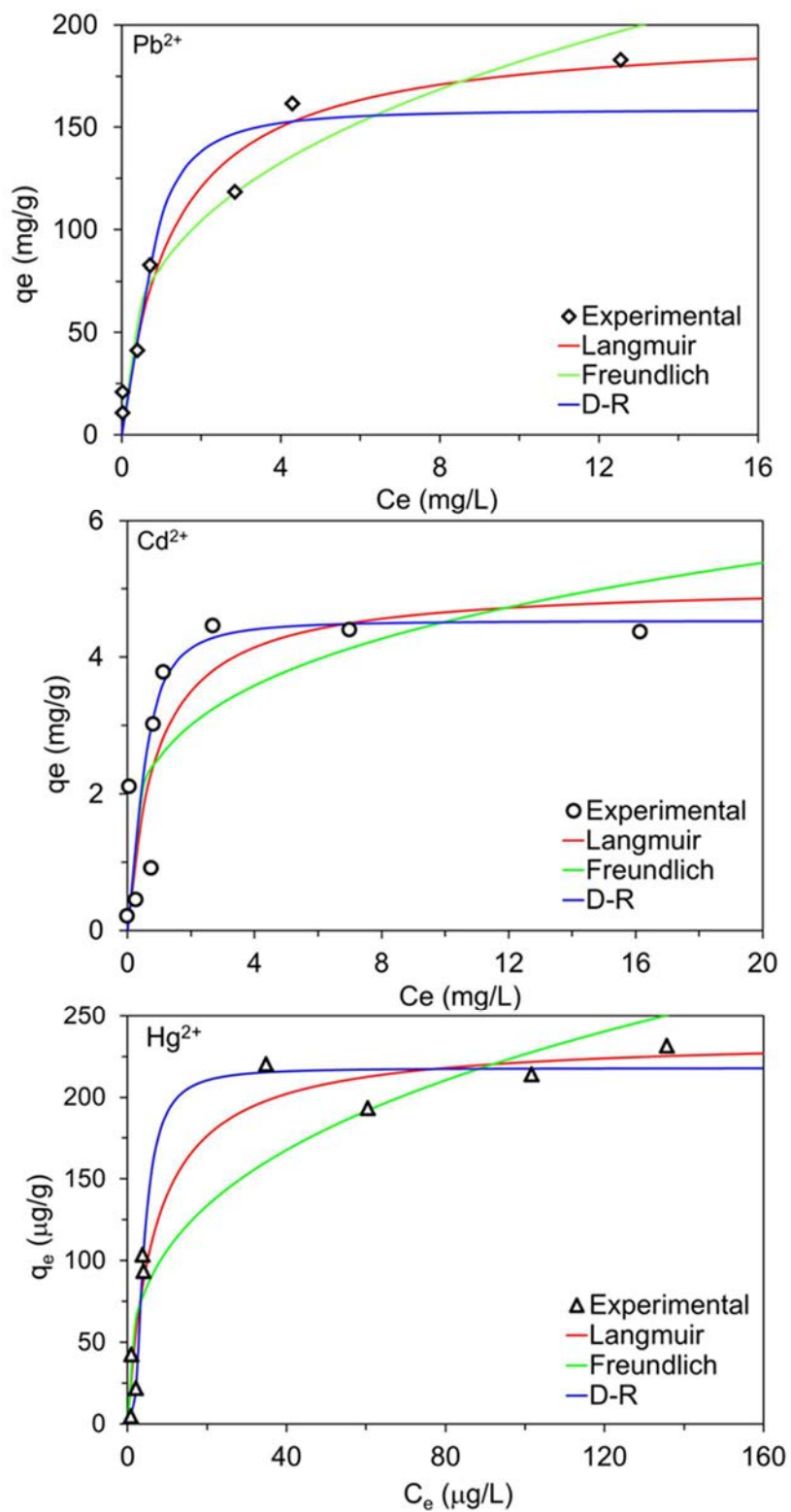


Figure 3.51. Two-parameter isotherms for the removal of Pb^{2+} , Cd^{2+} , and Hg^{2+} on ZB0. Conditions: pH = 4.5; contact time = 15 min; adsorbent dose = 5 g/L for Cd^{2+} and Hg^{2+} and 0.5 g/L for Pb^{2+} ; $T = 25 \pm 2$ °C.

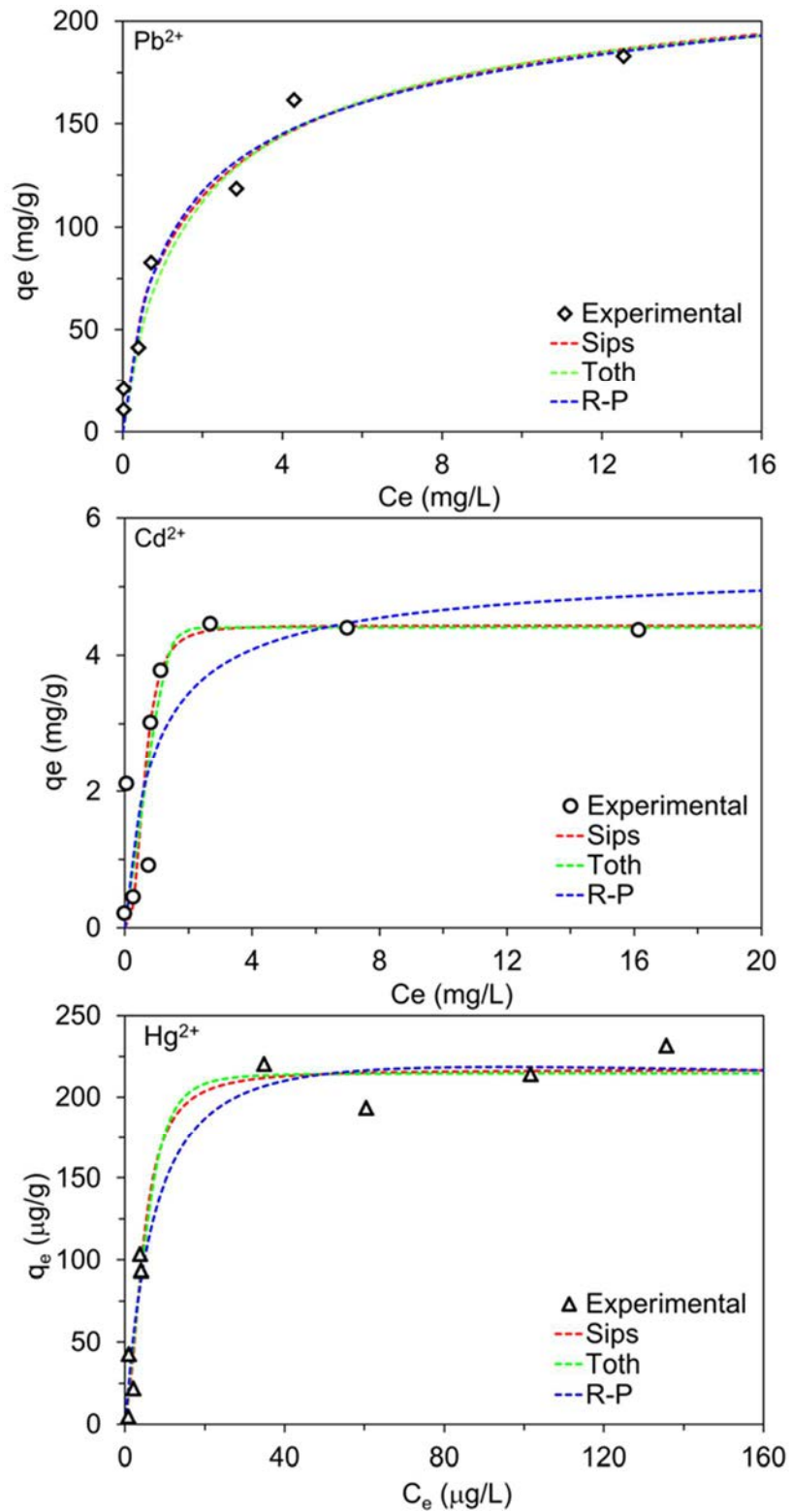


Figure 3.52 Three-parameter isotherms for the removal of Pb^{2+} , Cd^{2+} , and Hg^{2+} on ZBO. Conditions: pH = 4.5; contact time = 15 min; adsorbent dose = 5 g/L for Cd^{2+} and Hg^{2+} and 0.5 g/L for Pb^{2+} ; $T = 25 \pm 2$ °C.

3. RESULTS AND DISCUSSION

3.4.5 Competitive adsorption

The study of multi-cation adsorption allows the assessment of the degree of interference of other metal cations present in the adsorption process. In this sense, the competitive adsorption was evaluated using zeolite doses of 2 and 10 g/L at different contact times (ranged between 1 and 30 min), as shown in Table 3.47 and Figure 3.53.

Table 3.47. Competitive adsorption of Pb^{2+} , Cd^{2+} , and Hg^{2+} on ZB0 using different zeolite doses and contact times. Conditions: pH = 4.5; adsorbent dose = 2 and 10 g/L; $C_0 = 20$ mg/L for Pb^{2+} and Cd^{2+} , and 0.2 mg/L for Hg^{2+} ; $T = 25 \pm 2$ °C.

Cation	Adsorbent dose (g/L)	Contact time (min)	$q_{t,\text{experimental}}$ (mg/g)	Removal (%)
Pb^{2+}	2	5	10.47	98.8
		30	10.57	99.7
	10	5	2.15	99.9
		30	2.15	99.9
Cd^{2+}	2	5	2.15	20.3
		30	3.53	33.3
	10	5	1.83	85.1
		30	1.88	87.4
Hg^{2+}	2	5	0.042	42.2
		30	0.043	43.2
	10	5	0.018	86.0
		30	0.019	86.9

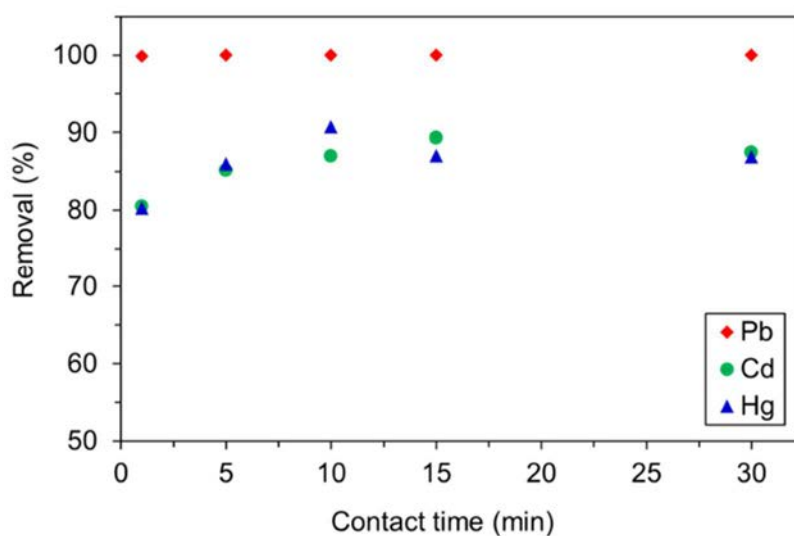


Figure 3.53. Influence of the contact time on the multi-cation adsorption using ZB0. Conditions: pH = 4.5; adsorbent dose = 10 g/L; $C_0 = 20$ mg/L for Pb^{2+} and Cd^{2+} , and 0.2 mg/L for Hg^{2+} ; $T = 25 \pm 2$ °C.

It seems that ZB0 presented a greater affinity for Pb^{2+} compared with Cd^{2+} and Hg^{2+} . The multi-component removal efficiency of Pb^{2+} on the zeolite remained practically unchanged in presence of Hg^{2+} and Cd^{2+} under the studied conditions.

High removal efficiencies of Pb^{2+} (almost 100 %) were reached both at very low contact time (1 min) and at longer time (i.e., 30 min), as can be seen in Figure 3.53. In all the studied cases, the residual concentration of Pb^{2+} from both the single solution and the cations mixture was remarkably low (in both cases lower than 0.02 mg/L). The Cd^{2+} and Hg^{2+} removal efficiencies, which were lower than that obtained for Pb^{2+} , greatly increased in proportion to the zeolite dose.

To evaluate the removal of Cd^{2+} and Hg^{2+} on the zeolite, the initial concentration of Pb^{2+} was varied (0-20 mg/L) using the best adsorption conditions (i.e., zeolite dose = 10 g/L; contact time = 30 min). In absence of Pb^{2+} in the solution medium, the elimination of such metal cations led to removal efficiencies ranged between 80 and 90 %. As the initial concentration of Pb^{2+} was increased, the Cd^{2+} and Hg^{2+} removal efficiencies were decreased due to the competition of the cations.

From the results, the selectivity of ZB0 seems to follow the next sequence: $\text{Pb}^{2+} > \text{Hg}^{2+} \sim \text{Cd}^{2+}$, which is quite similar to that reported for heavy metals removal on natural zeolites [213]. The hydrated radii of the studied metal cations are 4.01, 4.22, and 4.26 Å for Pb^{2+} , Hg^{2+} , and Cd^{2+} , respectively. So, the highest affinity of the zeolite for Pb^{2+} could be attributed to its smallest size that allows it to diffuse more easily to the zeolite surface. Structurally, the zeolite has a system of channels formed by 8-ring pore openings of 3.1 x 4.5 Å and 2.8 x 4.8 Å [20]. These two types of interconnected channels would be large enough for the accessibility of the metal cations through the channel system of NaP1. So, there would be no significant diffusion and steric limitations in the removal process of the studied metal cations on the zeolite.

3.4.6 Removal mechanism

For a better understanding of the adsorption mechanism between the zeolitic adsorbent (ZB0) and metal cations, SEM, FTIR, and μ -XRF analysis were developed to study the morphological, structural, and chemical properties of the zeolite before and after the competitive adsorption.

3. RESULTS AND DISCUSSION

After the Pb^{2+} , Cd^{2+} , and Hg^{2+} removal, ZB0 exhibited the typical morphology of the initial NaP1 zeolite that remained unchanged (Figure 3.54). Thus, the adsorption process of Pb^{2+} , Cd^{2+} , and Hg^{2+} at a pH 4.5 seems not to modify the zeolite structure. In addition, no precipitation of the studied heavy metals on the zeolite surface was observed in the SEM analysis.

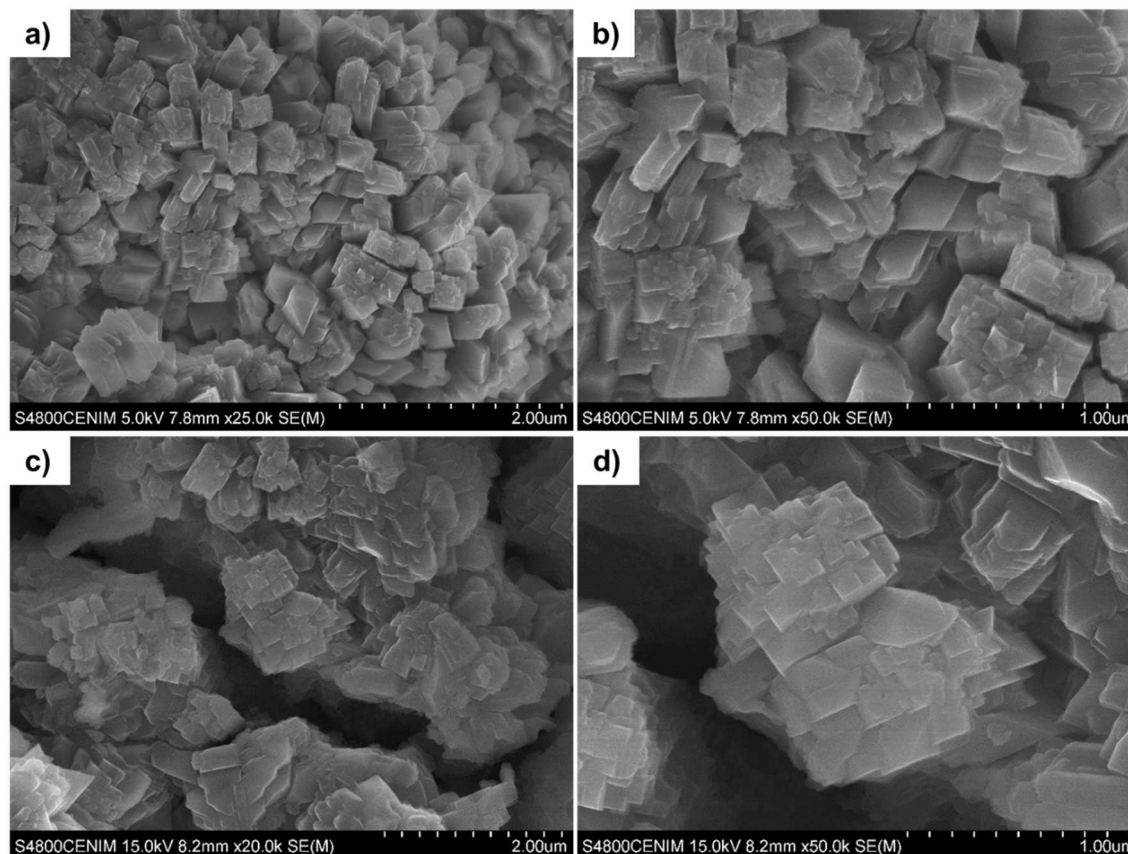


Figure 3.54. SEM images of the ZB0 zeolite before (a-b) and after (c-d) the multi-cation removal of Pb^{2+} , Cd^{2+} , and Hg^{2+} from aqueous solutions.

The comparison between the FTIR spectra of the initial zeolite with that obtained after the uptake of all the metal cations is shown in Figure 3.55. Before the adsorption, the results show the typical absorption bands of the initial NaP1 zeolite. The Pb^{2+} , Cd^{2+} , and Hg^{2+} adsorption seems to lead to very similar absorption bands to the characteristic vibration modes occurring in the initial zeolite. However, a slightly displacement of the bands associated to the T-O-T asymmetric (1003 cm^{-1}) and symmetric (678 cm^{-1}) stretching modes of the initial zeolite was observed, where T-atom corresponds to Si or Al. After the adsorption, these absorption bands were shifted to 1017 cm^{-1} and 686 cm^{-1} , which is attributed to the uptake of the studied cations on ZB0.

The reviewed literature reports changes in absorption bands that can be related to sorption processes of different contaminants from waters. For example, Mozgawa et al. [214] reported slight modifications in the intensity of absorption bands, around 650-715 cm^{-1} , of natural zeolites after the sorption of heavy metals. Zhu et al. [205] found shifts of bands to higher wave numbers that can be related to the coordination of metal cations with active groups on the sorbent.

According to the Lewis acid-base theory, metal cations such as Pb^{2+} , Cd^{2+} , and Hg^{2+} could act as Lewis acids, while the active sites of the zeolite (mainly OH^-) could be considered as Lewis bases. Thus, the metal cations could react with OH^- on the zeolite surface by bonding to one or more available electron pairs on the base.

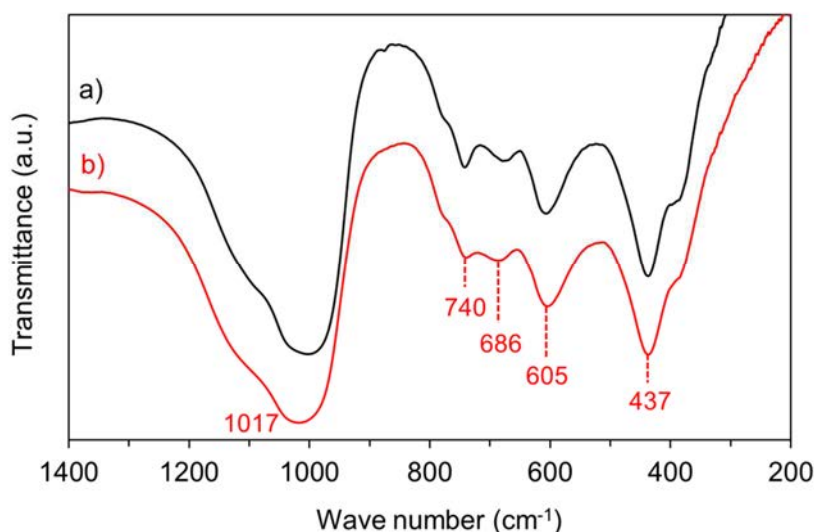


Figure 3.55. FTIR spectra of ZB0 before (a) and after (b) the multi-cation adsorption of Pb^{2+} , Cd^{2+} , and Hg^{2+} .

To evaluate possible changes in the chemical composition of the zeolite before and after the multi-cation adsorption, μ -XRF analysis was also performed. The chemical compositions (expressed as % wt.) of ZB0 after the adsorption process of the studied heavy metals compared with the initial zeolite are shown in Table 3.48.

Thus, the main chemical composition of ZB0 was: SiO_2 55.16 wt.%, Al_2O_3 26.74 wt.%, Na_2O 7.62 wt.%, and *ca* 10 wt.% corresponding to small amounts of CaO , TiO_2 , K_2O , Fe_2O_3 , and MgO . As can be seen, both lead and cadmium were detected in the chemical composition of ZB0 after adsorption, confirming their immobilization on the zeolite. Mercury identification was not possible due to its residual concentration was below the detection limit of the XRF technique. The amount of Na^+ present in the initial zeolite

3. RESULTS AND DISCUSSION

decreased as the heavy metals adsorption process progressed. This seems to indicate that the adsorption process could involve cation exchange between the extra-framework cations on the zeolite (mainly Na^+) and Pb^{2+} , Cd^{2+} , and Hg^{2+} . These results are in accordance with those obtained by Meng et al. [215]. The authors studied the removal of cations including heavy metals like Ag^+ , Pb^{2+} , etc. onto a zeolite A from halloysite, reporting higher concentrations of Na^+ in the aqueous solution after adsorption.

Table 3.48. Chemical composition (determined by μ -XRF) of ZB0 before and after the competitive adsorption of Pb^{2+} , Cd^{2+} , and Hg^{2+} .

Element	Before adsorption	After adsorption
	% wt.	% wt.
SiO_2	55.16	57.16
Al_2O_3	26.74	27.17
Na_2O	7.62	3.75
CaO	2.88	2.75
TiO_2	2.77	3.01
K_2O	2.02	2.23
Fe_2O_3	1.18	1.15
MgO	0.96	0.55
ZnO	0.41	0.49
CuO	0.26	0.29
PbO	-	0.86
CdO	-	0.61

3.4.7 Adsorption capacity of NaP1 compared with other adsorbents

Table 3.49 shows the comparison between the maximum adsorption capacity for Pb^{2+} , Cd^{2+} , and Hg^{2+} of the NaP1 zeolite obtained from the waste by the one-step zeolitization process and different adsorbents reported in the literature [202, 204, 212-218]. These sorbent materials included natural zeolites, clays, glasses, resins, nanocomposites, etc. with different adsorption capacities, depending on the different experimental conditions studied (pH, temperature, adsorbent dose, contact time, initial cation concentration, etc.).

3. RESULTS AND DISCUSSION

Table 3.49. Comparison of the maximum adsorption capacity of Pb^{2+} , Cd^{2+} , and Hg^{2+} using different sorbent materials

Adsorbent	q_{max} (mg/g)	Isotherm	pH	Dose (g/L)	Time (h)	T (°C)	Reference
Lead (Pb^{2+}) removal							
Ti (IV) iodovanadate	18.8	Langmuir	6	2	1	20	[216]
Bentonite	19.5	Freundlich	6	2	24	RT	[208]
Clinoptilolite	40.7	Sips	5	2	72	30	[206]
NaP1 from oil shale ash	70.6	R-P	7	1	5	20	[217]
Erionite	81.3	Sips	5	2	72	30	[206]
Modified natural zeolite	133	Freundlich	4.2	20	24	RT	[218]
NaP1 from aluminum waste	245.8	Sips	4.5	0.5	0.5	25	This thesis
Cadmium (Cd^{2+}) removal							
Clinoptilolite	2.5	Sips	5	2	72	30	[206]
NaP1 from aluminum waste	4.4	Sips	4.5	5	0.5	25	This thesis
Erionite	4.6	Sips	5	2	72	30	[206]
Bentonite	13.1	Freundlich	6	2	24	RT	[208]
NaP1 from oil shale ash	95.6	Sips	7	1	5	20	[217]
Curcumin formaldehyde resin	119.1	Langmuir	7	1	1	25	[219]
Mercury (Hg^{2+}) removal							
NaP1 from aluminum waste	0.22	Sips	4.5	5	0.5	25	This thesis
Perlite	0.35	Langmuir	6.5	14	1.33	20	[220]
Bentonite	1.7	Freundlich	6	10	36	RT	[208]
Organosilica	5.4	-	4.5	0.01	0.5	21	[221]
Ti (IV) iodovanadate	17.2	Langmuir	6	2	1.5	20	[216]
Starch/ SnO_2	192	Langmuir	6	0.4	1	25	[222]

In our case, the uptake of the metal cations was carried out in a very short time (30 min), indicating no significant diffusion limitations and no steric restrictions, due to the larger size of the pore openings of the zeolite, in the removal of Pb^{2+} , Cd^{2+} , and Hg^{2+} cations on NaP1 from Alw_x .

As can be observed the adsorption capacity for Pb^{2+} of the sample ZB0 studied is higher than those reported for the same cation, reaching a high Pb^{2+} removal in a very short contact time. The zeolite showed lower adsorption capacity for Cd^{2+} , and Hg^{2+} due to their larger size compared with Pb^{2+} .

3. RESULTS AND DISCUSSION

3.5 Removal of ammonium from aqueous solutions

In addition to the evaluation of the heavy metals removal on the synthesized zeolites (Section 3.4), the removal of other pollutants like ammonium present in aqueous media was also tested using the obtained zeolites as adsorbent.

The removal of ammonium (NH_4^+) from aqueous solutions by batch adsorption experiments on the NaP1 zeolite (sample ZB0) synthesized from the waste (Alw_x) via the bench-scale zeolitization process was evaluated. The effects of different experimental parameters, such as pH, contact time, adsorbent dose, and initial NH_4^+ concentration were evaluated (Table 3.50).

Table 3.50 Experimental conditions for the ammonium adsorption experiments using the zeolite NaP1 (sample ZB0) obtained from the waste.

Ammonium (NH_4^+) adsorption				
Conditions	Time (min)	pH	Adsorbent dose (g/L)	Initial concentration (mg/L)
pH	15	6-8	5	50
Contact time	2-360	7.5	5	50
Adsorbent dose	15	7.5	1-15	50
Initial concentration	15	7.5	10	10-1000

Adsorption kinetic models and equilibrium isotherms were applied using a non-linear regression method to evaluate the behavior of the zeolite in the adsorption process. The results showed that the NH_4^+ removal onto the zeolite was fast, leading to removal high removal percentages (88 %) in the first 15 min.

The immobilization of NH_4^+ on the studied zeolite was detected by the FTIR analysis, showing the typical absorption band (1400 cm^{-1}) of the NH_4^+ asymmetrical bending mode.

The NH_4^+ cations and alkali metals (mainly Na^+) from the zeolitic framework would be exchanged easily since these cations have the same charge and similar sizes. The governing mechanism of the adsorption process may be based on the exchange of the Na^+ cations in the zeolite structure by the NH_4^+ cations present in the aqueous solution.

3.5.1 Effect of pH

The pH plays a very important role in the adsorption process since it influences the chemical equilibrium between the ammonium ion (NH_4^+) and ammonia (NH_3), according to the reversible reaction [223]:



Likewise, the pH also promotes electrostatic interactions between sorbent materials and ions to be adsorbed, being an essential control parameter in adsorption processes.

The influence of pH on the ammonium adsorption capacity and removal efficiency for NaP1 was evaluated in the pH range of 6-8 (Figure 3.56) in order to select the most adequate conditions for further adsorption experiments. Although the highest ammonium uptake was reached at pH 7.5 leading to the highest adsorption capacity (8.76 mg/g) and removal efficiency (87.6 %), similar results were also obtained at pH 7 and 8. Thus, the NH_4^+ adsorption capacity for NaP1 was of 8.70 and 8.69 mg/g at pH 7 and 8, involving removal percentages of 87.0 and 86.9 %, respectively.

Similarly, studies about the NH_4^+ adsorption onto NaA zeolite from FA using the same adsorbate initial concentration (50 mg/L) also showed the best results at pH ranged between 7 and 8 with removal efficiency around 60 % [108]. In our case, using the zeolite (ZB0) obtained from the waste (Alw_x) through the bench-scale synthesis process higher removal efficiency (87.6 %) was obtained. Thus, the removal of the adsorbate from aqueous medium onto ZB0 could take place effectively at $\text{pH } 7.5 \pm 0.5$. The adsorption ability of the zeolite decreased slightly (only 3 % less than the highest removal efficiency) as the pH decreased from 7.5 to 6. This can be associated with the potential competition between H^+ protons and the NH_4^+ cations to be adsorbed onto ZB0.

Similar tendencies are shown in the literature for the ammonium sorption onto other adsorbent materials, such as volcanic tuff whose main component is clinoptilolite (a natural zeolite) [224] and NaA zeolite from halloysite mineral prepared by a two-step synthesis treatment (alkaline fusion followed by hydrothermal synthesis) [225].

3. RESULTS AND DISCUSSION

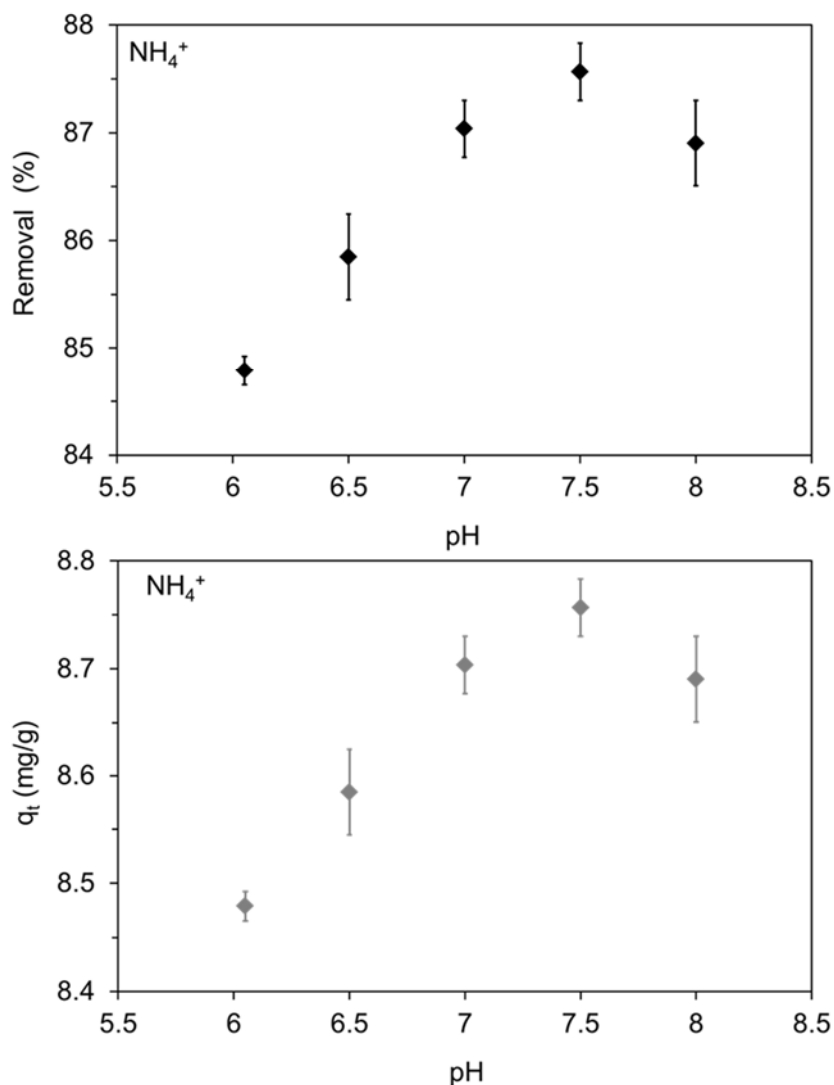


Figure 3.56. Influence of the pH on the NH_4^+ removal efficiency and adsorption capacity of the zeolite synthesized (ZB0) from the waste through the bench-scale synthesis process. Conditions: contact time = 15 min; adsorbent dose = 5 g/L; $C_0 = 50$ mg/L; $T = 28 \pm 2$.

As commented previously, lower pH conditions were not considered because mass losses caused by dissolution as well as dealumination of zeolites can take place at low pH, especially at $\text{pH} < 4$ [103]. Strong basic conditions ($\text{pH} > 8$) were not evaluated since the NH_4^+ concentration could decrease and the chemical equilibrium would be directed to the NH_3 (g) formation, as showed the NH_4^+ chemical equilibrium diagram determined for an initial concentration of 50 mL/g (Figure 3.57).

Therefore, the fixed pH for further adsorption tests was 7.5, where the zeolite mass remains unchanged and the adsorbate would exist mainly in the ionized form, i.e., NH_4^+ .

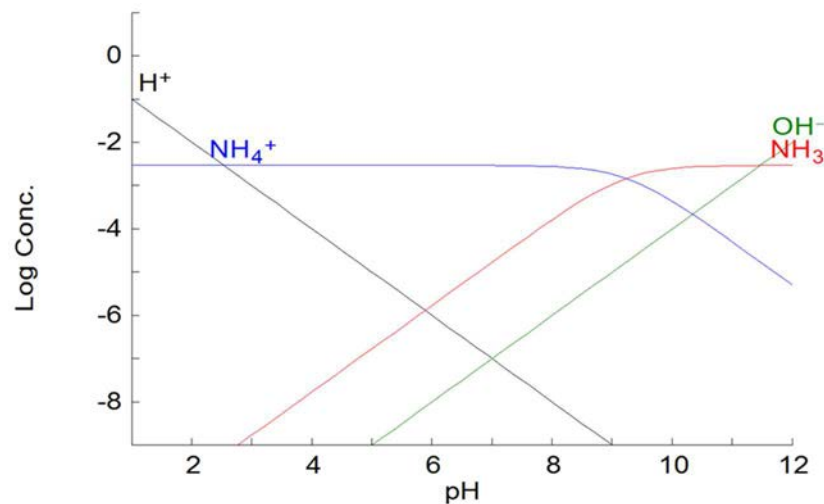


Figure 3.57 Chemical equilibrium diagram of NH_4^+ in aqueous solution determined for a fixed initial concentration (50 mg/L).

3.5.2 Effect of contact time: Adsorption kinetic

The influence of the contact time on the ammonium removal efficiency was studied from 1 to 360 min, as shown in Figure 3.58. The ammonium adsorption on ZB0 seems to be a very fast process where the equilibrium was reached within the first 5 min. Under the tested operating conditions, the highest removal efficiency of the zeolite was 88 %, which was reached at 15 min.

The short required contact time would involve a high affinity for the adsorbate, indicating a close electrostatic interaction between the NH_4^+ cations and the charged negatively functional groups on the zeolite surface. As the contact time increased, the removal efficiency of ZB0 was almost constant (86.3 and 85.4 % for 2 and 30 min), and then slightly decreased from 82 to 75.8 % for 60 and 360 min.

Some authors found that the NH_4^+ adsorption efficiency using natural zeolite was maintained from 30 min to longer contact times (up to 24 h) [226]. It seems to be related to the large number of available active sites on the adsorbent surface and the high adsorbate concentration gradient at the beginning of the adsorption process, resulting in a fast diffusion and rapid equilibrium. As the adsorbent sites are occupied, the adsorption capacity would decrease significantly.

3. RESULTS AND DISCUSSION

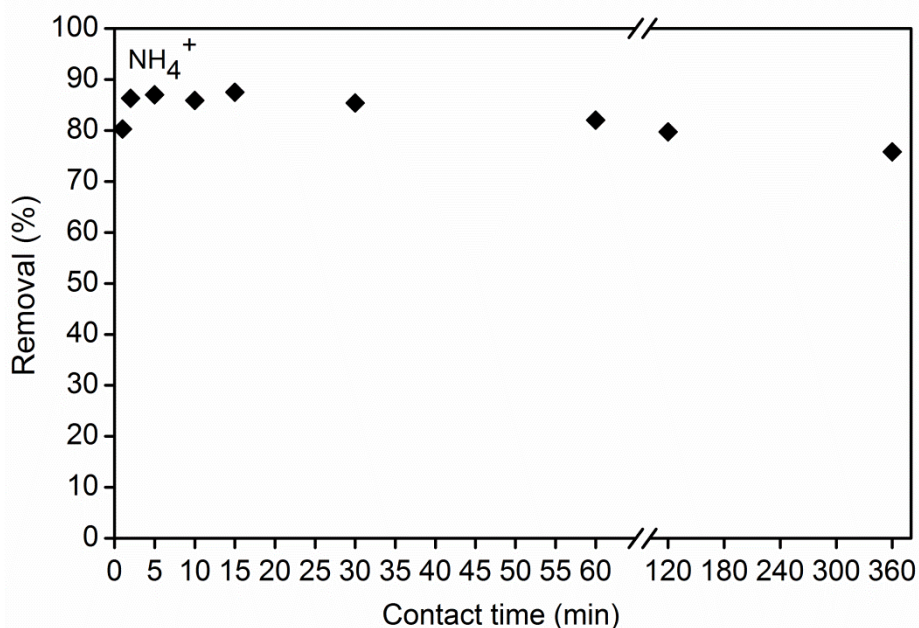


Figure 3.58. Effect of the contact time on the adsorption NH_4^+ onto ZB0. Conditions: pH = 7.5; adsorbent dose = 5 g/L; $C_0 = 50$ mg/L; $T = 28 \pm 2$ °C.

Additionally, the rapid adsorption would take place easily on the adsorbent surface, whereas the slower uptake process would occur inside the pores [144].

As a further increase in the contact time had no significant effect on the removal efficiency, the adsorption kinetic of NH_4^+ onto ZB0 was only studied between 1 and 60 min.

The kinetic analysis is essential for the process design in water treatment applications, thus the adsorption kinetic performance was evaluated by applying the pseudo-first [129] and pseudo-second-order [130] models and using the non-linear regression method. Apparently, only minor differences can be noticed between the plots obtained for the pseudo-second-order and the pseudo-first-order model (both shown in Figure 3.59).

Generally, although in most of the reviewed works [144, 227-229], the NH_4^+ adsorption kinetic has been evaluated according to linear regression methods, the pseudo-second-order model seems to provide the best results. However, the pseudo-first-order equation is usually more appropriate for the initial stage of adsorption processes (contact time of 20-30 min) not for the whole range [230]. In our case, the adsorption of NH_4^+ on ZB0 was significantly rapid, reaching high efficiencies of 80.3 and 86.3 % in 1 and 2 min, respectively.

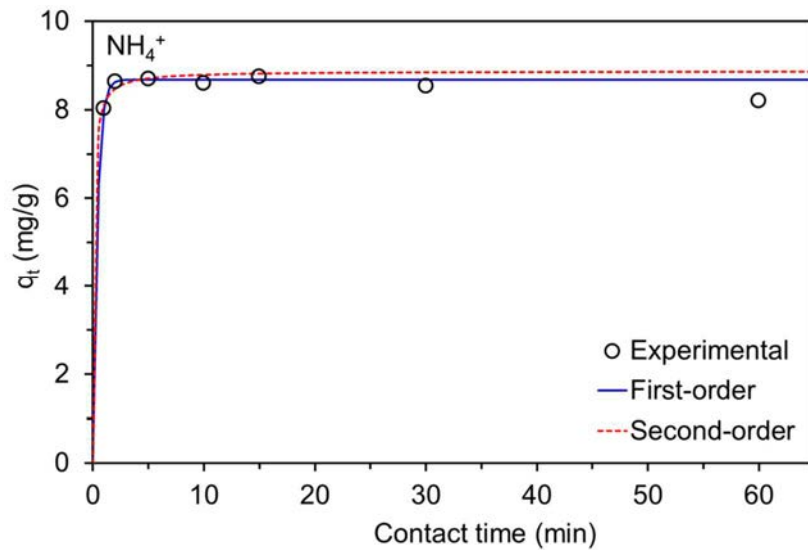


Figure 3.59 Pseudo-first-order and pseudo-second-order models for the adsorption of NH_4^+ onto ZB0. Conditions: pH = 7.5; adsorbent dose = 5 g/L; $C_0 = 50$ mg/L; $T = 28 \pm 2$ °C.

Thus, the pseudo-first-order kinetic model seems to describe better the experimental data since it model provided a more accurate correlation, i.e., the highest R^2 values (Table 3.51).

Table 3.51. Kinetic model parameters and error function values obtained for the NH_4^+ adsorption onto the NaP1 zeolite synthesized (ZB0) from the waste by the bench-scale synthesis process.

$q_{e,\text{experimental}}$ (mg/g)	Pseudo-first-order model $q_t = q_e(1 - e^{-k_1 t})$		Pseudo-second-order model $q_t = \frac{k_2 q_e^2 t}{1 + k_2 q_e t}$	
	8.75	$q_{e,\text{model}}$ (mg/g)	8.68	$q_{e,\text{model}}$ (mg/g)
k_1 (1/min)		2.60	k_2 (g/mg min)	1.20
R^2		0.961	R^2	0.895

It is considered that the NH_4^+ uptake by the zeolite ZB0 follows the common transport processes during the adsorption in solid-liquid systems characterized by four steps [95]:

- Bulk transport, which occurs quickly.
- Film diffusion where the adsorbate is transported from the bulk liquid phase to the active sites on the adsorbent external surface (solid phase), taking place slowly.
- Intra-particle diffusion where the adsorbate diffuses slowly from the exterior of the adsorbent to the most internal surface (i.e., pores) of the adsorbent.
- And finally, adsorptive attachment, which is a very fast process.

3. RESULTS AND DISCUSSION

3.5.3 Effect of adsorbent dose

The influence of the adsorbent dose on the removal efficiency and adsorption capacity of NaP1 for the ammonium uptake was studied from 1 to 15 g/L, as shown in Figure 3.60.

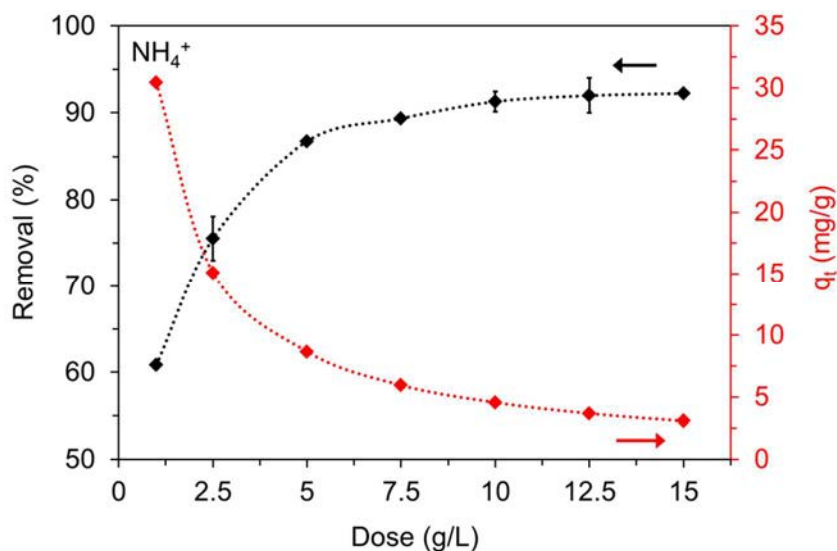


Figure 3.60. Effect of the adsorbent dose on the NH_4^+ removal efficiency and uptake capacity of ZB0. Conditions: pH = 7.5; contact time = 15 min; $C_0 = 50$ mg/L; $T = 28 \pm 2$ °C.

The increase of the zeolite dose led to the increase of the removal efficiency from 61 to 92 % for 1 and 15 g/L, while the NH_4^+ uptake capacity decreased from 30.4 to 3.1 mg/g for 1 and 15 g/L, respectively. The higher the adsorbent mass, the larger the adsorbent surface, and accordingly, the larger the number of adsorption sites on the surface of ZB0, accelerating the adsorption process.

The NH_4^+ cations would diffuse from the aqueous medium towards the surface of the zeolitic adsorbent due to the electrostatic attraction, tending to occupy the adsorption active sites. In this context, the higher the adsorbent dose, the larger the adsorbent sites will be available under the same adsorption conditions (i.e., under the same adsorbate mass gradient).

Both the removal efficiency and adsorption capacity of the zeolite were almost constant from 10 to 15 g/L, thus the selected adsorbent dose for developing the further adsorption tests was 10 g/L since it would be the lowest adsorbent dose that provides a very high removal efficiency (91 %).

3.5.4 Effect of initial adsorbate concentration: equilibrium isotherms

As the initial concentration increased, the amount of ammonium retained by ZB0 also increased gradually up to the adsorbent saturation, which was reached above an initial concentration of approximately 1000 mg/L under the tested conditions. The experimental data indicated that the maximum adsorption capacity of ZB0 was 37.9 mg/g. In general, higher adsorption capacities are obtained from the fit of isotherm models to the experimental data. The applied adsorption isotherms are illustrated in Figure 3.61 and Figure 3.62. The estimated parameters and error function values for the two-parameter and three-parameter models are shown in Table 3.52.

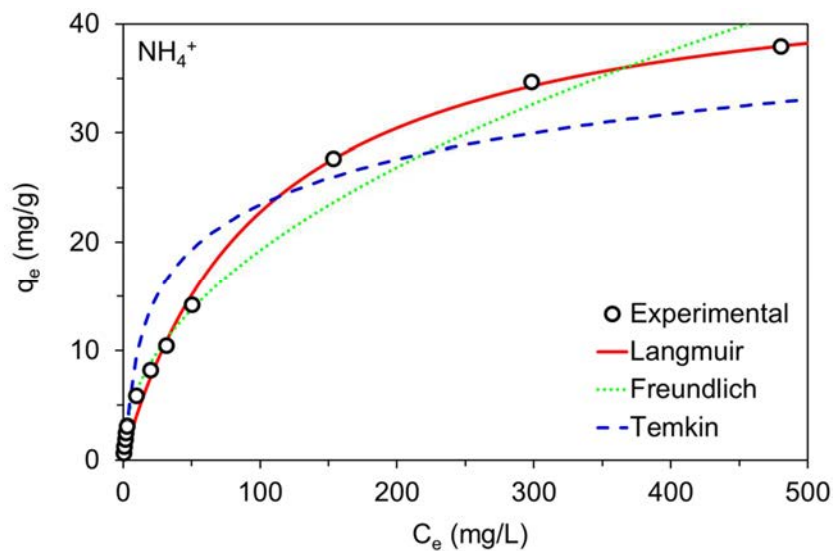


Figure 3.61 Two-parameter adsorption isotherms for the NH_4^+ uptake on ZB0. Conditions: pH = 7.5; contact time = 15 min; adsorbent dose = 10 g/L; $T = 28 \pm 2$ °C.

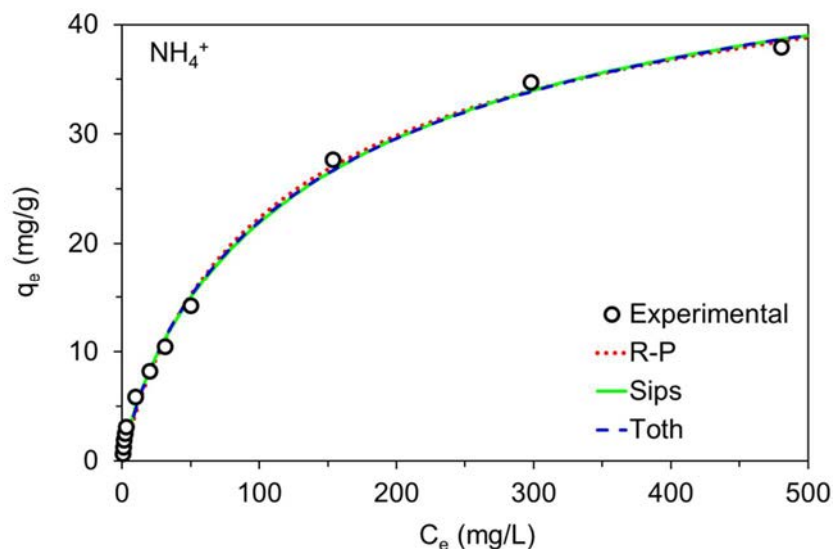


Figure 3.62. Three-parameter adsorption isotherms for the NH_4^+ uptake on ZB0. Conditions: pH = 7.5; contact time = 15 min; adsorbent dose = 10 g/L; $T = 28 \pm 2$ °C. R-P: Redlich-Peterson.

3. RESULTS AND DISCUSSION

Table 3.52. Isotherm models applied for the NH₄⁺ adsorption onto ZB0.

Two-parameter isotherm	Parameters	NH ⁴⁺
Langmuir [132]	q _{max} (mg/g)	46.05
$q_e = \frac{q_{max}k_L C_e}{1 + k_L C_e}$	k _L (L/mg)	0.01
	R ²	0.995
Freundlich [133]	k _F (mg/g)/(mg/L) ⁿ	2.09
$q_e = k_F C_e^n$	n	0.48
	R ²	0.981
Temkin [135]	A (L/g)	0.5
$q_e = \frac{RT}{b} \ln(AC_e)$	b (J/mol)	413.74
	R ²	0.901
Three-parameter isotherm	Parameters	NH ⁴⁺
Sips [136]	q _{max} (mg/g)	54.19
$q_e = \frac{q_{max}(k_S C_e)^n}{1 + (k_S C_e)^n}$	k _S x 10 ⁻³ (L/mg)	6.26
	n	0.83
	R ²	0.997
Toth [137]	q _{max} (mg/g)	58.46
$q_e = \frac{q_{max}k_T C_e}{[1 + (k_T C_e)^n]^{1/n}}$	k _T x 10 ⁻² (L/mg)	1.10
	n	0.68
	R ²	0.996
Redlich-Peterson [138]	k _{RP} (L/g)	0.52
$q_e = \frac{k_{RP} C_e}{1 + a_{RP} C_e^\beta}$	a _{RP} (mg/L) ^{-β}	0.02
	β	0.91
	R ²	0.996

The Langmuir isotherm was the only two-parameter model that provided the best data tendency in the whole range of initial concentrations (Figure 3.61). Thus, the Langmuir isotherm would indicate a homogeneous process and monolayer coverage of NH₄⁺ on the NaP1 surface. On the contrary, the Freundlich isotherm was only suited for the range of low initial concentrations, while the Temkin model was not fit satisfactorily to the experimental data.

The relation between the Freundlich exponent (n = 0.48 < 1) and the Langmuir separation factor (R_L = 0.94 and 0.11 for the lowest and highest initial adsorbate concentration) would indicate that the NH₄⁺ adsorption by ZB0 was favorable, according to the concave isotherm shape followed by experimental data [96, 139].

The experimental data were satisfactorily described by all the three-parameter models (Figure 3.62). Such models followed the same isotherm profile, providing the best fits for the experimental data. In particular, the Sips and Toth models provided the highest R^2 values.

The results show that the maximum amount of adsorbed NH_4^+ cation per mass of NaP1 (i.e., q_{max}) was of 54.19 and 58.46 mg/g, according to the Sips and Toth isotherm, respectively (Table 3.52). The Sips isotherm provided reliable results possibly due to the fact it combines both the Langmuir and Freundlich model, thus covering satisfactorily the whole initial concentration range. Thus, the NH_4^+ adsorption using ZB0 could be described by a homogeneous and heterogeneous process. The Redlich-Peterson isotherm is also a combination of both Langmuir and Freundlich model [139]. As the Redlich-Peterson exponent was close to 1 ($\beta = 0.91$), the process would be best described by the Langmuir isotherm instead of Freundlich [96].

Therefore, it suggests that the adsorption of the NH_4^+ cation onto ZB0 obtained from the waste can be more homogeneous rather than heterogeneous.

3.5.5 Adsorption capacity of NaP1 compared with other adsorbents

The maximum NH_4^+ removal capacity of the studied zeolite was compared with other adsorbent materials, mainly zeolites from natural or synthetic source (Table 3.53).

Table 3.53. Maximum adsorption capacity of NH_4^+ for several adsorbents.

Adsorbent	q_{max} (mg/g)	Isotherm	pH	T (°C)	Time (min)	Dose (g/L)	Reference
Natural zeolite	10.39	Langmuir	7	25	1440	32	[231]
Geopolymer	21.07	Sips	6	22	1440	5	[144]
Modified biochar	22.6	Langmuir	8-9	-	120	2	[85]
Natural zeolite	23.83	Sips	6.5	25	1440	3	[229]
Commercial activated carbon	28.92	Langmuir	-	22	120	10	[232]
Zeolite from FA	37.45	Langmuir	8	25	75	4	[109]
Hydrogel	42.74	Langmuir	6-7	30	30	2	[227]
NaP1 from aluminum waste	54.19	Sips	7.5	28	15	10	This Thesis
Zeolite from FA	95.42	Langmuir	7	25	60	2	[108]

3. RESULTS AND DISCUSSION

Although different operating conditions have been used for the uptake of NH_4^+ , in general, the results show that the required time to remove the adsorbate by ZB0 was shorter than most of the adsorbents given in Table 3.53. As can be seen, lower and higher NH_4^+ adsorption capacities were found in the literature [85, 108, 109, 144, 227, 229, 231, 232]. The NaP1 adsorbent from Al-waste showed a high removal capacity, being generally higher than natural zeolites. In addition, this zeolite can be considered as a low-cost adsorbent compared to other commercial materials like activated carbons. The studied NaP1 zeolite exhibited adequate sorption properties when it is compared to other sorbent materials obtained from common synthesis processes. In this sense, ZB0 showed promising adsorption characteristics, making it a potential adsorbent for the NH_4^+ removal from water. It is believed that this zeolite could be also used to remove other contaminants (e.g., radioactive metals, organic compounds, etc.) in aqueous media.

3.5.6 Removal mechanism

For a better evaluation of the removal mechanism between the zeolitic adsorbent (ZB0) and ammonium cation, FTIR analysis was performed to study the structural properties of the zeolite before and after the NH_4^+ adsorption process.

The driving forces for the adsorption process would be described by electrostatic interactions and cation exchange mechanisms. In this sense, the electrostatic attraction would take place between the NH_4^+ cations and ZB0, which showed a negatively charged surface in the studied pH conditions (ζ -potential = -57 mV at approximately pH = 7.5), as showed the ζ -potential analysis (see Section 3.3).

On the other hand, the adsorbate (NH_4^+) and alkali metals (mainly Na^+) from the zeolitic framework would be exchanged easily since these cations have similar crystal hydrated radii (3.31 and 3.58 Å for NH_4^+ and Na^+) [233], thus balancing the total charge of the NaP1 zeolite.

The adsorption would involve trapping the NH_4^+ cations inside the NaP1 structure, releasing innocuous cations (like Na^+) to the aqueous medium:



Structurally, the NaP1 zeolite presents two types of interconnected channels (3.1 x 4.5 Å and 2.8 x 4.8 Å) formed by 8-membered rings [20] that would be large enough for the accessibility of the NH₄⁺ cations through the zeolite channel system.

The comparison between the FTIR spectrum of the initial sample ZB0 with that obtained after the uptake of the adsorbate, is shown in Figure 3.63.

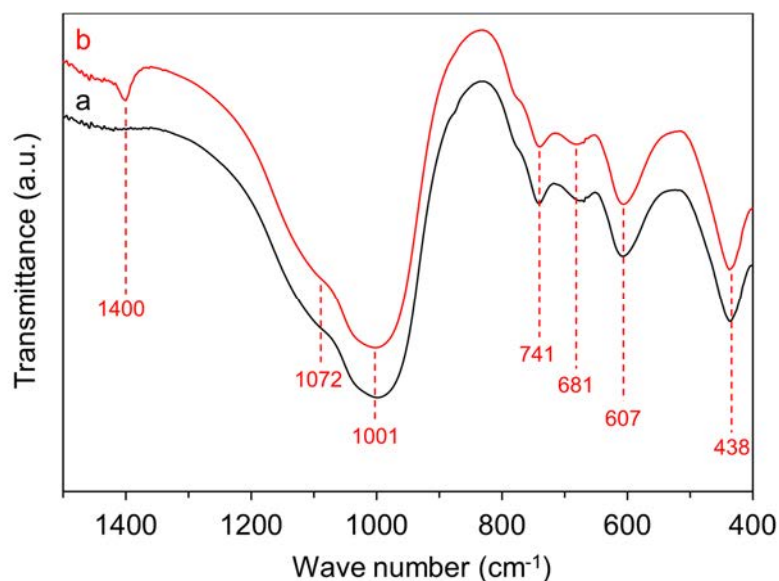


Figure 3.63. FTIR spectra of ZB0 before (a) and after (b) the NH₄⁺ adsorption.

Before NH₄⁺ adsorption, the spectrum shows the main absorption bands of NaP1: T-O-T asymmetrical stretching mode (band at 1000 cm⁻¹ with a shoulder at 1072 cm⁻¹), T-O-T symmetrical stretching mode (742-670 cm⁻¹), external linkage vibration (~ 607 cm⁻¹), and T-O bending mode (437 cm⁻¹) of the TO₄ tetrahedron. After NH₄⁺ adsorption onto zeolite, the corresponding spectrum shows very similar absorption bands (represented by dashed red lines in Figure 3.63) to the characteristic vibration modes occurring in the NaP1 framework before adsorption.

The results confirmed that the main change was observed at approximately 1400 cm⁻¹, attributing to the absorption band (ν₄ asymmetrical bending mode) of NH₄⁺ present in the NaP1 structure [234].

Therefore, the cation exchange of Na⁺ by NH₄⁺ may be considered as the governing mechanism of the adsorption process using the zeolitic adsorbent (ZB0) obtained from the waste by the bench-scale synthesis process.

4. CONCLUSIONS

From the results obtained in this Thesis the next conclusions can be inferred:

- The hazardous aluminum waste from the slag milling processes in the tertiary aluminum industry can be used as a raw material to synthesize different types of zeolites, with characteristics similar to those obtained from conventional and/or commercial materials, in spite of the complex and heterogeneous chemical and mineralogical composition of the waste.
- The most significant hazardous features of aluminum waste come from the following aspects:
 - Its spontaneous and exothermic reactivity derived from its high contents of metallic aluminum and aluminum nitride, evolving toxic gases such as ammonia (71 Nm³ per ton of waste) and/or inflammable and explosive gases like hydrogen (162 Nm³ per ton of waste).
 - Its powdery texture, constituted by particles of very fine granulometry (ranged between 2.5 and 93 μm), easily inhalable, which can reach the respiratory system.
 - Its leaching behavior, entailing the release of diverse harmful heavy metals under incorrect management and disposal.
- The synthesis process developed allows the total transformation of a hazardous waste into an added-value material, such as zeolites. The principal characteristics of this process are:
 - The only aluminum source is the hazardous waste.
 - A previous step of activation is not required, accordingly it can be considered as only one-step process, which is performed in mild experimental conditions.
 - Organic template is not needed for the design of the zeolites.
 - Different types of zeolites are obtained varying only some of the experimental conditions such as alkaline agent concentration and temperature.

4. CONCLUSIONS

- The synthesis, consisting of a zero solid waste and zero effluent process, allows taking advantage of the outputs (mother liquor and rinse water) without affecting to the properties of the zeolites.
- Significant saving of the consumptions of raw materials (water and alkalinizing agent) is achieved by the recycling of effluents, involving a cost reduction of NaOH (70 %) and water (68 %).
- The scaling up of the process achieves the same results of the lab-scale synthesis.
- The reaction yield reached in the zeolitization process involves up to 2.5 kg of zeolite per kg of waste, which is very much higher than that corresponding to zeolites obtained from other waste sources.
- The hydrothermal synthesis process resulted into three types of low Si/Al ratio zeolites, namely: NaP1, sodalite (SOD), and analcime (ANA). The optimal synthesis conditions to obtain the different types of zeolites are:
 - NaP1: 120 °C, 6 h, 1 M NaOH. Its “cauliflower-like” morphology is formed by nanometric crystals with well-defined edges (150-345 nm). Its estimated formula ($\text{Na}_{5.6}\text{Al}_6\text{Si}_{11.1}\text{O}_{34}\cdot 10\text{H}_2\text{O}$) is very similar to the theoretical ($\text{Na}_6\text{Al}_6\text{Si}_{10}\text{O}_{32}\cdot 12\text{H}_2\text{O}$) with a Si/Al ratio of 1.85.
 - SOD: 120 °C, 6 h, 5 M NaOH. It is characterized by a morphology composed of “raspberry-like” balls with distorted hexagonal tabular nanocrystals (40-350 nm). Its estimated formula ($\text{Na}_{2.2}\text{Al}_3\text{Si}_{3.1}\text{Cl}_{0.2}\text{O}_{11.9}\cdot 5\text{H}_2\text{O}$) corresponds to the theoretical of chloride-sodalite ($\text{Na}_4\text{Al}_3\text{Si}_3\text{O}_{12}\text{Cl}$) with a Si/Al ratio of 1.02.
 - ANA: 160 °C, 6 h, 1 M NaOH. It exhibits trapezohedral morphology with highly faceted crystals (4.6-11.2 μm). Its estimated formula ($\text{Na}_{0.9}\text{AlSi}_{1.7}\text{O}_{5.4}\cdot \text{H}_2\text{O}$) fits well with the theoretical ($\text{NaAlSi}_2\text{O}_6\cdot \text{H}_2\text{O}$) for a Si/Al ratio of 1.73.
- The three zeolites have good thermal stability up to 400 °C and can be precursors of ceramic-type phases as nepheline at temperatures above 800 °C.

- The high cation-exchange capacity of the NaP1 zeolite (2.73 meq NH_4^+ /g) is attributable to its gismondine framework, formed by an interconnected channel system, which enables its use in the treatment of water contaminated by highly toxic elements such as heavy metals (lead, cadmium, and mercury) and by other inorganic compounds as ammonium, which mean serious risks to water quality.
- The NaP1 zeolite from the waste shows suitable adsorption properties for the treatment of both acid (pH 4-6) and alkaline (pH > 7.5) aqueous effluents without any modification of its morphological and structural characteristics.
- NaP1 exhibits high removal efficiencies (98.9, 93.3, 99.3, and 88 % for Pb^{2+} , Cd^{2+} , Hg^{2+} , and NH_4^+ , respectively) even in very short times (~ 15 min). Its greater affinity for Pb^{2+} (183 mg/g) involves the smallest zeolite doses for the removal of this cation from aqueous solutions in both mono- and multi-cation systems.
- The removal of all the pollutants on the NaP1 zeolite takes place through fast kinetics, homogeneous and physical adsorption along with cation exchange processes.
- Therefore, the zeolitization process described in this Thesis can be considered as a green and feasible alternative to the traditional synthesis of zeolites from other raw materials. It implies a synergic effect on the environmental protection: firstly, the transformation of the hazardous aluminum waste into a zeolite can contribute to its end-of-waste condition, and secondly, the zeolite obtained from such waste can be considered as a promising adsorbent used for the removal of pollutants from aqueous effluents.

5. REFERENCES

- [1] *International Aluminium Institute. Statistics.* Available: <http://www.world-aluminium.org/statistics/primary-aluminium-production/#data>
- [2] P. E. Tsakiridis, P. Oustadakis, and S. Agatzini-Leonardou, Aluminium recovery during black dross hydrothermal treatment, *Journal of Environmental Chemical Engineering*, vol. 1, 23-32, 2013.
- [3] L. Fillali, Síntesis y caracterización microestructural de alúminas obtenidas a partir de un precursor no convencional, Tesis doctoral, Universidad Complutense de Madrid, 2015.
- [4] A. López-Delgado and H. Tayibi, Can hazardous waste become a raw material? the case study of an aluminium residue: A review, *Waste Management and Research*, vol. 30, 474-484, 2012.
- [5] *The Aluminum Association. Secondary Production.* Available: <http://www.aluminum.org/industries/production/secondary-production>
- [6] R. Galindo, I. Padilla, R. Sánchez-Hernández, J. I. Robla, G. Monrós, and A. López-Delgado, Production of added-value materials from a hazardous waste in the aluminium tertiary industry: Synergistic effect between hydrotalcites and glasses, *Journal of Environmental Chemical Engineering*, vol. 3, 2552-2559, 2015.
- [7] B. R. Das, B. Dash, B. C. Tripathy, I. N. Bhattacharya, and S. C. Das, Production of η -alumina from waste aluminium dross, *Minerals Engineering*, vol. 20, 252-258, 2007.
- [8] R. Galindo, I. Padilla, O. Rodríguez, R. Sánchez-Hernández, S. López-Andrés, and A. López-Delgado, Characterization of solid wastes from aluminum tertiary sector: The current state of Spanish industry, *Journal of Minerals and Materials Characterization and Engineering*, vol. 3, 55, 2015.
- [9] Directive 2008/98/EC of the European Parliament and of the Council of 19 November 2008 on waste and repealing certain Directives, *Official Journal of the European Union*, vol. L 312, 3-30, 2008.
- [10] European Waste Catalogue and Hazardous Waste List, *Environmental Protection Agency*, 2002.
- [11] *PRTR-España. Registro Estatal de Emisiones y Fuentes Contaminantes.* Available: <http://www.en.prtr-es.es>
- [12] H. Tayibi, Tratamiento de los polvos procedentes de la Metalurgia Secundaria del Aluminio, Tesis doctoral, Universidad Complutense de Madrid, 2004.
- [13] R. Galindo, A. López-Delgado, I. Padilla, and M. Yates, Synthesis and characterisation of hydrotalcites produced by an aluminium hazardous waste: A comparison between the use of ammonia and the use of triethanolamine, *Applied Clay Science*, vol. 115, 115-123, 2015.
- [14] R. Galindo, A. López-Delgado, I. Padilla, and M. Yates, Hydrotalcite-like compounds: A way to recover a hazardous waste in the aluminium tertiary industry, *Applied Clay Science*, vol. 95, 41-49, 2014.
- [15] A. López-Delgado, L. Fillali, J. Jiménez, and S. López-Andrés, Synthesis of α -alumina from a less common raw material, *Journal of Sol-Gel Science and Technology*, vol. 64, 162-169, 2012.
- [16] R. Sánchez-Hernández, A. López-Delgado, I. Padilla, R. Galindo, and S. López-Andrés, One-step synthesis of NaP1, SOD and ANA from a hazardous aluminum solid waste, *Microporous and Mesoporous Materials*, vol. 226, 267-277, 2016.

5. REFERENCES

- [17] R. Sánchez-Hernández, I. Padilla, S. López-Andrés, and A. López-Delgado, Eco-friendly bench-scale zeolitization of an Al-containing waste into gismondine-type zeolite under effluent recycling, *Journal of Cleaner Production*, vol. 161, 792-802, 2017.
- [18] A. F. Cronstedt, *Rön och beskrifning om en obekant bärg art, som kallas Zeolites* vol. 17:120. Svenska Vetenskaps akademiens. Handlingar, Stockholm, 1756.
- [19] X. Querol, N. Moreno, J. C. Urea, A. Alastuey, E. Hernández, A. López-Soler, and F. Plana, Synthesis of zeolites from coal fly ash: an overview, *International Journal of Coal Geology*, vol. 50, 413-423, 2002.
- [20] *International Zeolite Association (IZA)*. Available: <http://www.iza-structure.org/databases/>
- [21] S. Kulprathipanja, *Zeolites in industrial separation and catalysis*. John Wiley & Sons, 2010.
- [22] R. Xu, W. Pang, J. Yu, Q. Huo, and J. Chen, *Chemistry of zeolites and related porous materials: synthesis and structure*. John Wiley & Sons, Ltd, 2009.
- [23] R. M. Barrer, Zeolites and their synthesis, *Zeolites*, vol. 1, 130-140, 1981.
- [24] D. W. Breck, "Recent advances in zeolite science," in *Molecular sieve zeolites-I*. vol. 101, ed American Chemical Society, 1974, 1-19.
- [25] C. S. Cundy and P. A. Cox, The hydrothermal synthesis of zeolites: Precursors, intermediates and reaction mechanism, *Microporous and Mesoporous Materials*, vol. 82, 1-78, 2005.
- [26] N. M. Palmerola, Valorización de cenizas volantes para la síntesis de zeolitas mediante extracción de sílice y conversión directa. Aplicaciones ambientales, Tesis doctoral, Universitat Politècnica de Catalunya, 2002.
- [27] S. Shirani Lapari, Z. Ramli, and S. Triwahyono, Effect of different templates on the synthesis of mesoporous sodalite, *Journal of Chemistry*, vol. 2015, 6, 2015.
- [28] M. A. Cambor and J. Pérez-Pariente, Crystallization of zeolite beta: Effect of Na and K ions, *Zeolites*, vol. 11, 202-210, 1991.
- [29] C. Liu, W. Gu, D. Kong, and H. Guo, The significant effects of the alkali-metal cations on ZSM-5 zeolite synthesis: From mechanism to morphology, *Microporous and Mesoporous Materials*, vol. 183, 30-36, 2014.
- [30] X. Querol, F. Plana, A. Alastuey, J. L. Fernández Turiel, and A. López Soler, "Synthesis of industrial minerals from fly ash," in *Coal Science and Technology*. vol. 24, J. A. Pajares and J. M. D. Tascón, Eds., ed: Elsevier, 1995, 1979-1982.
- [31] L. A. Villaescusa, W. Zhou, R. E. Morris, and P. A. Barrett, Synthesis, characterization and control of faulting in STF/SFF topologies, a new family of intergrowth zeolites, *Journal of Materials Chemistry*, vol. 14, 1982-1987, 2004.
- [32] M. Fawer, D. Postlethwaite, and H.-J. Klüppel, Life cycle inventory for the production of zeolite a for detergents, *The International Journal of Life Cycle Assessment*, vol. 3, 71-74, 1998.
- [33] A. Shoumkova and V. Stoyanova, Zeolites formation by hydrothermal alkali activation of coal fly ash from thermal power station "Maritsa 3", Bulgaria, *Fuel*, vol. 103, 533-541, 2013.
- [34] M. Chareonpanich, O. Jullaphan, and C. Tang, Bench-scale synthesis of zeolite A from subbituminous coal ashes with high crystalline silica content, *Journal of Cleaner Production*, vol. 19, 58-63, 2011.

- [35] Y. W. Chiang, K. Ghyselbrecht, R. M. Santos, B. Meesschaert, and J. A. Martens, Synthesis of zeolitic-type adsorbent material from municipal solid waste incinerator bottom ash and its application in heavy metal adsorption, *Catalysis Today*, vol. 190, 23-30, 2012.
- [36] A. Y. Atta, B. Y. Jibril, B. O. Aderemi, and S. S. Adefila, Preparation of analcime from local kaolin and rice husk ash, *Applied Clay Science*, vol. 61, 8-13, 2012.
- [37] O. Gencel, M. Sutcu, E. Erdogmus, V. Koc, V. V. Cay, and M. S. Gok, Properties of bricks with waste ferrochromium slag and zeolite, *Journal of Cleaner Production*, vol. 59, 111-119, 2013.
- [38] C. Barca, D. Meyer, M. Liira, P. Drissen, Y. Comeau, Y. Andrès, and F. Chazarenc, Steel slag filters to upgrade phosphorus removal in small wastewater treatment plants: Removal mechanisms and performance, *Ecological Engineering*, vol. 68, 214-222, 2014.
- [39] N. Murayama, N. Okajima, S. Yamaoka, H. Yamamoto, and J. Shibata, Hydrothermal synthesis of $AlPO_4-5$ type zeolitic materials by using aluminum dross as a raw material, *Journal of the European Ceramic Society*, vol. 26, 459-462, 2006.
- [40] M. Sandoval, J. Henao, C. A. Rios, C. D. Williams, and D. C. Apperley, Synthesis and characterization of zeotype ANA framework by hydrothermal reaction of natural clinker, *Fuel*, vol. 88, 272-281, 2009.
- [41] H. Höller and U. Wirsching, Zeolite formation from fly-ash, *Fortschritte der mineralogie*, vol. 63, 21-43, 1985.
- [42] X. Querol, J. C. Umaña, F. Plana, A. Alastuey, A. Lopez-Soler, A. Medinaceli, A. Valero, M. J. Domingo, and E. Garcia-Rojo, Synthesis of zeolites from fly ash at pilot plant scale. Examples of potential applications, *Fuel*, vol. 80, 857-865, 2001.
- [43] J. C. U. Peña, Síntesis de zeolitas a partir de cenizas volantes de centrales termoeléctricas de carbón, Tesis doctoral, Universitat Politècnica de Catalunya, 2002.
- [44] W. Franus, M. Wdowin, and M. Franus, Synthesis and characterization of zeolites prepared from industrial fly ash, *Environmental Monitoring and Assessment*, vol. 186, 5721-5729, 2014.
- [45] S. Bohra, D. Kundu, and M. K. Naskar, One-pot synthesis of NaA and NaP zeolite powders using agro-waste material and other low cost organic-free precursors, *Ceramics International*, vol. 40, 1229-1234, 2014.
- [46] H. Kazemian, Z. Naghdali, T. Ghaffari Kashani, and F. Farhadi, Conversion of high silicon fly ash to Na-P1 zeolite: Alkaline fusion followed by hydrothermal crystallization, *Advanced Powder Technology*, vol. 21, 279-283, 2010.
- [47] C. Li, H. Zhong, S. Wang, J. Xue, and Z. Zhang, Removal of basic dye (methylene blue) from aqueous solution using zeolite synthesized from electrolytic manganese residue, *Journal of Industrial and Engineering Chemistry*, vol. 23, 344-352, 2015.
- [48] X. Xu, Y. Bao, C. Song, W. Yang, J. Liu, and L. Lin, Microwave-assisted hydrothermal synthesis of hydroxy-sodalite zeolite membrane, *Microporous and Mesoporous Materials*, vol. 75, 173-181, 2004.
- [49] M. Sathupunya, E. Gulari, and S. Wongkasemjit, ANA and GIS zeolite synthesis directly from alumatrane and silatrane by sol-gel process and microwave technique, *Journal of the European Ceramic Society*, vol. 22, 2305-2314, 2002.
- [50] P. Pal, J. K. Das, N. Das, and S. Bandyopadhyay, Synthesis of NaP zeolite at room temperature and short crystallization time by sonochemical method, *Ultrasonics Sonochemistry*, vol. 20, 314-321, 2013.

5. REFERENCES

- [51] G. G. Hollman, G. Steenbruggen, and M. Janssen-Jurkovičová, A two-step process for the synthesis of zeolites from coal fly ash, *Fuel*, vol. 78, 1225-1230, 1999.
- [52] H. Deng and Y. Ge, Formation of NaP zeolite from fused fly ash for the removal of Cu (II) by an improved hydrothermal method, *RSC Advances*, vol. 5, 9180-9188, 2015.
- [53] K. P. Dey, S. Ghosh, and M. K. Naskar, A facile synthesis of ZSM-11 zeolite particles using rice husk ash as silica source, *Materials Letters*, vol. 87, 87-89, 2012.
- [54] I. Othman Ali, A. M. Hassan, S. M. Shaaban, and K. S. Soliman, Synthesis and characterization of ZSM-5 zeolite from rice husk ash and their adsorption of Pb²⁺ onto unmodified and surfactant-modified zeolite, *Separation and Purification Technology*, vol. 83, 38-44, 2011.
- [55] R. d. A. Bessa, L. d. S. Costa, C. P. Oliveira, F. Bohn, R. F. do Nascimento, J. M. Sasaki, and A. R. Loiola, Kaolin-based magnetic zeolites A and P as water softeners, *Microporous and Mesoporous Materials*, vol. 245, 64-72, 2017.
- [56] J. Dufour, A. L. Iglesia, V. González, and J. C. Ruiz-Sierra, Viability of the use of pickling baths from aluminium surface treatment for synthesizing low Si/Al zeolites, *Journal of Environmental Science and Health . Part A: Environmental Science and Engineering and Toxicology*, vol. 32, 1807-1825, 1997.
- [57] J. Dufour, V. González, and A. La Iglesia, Optimization of 4A zeolite synthesis as recovery of wastes from aluminum finishing, *Journal of Environmental Science and Health, Part A*, vol. 36, 1257-1269, 2001.
- [58] C. Belviso, E. Agostinelli, S. Belviso, F. Cavalcante, S. Pascucci, D. Peddis, G. Varvaro, and S. Fiore, Synthesis of magnetic zeolite at low temperature using a waste material mixture: Fly ash and red mud, *Microporous and Mesoporous Materials*, vol. 202, 208-216, 2015.
- [59] A. M. Cardoso, A. Paprocki, L. S. Ferret, C. M. N. Azevedo, and M. Pires, Synthesis of zeolite Na-P1 under mild conditions using Brazilian coal fly ash and its application in wastewater treatment, *Fuel*, vol. 139, 59-67, 2015.
- [60] C. Liu, X. Gao, Y. Ma, Z. Pan, and R. Tang, Study on the mechanism of zeolite Y formation in the process of liquor recycling, *Microporous and Mesoporous Materials*, vol. 25, 1-6, 1998.
- [61] N. Keser Demir, B. Topuz, L. Yilmaz, and H. Kalipcilar, Synthesis of ZIF-8 from recycled mother liquors, *Microporous and Mesoporous Materials*, vol. 198, 291-300, 2014.
- [62] J. Xie, Z. Wang, D. Wu, Z. Zhang, and H. Kong, Synthesis of zeolite/aluminum oxide hydrate from coal fly ash: A new type of adsorbent for simultaneous removal of cationic and anionic pollutants, *Industrial & Engineering Chemistry Research*, vol. 52, 14890-14897, 2013.
- [63] G. Lin, Q. Zhuang, Q. Cui, H. Wang, and H. Yao, Synthesis and adsorption property of zeolite FAU/LTA from lithium slag with utilization of mother liquid, *Chinese Journal of Chemical Engineering*, vol. 23, 1768-1773, 2015.
- [64] J. Behin, S. S. Bukhari, H. Kazemian, and S. Rohani, Developing a zero liquid discharge process for zeolitization of coal fly ash to synthetic NaP zeolite, *Fuel*, vol. 171, 195-202, 2016.
- [65] M. R. Gonzalez, A. M. Pereyra, R. Zerbino, and E. I. Basaldella, Removal and cementitious immobilization of heavy metals: chromium capture by zeolite-hybridized materials obtained from spent fluid cracking catalysts, *Journal of Cleaner Production*, vol. 91, 187-190, 2015.
- [66] M. Maretto, F. Bianchi, R. Vignola, S. Canepari, M. Baric, R. Iazzoni, M. Tagliabue, and M. P. Papini, Microporous and mesoporous materials for the treatment of wastewater produced by petrochemical activities, *Journal of Cleaner Production*, vol. 77, 22-34, 2014.

- [67] V. K. Gupta and I. Ali, "Chapter 2-Water treatment for inorganic pollutants by adsorption technology," in *Environmental Water*, ed: Elsevier, 2013, 29-91.
- [68] M. Mazur, P. S. Wheatley, M. Navarro, W. J. Roth, M. Položij, A. Mayoral, P. Eliášová, P. Nachtigall, J. Čejka, and R. E. Morris, Synthesis of 'unfeasible' zeolites, *Nature Chemistry*, vol. 8, 58-62, 2016.
- [69] B. Yilmaz, N. Trukhan, and U. Müller, Industrial outlook on zeolites and metal organic frameworks, *Chinese Journal of Catalysis*, vol. 33, 3-10, 2012.
- [70] M. Moliner, C. Martínez, and A. Corma, Synthesis strategies for preparing useful small pore zeolites and zeotypes for gas separations and catalysis, *Chemistry of Materials*, vol. 26, 246-258, 2013.
- [71] M. S. Nabavi, T. Mohammadi, and M. Kazemimoghadam, Hydrothermal synthesis of hydroxy sodalite zeolite membrane: Separation of H₂/CH₄, *Ceramics International*, vol. 40, 5889-5896, 2014.
- [72] S. Zougar, K. Morakchi, A. Zazoua, S. Saad, R. Kherrat, and N. Jaffrezic-Renault, Characterization of ammonium ion-sensitive membranes in solution with electrochemical impedance spectroscopy, *Materials Science and Engineering C*, vol. 28, 1020-1023, 2008.
- [73] A. Hauer and F. Fischer, Open adsorption system for an energy efficient dishwasher, *Chemie Ingenieur Technik*, vol. 83, 61-66, 2011.
- [74] T. Nonnen, S. Beckert, K. Gleichmann, A. Brandt, B. Unger, H. Kerskes, B. Mette, S. Bonk, T. Badenhop, F. Salg, and R. Gläser, A thermochemical long-term heat storage system based on a salt/zeolite composite, *Chemical Engineering & Technology*, vol. 39, 2427-2434, 2016.
- [75] M. Ferrante, G. O. Conti, Z. Rasic-Milutinovic, and D. Jovanovic, *Health effects of metals and related substances in drinking water*. IWA Publishing, 2013.
- [76] Minamata Convention on Mercury: text and annexes, *United Nations Environment Programme, Geneva, Switzerland*, 2013.
- [77] K. Tanong, L. Coudert, G. Mercier, and J.-F. Blais, Recovery of metals from a mixture of various spent batteries by a hydrometallurgical process, *Journal of Environmental Management*, vol. 181, 95-107, 2016.
- [78] Directive 2013/39/EU of the European parliament and of the council of 12 August 2013 amending Directives 2000/60/EC and 2008/105/EC as regards priority substances in the field of water policy, *Official Journal of the European Union*, vol. L 226, 1-17, 2013.
- [79] J. K. Böhlke, R. L. Smith, and D. N. Miller, Ammonium transport and reaction in contaminated groundwater: Application of isotope tracers and isotope fractionation studies, *Water Resources Research*, vol. 42, 2006.
- [80] A. Casadellà, P. Kuntke, O. Schaetzle, and K. Loos, Clinoptilolite-based mixed matrix membranes for the selective recovery of potassium and ammonium, *Water Research*, vol. 90, 62-70, 2016.
- [81] A. Urriaga, I. Ortiz, A. Anglada, D. Mantzavinos, and E. Diamadopoulos, Kinetic modeling of the electrochemical removal of ammonium and COD from landfill leachates, *Journal of Applied Electrochemistry*, vol. 42, 779-786, 2012.
- [82] M. Sica, A. Duta, C. Teodosiu, and C. Draghici, Thermodynamic and kinetic study on ammonium removal from a synthetic water solution using ion exchange resin, *Clean Technologies and Environmental Policy*, vol. 16, 351-359, 2014.

5. REFERENCES

- [83] L. Megido, B. Suárez-Peña, L. Negral, L. Castrillón, S. Suárez, Y. Fernández-Nava, and E. Marañón, Relationship between physico-chemical characteristics and potential toxicity of PM10, *Chemosphere*, vol. 162, 73-79, 2016.
- [84] Real Decreto 817/2015, de 11 de septiembre, por el que se establecen los criterios de seguimiento y evaluación del estado de las aguas superficiales y las normas de calidad ambiental, *Boletín oficial del estado (BOE)*, vol. 219, 80582-80677, 2015.
- [85] T. M. Vu, V. T. Trinh, D. P. Doan, H. T. Van, T. V. Nguyen, S. Vigneswaran, and H. H. Ngo, Removing ammonium from water using modified corncob-biochar, *Science of the Total Environment*, vol. 579, 612-619, 2017.
- [86] P. B. Moraes and R. Bertazzoli, Electrodegradation of landfill leachate in a flow electrochemical reactor, *Chemosphere*, vol. 58, 41-46, 2005.
- [87] J.-F. Blais, Z. Djedidi, R. Cheikh, R. D. Tyagi, and G. Mercier, Metals precipitation from effluents: Review, *Practice Periodical of Hazardous, Toxic, and Radioactive Waste Management*, vol. 12, 135-149, 2008.
- [88] J. Perić, M. Trgo, and N. Vukojević Medvidović, Removal of zinc, copper and lead by natural zeolite-a comparison of adsorption isotherms, *Water Research*, vol. 38, 1893-1899, 2004.
- [89] S. Esplugas, J. Giménez, S. Contreras, E. Pascual, and M. Rodríguez, Comparison of different advanced oxidation processes for phenol degradation, *Water Research*, vol. 36, 1034-1042, 2002.
- [90] P.-S. Keng, S.-L. Lee, S.-T. Ha, Y.-T. Hung, and S.-T. Ong, Removal of hazardous heavy metals from aqueous environment by low-cost adsorption materials, *Environmental Chemistry Letters*, vol. 12, 15-25, 2014.
- [91] N. Moreno, X. Querol, C. Ayora, C. F. Pereira, and M. Janssen-Jurkovicová, Utilization of zeolites synthesized from coal fly ash for the purification of acid mine waters, *Environmental Science and Technology*, vol. 35, 3526-3534, 2001.
- [92] T. A. Kurniawan, G. Y. S. Chan, W.-H. Lo, and S. Babel, Physico-chemical treatment techniques for wastewater laden with heavy metals, *Chemical Engineering Journal*, vol. 118, 83-98, 2006.
- [93] V. K. Gupta, I. Ali, T. A. Saleh, A. Nayak, and S. Agarwal, Chemical treatment technologies for waste-water recycling-an overview, *RSC Advances*, vol. 2, 6380-6388, 2012.
- [94] J. D. Seader, E. J. Henley, and D. K. Roper, *Separation process principles*. Wiley, 1998.
- [95] W. J. Weber and E. H. Smith, Simulation and design models for adsorption processes, *Environmental Science and Technology*, vol. 21, 1040-1050, 1987.
- [96] H. N. Tran, S.-J. You, A. Hosseini-Bandegharaei, and H.-P. Chao, Mistakes and inconsistencies regarding adsorption of contaminants from aqueous solutions: A critical review, *Water Research*, vol. 120, 88-116, 2017.
- [97] P. S. Lawson, R. M. Sterritt, and J. N. Lester, Adsorption and complexation mechanisms of heavy metal uptake in activated sludge, *Journal of Chemical Technology and Biotechnology*, vol. 34, 253-262, 1984.
- [98] M. Ahmad, A. U. Rajapaksha, J. E. Lim, M. Zhang, N. Bolan, D. Mohan, M. Vithanage, S. S. Lee, and Y. S. Ok, Biochar as a sorbent for contaminant management in soil and water: A review, *Chemosphere*, vol. 99, 19-33, 2014.

- [99] S. Sen Gupta and K. G. Bhattacharyya, Adsorption of metal ions by clays and inorganic solids, *RSC Advances*, vol. 4, 28537-28586, 2014.
- [100] N. Koshy and D. N. Singh, Fly ash zeolites for water treatment applications, *Journal of Environmental Chemical Engineering*, vol. 4, 1460-1472, 2016.
- [101] M. Attari, S. S. Bukhari, H. Kazemian, and S. Rohani, A low-cost adsorbent from coal fly ash for mercury removal from industrial wastewater, *Journal of Environmental Chemical Engineering*, vol. 5, 391-399, 2017.
- [102] W. Qiu and Y. Zheng, Removal of lead, copper, nickel, cobalt, and zinc from water by a cancrinite-type zeolite synthesized from fly ash, *Chemical Engineering Journal*, vol. 145, 483-488, 2009.
- [103] R. Leyva-Ramos, J. E. Monsivais-Rocha, A. Aragon-Piña, M. S. Berber-Mendoza, R. M. Guerrero-Coronado, P. Alonso-Davila, and J. Mendoza-Barron, Removal of ammonium from aqueous solution by ion exchange on natural and modified chabazite, *Journal of Environmental Management*, vol. 91, 2662-2668, 2010.
- [104] T. H. Martins, T. S. O. Souza, and E. Foresti, Ammonium removal from landfill leachate by clinoptilolite adsorption followed by bioregeneration, *Journal of Environmental Chemical Engineering*, vol. 5, 63-68, 2017.
- [105] X. You, C. Valderrama, and J. L. Cortina, Simultaneous recovery of ammonium and phosphate from simulated treated wastewater effluents by activated calcium and magnesium zeolites, *Journal of Chemical Technology and Biotechnology*, 2017.
- [106] D. Guaya, C. Valderrama, A. Farran, C. Armijos, and J. L. Cortina, Simultaneous phosphate and ammonium removal from aqueous solution by a hydrated aluminum oxide modified natural zeolite, *Chemical Engineering Journal*, vol. 271, 204-213, 2015.
- [107] Y. Zhou, S. Xia, J. Zhang, B. T. Nguyen, and Z. Zhang, Insight into the influences of pH value on Pb(II) removal by the biopolymer extracted from activated sludge, *Chemical Engineering Journal*, vol. 308, 1098-1104, 2017.
- [108] Z. Jiang, J. Yang, H. Ma, X. Ma, and J. Yuan, Synthesis of pure NaA zeolites from coal fly ashes for ammonium removal from aqueous solutions, *Clean Technologies and Environmental Policy*, vol. 18, 629-637, 2016.
- [109] M. Zhang, H. Zhang, D. Xu, L. Han, D. Niu, B. Tian, J. Zhang, L. Zhang, and W. Wu, Removal of ammonium from aqueous solutions using zeolite synthesized from fly ash by a fusion method, *Desalination*, vol. 271, 111-121, 2011.
- [110] R. Apiratikul and P. Pavasant, Sorption of Cu^{2+} , Cd^{2+} , and Pb^{2+} using modified zeolite from coal fly ash, *Chemical Engineering Journal*, vol. 144, 245-258, 2008.
- [111] Y. J. O. Asencios and M. R. Sun-Kou, Synthesis of high-surface-area $\gamma\text{-Al}_2\text{O}_3$ from aluminum scrap and its use for the adsorption of metals: Pb (II), Cd (II) and Zn (II), *Applied Surface Science*, vol. 258, 10002-10011, 2012.
- [112] Y. Zhou, S. Xia, J. Zhang, Z. Zhang, and S. W. Hermanowicz, Adsorption characterizations of biosorbent extracted from waste activated sludge for Pb (II) and Zn (II), *Desalination and Water Treatment*, vol. 57, 9343-9353, 2016.
- [113] P. Scherrer, Estimation of the size and internal structure of colloidal particles by means of röntgen, *Nachrichten von der Gesellschaft der Wissenschaften zu Göttingen*, vol. 2, 96-100, 1918.

5. REFERENCES

- [114] F. Chung, Quantitative interpretation of X-ray diffraction patterns of mixtures. I. Matrix-flushing method for quantitative multicomponent analysis, *Journal of Applied Crystallography*, vol. 7, 519-525, 1974.
- [115] F. Chung, Quantitative interpretation of X-ray diffraction patterns of mixtures. II. Adiabatic principle of X-ray diffraction analysis of mixtures, *Journal of Applied Crystallography*, vol. 7, 526-531, 1974.
- [116] C. R. Hubbard, E. H. Evans, and D. K. Smith, The reference intensity ratio, I/I_c , for computer simulated powder patterns, *Journal of Applied Crystallography*, vol. 9, 169-174, 1976.
- [117] *Test Method 1311: Toxicity Characteristic Leaching Procedure (TCLP)*, United States Environmental Protection Agency (EPA) 1311, 1992.
- [118] *Light scattering. Laser diffraction (LD). Malvern Panalytical*. Available: <https://www.malvernpanalytical.com/en/products/technology/light-scattering/laser-diffraction>
- [119] K. S. W. Sing, "Reporting physisorption data for gas/solid systems with special reference to the determination of surface area and porosity (Recommendations 1984)," in *Pure and Applied Chemistry* vol. 57, ed, 1985, 603.
- [120] J. C. Groen, L. A. A. Peffer, and J. Pérez-Ramírez, Pore size determination in modified micro- and mesoporous materials. Pitfalls and limitations in gas adsorption data analysis, *Microporous and Mesoporous Materials*, vol. 60, 1-17, 2003.
- [121] M. Thommes, K. Kaneko, V. Neimark Alexander, P. Olivier James, F. Rodriguez-Reinoso, J. Rouquerol, and S. W. Sing Kenneth, "Physisorption of gases, with special reference to the evaluation of surface area and pore size distribution (IUPAC Technical Report)," in *Pure and Applied Chemistry* vol. 87, ed, 2015, 1051.
- [122] S. Brunauer, P. H. Emmett, and E. Teller, Adsorption of gases in multimolecular layers, *Journal of the American Chemical Society*, vol. 60, 309-319, 1938.
- [123] W. D. Harkins and G. Jura, Surfaces of solids. XIII. A vapor adsorption method for the determination of the area of a solid without the assumption of a molecular area, and the areas occupied by nitrogen and other molecules on the surface of a solid, *Journal of the American Chemical Society*, vol. 66, 1366-1373, 1944.
- [124] E. P. Barrett, L. G. Joyner, and P. P. Halenda, The determination of pore volume and area distributions in porous substances. I. Computations from nitrogen isotherms, *Journal of the American Chemical Society*, vol. 73, 373-380, 1951.
- [125] *Norma Cubana. Zeolitas naturales- Determinación de la capacidad de intercambio catiónico total - Método del cloruro de amonio*, NC 626: 2008, 2008.
- [126] G. Gillies, R. Raj, F.-D. Kopinke, and A. Georgi, Suspension stability and mobility of Trap-Ox Fe-zeolites for in-situ nanoremediation, *Journal of Colloid and Interface Science*, vol. 501, 311-320, 2017.
- [127] O. Larlus, S. Mintova, and T. Bein, Environmental syntheses of nanosized zeolites with high yield and monomodal particle size distribution, *Microporous and Mesoporous Materials*, vol. 96, 405-412, 2006.
- [128] S. Vallar, D. Houivet, J. El Fallah, D. Kervadec, and J. M. Haussonne, Oxide slurries stability and powders dispersion: optimization with zeta potential and rheological measurements, *Journal of the European Ceramic Society*, vol. 19, 1017-1021, 1999.

- [129] S. Y. Lagergren, Zur Theorie der sogenannten Adsorption gelöster Stoffe, *Kungliga Svenska Vetenskapsakademiens Handlingar*, vol. 24, 1-39, 1898.
- [130] G. Blanchard, M. Maunaye, and G. Martin, Removal of heavy metals from waters by means of natural zeolites, *Water Research*, vol. 18, 1501-1507, 1984.
- [131] W. J. Weber and J. C. Morris, Kinetics of adsorption on carbon from solution, *Journal of the Sanitary Engineering Division*, vol. 89, 31-60, 1963.
- [132] I. Langmuir, The adsorption of gases on plane surfaces of glass, mica and platinum, *Journal of the American Chemical Society*, vol. 40, 1361-1403, 1918.
- [133] H. M. F. Freundlich, Over the adsorption in solution, *The Journal of Physical Chemistry*, vol. 57, 385-471, 1906.
- [134] M. Dubinin and L. Radushkevich, Equation of the characteristic curve of activated charcoal, *Proceedings of the Academy of Sciences, Physical Chemistry Section. USSR, Section 55*, vol. 331-333, 875-890, 1947.
- [135] M. Temkin and V. Pyzhev, Kinetics of ammonia synthesis on promoted iron catalysts, *Acta Physicochimica. URSS*, vol. 12, 217-222, 1940.
- [136] R. Sips, On the structure of a catalyst surface, *Journal of Chemical Physics*, vol. 16, 490-495, 1948.
- [137] J. Toth, State equations of the solid-gas interface layers, *Acta chimica Academiae Scientiarum Hungaricae*, vol. 69, 311-328, 1971.
- [138] O. Redlich and D. L. Peterson, A useful adsorption isotherm, *Journal of Physical Chemistry*, vol. 63, 1024-1024, 1959.
- [139] K. Y. Foo and B. H. Hameed, Insights into the modeling of adsorption isotherm systems, *Chemical Engineering Journal*, vol. 156, 2-10, 2010.
- [140] M. Uğurlu and M. H. Karaoğlu, Adsorption of ammonium from an aqueous solution by fly ash and sepiolite: Isotherm, kinetic and thermodynamic analysis, *Microporous and Mesoporous Materials*, vol. 139, 173-178, 2011.
- [141] G. F. Malash and M. I. El-Khaiary, Piecewise linear regression: A statistical method for the analysis of experimental adsorption data by the intraparticle-diffusion models, *Chemical Engineering Journal*, vol. 163, 256-263, 2010.
- [142] K. R. Hall, L. C. Eagleton, A. Acrivos, and T. Vermeulen, Pore- and solid-diffusion kinetics in fixed-bed adsorption under constant-pattern conditions, *Industrial & Engineering Chemistry Fundamentals*, vol. 5, 212-223, 1966.
- [143] É. C. Lima, M. A. Adebayo, and F. M. Machado, "Kinetic and equilibrium models of adsorption," in *Carbon nanomaterials as adsorbents for environmental and biological applications*, ed: Springer 2015, 33-69.
- [144] T. Luukkonen, M. Sarkkinen, K. Kemppainen, J. Rämö, and U. Lassi, Metakaolin geopolymer characterization and application for ammonium removal from model solutions and landfill leachate, *Applied Clay Science*, vol. 119, Part 2, 266-276, 2016.
- [145] A. Gil and S. A. Korili, Management and valorization of aluminum saline slags: Current status and future trends, *Chemical Engineering Journal*, vol. 289, 74-84, 2016.

5. REFERENCES

- [146] P. E. Tsakiridis, Aluminium salt slag characterization and utilization-A review, *Journal of Hazardous materials*, vol. 217–218, 1-10, 2012.
- [147] A. Gil, Management of the salt cake from secondary aluminum fusion processes, *Industrial & Engineering Chemistry Research*, vol. 44, 8852-8857, 2005.
- [148] J. Marshall, PM 2.5, *Proceedings of the National Academy of Sciences*, vol. 110, 8756-8756, 2013.
- [149] M. Izquierdo and X. Querol, Leaching behaviour of elements from coal combustion fly ash: An overview, *International Journal of Coal Geology*, vol. 94, 54-66, 2012.
- [150] W. M. Gitari, O. O. Fatoba, L. F. Petrik, and V. R. K. Vadapalli, Leaching characteristics of selected South African fly ashes: Effect of pH on the release of major and trace species, *Journal of Environmental Science and Health, Part A*, vol. 44, 206-220, 2009.
- [151] A. López-Delgado, I. Padilla, R. Sánchez-Hernández, O. Rodríguez, and S. López-Andrés, Procedimiento de revalorización de un residuo procedente de la molienda de escorias de aluminio, Patente N° ES2617037, 15 Junio 2015.
- [152] J. L. Casci, Zeolite molecular sieves: preparation and scale-up, *Microporous and Mesoporous Materials*, vol. 82, 217-226, 2005.
- [153] M. M. J. Treacy and J. B. Higgins, "GIS - Na-P1," in *Collection of simulated XRD powder patterns for zeolites (fifth edition)*, ed Amsterdam: Elsevier Science B.V., 2007, 194-195.
- [154] P. Sharma, J.-g. Yeo, M. H. Han, and C. H. Cho, Knobby surfaced, mesoporous, single-phase GIS-NaP1 zeolite microsphere synthesis and characterization for H₂ gas adsorption, *Journal of Materials Chemistry A*, vol. 1, 2602-2612, 2013.
- [155] N. Murayama, H. Yamamoto, and J. Shibata, Mechanism of zeolite synthesis from coal fly ash by alkali hydrothermal reaction, *International Journal of Mineral Processing*, vol. 64, 1-17, 2002.
- [156] C.-F. Wang, J.-S. Li, L.-J. Wang, and X.-Y. Sun, Influence of NaOH concentrations on synthesis of pure-form zeolite A from fly ash using two-stage method, *Journal of Hazardous materials*, vol. 155, 58-64, 2008.
- [157] S. H. Park, C. B. Chung, and G. Seo, Preparation of small analcime particles with narrow size distributions from acid-treated larger analcime particles, *Microporous and Mesoporous Materials*, vol. 155, 201-207, 2012.
- [158] H.-L. Zubowa, H. Kosslick, D. Müller, M. Richter, L. Wilde, and R. Fricke, Crystallization of phase-pure zeolite NaP from MCM-22-type gel compositions under microwave radiation, *Microporous and Mesoporous Materials*, vol. 109, 542-548, 2008.
- [159] Z. Huo, X. Xu, Z. Lü, J. Song, M. He, Z. Li, Q. Wang, and L. Yan, Synthesis of zeolite NaP with controllable morphologies, *Microporous and Mesoporous Materials*, vol. 158, 137-140, 2012.
- [160] A. Baccouche, E. Srasra, and M. El Maaoui, Preparation of Na-P1 and sodalite octahydrate zeolites from interstratified illite-smectite, *Applied Clay Science*, vol. 13, 255-273, 1998.
- [161] Y. Huang, J. Yao, X. Zhang, C. Kong, H. Chen, D. Liu, M. Tsapatsis, M. R. Hill, A. J. Hill, and H. Wang, Role of ethanol in sodalite crystallization in an ethanol-Na₂O-Al₂O₃-SiO₂-H₂O system, *CrystEngComm*, vol. 13, 4714-4722, 2011.
- [162] H. Ghobarkar and O. Schäf, Effect of temperature on hydrothermal synthesis of analcime and viséite, *Materials Science and Engineering: B*, vol. 60, 163-167, 1999.

- [163] X. Ma, J. Yang, H. Ma, C. Liu, and P. Zhang, Synthesis and characterization of analcime using quartz syenite powder by alkali-hydrothermal treatment, *Microporous and Mesoporous Materials*, vol. 201, 134-140, 2015.
- [164] P. Plessis, T. Ojumu, and L. Petrik, Waste minimization protocols for the process of synthesizing zeolites from South African coal fly ash, *Materials*, vol. 6, 1688-1703, 2013.
- [165] C. Li and Z. Wu, Microporous materials characterized by vibrational spectroscopies, *Handbook of zeolite science and technology*, 423-513, 2003.
- [166] A. Chaisena and K. Rangsiwatananon, Synthesis of sodium zeolites from natural and modified diatomite, *Materials Letters*, vol. 59, 1474-1479, 2005.
- [167] M. Król, W. Mozgawa, J. Morawska, and W. Pichór, Spectroscopic investigation of hydrothermally synthesized zeolites from expanded perlite, *Microporous and Mesoporous Materials*, vol. 196, 216-222, 2014.
- [168] C. Grader and J.-C. Buhl, The intermediate phase between sodalite and cancrinite: Synthesis of nano-crystals in the presence of $\text{Na}_2\text{CO}_3/\text{TEA}$ and its thermal- and hydrothermal stability, *Microporous and Mesoporous Materials*, vol. 171, 110-117, 2013.
- [169] C. Günther, H. Richter, I. Voigt, A. Michaelis, H. Tzscheuschler, R. Krause-Rehberg, and J. M. Serra, Synthesis and characterization of a sulfur containing hydroxy sodalite without sulfur radicals, *Microporous and Mesoporous Materials*, vol. 214, 1-7, 2015.
- [170] E. R. Vance, D. J. Gregg, I. Karatchevtseva, J. Davis, and M. Ionescu, He and Au ion radiation damage in sodalite, $\text{Na}_4\text{Al}_3\text{Si}_3\text{O}_{12}\text{Cl}$, *Journal of Nuclear Materials*, vol. 453, 307-312, 2014.
- [171] A. Kumar, S. J. Dhoble, D. R. Peshwe, and J. Bhatt, Structural and Photoluminescence properties of nepheline-structure $\text{NaAlSiO}_4:\text{Dy}^{3+}$ nanophosphors, *Journal of Alloys and Compounds*, vol. 609, 100-106, 2014.
- [172] M. I. Martín, F. Andreola, L. Barbieri, F. Bondioli, I. Lancellotti, J. M. Rincón, and M. Romero, Crystallisation and microstructure of nepheline-forsterite glass-ceramics, *Ceramics International*, vol. 39, 2955-2966, 2013.
- [173] A. Ghafari-Nazari, F. Moztafzadeh, S. M. Rabiee, T. Rajabloo, M. Mozafari, and L. Tayebi, Antibacterial activity of silver photodeposited nepheline thin film coatings, *Ceramics International*, vol. 38, 5445-5451, 2012.
- [174] R. Dimitrijevic, V. Dondur, P. Vulic, S. Markovic, and S. Macura, Structural characterization of pure Na-nephelines synthesized by zeolite conversion route, *Journal of Physics and Chemistry of Solids*, vol. 65, 1623-1633, 2004.
- [175] A. Radulović, V. Dondur, P. Vulić, Z. Miladinović, G. Ćirić-Marjanović, and R. Dimitrijević, Routes of synthesis of nepheline-type polymorphs: An influence of Na-LTA bulk composition on its thermal transformations, *Journal of Physics and Chemistry of Solids*, vol. 74, 1212-1220, 2013.
- [176] S. Chandrasekhar and P. N. Pramada, Thermal studies of low silica zeolites and their magnesium exchanged forms, *Ceramics International*, vol. 28, 177-186, 2002.
- [177] S. Markovic, V. Dondur, and R. Dimitrijevic, FTIR spectroscopy of framework aluminosilicate structures: carnegieite and pure sodium nepheline, *Journal of Molecular Structure*, vol. 654, 223-234, 2003.
- [178] *Webmineral mineralogy database. Tridymite mineral data.* Available: <http://webmineral.com/data/Tridymite.shtml#WxFJXO6FPX7>

5. REFERENCES

- [179] L. Bandura, M. Franus, G. Józefaciuk, and W. Franus, Synthetic zeolites from fly ash as effective mineral sorbents for land-based petroleum spills cleanup, *Fuel*, vol. 147, 100-107, 2015.
- [180] M. Sprynskyy, M. Lebedynets, A. P. Terzyk, P. Kowalczyk, J. Namieśnik, and B. Buszewski, Ammonium sorption from aqueous solutions by the natural zeolite Transcarpathian clinoptilolite studied under dynamic conditions, *Journal of Colloid and Interface Science*, vol. 284, 408-415, 2005.
- [181] P. Sharma, J.-S. Song, M. H. Han, and C.-H. Cho, GIS-NaP1 zeolite microspheres as potential water adsorption material: Influence of initial silica concentration on adsorptive and physical/topological properties, *Scientific Reports*, vol. 6, 22734, 2016.
- [182] L. Ayele, J. Pérez-Pariente, Y. Chebude, and I. Díaz, Synthesis of zeolite A from Ethiopian kaolin, *Microporous and Mesoporous Materials*, vol. 215, 29-36, 2015.
- [183] A. H. Ören and A. Kaya, Factors affecting adsorption characteristics of Zn²⁺ on two natural zeolites, *Journal of Hazardous materials*, vol. 131, 59-65, 2006.
- [184] X. Querol, N. Moreno, J. C. Umaña, R. Juan, S. Hernández, C. Fernandez-Pereira, C. Ayora, M. Janssen, J. García-Martínez, A. Linares-Solano, and D. Cazorla-Amoros, Application of zeolitic material synthesised from fly ash to the decontamination of waste water and flue gas, *Journal of Chemical Technology & Biotechnology*, vol. 77, 292-298, 2002.
- [185] M. A. Longhi, E. D. Rodríguez, S. A. Bernal, J. L. Provis, and A. P. Kirchheim, Valorisation of a kaolin mining waste for the production of geopolymers, *Journal of Cleaner Production*, vol. 115, 265-272, 2016.
- [186] R. Sommerville, R. Blissett, N. Rowson, and S. Blackburn, Producing a synthetic zeolite from improved fly ash residue, *International Journal of Mineral Processing*, vol. 124, 20-25, 2013.
- [187] X. Querol, F. Plana, A. Alastuey, and A. López-Soler, Synthesis of Na-zeolites from fly ash, *Fuel*, vol. 76, 793-799, 1997.
- [188] M. Wdowin, M. Franus, R. Panek, L. Badura, and W. Franus, The conversion technology of fly ash into zeolites, *Clean Technologies and Environmental Policy*, vol. 16, 1217-1223, 2014.
- [189] S. S. Bukhari, J. Behin, H. Kazemian, and S. Rohani, Conversion of coal fly ash to zeolite utilizing microwave and ultrasound energies: A review, *Fuel*, vol. 140, 250-266, 2015.
- [190] L. Ayele, J. Pérez-Pariente, Y. Chebude, and I. Díaz, Conventional versus alkali fusion synthesis of zeolite A from low grade kaolin, *Applied Clay Science*, vol. 132-133, 485-490, 2016.
- [191] I. O. Ali, S. M. El-Sheikh, T. M. Salama, M. F. Bakr, and M. H. Fodial, Controllable synthesis of NaP zeolite and its application in calcium adsorption, *Science China Materials*, vol. 58, 621-633, 2015.
- [192] X. Qiu, Y. Liu, D. Li, and C. Yan, Preparation of NaP zeolite block from fly ash-based geopolymer via in situ hydrothermal method, *Journal of Porous Materials*, vol. 22, 291-299, 2015.
- [193] B. Szala, T. Bajda, J. Matusik, K. Zięba, and B. Kijak, BTX sorption on Na-P1 organo-zeolite as a process controlled by the amount of adsorbed HDTMA, *Microporous and Mesoporous Materials*, vol. 202, 115-123, 2015.
- [194] T. T. Wałek, F. Saito, and Q. Zhang, The effect of low solid/liquid ratio on hydrothermal synthesis of zeolites from fly ash, *Fuel*, vol. 87, 3194-3199, 2008.
- [195] C. Baerlocher and W. Meier, The crystal structure of synthetic zeolite Na-P1, an isotype of gismondine, *Zeitschrift für Kristallographie-Crystalline Materials*, vol. 135, 339-354, 1972.

- [196] J. Cama, C. Ayora, X. Querol, and J. Ganor, Dissolution kinetics of synthetic zeolite NaP1 and its implication to zeolite treatment of contaminated waters, *Environmental Science and Technology*, vol. 39, 4871-4877, 2005.
- [197] L. Bandura, R. Panek, M. Rotko, and W. Franus, Synthetic zeolites from fly ash for an effective trapping of BTX in gas stream, *Microporous and Mesoporous Materials*, vol. 223, 1-9, 2016.
- [198] Y. Huang, D. Dong, J. Yao, L. He, J. Ho, C. Kong, A. J. Hill, and H. Wang, In situ crystallization of macroporous monoliths with hollow NaP zeolite structure, *Chemistry of Materials*, vol. 22, 5271-5278, 2010.
- [199] M. Kosmulski, IEP as a parameter characterizing the pH-dependent surface charging of materials other than metal oxides, *Advances in Colloid and Interface Science*, vol. 171-172, 77-86, 2012.
- [200] N. Arancibia-Miranda, S. E. Baltazar, A. García, D. Muñoz-Lira, P. Sepúlveda, M. A. Rubio, and D. Altbir, Nanoscale zero valent supported by zeolite and montmorillonite: Template effect of the removal of lead ion from an aqueous solution, *Journal of Hazardous materials*, vol. 301, 371-380, 2016.
- [201] M. R. Das, J. M. Borah, W. Kunz, B. W. Ninham, and S. Mahiuddin, Ion specificity of the zeta potential of α -alumina, and of the adsorption of p-hydroxybenzoate at the α -alumina-water interface, *Journal of Colloid and Interface Science*, vol. 344, 482-491, 2010.
- [202] J. A. Menendez, M. J. Illán-Gómez, C. A. León y León, and L. R. Radovic, On the difference between the isoelectric point and the point of zero charge of carbons, *Carbon*, vol. 33, 1655-1657, 1995.
- [203] E. M. Flanigen, "A review and new perspectives in zeolite crystallization," ed: ACS Publications, 1973.
- [204] D. Datta and H. Uslu, Adsorptive separation of lead (Pb^{2+}) from aqueous solution using tri-n-octylamine supported montmorillonite, *Journal of Chemical & Engineering Data*, vol. 62, 370-375, 2017.
- [205] M. Zhu, L. Zhu, J. Wang, T. Yue, R. Li, and Z. Li, Adsorption of Cd (II) and Pb (II) by in situ oxidized Fe_3O_4 membrane grafted on 316L porous stainless steel filter tube and its potential application for drinking water treatment, *Journal of Environmental Management*, vol. 196, 127-136, 2017.
- [206] V. Hernández-Montoya, M. A. Pérez-Cruz, D. I. Mendoza-Castillo, M. R. Moreno-Virgen, and A. Bonilla-Petriciolet, Competitive adsorption of dyes and heavy metals on zeolitic structures, *Journal of Environmental Management*, vol. 116, 213-221, 2013.
- [207] Y. Yan, Q. Li, X. Sun, Z. Ren, F. He, Y. Wang, and L. Wang, Recycling flue gas desulphurization (FGD) gypsum for removal of Pb (II) and Cd (II) from wastewater, *Journal of Colloid and Interface Science*, vol. 457, 86-95, 2015.
- [208] Y. Fernández-Nava, M. Ulmanu, I. Anger, E. Marañón, and L. Castrillón, Use of granular bentonite in the removal of mercury (II), cadmium (II) and lead (II) from aqueous solutions, *Water, Air, & Soil Pollution*, vol. 215, 239-249, 2011.
- [209] X. Li, C. Bian, X. Meng, and F.-S. Xiao, Design and synthesis of an efficient nanoporous adsorbent for Hg^{2+} and Pb^{2+} ions in water, *Journal of Materials Chemistry A*, vol. 4, 5999-6005, 2016.

5. REFERENCES

- [210] A. Gil, S. Albeniz, and S. A. Korili, Valorization of the saline slags generated during secondary aluminium melting processes as adsorbents for the removal of heavy metal ions from aqueous solutions, *Chemical Engineering Journal*, vol. 251, 43-50, 2014.
- [211] R. R. Z. Tarpani, F. R. Lapolli, and M. Á. Lobo-Recio, Removal of aluminum from synthetic solutions and well water by chitin: batch and continuous experiments, *Desalination and Water Treatment*, vol. 53, 3531-3542, 2015.
- [212] E. Worch, *Adsorption technology in water treatment: Fundamentals, processes, and modeling*. De Gruyter, 2012.
- [213] S. Wang and Y. Peng, Natural zeolites as effective adsorbents in water and wastewater treatment, *Chemical Engineering Journal*, vol. 156, 11-24, 2010.
- [214] W. Mozgawa, M. Król, and T. Bajda, Application of IR spectra in the studies of heavy metal cations immobilization on natural sorbents, *Journal of Molecular Structure*, vol. 924-926, 427-433, 2009.
- [215] Q. Meng, H. Chen, J. Lin, Z. Lin, and J. Sun, Zeolite A synthesized from alkaline assisted pre-activated halloysite for efficient heavy metal removal in polluted river water and industrial wastewater, *Journal of Environmental Sciences*, vol. 56, 254-262, 2017.
- [216] M. Naushad, Z. A. AlOthman, M. R. Awual, M. M. Alam, and G. E. Eldesoky, Adsorption kinetics, isotherms, and thermodynamic studies for the adsorption of Pb^{2+} and Hg^{2+} metal ions from aqueous medium using Ti (IV) iodovanadate cation exchanger, *Ionics*, vol. 21, 2237-2245, 2015.
- [217] R. Shawabkeh, A. Al-Harashsheh, M. Hami, and A. Khlaifat, Conversion of oil shale ash into zeolite for cadmium and lead removal from wastewater, *Fuel*, vol. 83, 981-985, 2004.
- [218] M. Kragović, A. Daković, Ž. Sekulić, M. Trgo, M. Ugrina, J. Perić, and G. D. Gatta, Removal of lead from aqueous solutions by using the natural and Fe (III)-modified zeolite, *Applied Surface Science*, vol. 258, 3667-3673, 2012.
- [219] M. Naushad, T. Ahamad, Z. A. AlOthman, M. A. Shar, N. S. AlHokbany, and S. M. Alshehri, Synthesis, characterization and application of curcumin formaldehyde resin for the removal of Cd^{2+} from wastewater: Kinetics, isotherms and thermodynamic studies, *Journal of Industrial and Engineering Chemistry*, vol. 29, 78-86, 2015.
- [220] H. Ghassabzadeh, A. Mohadespour, M. Torab-Mostaedi, P. Zaheri, M. G. Maragheh, and H. Taheri, Adsorption of Ag, Cu and Hg from aqueous solutions using expanded perlite, *Journal of Hazardous materials*, vol. 177, 950-955, 2010.
- [221] M. A. O. Lourenço, P. Figueira, E. Pereira, J. R. B. Gomes, C. B. Lopes, and P. Ferreira, Simple, mono and bifunctional periodic mesoporous organosilicas for removal of priority hazardous substances from water: The case of mercury(II), *Chemical Engineering Journal*, vol. 322, 263-274, 2017.
- [222] M. Naushad, T. Ahamad, G. Sharma, A. a. H. Al-Muhtaseb, A. B. Albadarin, M. M. Alam, Z. A. AlOthman, S. M. Alshehri, and A. A. Ghfar, Synthesis and characterization of a new starch/ SnO_2 nanocomposite for efficient adsorption of toxic Hg^{2+} metal ion, *Chemical Engineering Journal*, vol. 300, 306-316, 2016.
- [223] L. Y. Zhang, H. Y. Zhang, W. Guo, and Y. L. Tian, Sorption characteristics and mechanisms of ammonium by coal by-products: slag, honeycomb-cinder and coal gangue, *International Journal of Environmental Science and Technology*, vol. 10, 1309-1318, 2013.

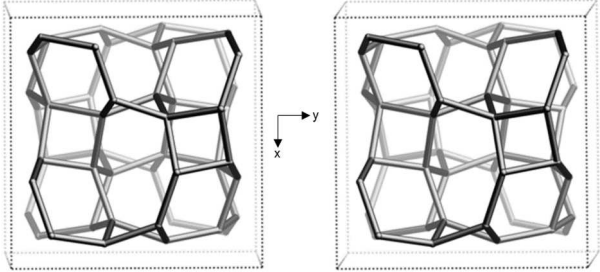
- [224] E. Marañón, M. Ulmanu, Y. Fernández, I. Anger, and L. Castrillón, Removal of ammonium from aqueous solutions with volcanic tuff, *Journal of Hazardous materials*, vol. 137, 1402-1409, 2006.
- [225] Y. Zhao, B. Zhang, X. Zhang, J. Wang, J. Liu, and R. Chen, Preparation of highly ordered cubic NaA zeolite from halloysite mineral for adsorption of ammonium ions, *Journal of Hazardous materials*, vol. 178, 658-664, 2010.
- [226] K. Saltalı, A. Sarı, and M. Aydın, Removal of ammonium ion from aqueous solution by natural Turkish (Yıldızeli) zeolite for environmental quality, *Journal of Hazardous materials*, vol. 141, 258-263, 2007.
- [227] Y. Zheng, Y. Liu, and A. Wang, Fast removal of ammonium ion using a hydrogel optimized with response surface methodology, *Chemical Engineering Journal*, vol. 171, 1201-1208, 2011.
- [228] K. Zare, H. Sadegh, R. Shahryari-ghoshekandi, M. Asif, I. Tyagi, S. Agarwal, and V. K. Gupta, Equilibrium and kinetic study of ammonium ion adsorption by Fe₃O₄ nanoparticles from aqueous solutions, *Journal of Molecular Liquids*, vol. 213, 345-350, 2016.
- [229] L. Lei, X. Li, and X. Zhang, Ammonium removal from aqueous solutions using microwave-treated natural Chinese zeolite, *Separation and Purification Technology*, vol. 58, 359-366, 2008.
- [230] Y. S. Ho and G. McKay, A comparison of chemisorption kinetic models applied to pollutant removal on various sorbents, *Process Safety and Environmental Protection*, vol. 76, 332-340, 1998.
- [231] F. Mazloomi and M. Jalali, Ammonium removal from aqueous solutions by natural Iranian zeolite in the presence of organic acids, cations and anions, *Journal of Environmental Chemical Engineering*, vol. 4, 1664-1673, 2016.
- [232] P. Vassileva, P. Tzvetkova, and R. Nickolov, Removal of ammonium ions from aqueous solutions with coal-based activated carbons modified by oxidation, *Fuel*, vol. 88, 387-390, 2009.
- [233] E. R. Nightingale, Phenomenological theory of ion solvation. Effective radii of hydrated ions, *Journal of Physical Chemistry*, vol. 63, 1381-1387, 1959.
- [234] K. Nakamoto, "Applications in inorganic chemistry," in *Infrared and raman spectra of inorganic and coordination compounds*, ed John Wiley & Sons, Inc., 2008, 149-354.

6. ANNEXES

ANNEX I FRAMEWORKS OF ZEOLITES

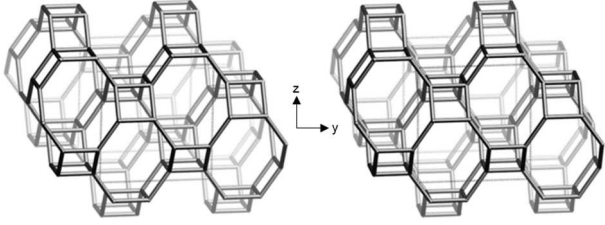
The main types of zeolite frameworks obtained in this thesis as well as their crystal characteristics are shown below. All data were adapted from the information provided by the Structure Commission of the International Zeolite Association (IZA-SC).

Framework Type ANA

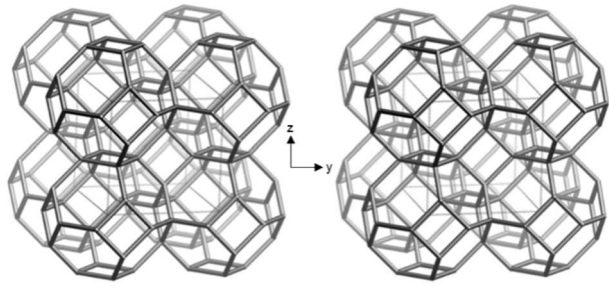
Zeolite Analcime	 <p>Framework viewed along [001]</p>			Framework Type ANA
Chemical Formula	Na ⁺ ₁₆ (H ₂ O) ₁₆ [Al ₁₆ Si ₃₂ O ₉₆]-ANA			
Unit Cell	Cubic	I a -3 d (# 230)		
	a = 13.5670 Å	b = 13.5670 Å	c = 13.5670 Å	
	α = 90.000°	β = 90.000°	γ = 90.000°	
Framework density	19.2 T/1000 Å ³			
Ring sizes (T-atoms)	8, 6, and 4			
Channels	Irregular channels formed by highly distorted 8-rings Dimensionality Sorption (molecular cross section > 3.4 Å): 0-dimensional Topological (pore opening > 6-ring): 3-dimensional			
Accessible volume	0.00 %			

6. ANNEXES

Framework Type GIS

Zeolite Gismondine	 <p style="text-align: center;">Framework viewed along [100]</p>			Framework Type GIS
Chemical Formula	$[\text{Ca}^{2+}_4(\text{H}_2\text{O})_{16}] [\text{Al}_8\text{Si}_8\text{O}_{32}]\text{-GIS}$			
Unit Cell	Tetragonal		I 4 ₁ /a m d (# 141)	
	$a = 9.8010 \text{ \AA}$	$b = 9.8010 \text{ \AA}$	$c = 10.1580 \text{ \AA}$	
	$\alpha = 90.000^\circ$	$\beta = 90.000^\circ$	$\gamma = 90.000^\circ$	
Framework density	$15.3 \text{ T}/1000 \text{ \AA}^3$			
Ring sizes (T-atoms)	8 and 4			
Channels	Dimensionality Sorption (molecular cross section > 3.4 Å): 0-dimensional Topological (pore opening > 6-ring): 3-dimensional			
Accessible volume	9.38 %			
Related zeolites	NaP1 (sodium aluminum silicate hydrate, also called zeolite P1) NaP2 MAP (low-silica NaP), etc.			

Framework Type SOD

Zeolite Sodalite	 <p>Framework viewed along [001]</p>			Framework Type SOD
Chemical Formula	Na ⁺ ₈ Cl ⁻ ₂ [Al ₆ Si ₆ O ₂₄]-SOD			
Unit Cell	cubic	P -4 3 n (# 218)		
	a = 8.8700 Å	b = 8.8700 Å	c = 8.8700 Å	
	α = 90.000°	β = 90.000°	γ = 90.000°	
Framework density	17.2 T/1000 Å ³			
Ring sizes (T-atoms)	6 and 4			
Channels	Apertures formed by 6-rings only Dimensionality Sorption (molecular cross section > 3.4 Å): 0-dimensional Topological (pore opening > 6-ring): 0-dimensional			
Accessible volume	0.00 %			
Related zeolites	Hydro-sodalite (Na ₆ [AlSiO ₄] ₆ ·8H ₂ O) Anhydrous sodalite (Na ₆ [AlSiO ₄] ₆)			

ANNEX II PUBLICATIONS

Journal of Minerals and Materials Characterization and Engineering, 2015, 3, 55-64
Published Online March 2015 in SciRes. <http://www.scirp.org/journal/jmmce>
<http://dx.doi.org/10.4236/jmmce.2015.32008>



Characterization of Solid Wastes from Aluminum Tertiary Sector: The Current State of Spanish Industry

Roberto Galindo¹, Isabel Padilla¹, Olga Rodríguez¹, Ruth Sánchez-Hernández¹, Sol López-Andrés², Aurora López-Delgado¹

¹National Centre for Metallurgical Research, CENIM-CSIC, Madrid, Spain

²Department of Crystallography and Mineralogy, Faculty of Geology, UCM, Madrid, Spain

Email: alopezdelgado@cenim.csic.es

Received 9 February 2015; accepted 27 February 2015; published 4 March 2015

Copyright © 2015 by authors and Scientific Research Publishing Inc.

This work is licensed under the Creative Commons Attribution International License (CC BY).

<http://creativecommons.org/licenses/by/4.0/>



Open Access

Abstract

Aluminum recycling is an important activity that allows returning this metal to the market saving energy and resources. This activity generates slag and dross, both hazardous materials, which are recovered by other industries (tertiary sector). In that process, new wastes are produced, but most of them are disposed in security storage facilities because of their hazardousness and scarce marketable value. In Spain, the statistical data analysis on waste reveals that this sector is increasing every year. This study aims to characterize the wastes generated by the tertiary aluminum industries in Spain. Samples were collected in different aluminum recycling industries and characterized by chemical analyses, X-ray fluorescence, X-ray diffraction and particle size determination. Wastes rich in aluminum oxide and alkaline elements also comprise metallic aluminum and aluminum nitride. Such components are the main responsible for the waste hazardousness since they generate toxic gases in the presence of water. Besides, their fine granulometry ($x_{50} < 30 \mu\text{m}$) also contributes highly to the hazardousness.

Keywords

Hazardous Aluminum Waste, Characterization, Recycling, Slag/Dross



Contents lists available at ScienceDirect

Microporous and Mesoporous Materials

journal homepage: www.elsevier.com/locate/micromeso

One-step synthesis of NaP1, SOD and ANA from a hazardous aluminum solid waste

Ruth Sánchez-Hernández^a, Aurora López-Delgado^{a,*}, Isabel Padilla^a, Roberto Galindo^a, Sol López-Andrés^b^a National Centre for Metallurgical Research, CSIC, Avda. Gregorio del Amo 8, Madrid, 28040, Spain^b Department of Crystallography and Mineralogy, Faculty of Geology, University Complutense of Madrid, C/ José Antonio Novais s/n, Madrid, 28040, Spain

ARTICLE INFO

Article history:

Received 16 October 2015

Received in revised form

15 January 2016

Accepted 18 January 2016

Available online 5 February 2016

Keywords:

NaP1

Sodalite and anakime

Hazardous waste

One-step hydrothermal synthesis

High-CEC zeolite

ABSTRACT

NaP1, SOD, and ANA zeolites were synthesized from a hazardous aluminum waste as main aluminosilicate source by a one-step hydrothermal synthesis. This allowed the total transformation of the waste and no other solid residues were produced. The conversion of the waste into zeolites led to yields of ~2.5 kg of zeolite per kg of waste. Experimental parameters such as stirring, time, temperature, and concentration of alkalinizing agent (NaOH solution) were studied to determine the best synthesis conditions. Samples were characterized by different techniques such as XRD, SEM-EDS, FTIR, TG-DTA; textural properties such as BET specific surface area, zeta potential, granulometry and cation-exchange capacity (CEC) were also determined. Temperature and alkali concentration were the parameters with strongest influence in the formation of the different zeolites. Thus, the optimal conditions to obtain NaP1 and ANA were 1 M NaOH solution for 6 h at 120 and 200 °C, respectively, while SOD was prepared at 120 °C for 6 h, using a very much higher alkali concentration (5 M). These zeolites exhibited similar characteristics to those obtained from conventional chemical reagents. Besides, the mother liquor from the synthesis of NaP1 was recycled twice in order to reduce water and alkalinizing agent consumption. In this case, the only crystalline phase obtained was NaP1 showing morphological, textural and crystalline characteristics very similar to those of NaP1 prepared from fresh solutions. The results show that the aluminum waste can be transformed into different types of zeolites, considered as value-added materials, with promising adsorption properties.

© 2016 Elsevier Inc. All rights reserved.



⑪ Número de publicación: **2 617 037**

⑫ Número de solicitud: 201531811

⑬ Int. Cl.:

C01B 39/02 (2006.01)

B01J 29/06 (2006.01)

⑭

PATENTE DE INVENCION

B1

⑮ Fecha de presentación:

15.12.2015

⑯ Fecha de publicación de la solicitud:

15.06.2017

Fecha de la concesión:

04.04.2018

⑰ Fecha de publicación de la concesión:

11.04.2018

⑱ Titular/es:

CONSEJO SUPERIOR DE INVESTIGACIONES
CIENTÍFICAS (CSIC) (85.0%)
C/ Serrano, nº 117
28006 Madrid (Madrid) ES y
UNIVERSIDAD COMPLUTENSE DE MADRID
(15.0%)

⑲ Inventor/es:

LÓPEZ DELGADO, Aurora;
PADILLA RODRÍGUEZ, Isabel;
SÁNCHEZ HERNÁNDEZ, Ruth;
RODRIGUEZ LARGO, Olga y
LÓPEZ ANDRÉS, Sol

⑳ Agente/Representante:

PONS ARIÑO, Ángel

㉑ Título: PROCEDIMIENTO DE REVALORIZACIÓN DE UN RESIDUO PROCEDENTE DE LA MOLIENDA DE ESCORIAS DE ALUMINIO

㉒ Resumen:

Procedimiento de revalorización de un residuo procedente de la molienda de escorias de aluminio. El objeto de la invención es un procedimiento de revalorización de residuos peligrosos procedentes de la molienda de escorias de aluminio mediante su transformación en zeolitas. Se contempla la utilización como materia prima de los finos de granulometría inferior a 200 μm obtenidos en el proceso de molienda de escorias de aluminio, recuperados tanto por separación granulométrica como por sistemas de captación.

Mediante el procedimiento objeto de la presente invención se consigue transformar un residuo peligroso en un producto comercial como las zeolitas, permitiendo además la recuperación de los gases liberados como el amoníaco y el hidrógeno, que pueden ser destinados a otros usos, así como, la recuperación de las sales obtenidas por evaporación de las aguas de lavado.

El procedimiento se ha optimizado recirculando las aguas madres resultantes tras la separación de las zeolitas.

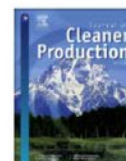
ES 2 617 037 B1

Aviso: Se puede realizar consulta prevista por el art. 37.3.8 LP 11/1986.



Contents lists available at ScienceDirect

Journal of Cleaner Production

journal homepage: www.elsevier.com/locate/jclepro

Eco-friendly bench-scale zeolitization of an Al-containing waste into gismondine-type zeolite under effluent recycling

Ruth Sánchez-Hernández^a, Isabel Padilla^a, Sol López-Andrés^b, Aurora López-Delgado^{a,*}^a National Centre for Metallurgical Research, CSIC, Avda. Gregorio del Amo 8, Madrid, 28040, Spain^b Department of Crystallography and Mineralogy, Faculty of Geology, University Complutense of Madrid, C/ José Antonio Nováis 12, Madrid, 28040, Spain

ARTICLE INFO

Article history:

Received 15 February 2017

Received in revised form

3 May 2017

Accepted 30 May 2017

Available online 4 July 2017

Keywords:

Aluminum waste

Eco-friendly zeolitization

Bench-scale

NaP1

Mother liquor recycling

High-CEC zeolite

ABSTRACT

The feasibility of developing an eco-friendly bench-scale zeolitization process of NaP1 from an Al-containing waste and under recycling of effluents was evaluated. Prior lab-scale tests were performed to optimize the synthesis conditions. The mixture of effluents, i.e., mother liquors (ML) from the synthesis and rinse water (RW) from the cleaning step of the zeolites, was recycled several times to study the reduction of raw materials (NaOH and water) and accordingly the reduction of costs. The bench-scale process allows the complete transformation of the waste into NaP1 zeolite, reaching equivalent reaction yields (2.5 ton of zeolite per ton of waste) to the lab-scale process and avoiding the generation of new solid residues. The effect of the recycling of effluents on the physical-chemical properties of the resulting zeolites was investigated. NaP1 zeolite was the only crystalline phase obtained, showing morphological, textural and crystalline characteristics closely similar to NaP1 synthesized from fresh NaOH aqueous solutions and from pure chemical reagents. NaOH and water consumption savings of 80 and 67%, respectively, were obtained, representing a cost reduction around 70%. These results show that the bench-scale process to obtain NaP1 from an Al-waste with recycling of effluents can be a more sustainable alternative compared with the traditional synthesis methods.

© 2017 Elsevier Ltd. All rights reserved.

ANNEX III CONGRESS AND AWARDS

Congress **Simposio del Grupo Especializado de Cristalografía y Crecimiento****Cristalino, GE3C**

Bilbao, Spain. June 23-26, 2014

Title *Síntesis de zeolita NaP1 a partir de residuos industriales***Authors** **Ruth Sánchez-Hernández**, Isabel Padilla, Sol López-Andrés, Roberto Galindo, Aurora López-Delgado**Type** Oral presentation

Congress **Sustainable Materials Science and Technology**

Paris, France. July 15-17, 2015

Title *Al-waste zeolites and their application as cadmium adsorbents***Authors** **Ruth Sánchez-Hernández**, Isabel Padilla, Edgar Winter Júnior, Ana L.R. Mercê, Sol López-Andrés, Denise A. Fungaro, Roberto Galindo, Aurora López-Delgado**Type** Oral presentation

6. ANNEXES

Congress XXXV Reunión Bienal RSEQ (Simposio de Química Sostenible)
A Coruña, Spain. July 19-23, 2015

Title *Síntesis a escala piloto de NaP1 a partir de un residuo peligroso y su utilización como adsorbente de mercurio*

Authors Ruth Sánchez-Hernández, Isabel Padilla, Sol López-Andrés, Roberto Galindo, Aurora López-Delgado

Type Oral presentation

Congress IV Meeting of The Italian and Spanish Crystallographic Associations (IV MISCA)
Tenerife, Spain. June 21-25, 2016

Title *Thermal transformation of sodium zeolites into pure nepheline*

Authors Sol López-Andrés, Ruth Sánchez-Hernández, Isabel Padilla, Aurora López-Delgado

Type Poster

Congress Junior Euromat 2016
Lausanne, Switzerland. July 10-14, 2016

Title *Recycling of mother liquors from the zeolitization of a hazardous aluminium waste*

Authors Ruth Sánchez-Hernández, Aurora López-Delgado, Isabel Padilla, Sol López-Andrés

Type Oral presentation

Congress 6th EuCheMS

Sevilla, Spain. September 11-15, 2016

Title *Complete transformation of hazardous aluminium waste into an adsorbent zeolitic material for water remediation***Authors** Ruth Sánchez-Hernández, Aurora López-Delgado, Isabel Padilla, Sol López-Andrés**Type** Oral presentation

Congress Journal of Thermal Analysis and Calorimetry Conference and Thermoanalytical Conference (JTACC+V4)

Budapest, Hungary. June 6-9, 2017

Title Kinetic study of nepheline crystallization obtained by thermal transformation of sodalite zeolite**Authors** Ruth Sánchez-Hernández, Isabel Padilla, Maximina Romero, Sol López-Andrés, Aurora López-Delgado**Type** Poster

6. ANNEXES

AWARD Certamen de Fotografía Científica FOTCIENCIA13
FECYT & CSIS

Title *Mundo Sostenible*

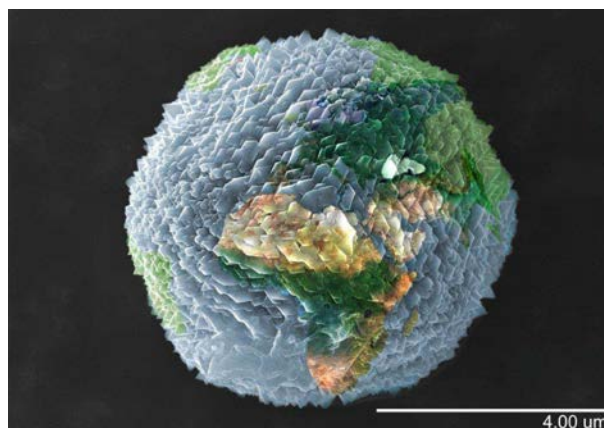
Author Ruth Sánchez Hernández

Co-author Antonio Tomás López

Type SEM image awarded with the **first prize** of the micro category

Abstract: El progresivo agotamiento de los recursos naturales del Planeta Tierra, unido a la ingente producción de residuos, priorizan la búsqueda de alternativas más respetuosas con el medio ambiente. La imagen muestra un cristal de zeolita obtenido en el laboratorio a partir de un residuo peligroso de aluminio. Las zeolitas son minerales con numerosas aplicaciones industriales. En la naturaleza se originan por reacciones entre rocas volcánicas en diferentes medios. En el laboratorio se preparan y diseñan a partir de reactivos químicos para dotarlas de características especiales para diferentes usos. También, se sintetizan a partir de residuos. Ésta última opción, permite minimizar el impacto medioambiental que genera la acumulación de residuos en vertederos, y a su vez, aprovechar residuos de manera sostenible para obtener materiales de valor añadido, como zeolitas, disminuyendo el consumo de recursos naturales. La zeolita de la imagen se utiliza para eliminar metales pesados en aguas, consiguiendo resolver dos problemáticas ambientales: el aprovechamiento de residuos, y el tratamiento de aguas contaminadas.

Proyecto CTM2012-34449 y Ayuda Predoctoral BES-2013-066269.



ANNEX IV LIST OF TABLES

Table 1.1 Classification of zeolites according to their pore sizes and openings. (Adapted from reference [22]).	11
Table 1.2 Water treatment technologies. (Adapted from references [92, 93]).	21
Table 2.1 Experimental conditions used for the lab-scale synthesis of zeolites from aluminum waste (Alw_x).	34
Table 2.2 Experimental conditions used for the bench-scale synthesis of zeolites from aluminum waste (Alw_x).	36
Table 3.1 Chemical composition of the different waste samples (Alw_1 - Alw_9) and the representative waste sample (Alw_x) determined by X-ray fluorescence (XRF).	60
Table 3.2 Aluminum nitride (AlN) and metallic aluminum (Al) contents present in the waste samples determined by the Kjeldhal method and AAS, respectively.	61
Table 3.3 Content of aluminum in the different aluminum phases of the waste sample Alw_x .	62
Table 3.4 Semi-quantitative analysis of crystalline phases in Alw_x determined by the Chung method [114, 115].	65
Table 3.5 Microchemical point analyses of the representative waste sample Alw_x (according to Figure 3.3).	66
Table 3.6 Microchemical point analyses of the representative waste sample Alw_x (according to Figure 3.4).	67
Table 3.7 Particle size distribution of the waste samples according to their particle diameters d_{10} , d_{50} and d_{90} .	68
Table 3.8 Concentrations of elements present in the leachates after acid treatment.	71
Table 3.9 Concentrations of elements present in the leachates after aqueous treatment.	72
Table 3.10 Experimental lab-scale synthesis conditions used to obtain zeolites from the waste, zeolitic phases and reaction yields obtained.	75
Table 3.11 Peak parameters (2θ and FWHM) and crystallite sizes (D_{hkl}) calculated for the samples obtained from the waste via the lab-scale synthesis.	76
Table 3.12 Miller indices (hkl), peak parameters (2θ and FWHM), and relative intensities (I_{rel}) for NaP1 obtained for 6 h (sample Z3) and 24 h (sample Z4).	80
Table 3.13 Miller indices (hkl), peak parameters (2θ and FWHM), and relative intensities (I_{rel}) for SOD (sample Z7).	83
Table 3.14 Miller indices (hkl), peak parameters (2θ and FWHM), and relative intensities (I_{rel}) for ANA (sample Z13).	86
Table 3.15 Influence of the initial liquid/solid ratio on the crystallinity of NaP1 from the waste.	89
Table 3.16 Characteristic IR bands of zeolites [165].	97
Table 3.17 Assignments of bands observed by FTIR for NaP1 (Z3), SOD (Z7), and ANA (Z13) synthesized from the waste.	98
Table 3.18 TG-DTA analyses of the NaP1 (Z3), SOD (Z7), and ANA (Z13) zeolites obtained from the waste.	101
Table 3.19 Chemical formula of NaP1, SOD, and ANA obtained from the waste via direct synthesis on lab scale.	102
Table 3.20 Specific surface area (S_{BET}), external area (S_{EXT}), and particle size distribution (PSD) of NaP1, SOD, and ANA synthesized from the waste.	109

6. ANNEXES

Table 3.21 Zeta-potential (ζ -potential) and cation-exchange capacity (CEC) of NaP1, SOD, and ANA obtained from the waste. Aqueous suspensions of zeolite prepared at initial pH 7 and 25 °C.	111
Table 3.22 Experimental lab-scale synthesis conditions to obtain zeolites from the waste with mother liquor recycling, zeolitic phases, and reaction yields obtained.	113
Table 3.23 Peak parameters (2θ and FWHM) and crystallite sizes (D_{hkl}) calculated for the samples obtained from the waste via the lab-scale synthesis of NaP1 with mother liquor recycling.	115
Table 3.24 Specific surface area (S_{BET}) and external area (S_{EXT}) of NaP1 obtained without mother liquor recycling (Z16) and after the first (Z17) and second recycling cycle (Z18).	119
Table 3.25 Chemical composition determined by ICP-OES, pH, and conductivity (CE) of the mother liquors obtained in the synthesis of NaP1 after the first (ML1) and second (ML2) recycling.	119
Table 3.26 Peak parameters (2θ and FWHM) and crystallite sizes (D_{hkl}) calculated for the samples obtained from the waste via the lab-scale synthesis of SOD and ANA with mother liquor recycling.	120
Table 3.27 Zeolites obtained from different precursors by conventional hydrothermal processes.	123
Table 3.28 Zeolitic phase, yield (expressed as tons of zeolite per ton of waste), crystallinity, peak parameters (2θ and FWHM), and crystalline sizes (D_{hkl}) obtained in the bench-scale synthesis process with and without ML and RW recycling.	129
Table 3.29 Peak parameters of a commercial zeolite (P1-X) characterized by NaP1 and traces of X zeolite.	131
Table 3.30 Assignments of bands observed by FTIR for the NaP1 zeolites obtained from the waste by the bench-scale synthesis without recycling (ZB0) and with effluents recycling (ZB1, ZB2, and ZB3) compared with a commercial zeolite (P1-X).	132
Table 3.31 Chemical composition (determined by μ -XRF) of NaP1 synthesized from the waste by bench-scale synthesis without recycling (ZB0) compared with a commercial zeolite (P1-X). Standard deviation = ± 0.1	133
Table 3.32 EDS analysis of the NaP1 zeolite synthesized from the waste by the bench-scale zeolitization process without (ZB0) and with effluent recycling (ZB1, ZB2, and ZB3).	135
Table 3.33 TG-DTA analyses of the initial NaP1 zeolite (ZB0), and the recycled zeolites (ZB1, ZB2, and ZB3) from the waste.	138
Table 3.34 Specific surface area (S_{BET}) and external area (S_{EXT}) values of the NaP1 zeolites from the waste through the bench-scale synthesis without (ZB0) and with (ZB1, ZB2, and ZB3) recycling. Outgassing conditions: 60 °C for 24 h.	140
Table 3.35 Specific surface area (S_{BET}), external area (S_{EXT}), total, meso and micropore volume values (V_{total} , V_{meso} , and V_{micro}) of NaP1 from the waste through the bench-scale synthesis without recycling (ZB0) and after three recycling cycles (ZB3) compared with a commercial zeolite (P1-X). Outgassing conditions: 350 ° for 24 h.	141
Table 3.36 Characteristic parameters (d_{10} , d_{50} , and d_{90}) of the particle size distribution (PSD) for the NaP1 zeolite synthesized with fresh alkalizing agent (Z0) and with effluent recycling (Z1, Z2, and Z3) on bench scale.	143
Table 3.37 Zeta-potential (ζ -potential) of NaP1 from the waste through the bench-scale synthesis without (ZB0) and with (ZB1, ZB2, and ZB3) recycling compared with a commercial zeolite (P1-X). Aqueous suspensions of zeolite prepared at initial pH 7 and 25 °C.	144
Table 3.38 Cation-exchange capacity (CEC) values of the NaP1 zeolites from the waste via the bench-scale synthesis without (ZB0) and with (ZB1, ZB2, and ZB3) recycling compared with a commercial zeolite (P1-X).	146

Table 3.39 Chemical composition, pH, and conductivity (CE) of the mother liquors (ML) obtained after the synthesis from fresh NaOH solution (MLZB0) and from the first (MLZB1) and second (MLZB2) recycling.	147
Table 3.40 LCI of the production of 1 ton of NaP1 through the bench-scale synthesis process with and without discharge of effluents (ML and RW).	148
Table 3.41 Cost estimation based on the production of one ton of NaP1 obtained from the waste by the zeolitization process with and without liquid effluents recycling.	150
Table 3.42 Conditions studied in the single- and multi-metal cation adsorption experiments using the zeolite NaP1 (sample ZB0) synthesized from the waste.	153
Table 3.43 Crystallinity, peak parameters (2θ and FWHM), and crystalline sizes (D_{hkl}) obtained for the initial NaP1 zeolite (sample ZB0 at pH 10 ± 0.5) compared with NaP1 in aqueous solution at pH 6 and 4.	158
Table 3.44. Kinetic model parameters and error function values calculated for the single adsorption of the Pb^{2+} , Cd^{2+} , and Hg^{2+} cations onto ZB0.	160
Table 3.45. Parameters obtained from the intra-particle diffusion model applied to the adsorption of Pb^{2+} , Cd^{2+} , and Hg^{2+} using ZB0.	162
Table 3.46. Isotherm models: parameters and error function (R^2) values obtained for the removal of the Pb^{2+} , Cd^{2+} , and Hg^{2+} cations onto ZB0.	167
Table 3.47. Competitive adsorption of Pb^{2+} , Cd^{2+} , and Hg^{2+} on ZB0 using different zeolite doses and contact times. Conditions: pH = 4.5; adsorbent dose = 2 and 10 g/L; $C_o = 20$ mg/L for Pb^{2+} and Cd^{2+} , and 0.2 mg/L for Hg^{2+} ; T = 25 ± 2 °C.	170
Table 3.48. Chemical composition (determined by μ -XRF) of ZB0 before and after the competitive adsorption of Pb^{2+} , Cd^{2+} , and Hg^{2+}	174
Table 3.49. Comparison of the maximum adsorption capacity of Pb^{2+} , Cd^{2+} , and Hg^{2+} using different sorbent materials.	175
Table 3.50 Experimental conditions for the ammonium adsorption experiments using the zeolite NaP1 (sample ZB0) obtained from the waste.	176
Table 3.51. Kinetic model parameters and error function values obtained for the NH_4^+ adsorption onto the NaP1 zeolite synthesized (ZB0) from the waste by the bench-scale synthesis process.	181
Table 3.52. Isotherm models applied for the NH_4^+ adsorption onto ZB0.	184
Table 3.53. Maximum adsorption capacity of NH_4^+ for several adsorbents.	185

ANNEX V LIST OF FIGURES

Figure 1.1 Main Spanish industrial areas dedicated to the recovery and/or disposal of aluminum wastes.(Adapted from Galindo et al. [8]).	5
Figure 1.2 Total and recovered amount of hazardous aluminum waste (Alw) from the Spanish tertiary industry during the period 2010-2016 (European Waste Catalogue code: 100321).	5
Figure 1.3 Waste prevention and management according to the Waste Framework Directive (WFD) [9].	7
Figure 1.4 Examples of zeolite frameworks: ANA (analcime), GIS (gismondine), LTA (Linde type A), and SOD (sodalite). (Adapted from reference [20]).	8
Figure 1.5 a) PBU of zeolites; b) Examples of some CBU; c) LTA-framework formed by sodalite cages represented in green. (Adapted from reference [20]).	9
Figure 1.6 NaP1 zeolite (GIS-type framework).	10
Figure 1.7 Channel systems (represented in blue) and ring sizes (dimensions expressed in Å) of the ANA, GIS, and LTA zeolites. (Adapted from reference [20]).	11
Figure 1.8 Steps that can take place during adsorption between an adsorbate and adsorbent (Adapted from Tran et al. [96]).	22
Figure 1.9 Main parameters that influence the adsorption processes.	23
Figure 2.1 a) Homogenization and separation of different aluminum waste fractions. b) Representative sample of the aluminum waste (Alw _x) used for the synthesis of zeolites.	30
Figure 2.2 a) Reactor used for the lab-scale synthesis experiments of zeolites from aluminum waste. b) Wet zeolite sample obtained after filtration. c) Dry zeolite sample.	32
Figure 2.3 Bench-scale synthesis set up (facilities of the company <i>Archroma S.A.</i>). a) Reactor and thermal fluid heating and agitation system. b) Control system of synthesis parameters: temperature, pressure, and agitation. c) Loading of mother liquor and rinse water in the reactor.	36
Figure 2.4 a) Separation of the zeolites and mother liquor by filtration. b) Wet zeolite sample. c) Dry zeolite samples.	37
Figure 2.5 Main stages of the synthesis process of zeolites from the aluminum waste.	38
Figure 2.6 Main properties of the zeolites obtained from aluminum wastes analyzed by different characterization techniques.	39
Figure 3.1 Volumes of NH ₃ and H ₂ released by the wastes.	63
Figure 3.2 XRD pattern of the representative waste sample Alw _x used for the synthesis of zeolites.	64
Figure 3.3 General morphology of the representative waste sample Alw _x used for the synthesis of zeolites. SEM images at magnification x1,000 (a) and x2,000 (b).	66
Figure 3.4 Characteristic phases of Alw _x : Spinel (1) and metallic aluminum (2), SEM image at magnification x1,000; quartz (3), SEM image at magnification x250; and halite (4), SEM image at magnification x400.	67
Figure 3.5 Particle size distribution (PSD) of the waste samples.	70
Figure 3.6 XRD patterns of zeolite NaP1 obtained from the waste at 120 °C for 3 h using 1 M NaOH without (Z1) and with (Z2) agitation. P1 = NaP1 (ICDD PDF 01-071-0962).	78
Figure 3.7 XRD patterns of zeolite NaP1 obtained from the waste at 120 °C and with 1 M NaOH for 3 h (Z2), 6 h (Z3), and 24 h (Z4) with stirring. P1 = NaP1 (ICDD PDF 01-071-0962).	79
Figure 3.8 SEM images of the zeolite NaP1 obtained at 120 °C with 1 M NaOH and a liquid/solid ratio of 25 mL/g for different times: (a-b) 6 h (sample Z3) and (c-e) 24 h (sample Z4).	81

6. ANNEXES

Figure 3.9 XRD patterns of the samples obtained from the waste at 120 °C for 6 h with a NaOH concentration of 1 M (Z3), 3 M (Z5), 4 M (Z6), and 5 M (Z7). P1 = NaP1 (ICDD PDF 01-071-0962) and S = hydroxy-sodalite (ICDD PDF 01-076-1639) and/or chloride-sodalite (ICDD PDF 01-086-1844).	82
Figure 3.10 SEM images of the SOD zeolite obtained at 120 °C for 6 h with a liquid/solid ratio of 25 mL/g and different NaOH concentrations: (a-b) 3 M (sample Z5) and (c-d) 5 M (sample Z7)..	84
Figure 3.11 XRD patterns of the samples synthesized with 1 M NaOH for 6 h at 80 °C (Z8), 90 °C (Z9), 100 °C (Z10), 120 °C (Z3), 140 °C (Z11), 160 °C (Z12), and 200 °C (Z13). P1 = NaP1 (ICDD PDF 01-071-0962), A = analcime (ICDD PDF 00-041-1478), and Q = quartz (ICDD PDF 00-046-1045).	85
Figure 3.12 SEM images of the zeolite ANA obtained with 1 M NaOH and a liquid/solid ratio of 25 mL/g for 6 h at different temperatures: (a-b) 160 °C (sample Z12) and (c-d) 200 °C (sample Z13).	87
Figure 3.13 XRD patterns of zeolite NaP1 obtained at 120 °C for 6 h with different liquid/solid ratios of the reaction suspension: 25 mL/g (Z3), 15 mL/g (Z14), and 7.5 mL/g (Z15). P1 = NaP1 (ICDD PDF 01-071-0962).	88
Figure 3.14 SEM images at different magnifications of the zeolite NaP1 (sample Z3) obtained from the waste at 120 °C for 6 h using 1 M NaOH and a liquid/solid ratio of 25 mL/g.	91
Figure 3.15 SEM images at different magnifications of the zeolite SOD (sample Z7) obtained from the waste at 120 °C for 6 h using 5 M NaOH and a liquid/solid ratio of 25 mL/g.....	92
Figure 3.16 SEM images at different magnifications of the zeolite ANA (sample Z13) obtained from the waste at 200 °C for 6 h using 1 M NaOH and a liquid/solid ratio of 25 mL/g.	94
Figure 3.17 EDS spectra and microchemical point analyses of NaP1 (Z3), SOD (Z7), and ANA (Z13) obtained from the waste.	95
Figure 3.18 FTIR spectra (“finger print” region) of NaP1 (Z3), SOD (Z7), and ANA (Z13) synthesized from the waste.....	98
Figure 3.19 TG-DTA curves of NaP1 (Z3), SOD (Z7), and ANA (Z13) obtained from the waste. (TG (relative mass loss, %): green curve. DTA analysis (°C/mg): blue curve).....	100
Figure 3.20 XRD patterns obtained after the thermal treatment of NaP1 (Z3) at 400, 800, and 1000 °C for 4 h in air atmosphere. P1 = NaP1 (ICDD PDF 01-071-0962) and Ne = nepheline (ICDD PDF 00-035-0424).	104
Figure 3.21 XRD patterns obtained after the thermal treatment of ANA (Z13) at 400, 800, and 1000 °C for 4 h in air atmosphere. A = analcime (ICDD PDF 00-041-1478) and Ne = nepheline (ICDD PDF 00-035-0424).	105
Figure 3.22 XRD patterns obtained after the thermal treatment of SOD (Z7) at 400, 800, and 1000 °C for 4 h in air atmosphere. S = hydroxy-sodalite (ICDD PDF 01-076-1639) and/or chloride-sodalite (ICDD PDF 01-086-1844), and Ne = nepheline (ICDD PDF 00-035-0424).	106
Figure 3.23 a) Nitrogen adsorption/desorption isotherms, and b) distribution of pore diameter of NaP1 (Z3), SOD (Z7), and ANA (Z13) obtained from the waste.	108
Figure 3.24 Particle size distribution of NaP1 (Z3), SOD (Z7), and ANA (Z13) synthesized from the waste.	110
Figure 3.25 XRD patterns of NaP1 synthesized at 120 °C for 6 h after the first (Z17) and second (Z18) mother liquor recycling compared with the initial NaP1 zeolite (Z16) obtained with 1 M NaOH. P1 = NaP1 (ICDD PDF 01-071-0962).....	115
Figure 3.26 SEM images and EDS spectrum and microchemical point analysis of NaP1 obtained from the second mother liquor recycling (sample Z18).....	117
Figure 3.27 a) Nitrogen adsorption/desorption isotherms and b) pore diameter distribution of NaP1 obtained without recycling (Z16) and after the first (Z17) and second recycling cycle (Z18).	118

Figure 3.28 XRD patterns of SOD synthesized at 120 °C for 6 h after the first (Z20) and second (Z21) mother liquor recycling compared with the initial SOD zeolite (Z19) obtained with 5 M NaOH. S = hydroxy-sodalite (ICDD PDF 01-076-1639) and/or chloride-sodalite (ICDD PDF 01-086-1844) and P1 = NaP1 (ICDD PDF 01-071-0962).....	121
Figure 3.29 XRD patterns of ANA synthesized at 200 °C for 6 h after the first (Z23) and second (Z24) mother liquor recycling compared with the initial ANA zeolite (Z22) obtained with 1 M NaOH. A = analcime (ICDD PDF 00-041-1478).....	122
Figure 3.30 Zeolitic phases and their corresponding crystalline sizes as a function of the temperature and NaOH concentration tested to obtain the NaP1, SOD, and ANA zeolites from the waste through the simple one-step zeolitization process.....	125
Figure 3.31 XRD patterns of NaP1 synthesized from the waste by bench-scale synthesis with fresh NaOH solution (ZB0) and with effluents re-used: first (ZB1), second (ZB2), and third (ZB3) recycling cycle. All peaks were identified with NaP1 (ICDD PDF 01-071-0962).....	128
Figure 3.32 XRD pattern of a commercial zeolite (P1-X) characterized by NaP1 zeolite along with traces of zeolite X. All peaks were identified with NaP1 (ICDD PDF 01-071-0962) and zeolite X (ICDD PDF 00-038-0237).....	130
Figure 3.33 FTIR spectra of NaP1 obtained from the waste by bench-scale synthesis with liquid discharge (ZB0) and under the first (ZB1), second (ZB2), and third (ZB3) effluent recycling cycle. Wave number values shown for the commercial zeolite (P1-X).....	131
Figure 3.34 SEM images at different magnifications of NaP1 from the waste via bench-scale synthesis. Sample ZB0 obtained using fresh alkalizing agent (a-c) and samples ZB1, ZB2, and ZB3 prepared after the first (d), second (e), and third (f) effluent recycling cycle, respectively...	134
Figure 3.35 TG-DTA curve of the initial NaP1 zeolite (ZB0) obtained from the waste by the bench-scale synthesis.	136
Figure 3.36 TG-DTA curve of the NaP1 zeolite obtained after the first mother liquor recycling (ZB1) by the bench-scale synthesis.	136
Figure 3.37 TG-DTA curve of the NaP1 zeolite obtained after the second mother liquor recycling (ZB2) by the bench-scale synthesis.	137
Figure 3.38 TG-DTA curve of the NaP1 zeolite obtained after the third mother liquor recycling (ZB3) by the bench-scale synthesis.	137
Figure 3.39 Nitrogen adsorption/desorption isotherms of NaP1 synthesized from the waste by bench-scale synthesis using fresh NaOH solution (ZB0) and after effluent recycling (ZB1, ZB2, and ZB3). Outgassing conditions: 60 °C for 24 h.	140
Figure 3.40 Particle size distribution of the NaP1 zeolite synthesized with fresh alkalizing agent (Z0) and with effluent recycling (Z1, Z2, and Z3) on bench scale.	143
Figure 3.41 ζ -potentials for NaP1 from the waste through the bench-scale synthesis without (ZB0) recycling and after the first recycling (ZB1) compared with a commercial zeolite (P1-X).	144
Figure 3.42 Point of zero charge (PZC) for ZB0 obtained from the waste through the bench-scale synthesis without effluents.....	146
Figure 3.43 Effect of the solution pH on the stability of Pb^{2+} , Cd^{2+} , and Hg^{2+} in aqueous medium at 25 °C \pm 2. C/C_0 : final concentration referred to the initial cation concentration (20 mg/L for Pb^{2+} and Cd^{2+} , and 0.2 mg/L for Hg^{2+}).....	154
Figure 3.44 Chemical equilibrium diagrams of Pb^{2+} , Cd^{2+} , and Hg^{2+} in aqueous solution determined for the next initial concentrations: 20 mg/L for Pb^{2+} and Cd^{2+} , and 0.2 mg/L for Hg^{2+}	155
Figure 3.45 Influence of the solution pH on the removal efficiency of Hg^{2+} by ZB0. Conditions: zeolite dose = 10 g/L; C_0 = 0.2 mg/L; T = 25 \pm 2 °C.....	156

6. ANNEXES

Figure 3.46. Comparison of the XRD patterns of the sample ZB0 at different pH: initial sample of zeolite (ZB0) at pH 10 ± 0.5 (a); ZB0 samples in aqueous solutions at pH 4 (b) and at pH 6 (c). All diffraction peaks were identified by the NaP1 zeolite (ICDD PDF 01-071-0962).	158
Figure 3.47. Effect of the contact time for the single-cation adsorption of Pb^{2+} , Cd^{2+} , and Hg^{2+} onto ZB0. Conditions: pH = 4.5; adsorbent dose = 5 g/L for Cd^{2+} , and Hg^{2+} , and 0.5 g/L for Pb^{2+} ; C_0 = 20 mg/L for Pb^{2+} and Cd^{2+} , and 0.2 mg/L for Hg^{2+} ; $T = 25 \pm 2$ °C.....	160
Figure 3.48 Pseudo-first-order and pseudo-second-order models for the single-cation adsorption of Pb^{2+} , Cd^{2+} , and Hg^{2+} onto ZB0. Conditions: pH = 4.5; adsorbent dose = 5 g/L for Cd^{2+} , and Hg^{2+} , and 0.5 g/L for Pb^{2+} ; C_0 = 20 mg/L for Pb^{2+} and Cd^{2+} , and 0.2 mg/L for Hg^{2+} ; $T = 25 \pm 2$ °C.	161
Figure 3.49. Intra-particle diffusion models of the adsorption of Pb^{2+} , Cd^{2+} , and Hg^{2+} onto ZB0. Conditions: pH = 4.5; adsorbent dose = 5 g/L for Cd^{2+} and Hg^{2+} , and 0.5 g/L for Pb^{2+} ; C_0 = 20 mg/L for Pb^{2+} and Cd^{2+} , and 0.2 mg/L for Hg^{2+} ; $T = 25 \pm 2$ °C.....	163
Figure 3.50. Effect of the zeolite dose on the single-cation adsorption efficiency and uptake capacity of Pb^{2+} , Cd^{2+} , and Hg^{2+} onto ZB0. Conditions: pH = 4.5; contact time = 30 min; C_0 = 20 mg/L for Pb^{2+} and Cd^{2+} , and 0.2 mg/L for Hg^{2+} ; $T = 25 \pm 2$ °C.....	165
Figure 3.51. Two-parameter isotherms for the removal of Pb^{2+} , Cd^{2+} , and Hg^{2+} on ZB0. Conditions: pH = 4.5; contact time = 15 min; adsorbent dose = 5 g/L for Cd^{2+} and Hg^{2+} and 0.5 g/L for Pb^{2+} ; $T = 25 \pm 2$ °C.....	168
Figure 3.52 Three-parameter isotherms for the removal of Pb^{2+} , Cd^{2+} , and Hg^{2+} on ZB0. Conditions: pH = 4.5; contact time = 15 min; adsorbent dose = 5 g/L for Cd^{2+} and Hg^{2+} and 0.5 g/L for Pb^{2+} ; $T = 25 \pm 2$ °C.....	169
Figure 3.53. Influence of the contact time on the multi-cation adsorption using ZB0. Conditions: pH = 4.5; adsorbent dose = 10 g/L; C_0 = 20 mg/L for Pb^{2+} and Cd^{2+} , and 0.2 mg/L for Hg^{2+} ; $T = 25 \pm 2$ °C.	170
Figure 3.54. SEM images of the ZB0 zeolite before (a-b) and after (c-d) the multi-cation removal of Pb^{2+} , Cd^{2+} , and Hg^{2+} from aqueous solutions.	172
Figure 3.55. FTIR spectra of ZB0 before (a) and after (b) the multi-cation adsorption of Pb^{2+} , Cd^{2+} , and Hg^{2+}	173
Figure 3.56. Influence of the pH on the NH_4^+ removal efficiency and adsorption capacity of the zeolite synthesized (ZB0) from the waste through the bench-scale synthesis process. Conditions: contact time = 15 min; adsorbent dose = 5 g/L; C_0 = 50 mg/L; $T = 28 \pm 2$	178
Figure 3.57 Chemical equilibrium diagram of NH_4^+ in aqueous solution determined for a fixed initial concentration (50 mg/L).	179
Figure 3.58. Effect of the contact time on the adsorption NH_4^+ onto ZB0. Conditions: pH = 7.5; adsorbent dose = 5 g/L; C_0 = 50 mg/L; $T = 28 \pm 2$ °C.....	180
Figure 3.59 Pseudo-first-order and pseudo-second-order models for the adsorption of NH_4^+ onto ZB0. Conditions: pH = 7.5; adsorbent dose = 5 g/L; C_0 = 50 mg/L; $T = 28 \pm 2$ °C.	181
Figure 3.60. Effect of the adsorbent dose on the NH_4^+ removal efficiency and uptake capacity of ZB0. Conditions: pH = 7.5; contact time = 15 min; C_0 = 50 mg/L; $T = 28 \pm 2$ °C.....	182
Figure 3.61 Two-parameter adsorption isotherms for the NH_4^+ uptake on ZB0. Conditions: pH = 7.5; contact time = 15 min; adsorbent dose = 10 g/L; $T = 28 \pm 2$ °C.	183
Figure 3.62. Three-parameter adsorption isotherms for the NH_4^+ uptake on ZB0. Conditions: pH = 7.5; contact time = 15 min; adsorbent dose = 10 g/L; $T = 28 \pm 2$ °C. R-P: Redlich-Peterson.	183
Figure 3.63. FTIR spectra of ZB0 before (a) and after (b) the NH_4^+ adsorption.	187